UTILIZATION OF CARBONATED WATER INJECTION (CWI) AS A MEANS OF IMPROVED OIL RECOVERY IN LIGHT OIL SYSTEMS: PORE-SCALE MECHANISMS AND RECOVERY EVALUATION

A Thesis

Submitted to Faculty of Graduate Studies and Research

In Partial Fulfilment of the Requirements

For the Degree of

Doctor of Philosophy

in

Petroleum Systems Engineering

University of Regina

By

Nader Mosavat

Regina, Saskatchewan

September 2014

UNIVERSITY OF REGINA

FACULTY OF GRADUATE STUDIES AND RESEARCH

SUPERVISORY AND EXAMINING COMMITTEE

Nader Mosavat, candidate for the degree of Doctor of Philosophy in Petroleum Systems Engineering**,** has presented a thesis titled, **Utilization of Carbonated Water Injection (CWI) as a Means of Improved Oil Recovery in Light Oil Systems: Pore-Scale Mechanisms and Recovery Evaluation,** in an oral examination held on August 28, 2014. The following committee members have found the thesis acceptable in form and content, and that the candidate demonstrated satisfactory knowledge of the subject material.

External Examiner:	Dr.Peyman Pourafshary, Sultan Qaboos University
Supervisor:	Dr. Farshid Torabi, Petroleum Systems Engineering
Committee Member:	*Dr. Paitoon Tontiwachwuthikul, Process Systems Engineering
Committee Member:	Dr. Nader Mobed, Department of Physics
Committee Member:	Dr. Raphael Idem, Process Systems Engineering
Committee Member:	**Dr. Fanhua Zeng, Petroleum Systems Engineering
Chair of Defense:	Dr. Taehan Bae, Department of Mathematics & Statistics

*Questions Provided
**Not present at defense

Abstract

In this study, the performance of secondary and tertiary carbonated water injection (CWI) was investigated at various operating conditions through sequences of laboratory experiments and numerical simulations. According to the results of CO_2 solubility tests measured at constant temperatures, an increase in solubility value is observed for both water and oil phases when the pressure increases in the range of P = 0.7–10.3 MPa. Furthermore, it was found that the solubility of CO_2 reduces with increased temperature. In addition, the results obtained from swelling/extraction tests revealed that the oil swelling factor increases as the pressure rises until a certain pressure called extraction pressure, P_{ext} is reached. Afterward, the swelling factor reduces due to substantial extraction of lighter hydrocarbons from the oil to the CO_2 phase. Comparison of the CO_2 solubility values in oil at extraction pressures corresponding to different experimental temperatures also showed that the major hydrocarbon extraction occurs when a certain amount of CO_2 has dissolved in the oil phase, which is called threshold CO_2 solubility, χ_{th}.

Results of sand-pack CWI flooding tests revealed that the recovery factor (RF) substantially increases up to a pressure of P = 5.6 MPa followed by slow growth until the pressure reaches P = 10.3 MPa. The same turning point of about P = 5.6 MPa was also observed in the plot of CO_2 solubility in brine versus the operating pressure. Therefore, the value of CO_2 solubility in brine controls the efficiency of the CWI. Additionally, lower recovery factor was obtained when temperature was increased from T = 25 °C to 40 °C. The same impact was observed when the carbonation level of the injected brine was reduced from CL = 100% to CL = 50%. From a CO_2 storage point of view, the

amount of CO_2 stored by the end of secondary and tertiary CWI for different operating pressures was determined, and the values ranged from 40.7% to 61.1% of total injected CO_2. Thus, it was concluded that CWI has great potential for permanent storage of the injected CO_2 while significantly improving oil recovery in light oil systems.

It was observed that the tuned PR-EOS model constructed using CMG WINPROP is capable of accurately reproducing the fluids' basic characteristics, as well as the properties of CO_2–oil and CO_2–brine mixtures, such as saturation pressure and solubility. The fluid model was incorporated into the compositional and unconventional reservoir simulator, CMG GEM, in order to reproduce the CWI flooding tests conducted in this study. The simulation results showed that the CWI process can be simulated using the commercial software, CMG, by modifying the fluid model and history matching the laboratory flooding tests. Understanding the details of oil recovery mechanisms during CWI is of great importance, and precise observations of the fluid-fluid and fluid-solid interactions were carried out in this study through visual micro-model displacement tests. It was found that major wettability trapping along with minor snap-off and pore-doublet trapping mechanisms were attributed to relatively high residual oil saturation after primary water flooding. However, it was observed that injection of carbonated water is able to favourably adjust the wettability of the utilized glass micro-model toward the water-wetting condition. The observations of the CWI process in the micro-model demonstrated the main recovery mechanisms contributing to improvement of the oil recovery are oil swelling and viscosity reduction as a result of CO_2 mass transfer from the brine to the in-place oil phase. It was also revealed that the trapped oil ganglia can be produced by continued injection of carbonated water for higher pore volumes.

Acknowledgements

I would like to express my sincere gratitude to my supervisor Dr. Farshid Torabi for his guidance, encouragement, patience, and enlightenment throughout the course of this work at the University of Regina. His valuable input during different tasks of this research was extremely helpful. He provided countless academic and self-development opportunities, which ultimately helped me in completion of my research and growth in this profession. I also wish to thank Dr. Raphael Idem, Dr. Nader Mobed, Dr. Paitoon Tontiwachwuthikul, and Dr. Bill Zeng for their advice and support of this work and enthusiasm in serving as members of my graduate advisory committee.

I would like to thank to the Petroleum Technology Research Centre (PTRC), Sustainable Technologies for Energy Production System (STEPS) program, and Faculty of Graduate Studies and Research (FGSR) for funding this research project.

Many thanks to Mr. Ali Abedini who helped me during some of the experiments in this study. His knowledge and practical experiences were always helpful to me during different tests and technical discussions. I also would like to thank Dr. Ali Kavousi for all his support and encouragement.

I also wish to thank the Engineering Design Lab/Workshop at the University of Regina, particularly Mr. Harald Berwald and Mr. Harlan Berwald for their constructive discussions and feedback in designing the new apparatuses.

Thanks are also extended to all the faculty members, staff, and students at the Faculty of Engineering and Applied Science at The University of Regina who have offered help and made the past several years enjoyable and worthwhile.

Dedication

To

The memory of my father-in-law, Mr. Ebrahim Razeghi, for his unconditional support, friendship, and encouragement. I miss him every day, but I believe that he is somewhere above and watching over this process through to its completion.

To

My dearest wife, Samaneh, for her love, trust, patience, and continuous encouragement. For being my best friend and the "soul out of my soul".

To

My parents and family, for their love, invaluable advice, motivation, and support.

Table of Contents

List of Tables

List of Figures

Nomenclature

Symbols

CL	Carbonation level (%)
D	Grain diameter in porous medium (m)
dP	Differential pressure across the sand-pack (kPa)
f_{CO2}	Fugacity of CO_2 (Pa)
k_{abs}	Absolute permeability (mD)
k_{eff}	Effective permeability (mD)
k_h	Horizontal permeability (mD)
$K_{H,CO2}$	Henry's constant for CO_2 (m^3.Pa/mole)
K_i	Equilibrium k-value for component i
k_{ro}	Relative permeability to oil
k_{rw}	Relative permeability to water
k_v	Vertical permeability (mD)
l_g	Length of micro-model's glass (cm^3)
l_p	Length of micro-model's engraved pattern (cm^3)
M	Mobility (D/Pa.s)
$m_{CO2,f}$	Final mass of CO_2 (gr)
$m_{CO2,i}$	Initial mass of CO_2 (gr)
m_{dis}	Mass of CO_2 dissolved in the oil (gr)
MMP_{actual}	Actual value of minimum miscibility pressure (MPa)
MMP_{approx}	Approximated value of minimum miscibility pressure (MPa)
M_o	Mobility of the oil phase (D/Pa.s)

m_{oil}	Mass of the oil sample (gr)
MW_{CO2}	Molecular weight of CO_2 (44.01 gr/mol)
MW_o	Oil molecular weight (gr/mole)
N_{CA}	Complete capillary number
P	Pressure (MPa)
P_{atm}	Atmospheric pressure (101.1 kPa)
P_c	Critical pressure (MPa)
P_{ext}	Light-component extraction pressure (MPa)
P_f	Final pressure (MPa)
P_i	Initial pressure (MPa)
P_{liq}	CO_2 liquefaction pressure (MPa)
P_{max}	Maximum operating pressure (MPa)
P_R	Reservoir pressure (MPa)
P_{sat}	Saturation pressure (MPa)
q_{inj}	Injection flow rate (cm^3/min)
R	Universal gas constant (8.314 J/mol.K)
Re	Reynolds number
s	Brine salinity (mole/kg)
SF	Swelling factor
S_{or}	Residual oil saturation (%)
S_{wi}	Initial water saturation (%)
T	Temperature (°C)
t	Injection time (s)
t_{BT}	Breakthrough time in micro-model study (s)
T_c	Critical temperature (°C)

$T_{c,CO2}$	CO_2 critical temperature (31 °C)
T_{exp}	Experimental temperature (°C)
T_R	Reservoir temperature (°C)
V_c	Critical volume (cm^3)
$V_{CO2,f}$	Final CO_2 volume (cm^3)
$V_{CO2,i}$	Initial CO_2 volume (cm^3)
$V_{CO2\text{-}Oil}$	Volume of CO_2–oil mixture (cm^3)
v_L	Displacing liquid velocity (m/s)
V_{oil}	Oil volume (cm^3)
w	Accentric factor
w_g	Width of micro-model's glass (cm^3)
w_p	Width of micro-model's engraved pattern (cm^3)
$X_{1,eq}$	Water mass fraction in aqueous phase
$X_{2,eq}$	CO_2 mass fraction in aqueous phase
X_3	Total CO_2 mass fraction
x_{CO2}	Molar fraction of CO_2 in water
x_i	Equilibrium liquid composition of component i
$Y_{1,eq}$	Water mass fraction in gas phase
$Y_{2,eq}$	CO_2 mass fraction in gas phase
y_i	Equilibrium gas composition of component i
Z	Gas compressibility factor

Greeks

ϕ	Porosity (%)

ΔP	Pressure difference (kPa)
μ_d	Liquid dye viscosity (mPa.s)
θ	Contact angel (°)
μ	Viscosity (mPa.s)
μ_b	Water viscosity (mPa.s)
μ_L	Displacing liquid viscosity (mPa.s)
μ_o	Oil viscosity (mPa.s)
ρ_b	Brine density (kg/m^3)
ρ_{CO2}	CO_2 density (kg/m^3)
ρ_d	Liquid dye density (kg/m^3)
ρ_L	Displacing liquid density (kg/m^3)
ρ_o	Oil density (kg/m^3)
σ_{eq}	Equilibrium interfacial tension (N/m)
χ_b	CO_2 solubility (mole CO_2/kg brine)
$\chi_{b,max}$	Maximum CO_2 solubility (mole CO_2/kg water)
χ_o	CO_2 solubility in oil (gr CO_2/ 100 gr oil)
$\chi_{o,max}$	Maximum CO_2 solubility in oil (gr CO_2/ 100 gr oil)
χ_{th}	Threshold CO_2 solubility in oil (gr CO_2/ 100 gr oil)
χ_w	CO_2 solubility (mole CO_2/kg water)

Abbreviations

API	American petroleum institute
ASTM	American Society for Testing and Materials
BIC	Binary interaction coefficient

BL	Buckley-Leverett
BPR	Back pressure regulator
BT	Breakthrough time
CCS	Carbon capture and storage
CW	Carbonated water
CWI	Carbonated Water Injection
DPI	Dots per inch
EOR	Enhanced oil recovery
EOS	Equation of state
GC	Gas Chromatography
GHG	Greenhouse gas
GI	Gas infusion
GWR	Gas to water ratio
HCPV	Hydrocarbon pore volume
IEA	International energy agency
IFT	Interfacial tension
IOR	Improved oil recovery
IPCC	Intergovernmental panel on climate change
JST	Jossi-Stiel-Thodos
MMP	Minimum miscibility pressure (MPa)
MW	Molecular weight
NAPL	Non-aqueous phase liquid
OOIP	Original oil in place
OOIP	Original oil in place
ppm	Parts per million

PR	Peng-Robinson
PV	Pore volume
PVT	Pressure-Volume-Temperature
RF	Recovery factor
SCWI	Secondary carbonated water injection
SG	Specific gravity
SIR	Stored to injected ratio
SRK	Soave-Redlich-Kwong
STB	Stock tank barrel
TCWI	Tertiary carbonated water injection
TDS	Total dissolved solids
VIT	Vanishing interfacial tension
VLE	Vapour-liquid equilibrium
WAG	Water alternating gas
WF	Water flooding

Unit conversion:

1 mD $\approx$ 0.000987 μm^2

CHAPTER ONE: Introduction

1.1. Energy demand and climate change

Global energy demand is expected to increase approximately 35% between 2010 and 2040 where crude oil will remain the largest source of energy with its contribution to the world's energy supply growing to around 25% (Exxonmobil, 2013). **Figure 1.1** demonstrates the explosive growth of various contributors to providing global primary energy. It is obvious from the figure that the hydrocarbon-based recourses are of primary importance, vastly outweighing the use of nuclear and renewable energy sources. World consumption of petroleum and other petrochemicals are projected to grow from 85.7 to 97.6 and 112.2 million barrels per day in 2008, 2020, and 2035, respectively. To satisfy this increase in world crude oil demand, hydrocarbon liquid production needs to increase by 26.6 million barrels per day from 2008 to 2035 (International Energy Outlook 2011).

On the other hand, using fossil fuels for energy production creates large amounts of environmental pollutants, which cause severe impacts on the global environment by increasing concentrations of the anthropogenic greenhouse gases (GHG) in the atmosphere, particularly CO_2. According to the Intergovernmental Panel on Climate Change (IPCC), global GHG emissions must be reduced by 50 to 80 percent by 2050 to avoid dramatic consequences of global warming (Solomon *et al.*, 2007; IPCC, 2007). An option to mitigate climate change is to prevent release of CO_2 to the atmosphere by storing it in geological reservoirs. Of the various options for storing CO_2 underground, depleted oil and gas fields have substantial capacities since these fields are known to have

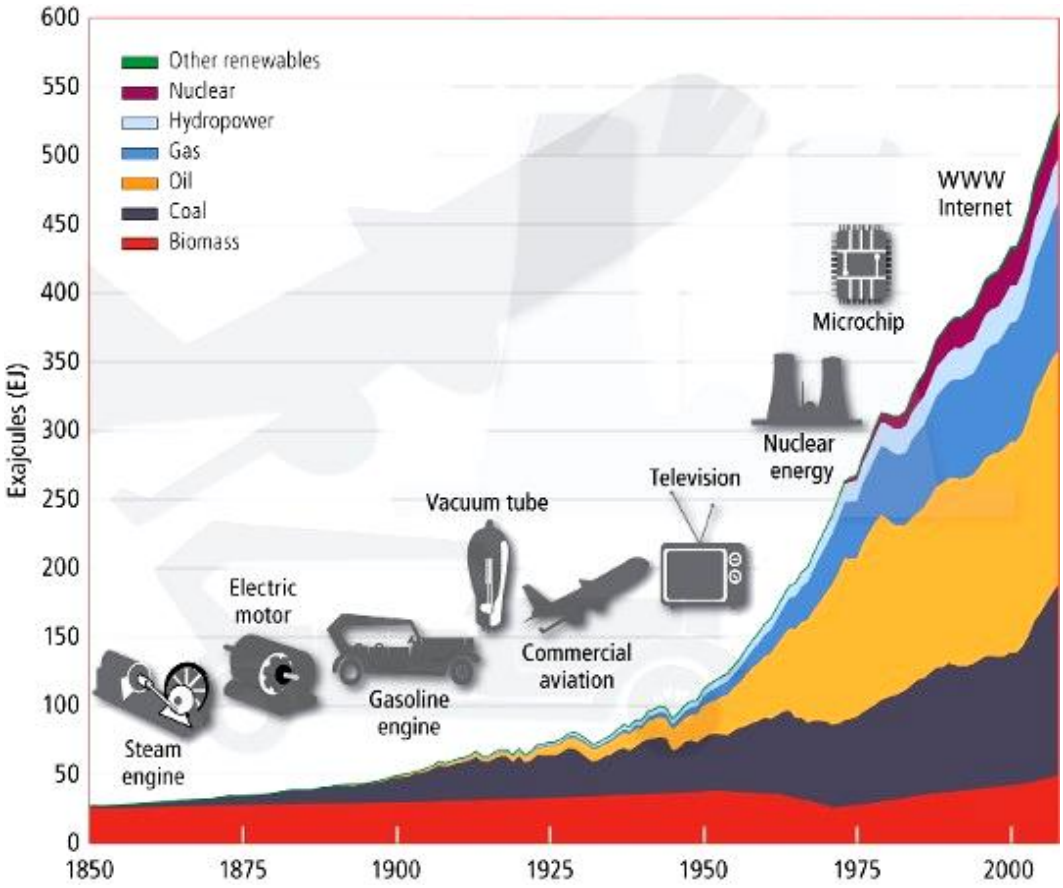

Figure 1.1: World primary energy use (IIASA magazine, summer 2012).

held gases and liquids for millions of years and their geology is already known (IEA Greenhouse Gas, 2009).

1.2. Oil recovery phases: processes and mechanisms

Over the lifetime of an oil reservoir, the recovery process usually includes three phases: primary, secondary and tertiary oil recovery, as illustrated in **Figure 1.2**. The first producing phase of a reservoir is known as the primary production phase where a new field is found and wells are drilled into the formation. Primary recovery is characterized by natural flow of oil from the reservoir to production wells, driven by the pressure gradient across the reservoir rock, which is generally a sandstone or carbonate (limestone and dolomite) formation. After the oil production has started, the reservoir energy from reservoir pressure eventually depletes and the wells cease to produce. This requires a stage called "artificial lift" wherein fluids are pushed or lifted to the surface and production can be prolonged. Eventually, the pore pressures are so thoroughly depleted and move so slowly within the formation that the wells produce uneconomic volumes. At this point, a considerable amount of oil with as much as 80–90% still trapped in the pore spaces of the rock (Melzer, 2012).

The field may be abandoned after fluid pressures deplete or it can be converted to what is called a secondary phase of production wherein a substance is injected to re-pressurize the formation. Secondary or improved oil recovery (IOR) involves gas (e.g. N_2, CO_2) or liquid (e.g., water) injection with the major objective of pressure maintenance. New injection wells are drilled or converted from producing wells and the

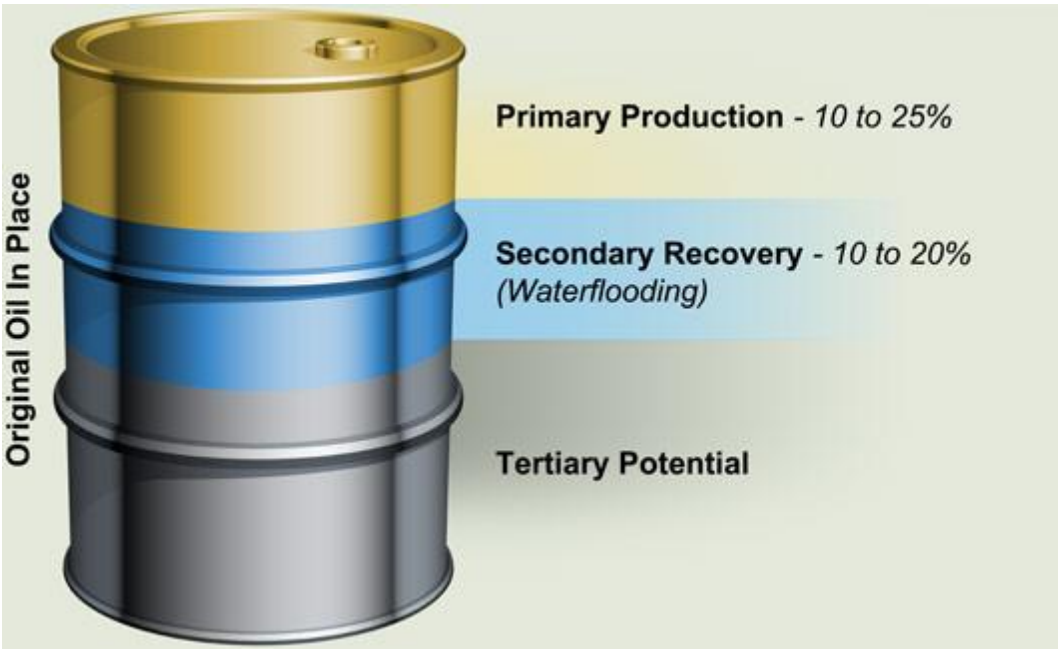

Figure 1.2: Oil recovery phases showing the approximate recovery factors for each phase (http://www.midconenergypartners.com).

injected fluid sweeps oil to the remaining producing wells. This secondary phase is often very efficient and can match or surpass the primary phase of production.

As mentioned earlier, water is the common injectant in the secondary phase of production since water is relatively inexpensive. Normally fresh water is not used during the water flooding, but, rather, the produced water from the formation is repeatedly recycled back into the formation. Ultimately, in most reservoirs, the injected water bypasses 50–70% of the original oil in place (OOIP) remains in the reservoir after water flooding as it, which is immiscible with the oil.

To produce more residual oil from the reservoir, third phase (i.e., tertiary phase) of production may be initiated. This uses an injectant that reacts with the oil to change its properties and allow it to flow more freely within the reservoir. This phase is also called Enhanced Oil Recovery (EOR) and can be divided into thermal methods (e.g. steam injection) and non-thermal methods (i.e., chemical methods and miscible gas flooding) in which chemical and/or thermal reactions and/or dissolution processes are involved and the injection fluid (e.g., CO_2) reacts with the reservoir oil.

One of the most proven EOR methods is carbon dioxide (CO_2) flooding. CO_2 has the capability of mixing with the oil to swell it, make it lighter, and detach it from the rock surfaces, thereby enabling the oil to flow more freely within the reservoir and recovered at the producer well. Injection of CO_2 into depleted oil reservoirs to improve oil recovery has been implemented in many reservoirs around the world for more than 40 years. **Figure 1.3** depicts the oil production history in Weyburn, Saskatchewan, Canada, including primary and waterflooding, vertical infill drillings, pre CO_2 horizontal infill drillings, and CO_2 EOR phases.

A major drawback of gas flooding methods (such as CO_2 flooding) is that the sweep efficiency is poor particularly in thick reservoirs. This method is often not economically feasible. **Figure 1.4(a)** shows schematics of a likely scenario for low sweep efficiency. Due to large density contrasts between the injected CO_2 and the oil phase, gas override is observed. The injected gas rises upwards and bypasses the OOIP so that only a limited portion of the oil in place contacts the injected gas. Alternating the gas injection with water injection, attempts to minimize the gas override. However, Figure 1.4**(b)** shows the sweep efficiency is still low. Carbonated water, which is water (or brine) with dissolved CO_2, has proven to overcome these problems and achieve a more stable front. Figure 1.4**(c)** illustrates the typical sweep efficiency of a CWI process in a typical 2-D plane section of an oil reservoir.

The CO_2 solubility in the brine or oil phase and its influences on the brine or oil physical properties can be determined by experimental studies and by using available modelling packages or correlations. However, the available models can only be used in limited situations and, hence, may not be applicable in a wide range of operating conditions, particularly for CO_2-based EOR and CO_2 storage processes. Physical fluid properties including brine density and viscosity, CO_2 solubility in brine, oil viscosity and density, CO_2 solubility in oil, and oil swelling factor are the key parameters required to design and simulate the oil recovery and CO_2 storage processes (Simon and Graue, 1965; Jamaluddin *et al.*, 1991; Srivastava *et al.*, 1995; Costa *et al.*, 2012; Abedini and Torabi, 2013).

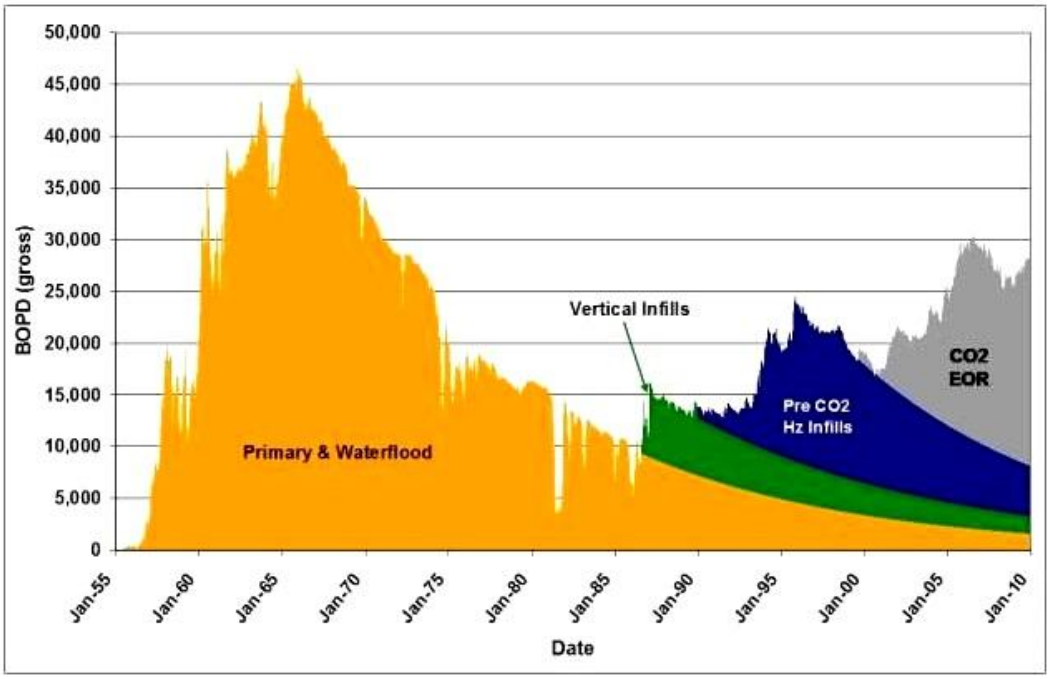

Figure 1.3: Oil recovery phases in Weyburn field (Cenovus Energy Inc., 2010).

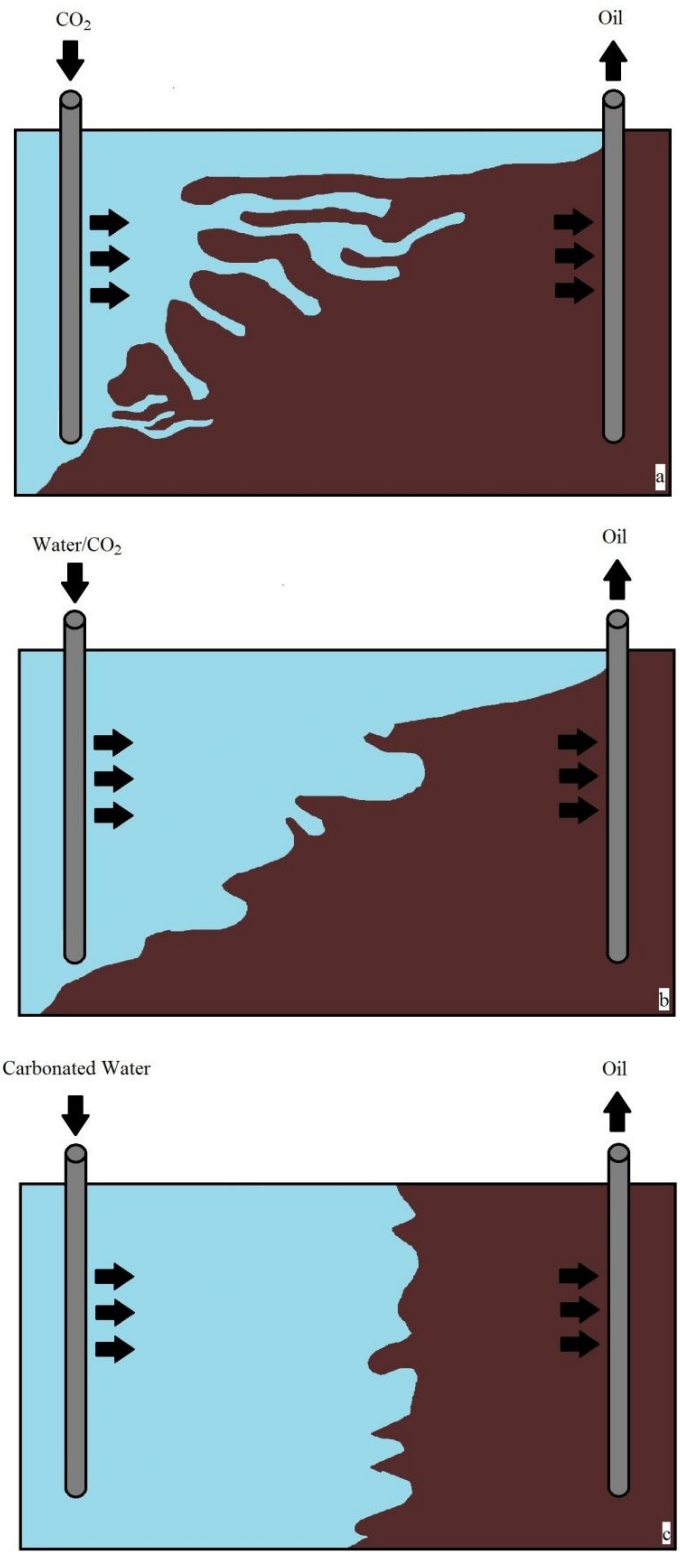

Figure 1.4: Schematic illustration of the oil sweep efficiency in a 2-D cross-section of a typical reservoir: (a) CO_2 injection, (b) CO_2-WAG injection, and (c) CWI.

1.3. CO_2 solubility promoter solvents

Although CO_2 solubility in water is significant compared to other gases, the amount of CO_2 delivered by carbonated water is still low and only a small fraction of that will be diffused into the crude oil (specifically heavy oils) during CWI. In fact, CO_2 content is a key parameter that plays an important role in CWI. The low CO_2 content can adversely affect the CWI performance and consequently results in a low recovery factor. Therefore, it is important to use a CO_2 solubility promoter (called co-solvents) to increase the solubility of CO_2 in water prior to injection (Shu, 1983; Kamps *et al*., 2000). Thus more CO_2 is delivered to the reservoir and subsequently to the oil phase. This will result in relatively higher oil swelling, viscosity reduction and ultimately improve the performance of CWI. One example of a co-solvent is acetone. Several studies have shown that the presence of acetone in water could increase CO_2 solubility significantly (Jodecke *et al.*, 2004; Jodecke *et al.*, 2007; Riazi, 2011).

Generally, CO_2 co-solvents can be divided into two groups: physical and chemical absorbent agents. Chemical absorption is characterized by the occurrence of a chemical reaction between the gas (CO_2) component and a component in the liquid (water) phase. However, use of such co-solvents (chemical absorption) would not readily allow CO_2 to be released and diffused into the oil phase; thus, a slug of demoter or heated fluid would be required to release CO_2 from the carbonated water (Riazi, 2011).

A physical absorbent on the other hand, does not react chemically with the absorbed CO_2 and, hence allows the partitioning of CO_2 when it comes in contact with oil and ultimately improves the recovery performance of CWI.

It has been suggested that to increase the amount of CO_2 available for reducing oil viscosity, first a slug of CW containing a CO_2 solubility promoter to increase dissolved CO_2 in water should be injected into the formation. Then, a slug of a CO_2 solubility demoter or a heated fluid should be injected into the formation to decrease the solubility of the CO_2 in the aqueous slug to release CO_2 from CW. The CO_2 solubility promoter reacts with the CO_2 in the CW and increases CO_2 solubility (Winston, 1983; Winston, 1984).

1.4. Carbonated water injection (CWI)

1.4.1. Process overview

CO_2 is increasingly considered as having potential applications as a possible EOR/IOR process for mature oil reservoirs. Additionally, these reservoirs provide long-term storage potential for CO_2 as an acceptable solution to the challenges of continuous use of fossil fuels, climate change, and compliance with national and international commitments to reduce CO_2 emissions.

Since CO_2 solubility in water is high compared to other gases such as C_1H_4, C_2H_4, and C_2H_6, an effective injection strategy could be carbonated water (CO_2-enriched water) injection. Carbonated water has attracted attention as a potential flooding agent for more than 50 years. Previous studies in the laboratory and in the field showed that waterflooding efficiency could be considerably improved by CWI. Moreover, CWI has proven to be an effective alternative injection strategy that can eliminate many of the deficiencies of direct CO_2 injection, including poor sweep efficiency due to a high CO_2

mobility. In addition, CWI provides the opportunity to use CO_2 for both enhanced oil recovery and sequestration purposes.

One of the main advantages of utilizing CWI is that dissolution of injected CO_2 in the oil phase causes an increase in oil mobility. CO_2 mobility in the oil phase is affected in two ways: oil phase swelling and viscosity reduction. Swelling of the oil phase leads to a higher relative permeability to oil, which in turn, favourably affects oil mobility.

In CWI, dissolved CO_2 transfers from the injected water to the oil phase, so the CO_2 front advances more gradually than the water front. The injected carbonated water sweeps considerably more oil than a water flood and better than a CO_2 flooding because of the lower mobility (viscosity may increase by 5% at reservoir pressure of P = 3.4 MPa) and density contrasts reported by researchers (Green and Willhite, 1998). On the other hand the CO_2 injection rate in CWI is lower than that of CO_2 injection because the amount of injected CO_2 is limited by the CO_2 solubility in water. Therefore the oil response to the injected CO_2 (i.e., swelling and viscosity reduction) in the reservoir is more deliberate when CWI technique is utilized.

Furthermore, most of the oil resources in the world are under waterflood, and, therefore, it may not be feasible to shut down those projects and switch to other EOR techniques while there is still potential for improving the performance of water flooding by injecting carbonated water. With current oil prices showing potential to increase and enhancements in water flooding by injecting carbonated water, there is a large opportunity to increase the oil production by using CWI instead of pure CO_2, pure water, or water alternating gas (WAG). In addition, CWI provides a bridge between reducing GHG and using CO_2 to increase oil recovery.

1.4.2. Operational issues of CWI

Practical issues arise in preparing large scale CW at the desired pressure and temperature conditions are safety and economic considerations. One of the well-known technologies to make carbonated water is the use of a gas infusion (GI) generator (**Figure 1.5**). The GI generator includes hydrophobic micro hollow fibers that provide surface area between the water and gas for high mass transfer efficiency (i.e., bubble-free CO_2 transfer) to produce high dissolved gas concentrations (**Figure 1.6**).

Another important practical issue associated with CWI is corrosion of the facilities due to formation of carbonic acid (H_2CO_3) because of CO_2 dissolution in water. The acid, in sufficient quantities, may promote corrosion of carbon steel. The critical factors in this process are the partial pressure of CO_2, temperature, pH of the CW and velocity of the fluid within the pipes.

Formation of carbonic acid due CO_2 dissolution in water may lead to injectivity problems because the acid reacts with the carbonated rocks and some solids precipitation may occur. Moreover, presence of carbonic acid may cause severe corrosion in steel pipelines, tubing, and surface equipment.

As a result of the dissolved CO_2 in water, some operational problems such as precipitation of asphaltene and paraffins and the formation of calcium sulfate scale may take place. These changes during CWI cause blockage in the reservoir and pipeline facilities and consequently affect the fluid flow processes.

Another issue is water weakening effect. This refers to the deformation of reservoir layers (especially for chalk layers) during water flooding. This effect causes several issues, such as reservoir compaction and seabed subsidence. The effect of

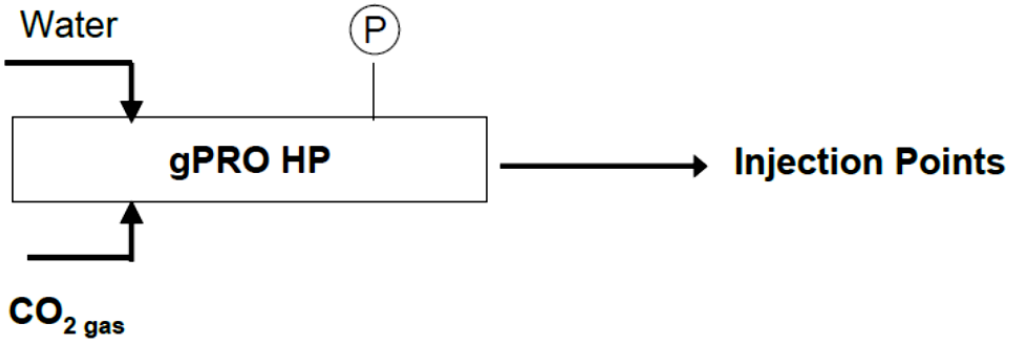

Figure 1.5: Schematics of the gPRO HP setup for preparation of carbonated water mixing water and CO_2 at a certain pressure and temperature (www.gproinfo.com).

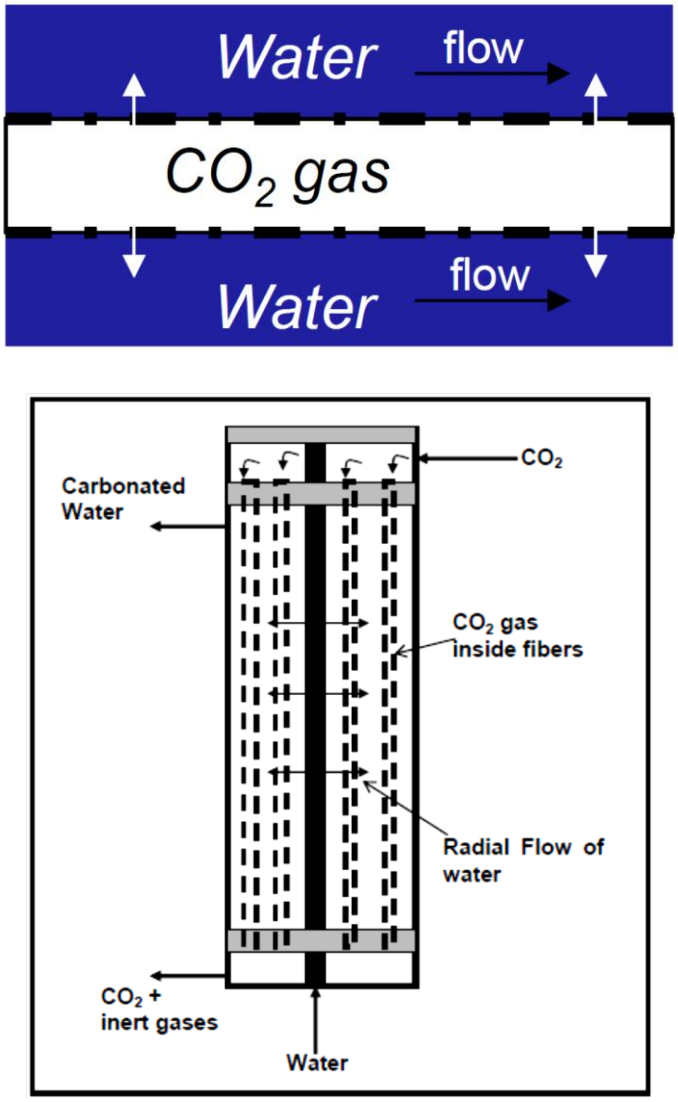

Figure 1.6: Schematics of the process of CO_2 mass transfer in a GI unit (a) micro scale (b) macro scale (www.gproinfo.com).

dissolved CO_2 in water on rock–fluid interaction has been studied by different research groups (Sayegh *et al.*, 1990; Hiorth, *et al.*, 2008; Korsnes *et al.*, 2008). The mechanical strength of high porosity chalk is affected by using carbonate water as IOR fluid and the water-weakening effect is enhanced due to increased dissolution of chalk in the presence of CO_2 (Madland *et al.*, 2006).

1.4.3. Buckley–Leverett (BL) theory for CWI

The whole process of CWI can be described on the basis of the BL study (Buckley and Leverett, 1942). The detailed derivation and mathematical model can be found in de Nevers (1964). The calculation is only valid when all the assumptions for BL equation are met, plus:

- There is no dissolution of oil in water or vice versa.
- The formation pressure is high enough that no CO_2 gas phase is formed anywhere in the formation.
- In those parts of the formation where CO_2 is present, at any given point in the formation, the oil and water are in equilibrium.
- Molecular diffusion and convective diffusion (dispersion) of CO_2 in the flow direction are zero (i.e., CO_2 moves forward only by flow of the oil and water phases, not by diffusion within them).

The cumulative oil and CO_2 production, the water saturation, and the CO_2 concentrations in the reservoir for a plain water flooding and a CWI are presented in **Figure 1.7**. From this graph it is clear that the cumulative oil production is higher when injecting carbonated water is used instead of pure water (Figure 1.7**d**). Figure 1.7**a** illustrates how the water first propagates with a constant CO_2 concentration (G–E). The

water saturation here is higher than the water saturation of the plain water flood. The additional oil produced from this area flows forward and forms an oil bank (C–B). This oil contains no CO_2. The section (E–C) is the carbonated zone. The difference between a plain water flood and a CWI is also illustrated in Figure 1.7d, where the oil production is similar up to point B. Between points (B–E) the additional oil is recovered. Figure 1.7c illustrates the cumulative production of CO_2. Assume that the total amount of CO_2 injected is the projection on the y-axis of point D (Figure 1.7c). Then, this will also be the point that the CWI process will stop and no more CO_2 will be produced (Steffens, 2010).

As a reason for the decreased residual oil saturation (difference between F and G), de Nevers gives the swelling followed by shrinking method. This method implies two processes. The first process is oil swelling due to dissolution of CO_2 in the oil. The oil becomes more mobile and producible so that the oil saturation increases when applying CWI. The second process is oil shrinking. This is due to the plain water flood which follows the carbonated water flood. The injected pure water extracts the CO_2 from the oil phase so that the oil shrinks. The oil shrinking results in an oil saturation even lower than the initial residual oil saturation.

1.4.4. Sweep and displacement efficiencies

In a CWI process, gravity segregation is usually similar to water flood and much less than for a pure CO_2 gas flood. CO_2 dissolution results in a 1–4% increase in the density of pure water or brine. Particularly, in the case of heavy oil, the lower density contrast when injected with CO_2 saturated water will minimize the gas-overrun as well as water under-run effect.

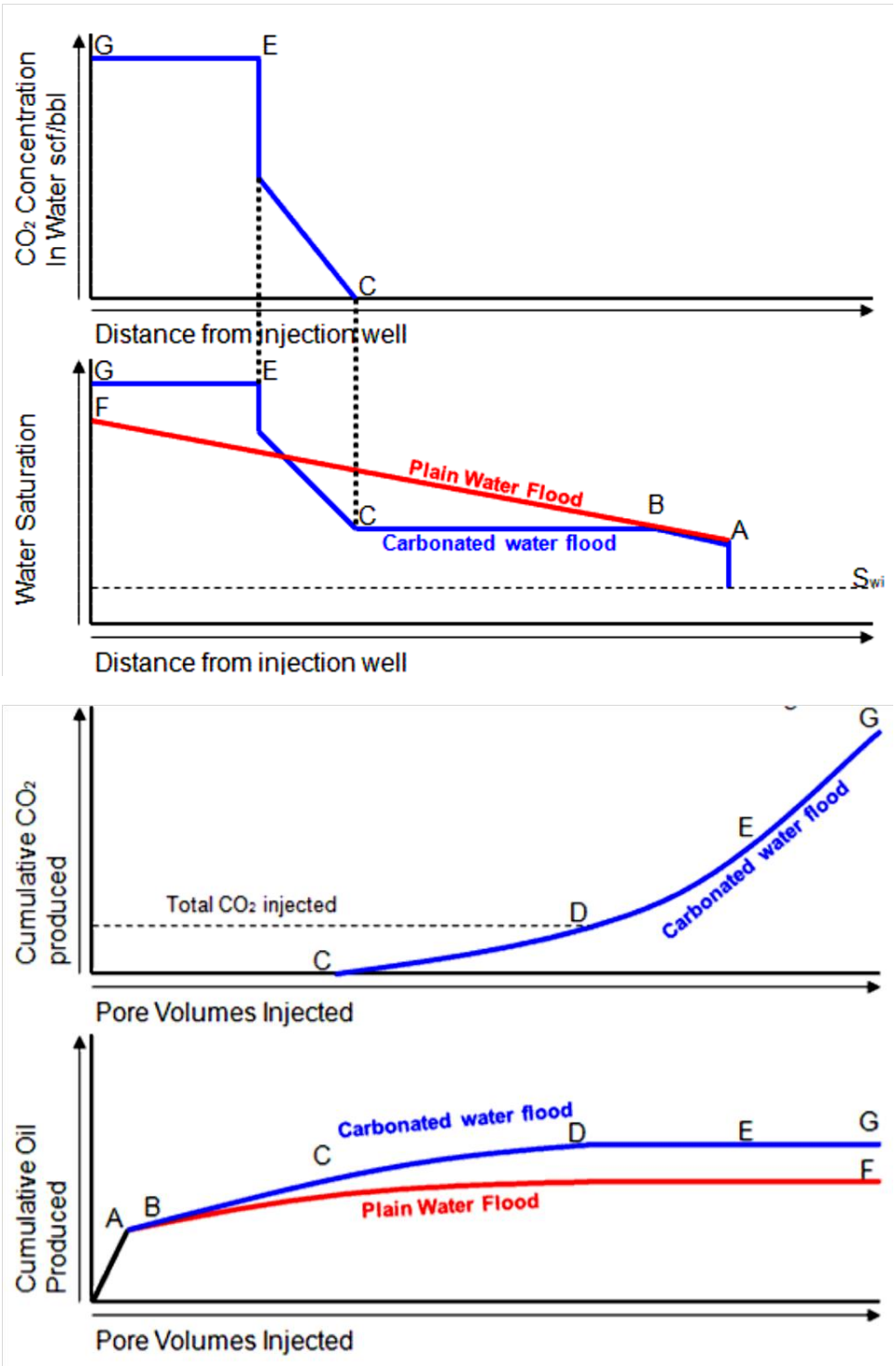

Figure 1.7: Comparison of plain water flood and CWI according to Buckley–Leverett theory by de Nevers (1964): a) CO_2 concentration as a function of distance from injector; b) Water saturation as a function of distance; c) Cumulative CO_2 production as a function of injected pore volume; d) Cumulative oil production as a function of injected pore volume (Steffens, 2010).

In the illustration for production curves for a typical carbonation level in **Figure 1.8**, it appears that higher carbonation levels give higher oil recoveries. Initially, oil production is similar in both cases at water breakthrough. Then water production continues for a while until CO_2 breakthrough at the producer well. From that point on, incremental oil is visible with drastic viscosity reduction surrounding the producer. After a certain time, there is no increase in cumulative oil production since the flow at the producer is mostly CO_2 and its production rate goes up significantly.

Generally, at low carbonation levels, increasing carbonation leads to a large change in recovery until reaching a threshold, after which adverse effects may occur. The carbonation level of the injected water for which this calculation method works, is limited by the reservoir pressure, temperature, and brine salinity. At a given temperature and pressure, the CO_2 solubility in pure water curves sets a maximum carbonation level at which no free CO_2 gas is present. If a carbonation level of higher than this (i.e., $CL >$ 100%) is chosen, free CO_2 gas will be formed. Thus, it appears that the carbonation level should be chosen not higher than CL = 100% to avoid generation of free gaseous CO_2. In other words, the carbonation level should always be high enough that the bubble point pressure of the CO_2–water solution is at or near reservoir pressure.

The advance of the gas–water front is illustrated in **Figure 1.9**. Consequently, there are three distinct regions along the flow path from the injector to producer. The black curve corresponds to the solution from BL for conventional water flood. There is a slight difference in the red curve constructed for CWI.

In Region I, CO_2 concentration in water is equal to the injected concentration and is nearly constant over time; hence, water saturation, S_w is fairly high, accordingly, as a

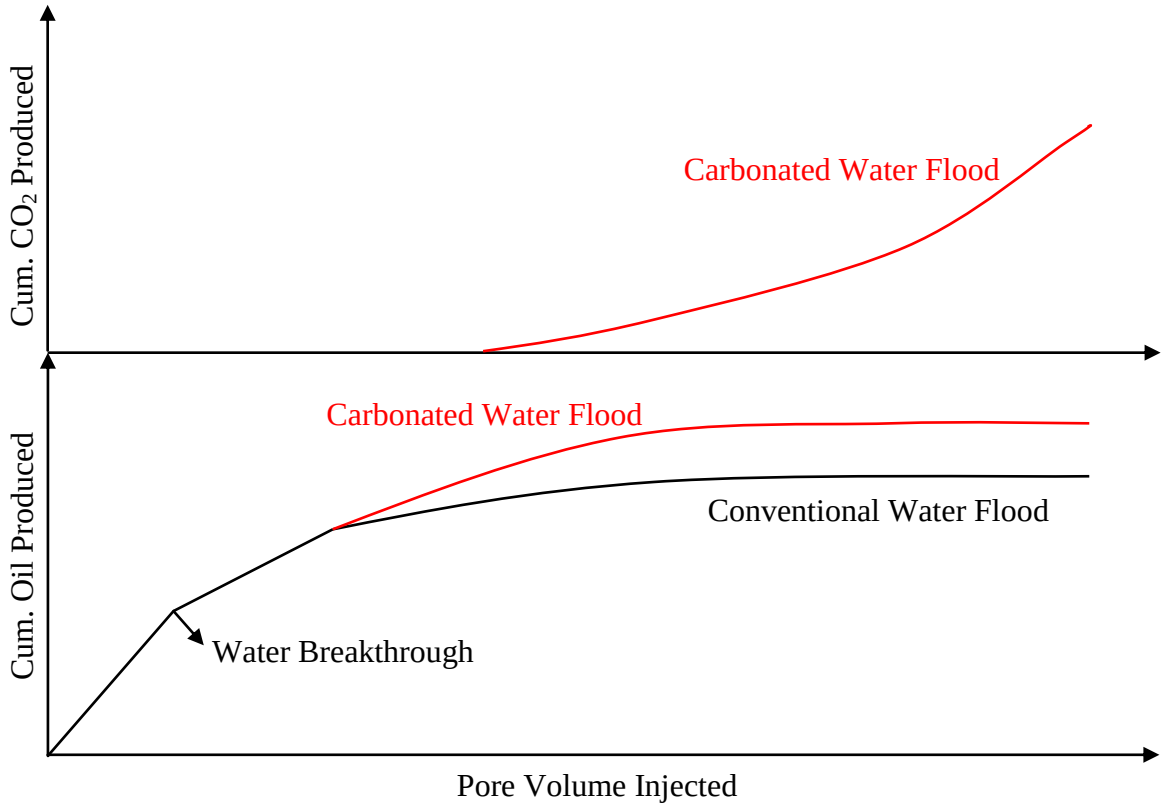

Figure 1.8: Cumulative injected volumes in a CWI process and conventional water flooding (rebuilt from Steffens, 2010).

result of increasing density and viscosity, as mentioned earlier. CWI forms a flood-bank with higher water saturation, and the incremental oil recovered, causing the difference of the region between the black and red curves in both Region I and II. The performance in Region III is identical to that of in the BL solution. In addition, the blue line in Figure 1.6 denotes CO_2 concentration in water. Similar to S_w, a high concentration is expected in the vicinity near the injector due to the density difference. As a result, gas breakthrough always comes later than water and, simultaneously, increases with time until the flood-bank arrives, and, then, apparently, no more oil produced as only gas and water flow.

The presence of CO_2 leads to the modification of the material balance. It is the mass transfer process when CO_2 diffuses from injected water into the oil with subsequent viscosity reduction. Two material balance equations are involved in describing each phase's saturation in the continuous changing phase in Region II and at the shock front.

When applied as tertiary recovery, CWI is able to remobilize oil droplets shielded by WF and thus produce more oil. In secondary mode, CWI is able to produce more oil than WF does for the same PV injected.

1.5. Motivation

The principal reason for waterflooding an oil reservoir is to increase the oil-production rate and ultimately improve the oil recovery. This is accomplished by injection of water to increase the reservoir pressure during the secondary production phase. Meanwhile, the injected water displaces oil from the pore spaces towards the production well and enhances the pore-scale oil mobility. The efficiency of waterflooding is determined by many factors such as reservoir fluid properties and rock characteristics.

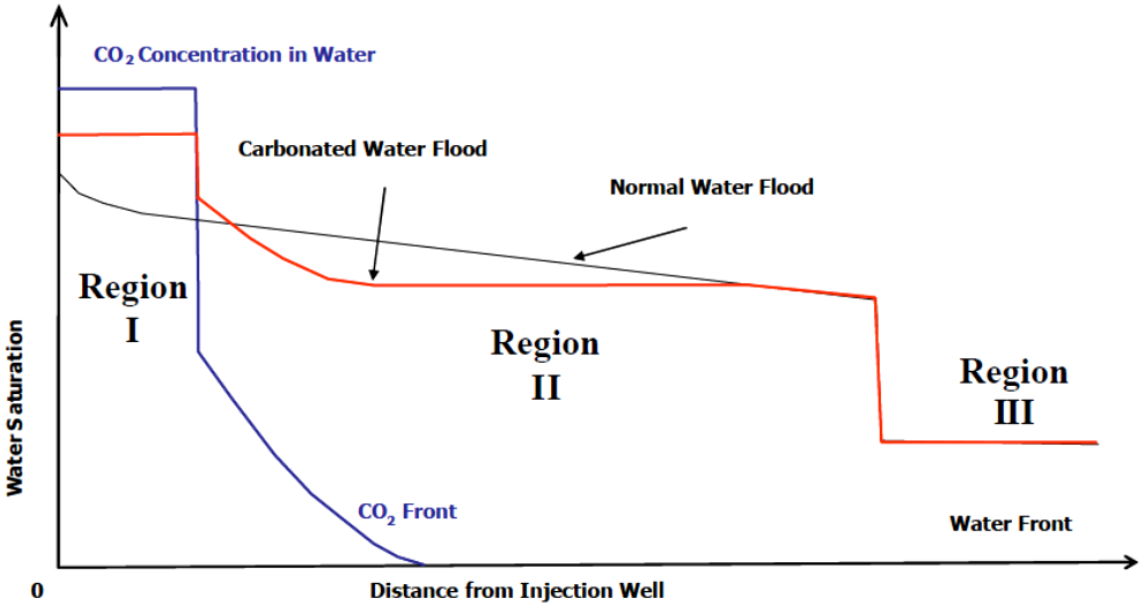

Figure 1.9: Water Saturation in a Carbonated Water Flood and Normal Water Flood (Steffens, 2010).

Many researchers have conducted numerous studies to improve the efficiency of conventional water flooding using various innovative methods. Among many options to improve the performance of water flooding, literature shows that application of CWI is considered as a beneficial alternative to conventional water flooding. It is believed that both virgin and water flooded oil reservoirs can be suitable candidates for CWI process. Although some portions of the global oil reservoirs, especially light oil reservoirs, are already water flooded, there are many reservoirs that are not yet water flooded, or are currently under water flooding. The first part of this study deals with the application of CWI in the secondary phase, addressing the application of CWI in later reservoirs. Since water flooding of a typical reservoir occurs over decades, depending on the size of the reservoir, initial pressure, and etc., switching current water flooding to CWI is economical and results in much better microscopic and macroscopic sweep efficiencies.

Although the amount of CO_2 that is stored inside the reservoir using CWI is lower compared to conventional CO_2 flooding, large field-scale operations would benefit from enhanced oil recovery while storing some portion of injected CO_2. It is believed that considering CWI at field scale operations is also valuable in terms of a solution to climate change and global warning issues. Moreover, in some areas, the amount of locally captured CO_2 is very limited, or it is not economically feasible to transport CO_2 to the injection site. Therefore, improving the oil recovery together with storing locally accumulated CO_2 are considered key advantages of CWI.

A significant advantage of CWI is that it can be operated with a relatively lower amount of CO_2 compared to CO_2 flooding. Therefore, CWI can be easily utilized in both onshore and offshore reservoirs where pipelines are neither economical nor feasible.

1.6. Knowledge gap

Although the literature provides some experimental results of carbonated water floods in different sand-packs and different core characteristics, lack of flooding tests with consistent experimental conditions are obvious. Therefore, additional efforts are required to solve various operational challenges of the CWI process in various oil systems. In this regard, comprehensive experimental and simulation studies on the application of CWI at consistent operating conditions are of significant value. Hence, the results would be more comparable and more conclusive findings could be achieved. The main objective of this study is to provide a comparative evaluation of CWI processes under consistent laboratory and operating conditions. A total of 28 solubility measurement tests and 17 flooding experiments were conducted. Additionally, details of the CWI process were investigated using visual micro-model tests by analysing the wettability behaviour and recovery mechanism at the pore scale. This study provides a beneficial learning of how CWI performs and new insight on the impact of various parameters on this process. For example, through this study, the optimum pressure for CWI was found to be around P = 5.9 MPa for a temperature of T = 25 °C. This type of data is highly valuable for future design and implementation of practical CWI techniques at field scale. It should also be noted that most of the previous research was performed at a very limited ranges of pressures and temperatures and did not cover the range of operating conditions of this study.

1.7. Scope of this study

In this investigation, performance of CWI was analysed at various operational conditions through carefully designed laboratory phase behaviour and flooding tests. The study was initiated with a comprehensive phase behaviour study of CO_2–water, CO_2–brine, and CO_2–oil mixtures along with PVT modeling using WINPROP modulus of CMG software. Then, performance of CWI was investigated by conducting various sand-pack flooding experiments at different operating pressures ranging from P = 0.7 to 10.3 MPa, operating temperatures of T = 25 and 40 °C, carbonation levels of CL = 50 and 100%, and different CWI schemes (i.e., secondary and tertiary scenarios). It was aimed to systematically analyse the CO_2 solubility, oil recovery factor, CO_2 storage capacity, and oil recovery mechanisms at various operating conditions in order to optimize the CWI scenarios in light oil systems. Through the next phase of this study, complete phase behaviour modeling was conducted using experimental PVT data imported for the purpose of compositional flooding simulations. Finally, various pore scale visualization tests were carried out using transparent glass micro-models that were designed, constructed, and calibrated during this study. Results obtained by laboratory PVT experiments, flooding tests, PVT modeling, flooding simulation, and micro-model studies were utilized to analyse different aspects of CWI in both pore and laboratory scale studies and provided a conclusive evaluation of the application of CWI in light oil systems.

1.8. Research objectives

The main objective of this research was to determine the applicability of CWI technique to enhance oil recovery under various operating conditions. This was

accomplished through conducting a comprehensive literature review, and experimental and theoretical studies to investigate recovery mechanisms and the performance of CWI. A series of laboratory experiments and interpretations were carried out and are summarized herein.

- Physical properties of the brine and oil samples such as viscosity, density, and asphaltene content were measured at various operating conditions.
- The phase behaviours of various CO_2-saturated systems including CO_2–water, CO_2–brine, and CO_2–oil systems were investigated. This was accomplished through conducting a series of CO_2 solubility measurement tests in pure water, brine, and crude oil. Impacts of various operating parameters (i.e., pressure and temperature), as well as brine salinity on CO_2 solubility in pure water and brine were determined. Furthermore, a series of solubility and swelling/extraction tests were implemented under desired operating conditions in order to examine the CO_2 solubility in the oil phase and oil swelling factor, respectively. In addition a comprehensive interpretation was conducted on swelling/extraction curves at various temperatures to recognize the details of the mutual interactions in CO_2–oil system.
- CWI tests in both secondary and tertiary schemes at various operating pressures, temperatures, injection rates, and carbonation levels were studied to examine the performance of CWI. Furthermore, comparisons of results, analysis of obtained data, and interpretation of findings were conducted.
- Visual glass micro-models were designed, constructed, and utilized in order to visualize the displacement efficiency of CWI at pore scale. Based on the image

processing on the captured high quality images, various pore-scale mechanisms, fluid interactions, and residual oil trapping mechanisms were examined and results were interpreted in order to understand the details of fluid-fluid and fluid-solid interactions during the CWI process.

In addition to the experimental studies listed above, a comprehensive numerical simulation study was conducted in order to:

- Provide a complete phase behaviour model capable of modelling various characteristics of the brine and oil samples along with their interactions with CO_2 at different operating conditions.
- Incorporate the EOS-based fluid model to a compositional simulator to model the laboratory displacement experiments. The compositional model was then utilized to verify the fluid production and pressure change along the sand-pack model.

CHAPTER TWO: Literature review

2.1. CO_2 solubility in water, brine, and oil phases

The solubility of CO_2 in pure water and brine has been measured for a wide range of pressures (*P*), temperatures (*T*), and ionic strengths or salinity (*s*) by various researchers (Bamberger *et al.*, 2000; Sabirzyanov *et al.*, 2003; Chapoy *et al.*, 2004; Valtz *et al.*, 2004; Han *et al.*, 2009; Liu *et al.*, 2011). Experimental solubility data of CO_2 in aqueous NaCl solutions are not as extensive as those in pure water. However, different data sets have been reported for the ternary CO_2–H_2O–NaCl system (Rumpf *et al.*, 1994; Gu, 1998; Kiepe *et al.*, 2002; Koschel *et al.*, 2006). Diamond and Akinfiev (2003) surveyed the solubility data of CO_2 in water from T = -1.5 to 100 °C and P = 0.1 to 100 MPa. Duan and Sun (2003) and Duan *et al.* (2006) also evaluated the solubility data of CO_2 in pure water and various brine solutions containing Na^+, K^+, Ca^{2+}, Mg^{2+}, Cl^-, and $SO4^{2-}$. They provided a complete list of all the reliable experimental data sets for CO_2 solubility in pure water at temperatures from T = 273 to 533 K and at pressures up to 200 MPa. Mao *et al.*, (2013) provided a detailed summary of solubility data of CO_2 in water and aqueous NaCl solutions for a wide range of pressures (0.1–150 MPa), temperatures (0–350 °C), and ionic strengths (0–4.5 mol/kg).

The effect of dissolved solids on the CO_2 solubility in water was also studied by Enick and Klara (1989). They developed a correlation to calculate the solubility of CO_2 in brine that is applicable at reservoir conditions, taking into consideration the effect of dissolved solids. They assumed that solubility only depended on TDS, regardless of the type of salt. **Table 2.1** shows the comparison between the solubility of CO_2 in various

Table 2.1: CO_2 solubility in water and brines with various compositions and salt concentrations at constant pressure of P = 9.0 MPa and T = 93.3 °C (Mohamed *et al.*, 2013).

Salt Concentration, wt.%	0	1	5	10
Brine Composition	**CO_2 Solubility, weight fraction**			
NaCl	0.0134	0.0130	0.0115	0.0098
$CaCl_2$		0.0130	0.0115	0.0096
$MgCl_2$		0.0128	0.0105	0.0083

brines and salt concentrations (Mohamed *et al.*, 2013). The CO_2 solubility values in water, NaCl and $CaCl_2$ brines at a pressure of P = 9.0 MPa and temperature of T = 93.3 °C were obtained from Prutton and Savage (1945), Nighswander *et al.* (1989), and Duan *et al.* (2006). They calculated the solubility of CO_2 in $MgCl_2$ brines based on the equation developed by Enick and Klara (1989).

Although the literature provides a good database of data, reliable experimental CO_2 solubility data in both pure water and brine is still required, particularly for the operating conditions existing in EOR processes.

CO_2 solubility in crude oil is a function of several thermodynamic parameters, mainly saturation pressure, temperature, and crude oil properties (Simon and Graue, 1965; Jamaluddin *et al.*, 1991; Srivastava *et al.*, 1995; Emera and Sarma, 2006). Several mathematical correlations have also been developed to estimate the CO_2 solubility in crude oil. However, such correlations are only accurate in particular ranges of operating conditions and fluid properties. Therefore, detailed investigations of CO_2 solubility in crude oil and oil swelling factor, as a result of CO_2 dissolution, are required to thoroughly distinguish the important mechanisms associated with CO_2-based EOR techniques.

2.2. Lab-scale CWI

CW has attracted attention as a potential flooding agent for more than 50 years. The advantage of combining CO_2 with water lies in the increased oil mobility, M_o, due to the dissolution of injected CO_2 in the oil phase. Mobility, M, is defined as the ratio of the permeability of a porous medium to a fluid, k_{eff}, to the viscosity of that fluid, μ. It is

believed that dissolved CO_2 in the oil phase enhances the mobility of the oil in two ways: oil viscosity reduction and oil swelling. From the mobility equation, the viscosity is the denominator, meaning a reduction in oil viscosity results in higher oil mobility. Moreover, swelling of the oil leads to a higher relative permeability to that oil, which, in turn, favourably affects oil mobility.

CWI may have a better performance over direct injection of CO_2 because of its higher sweep performance. In water flooded reservoirs, CWI can alleviate the adverse effect of high water saturation and the water shielding effect as a result of mixing with the resident water (Sohrabi *et al.*, 2008; Sohrabi *et al.*, 2009). This might, in turn increase the rate of CO_2 diffusion into the oil and the subsequent oil swelling. It has been shown that in direct CO_2 injection, due to low sweep efficiency and gravity segregation, the time scale of diffusion can be several years (Solomon, 2007). In terms of CO_2 storage, in CWI, CO_2 is dissolved in water (and later in the oil) rather than staying as a free phase, thereby providing a safer method of CO_2 storage compared to direct CO_2 injection. However, CWI has been considered mainly as a method of enhancing oil recovery. Thus, its CO_2 storage potential has been noted as an additional advantage rather than being the main driver, as it would be in a carbon capture and storage (CCS) program.

CWI was first introduced as an improved secondary oil recovery process by Oil Recovery Corporation (ORCO). Sand-pack experiments, conducted by Monteclaire Research in the late 1940s for ORCO, showed that the residual oil saturation could be further reduced up to 15% of pore volume (PV) if CW was used after WF (Lake *et al.*, 1984). From 1948 to 1952, another set of experiments using CW and fresh core samples were performed by Earlougher Engineering at various operating pressures which ranged

from P = 5.5 MPa to P = 6.9 MPa with various oil samples from 28 °API to 50 °API. Their results indicated that the oil saturation after CWI was 2% to 26% PV less than that of WF. The lab report issued afterwards pointed out that the observed incremental recovery could not be accounted solely by oil swelling so it probably was due to a combination of changes in properties of both the rock and fluid (Lake *et al.*, 1984).

Various researchers (Martin, 1951a; Martin, 1951b; Johnson, 1952; Holm, 1959; Holm, 1963; de Nevers, 1966; Latil, 1980; Tran, 2009; Steffens, 2010) reported CWI results in sand-packs and core samples at various operating pressures and temperatures. Martin (1951a) reported an improvement of about 12% in oil recovery by using CW as the injection fluid. He also showed that oil recovery enhancement was positively correlated with the carbonation level (Martin, 1951b). In the same year, Saxon *et al.* (1951) conducted several coreflood laboratory tests with CO_2 and CW. However, unlike Martin's results, no significant difference between water and CW was reported in this study. Later in 1952, Johnson *et al.* continued Saxon *et al.*'s (1951) study and investigated the effect of CWI on oil recovery using coreflood experiments. Johnson *et al.* (1952) stated that for the oil viscosities of μ_o = 1.42 mPa.s and 2.86 mPa.s (under the prescribed experimental conditions) recovery improvement using CW was between 15% to 25%. They presented charts, which showed no recovery from brine injection while substantial recoveries were obtained when CW was injected. Additional oil recovery was also reported during the subsequent depressurisation period at the end of the CWI stage (i.e., blow out process). They showed higher oil recovery by CWI at a lower temperature, which could be due to higher CO_2 solubility in oil at a lower temperature, causing a greater expansion in oil volume and consequently greater oil recovery. They

demonstrated that as the percentage of light hydrocarbons (i.e., C_3 and higher) was increased, the volume expansion became greater. They also reported that carbonation of outlet water never reached that of the injection water even after 130 PVs had been passed through the core. Based on material balance, they showed that the difference was about 7% of the total CO_2, which indicated that the process of CO_2 dissolution into the retained oil in the porous media continued for some time.

In 1959, Holm observed 21% and 19% increases in recovery factor (compared to WF) for temperatures of T = 21.1 and 37.8 °C, respectively, when CW was injected into the same cores. In another set of experiments, CW was injected as a slug driven by plain water. Improvements on recovery factor were 5%, 23%, and 69% (compared to WF) for oil samples with viscosities of 0.8, 5, and 90 mPa.s, respectively.

Various sand-pack flooding experiments were carried out by Shell with respect to CWI (van Dijk, 1965; Dumore *et al.*, 1982; Falls, 1986; Falls *et al.*, 1986; Gorell and Falls, 1986). In their flooding study, CW was able to recover 12% PV to 23% PV more oil than WF at 5 PV injections, depending on oil viscosities.

Panteleev and Tumasyan (1972) carried out the first study on wettability alteration of the porous media. They claimed that CW imbibition took place faster and recovered more oil than plain water (i.e. 37.3% oil recovery by CW imbibition compared to 26.5% oil production by water imbibition). They also showed that both oil recovery and imbibition rate increased as the concentration of CO_2 in water increased.

In 1981, Institut Francais du Petrole (IFP) conducted a series of core flooding experiments using oil samples from Bati Raman oil field and gas samples from Dodan field (Khatib & Earlougher, 1981). The experiment temperature and pressure were set at

T = 65 °C and P = 2.8 MPa, respectively. Both high viscosity (μ_o = 290 mPa.s) and medium viscosity oil (μ_o = 42 mPa.s) were used in their study. Experiments consisted of a series of injection cycles with plain water, CO_2, and CW with 24 hours shutdown between changes in injectants. This resulted in 14% to 15% improvement in the oil recovery.

Mayers *et al.* (1988) reported two groups of core flooding experiments they completed in 1981 and 1985. The study used core plugs with lengths between 12.2 cm and 14.5 cm, and diameters between 4.6 cm and 5.1 cm. The viscosities of the oil samples used in the study were 475 mPa.s and 406 mPa.s at the experimental temperature (T = 51.7 °C). Oil recovery improvement was between 13% PV and 24% PV, with an average of 17% PV for the 1981 data group and 19.4% PV for the 1985 data group.

In 1992, Perez *et al*., studied carbonated water imbibitions in a fractured reservoir. The carbonation pressures varied from P = 0.3 MPa to 3.4 MPa. Spontaneous imbibition of plain water and carbonated water into a number of core plugs showed that the latter was able to recover 10% HCPV to 16% HCPV more oil than the former. A similar study was also carried out by Cardoza *et al.* (1992). They confirmed that the CO_2 dissolved in water increased both the oil recovery rate and the ultimate oil recovery by imbibition mechanism compared to unadulterated water.

Flumerfelt and Li (1993) followed the work of Perez *et al.* (1992) using two different oil types (kerosene and crude oil) and low permeability fractured dolomite rock samples. They investigated the effect of surfactants on the performance of CWI. The study reported that compared to water injection, the additional oil recovery by CW with surfactant was 50% whereas CW alone was 20%.

Asghari *et al.* (2009) also showed that injection of carbonated water led to recovery of an additional 16.9 % OOIP in the for consolidated core trial and about 14 % OOIP in the sand-pack trial. The experimental temperature and pressure were T = 40 °C and P = 8.3 MPa, respectively, and the oil viscosity ranged between 1800–2000 mPa.s. For the consolidated core set, a 17 hours soaking period was used, and two soaking periods of 25 hours and 34 hours were used for the unconsolidated sand-pack dataset. Carbonated water soaking periods were found to be very favourable compared to the oil recovery in all cases.

A comprehensive study was carried out on CWI by the Centre for EOR and CO_2 Solutions at the Herriot Watt Institute of Petroleum Engineering Centre, in which the first phase of the project started in 2006. Experimental and numerical studies were performed through both micro-model and core experiments, and mathematical modeling and numerical simulations. Micro model CWI experiments were carried out at P = 13.8 MPa and temperature of T = 38 °C using mineral oil (μ_o = 16.5 mPa.s) and *n*-Decane (Sohrabi *et al.*, 2011). They found that CWI, compared to conventional water injection, improved oil recovery and the additional oil recovery was a result of improved sweep efficiency, oil swelling, viscosity reduction, and coalescence of the isolated oil ganglia, all attributed to diffusion. They also proposed that CWI can be carried out in combination with reservoir depressurisation, carried out subsequent to CWI or in a cyclic manner in which carbonated and plain water cycles are injected in succession (Riazi *et al.*, 2009). Reported oil recovery increases were 8.8% and 23.8% HCPV for two samples, respectively. They also reported the underlying physical processes and the pore-scale mechanisms of fluid–fluid and fluid–solid interactions during CWI. Their results showed that CWI, compared

to unadulterated water injection, improved oil recovery in both secondary (before WF) and tertiary (after WF) injection modes. The improvement was higher when CW was injected before WF (secondary mode). Based on the results of their flow visualisation, a mathematical model was developed that accounted for the pore-scale mechanisms observed during the experiments (Riazi *et al.*, 2011). In a different part of their study, they stated that injection of CW in watered-out reservoirs may also be attractive from an aspect of CO_2 storage. They used a moderately viscous crude oil with viscosity of μ_o = 158 mPa.s, measured at the test conditions of P = 17.2 MPa and T = 37.8 °C. They found that the CO_2 retention factor in CWI is generally higher than those estimated in a typical immiscible CO_2 flooding (Kechut *et al.*, 2011). All their measurements revealed that a relatively high percentage of the total volume of CO_2 injected (in the CW), about 46% was stored at the end of the tertiary CWI (Kechut *et al.*, 2010).

The results of 8 sand-pack experiments were summarized by Dong *et al.* (2011). They found that 2 PV/day is the optimal injection speed for their setup. In addition, higher flooding rates gave more optimal RF but scalability to field applications decreased.

2.3. Field-scale CWI

As already discussed, CWI has distinct advantages, compared to conventional water injection for oil recovery improvement, as reported in the literature. Despite some encouraging laboratory core flooding results, only a few EOR field applications were found in the literature. Some of the applications of CWI were for well stimulation, whilst

others were applied to clean up the ground water from oil based contamination. In this section, details of some of these field-scale CWI experiences are presented and discussed.

The first reported CWI field trial took place in Allegany County near Richburg, New York in 1947 (Martin and Tuckahoe, 1959). The production data for this field showed a significant improvement in production rate from 92 to 1260 barrels/acre/year as a result of injection of CW instead of water.

The next CWI field test was the K&S project in the 1950's (Martin, 1951b; Hickok *et al.*, 1960; Christensen, 1961; Hickok, and Ramsay, 1962;). It was a field located 10 mile north of Bartlesville, OK, with 35 injectors and 24 producers in a regular 10 acre 5 spot pattern. Production of the field started with pressure depletion in 1907 and ended in 1934 due to economic reasons. In 1958, co-injection of CO_2 and water in the same tubing was started. This carbonation process was completed by April 1, 1960. The improved production in 1959 was 123,000 STB more than the total primary oil produced from 1905 to 1934. It was estimated that carbonated water could produce 37% more oil than WF.

Another field program was in the Domes Unit in 1965 (Scott and Forrester, 1965). The field started production in 1910 and by 1953, 90 wells were drilled and completed. Secondary development started in 1961. During the process, 13 producers were converted into injectors and three new injectors were also drilled. CO_2 and water injection started in September and October that year. By March 1962, about one third of PV equivalent carbonated water was injected, followed by plain water. It was estimated that the slug injection of carbonated water gave about 9% additional oil recovery (Riazi, 2011).

In another field scale application (Tumasyan *et al.*, 1973), the oil recovery improvement by CWI compared to WI was reported to be 14 to 16%. The effect of water saturation was experimentally investigated by the same authors, demonstrating that water saturation had an adverse effect on the oil recovery performance of CWI.

In some studies, CWI was considered a stimulating agent to improve the well injectivity. When CO_2 is dissolved in water, carbonic acid is formed. The injected carbonated water will react with the carbonate materials in the rock to form bicarbonates, which are much more soluble, especially in the vicinity of the wellbore, and results in improved permeability, which improves water injectivity (Ramsay and Small, 1964; Hickok and Ramsay, 1962). Therefore, in some fields, CWI was used for the purpose of well stimulation (Kraus *et al.*, 1970). The results of this application in the Aleksandrovsk (Tuimazy) fieldshowed a significant improvement in the water intake rate of the wells after CWI (Kislyakov *et al.*, 1967).

Another application for carbonated water is cleaning up the ground water from oil-based contamination. **Figure 2.1** gives a conceptual description of the process (Li *et al.*, 2007). CWI was injected in a pilot field scale trial to evaluate the recovery of volatile, light non-aqueous phase liquids from ground water (Nelson *et al.*, 2009). In this technique, CW is injected into the subsurface; as a result, the nucleation of CO_2 bubbles at and away from the injection point takes place. The nucleating bubbles coalesce, rise, and volatilize residual oil ganglia. A 78% and 50% recovery of the pentane and less volatile hexane, respectively, were reported using this technique.

2.4. Theoretical modelling of CWI

The impact of CO_2 diffusion in CO_2 injection, as a tertiary oil recovery mechanism, has been investigated by several researchers. Theoretical studies provide useful information for the oil recovery process by CO_2 injection (Laidlaw and Wardlaw, 1983). In addition, the effect of relevant parameters on the performance of CWI, and the sensitivity of those parameters on the mass transfer process during CWI have been studied and are summarized in this section.

In 1964, de Nevers developed a calculation method to predict the performance of CWI. That method takes into account the effects of oil viscosity reduction and oil swelling, due to CO_2 being transferred to the reservoir oil from the carbonated flood water. The calculation shows the effect of slug size and carbonation level in the slug on oil recovery. Based on sample calculation, de Nevers concluded that oil viscosity reduction due to dissolution of CO_2 is the most important mechanism of incremental oil recovery.

Ramesh and Dixon (1972) later reported an improved three phase black oil model for compressible fluids, which could handle heterogeneous reservoir properties, gravity and capillary forces without free hydrocarbon gas in the reservoir. Simultaneous saturation of CO_2 in oil and water phases was assumed, where CO_2 solubility was proportional to the relative capabilities of these phases to dissolve CO_2 at the saturation point at the prevailing block pressure. The developed mathematical model was used to simulate the experimental work reported by Holm (1959) to show the applicability of the model.

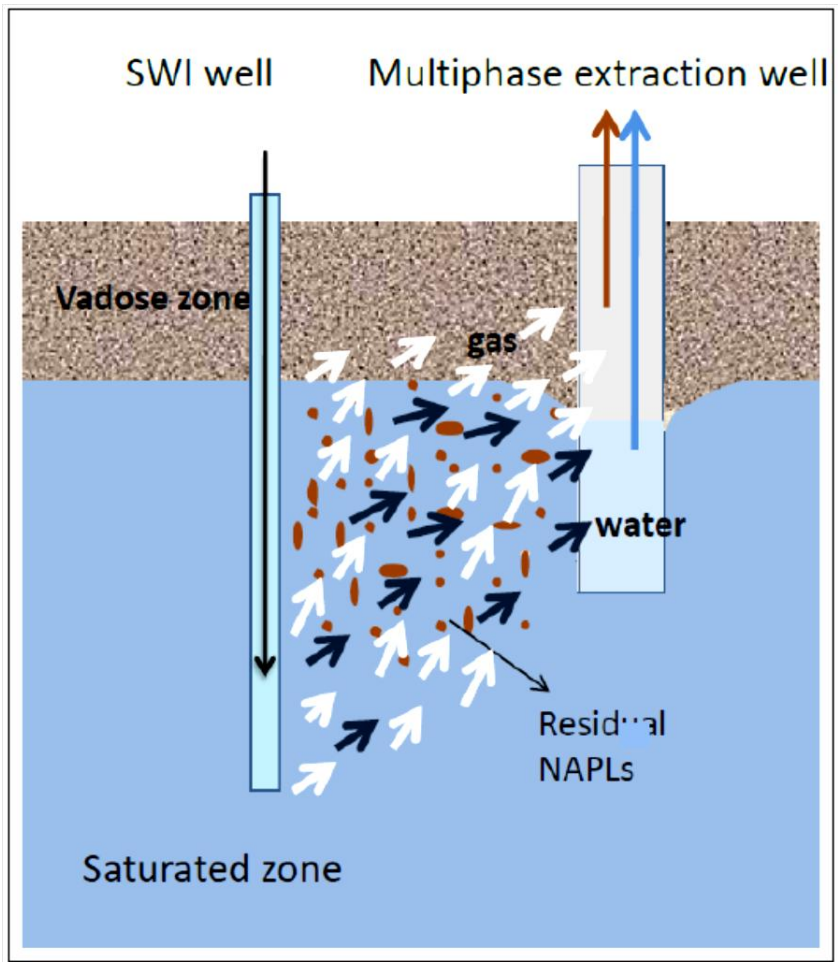

Figure 2.1: Conceptual model of supersaturated water injection for NAPL recovery (Li *et al.*, 2007).

Shenawi *et al.* (1994) developed a semi-analytical iterative model to describe the imbibitions of CWI in a naturally fractured reservoir. Their model was able to predict oil and water saturation distributions and oil recovery factor for a range of oil/water viscosity ratios. The new correlations were introduced, and their validity was checked with limited laboratory data.

Shenawi and Wu (1994), in another publication, presented the simulation of CW imbibition in naturally fractured reservoirs using a compositional simulator (COMABS). It should be noted the COMBAS simulator allows the partitioning of CO_2 from the injected water phase into the oil phase, based on the CO_2 solubility in each phase. The results of this simulation indicated that CW enhances the water imbibition rate close to the imbibing core face.

Riazi *et al.* (2011) developed a mathematical model that simulates the dynamic process during oil swelling as a result of the partitioning of CO_2 from CW and its dissolution into oil at the pore scale. Their model successfully simulated the swelling of an oil drop both when it is separated from a CO_2 source by a water layer and when it is in direct contact with CW. In their study, the sensitivity of pertinent parameters was studied for both direct (i.e., oil–CW) and indirect (i.e., oil–water–CO_2) contact scenarios using two different evaluation methods. They concluded that CO_2 molar density and solubility are the main parameters affecting the degree of swelling of the oil ganglion during CWI.

CHAPTER THREE: Phase behaviour study

3.1. Introduction

Knowledge of the physical and chemical properties of CO_2, brine, and oil as well as the interactions between them in binary or ternary systems (i.e., CO_2–brine, CO_2–oil, and CO_2–brine–oil systems), together with their effects on oil recovery and CO_2 storage capacity, are crucial for any CO_2-based EOR and carbon capture and storage (CCS) project. One of the major parameters that most influence the performance of EOR processes is the CO_2 solubility in the oil phase because it results in oil viscosity reduction and swelling, consequently enhancing oil recovery (Orr *et al.*, 1982; Abedini and Torabi, 2013; Mosavat and Torabi, 2014). Moreover, one of the main trapping mechanisms involved in the storage of CO_2 in deep saline aquifers is solubility and most of the injected CO_2 is trapped through dissolution into the formation brine (Lindeberg and Wessel-Berg, 1997; Ennis-King and Paterson, 2005; Nghiem *et al.*, 2009). Therefore, a better understanding of solubility and its effects on oil recovery and CO_2 storage mechanisms are essential in the success of CO_2-based EOR and CO_2 storage projects.

The CO_2 solubility in the brine or oil phases and its effects on the brine or oil physical properties can be determined by experimental studies and available modelling packages. Laboratory studies are relatively expensive and time consuming, as they require testing of a wide range of data. On the other hand, the available models can only be used in limited situations, and hence, may not be applicable in a wide range of operating conditions.

Physical properties, including brine density, viscosity, CO_2 solubility in brine, oil swelling factor, viscosity, density, and CO_2 solubility in oil are required to design and simulate the oil recovery process by CWI. During this chapter, the effects of CO_2 on the physical properties of both brine and crude oil samples will be determined by two methods, by experimental study and by the use of reliable available mathematical models.

3.2. CO_2 phase behaviour

CO_2-based EOR processes have been implemented for more than 60 years in the oil and gas industry to improve oil recovery from geological hydrocarbon reservoirs. CO_2 has proven to be a promising agent for improving oil recovery in various injection schemes such as pure CO_2 flooding, water-alternating-gas (WAG) flooding, and CWI.

The state of CO_2 in the reservoir directly depends on the pressure and temperature. However, for most practical EOR applications, CO_2 exists either as a gas or as supercritical fluid. Supercritical CO_2 exists when the operating conditions are above critical temperature and critical pressure of CO_2. Supercritical CO_2 combines useful properties of gas and liquid phases, and its behaviours are near gaseous CO_2 under certain circumstances and near liquid CO_2 in other circumstances. Supercritical CO_2 provides a gas-like characteristic when it fills a container and it takes the shape of the container meaning that the molecular motion is quite similar to gas molecules. On the other hand, a supercritical CO_2 behaves like a liquid because its density is close to the liquid phase and, hence, it shows a similarity to liquid CO_2 in terms of dissolution.

As shown in the phase diagram in **Figure 3.1**, CO_2 can be injected into an oil reservoir in different forms depending on the reservoir pressure and temperature.

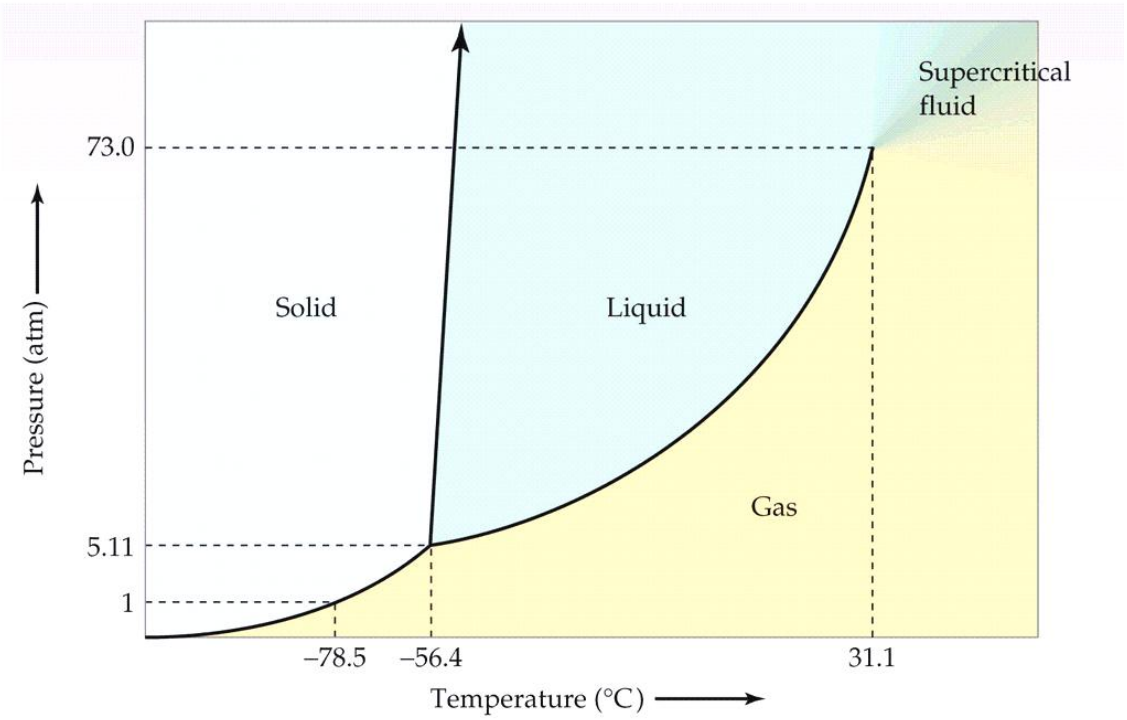

Figure 3.1: Carbon dioxide (CO_2) pressure–temperature phase diagram.

A review study on CO_2 properties (Whitson and Brule, 2000) indicated that density, gas compressibility factor, and viscosity are strongly dependent on the operating pressure and temperature.

3.3. The physical properties of the fluids

The CO_2 used in this study was sourced from a high purity CO_2 cylinder (99.99%, Praxair Co.). Synthetic brine of 20,000 ppm NaCl was prepared using deionized water. The density and viscosity of the brine were measured to be ρ_b = 1010.2 kg/m^3 and μ_b = 0.90 mPa.s, respectively, at the temperature of T = 25 °C and atmospheric pressure (i.e., P_{atm} = 101.1 kPa). The properties of the brine and CO_2 used in this study are shown in **Table 3.1**. A DV-II+Viscometer (Can-AM Instruments LTD.) was used to measure brine viscosity at different temperatures of T = 25 and 40 °C. The light stock tank oil sample used in this study was a mixture of few samples taken from the Bakken formation in Saskatchewan, Canada. The various hydrocarbon group compositional analyses and the distribution of the carbon number of the oil sample are presented in **Table 3.2** and **Figure 3.2**, respectively. Density and viscosity of the crude oil sample were ρ_o = 799.0 kg/m^3 and μ_o = 2.76 mPa.s respectively at a temperature of T = 25 °C and atmospheric pressure of P_{atm} = 101.1 kPa. The asphaltene content (*n*-Pentane insoluble) of the crude oil sample was also measured to be 1.23 wt.%. The MMP of the CO_2–oil mixture was determined using a swelling/extraction test and was estimated to be MMP = 8.5 MPa at the constant temperature of T = 25 °C. **Table 3.3** summarizes different characteristics of the crude oil sample used in this study. The same viscometer was used to measure the oil viscosity at various temperatures and atmospheric pressure and the results are depicted in **Figure 3.3**.

Table 3.1: The physical properties of the brine sample and CO_2 used in this study at atmospheric pressure (i.e., P_{atm} = 101.3 MPa) and two temperatures of T = 25 °C and 40 °C.

Fluid	Density P_{atm}, 25 °C (kg/cm^3)	Density P_{atm}, 40 °C (kg/cm^3)	Viscosity P_{atm}, 25 °C (mPa.s)	Viscosity P_{atm}, 40 °C (mPa.s)
Brine	1010.2	1008.2	0.90	0.70
CO_2	1.8093	1.7205	0.0149	0.0156

Table 3.2: Compositional analysis of the light crude oil under study at T = 21°C and atmospheric pressure.

Carbon number	Mole %	Carbon number	Mole %	Carbon number(s)	Mole %
C_1	0	C_{12}'s	4.48	C_{28}'s	0.44
C_2	1.58	C_{13}'s	4.02	C^{29}'s	0.33
C_3	0.92	C_{14}'s	3.32	C_{30+}'s	2.85
i-C_4	0	C_{15}'s	3.06		
n-C_4	3.88	C_{16}'s	2.37	C_1–C_6's	22.48
i-C_5	2.20	C_{17}'s	2.06	C_{7+}'s	77.52
n-C_5	4.03	C_{18}'s	1.91		
C_5's	0.49	C_{19}'s	1.51	C_1–C_{14}'s	78.82
i-C_6	3.07	C_{20}'s	1.29	C_{15+}'s	21.18
n-C_6	2.95	C_{21}'s	1.29		
C_6's	3.37	C_{22}'s	0.76	C_1–C_{29}'s	97.15
C_7's	13.87	C_{23}'s	0.87	C_{30+}'s	2.85
C_8's	10.46	C_{24}'s	0.71		
C_9's	8.19	C_{25}'s	0.66		
C_{10}'s	6.38	C_{26}'s	0.57		
C_{11}'s	5.61	C_{27}'s	0.49		

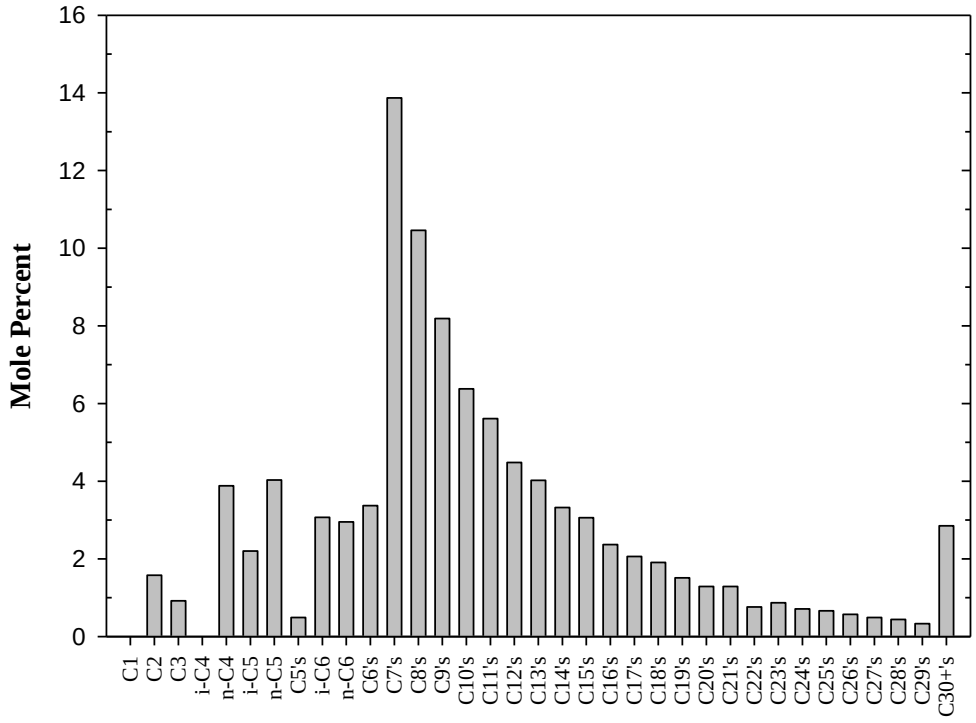

Figure 3.2: Gas Chromatography (GC) compositional analysis result for Bakken crude oil sample used in this study.

Table 3.3: Physical properties of the oil sample used in this study at P_{atm} = 101.1 kPa and T = 25 °C.

Property	Value
Molecular weight	223 gr/mol
Density at 101.1 kPa & 25 °C	799 kg/m^3
Viscosity at 101.1 kPa & 25 °C	2.76 mPa.s
n-C5 insoluble asphaltene	1.23 wt.%

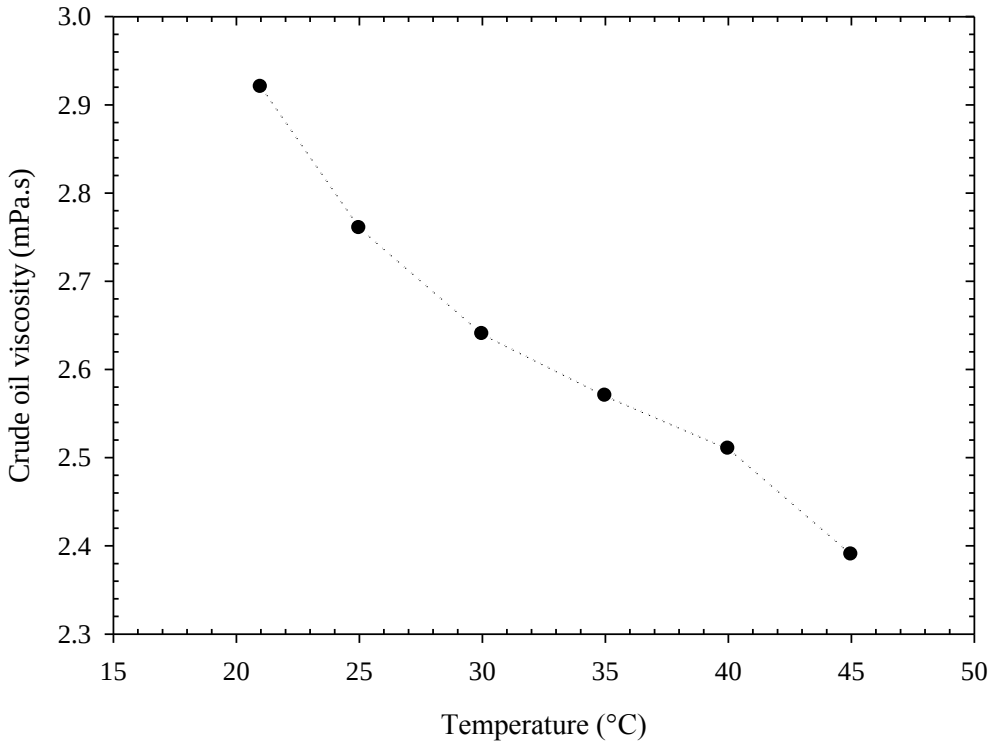

Figure 3.3: Measured values of crude oil viscosities with changes in temperature at atmospheric pressure (i.e., P_{atm} = 101.1 kPa).

3.4. CO_2–brine system

In CWI, CO_2 is dissolved in water and transported through the reservoir by the flood water. CO_2 solubility in water is normally higher compared to other gases and this makes it suitable for CWI as an improved oil recovery technique (**Figure 3.4**). When CO_2 dissolves, it interacts with water molecules to hydrate itself (i.e., the electronegative oxygen atoms of CO_2 form strong H-bonds with H atoms of water molecules). This interaction is very strong and can cause further dissolution of additional CO_2 molecules. Some of the H_2O bonds to CO_2 and releases protons to increase H^+ ions in water (and CO_2 converts into HCO_3^-). When an equilibrium state is established H_2CO_3 (carbonic acid) will be produced as shown in the reaction below:

$$CO_2\ (aq) + H_2O \leftrightarrow H_2CO_3\ (aq)$$

This reaction is kinetically slow, and at equilibrium, only a small fraction (0.2 – 1%) of the dissolved CO_2 is actually converted to H_2CO_3. Most of the CO_2 remains as dissolved molecular CO_2 in the water and carried to the reservoir in CWI.

The poor solubility of hydrocarbons or other gases (O_2, N_2, or H_2) in water might be explained by the fact that these gases occupy the intermolecular spaces and stay there by interaction with surrounding molecules by weak van der Waals forces or very weak electronic interaction by use of their pi electrons (C_2H_2) or lone pairs (such as O_2) in the water. Therefore, the attractive forces between water molecules and hydrocarbon or other gases are weaker than that for CO_2. This will result in lower solubility of these gases in water compared to CO_2.

Solubility of CO_2 in pure water has been well documented in the literature for a range of temperatures and pressures of T = 10 °C to 3000 °C and P = 0 to 200 MPa,

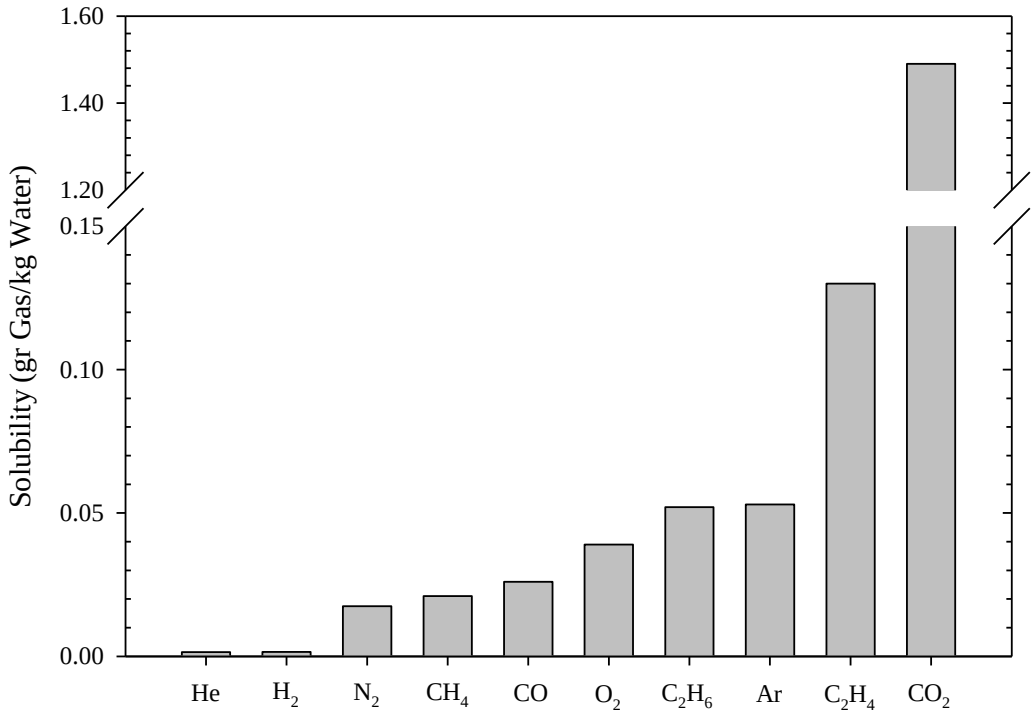

Figure 3.4: Solubility of different gases in pure water at pressure of P = 101.3 kPa and temperature of T = 25 °C (www.engineeringtoolbox.com).

respectively. It is believed that pressure, temperature, and water salinity, *s*, are the key parameters affecting CO_2 solubility in water. Since operating pressure mainly determines the water capacity to dissolve CO_2 at surface prior to injection, the impact of operating pressure on CO_2 solubility in water is an important issue in the CWI process.

The amount of CO_2 that can be dissolved in saline brine can be estimated by utilizing previous experimental studies. The solubility of CO_2 in fresh water increases with increasing pressure, decreasing temperature, and can be estimated from past experimental works (Crawford and others, 1963; Holm, 1963, Jarrell *et al.*, 2002). A series of solubility curves was used to generate a relational database table of solubilities at different pressure and temperature combinations (Kansas Geological Survey, 2003). **Figure 3.5** shows the effect of operating pressure and temperature on the CO_2 solubility in pure water. The solubilities of fresh water in this plot are adjusted according to the salinity of the brine (independent of pressure and temperature) and presented in **Figure 3.6**. This figure uses percent solubility retained as a function of salinity (Martin, 1951a; Johnson, 1952; Johnson *et al.*, 1952; Chang *et al.*, 1996; Jarrell *et al.*, 2002) and depicts that water salinity has significant effects on CO_2 solubility. For example at zero salinity, 100% of the solubility is retained, meaning the solubility is the same as in fresh water. However at a higher water salinity (e.g., salinity of 10 wt.%) the CO_2 solubility is decreased by 30.5%. In this matter, Henry's constant is an important parameter that influences the solubility of gas in water. The Henry's constant for CO_2, $K_{H,CO2}$, is defined as the limit of fugacity to concentration ratio of CO_2 in the water phase and has the dimension of pressure:

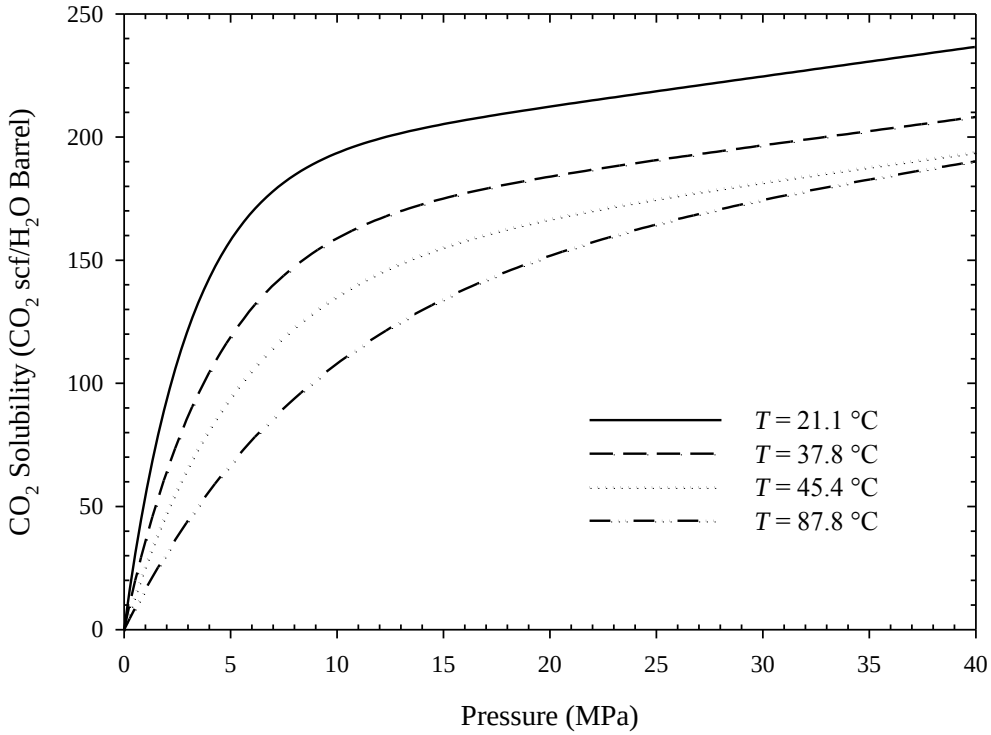

Figure 3.5: CO_2 solubility in fresh water at various pressures and temperatures (rebuilt from Kansas Geological Survey, 2003).

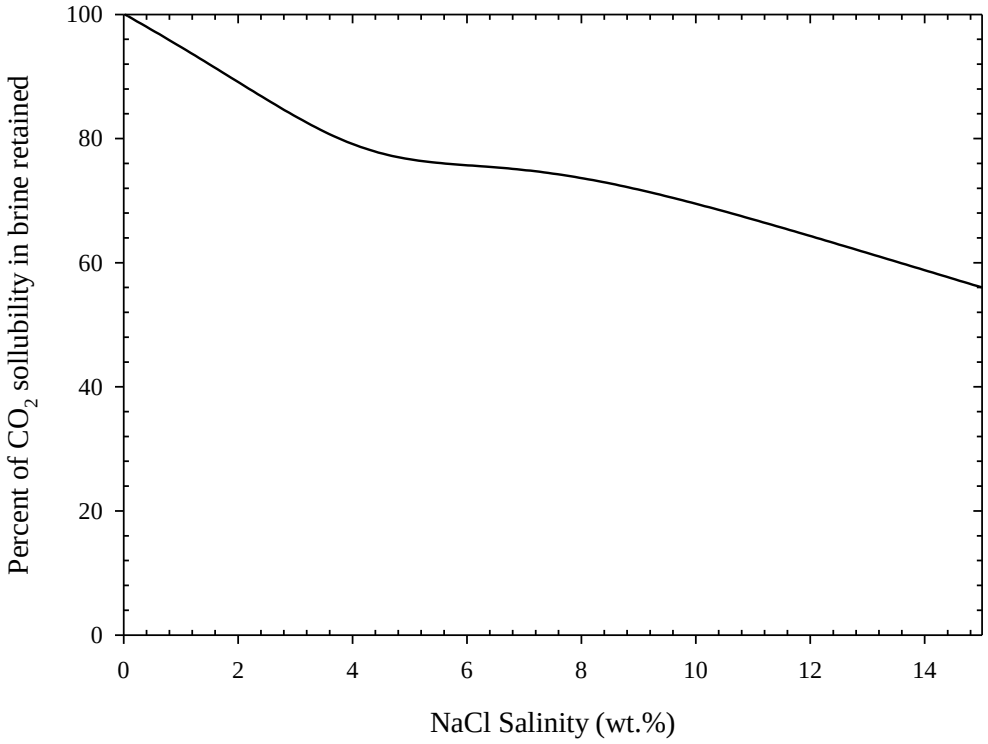

Figure 3.6: Effect of water salinity on the CO_2 solubility in water (rebuilt from Kansas Geological Survey, 2003).

$$K_{H,CO_2}(T,p) = \lim_{x_{CO_2}\to 0}\left(\frac{f_{CO_2}}{x_{CO_2}}\right) \quad \text{.....} \quad (3.1)$$

where x_{CO2} is the molar fraction of CO_2 in water, f_{CO2} is fugacity of CO_2, $K_{H,CO2}$ is Henry's constant. In addition, reviewed literature revealed that the water density and viscosity change only slightly when saturated with CO_2, dependingt on saturation pressure and temperature.

Similar to the solubility of CO_2 in the water phase, some portion of the water phase changes to the gaseous CO_2 phase, which is significantly smaller than the CO_2 solubility in the water phase. **Figure 3.7** presents the concentration of water in gaseous CO_2 and the CO_2 solubility in aqueous phase for a range of salinity values (TOUGH2_ECO2N user guide, 2005). Regarding CWI, equilibrium between aqueous and gas phases correspond to a dissolved CO_2 mass fraction in the aqueous phase, $X_{2,eq}$, in the order of a few percent, while the mass fraction of water in the gas phase, $Y_{1,eq}$, is a fraction of one percent, so that gas phase CO_2 mass fraction $Y_{2,eq} = 1 - Y_{1,eq}$ is larger than 99%. The relationship between CO_2 mass fraction X_3 and phase composition of the fluid mixture is presented in **Figure 3.8** and as follows:

- $X_3 < X_{2,eq}$ corresponds to single-phase liquid conditions;
- $X_3 > Y_{2,eq}$ corresponds to single-phase gas;
- intermediate values ($X_{2,eq} \leq X_3 \leq Y_{2,eq}$) correspond to two-phase conditions with different proportions of aqueous and gas phases.

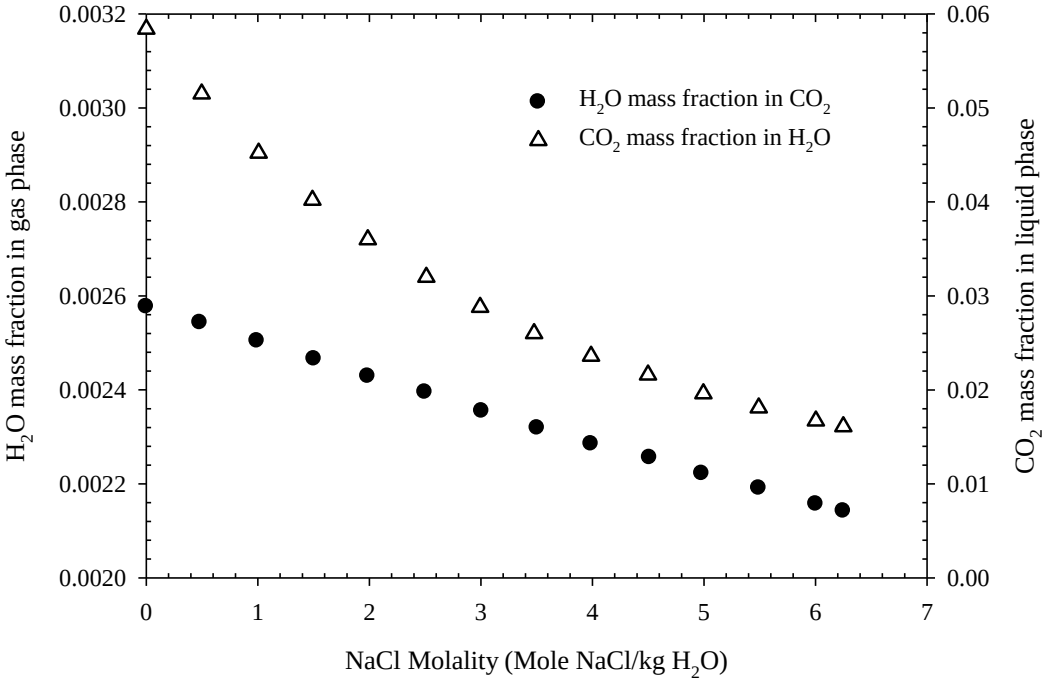

Figure 3.7: Concentration of water in gas and CO_2 in the liquid (aqueous) phase at various salinities and pressure of P = 21.6 MPa and temperature of T = 45 °C (rebuilt from: TOUGH2_ECO2N user guide, 2005).

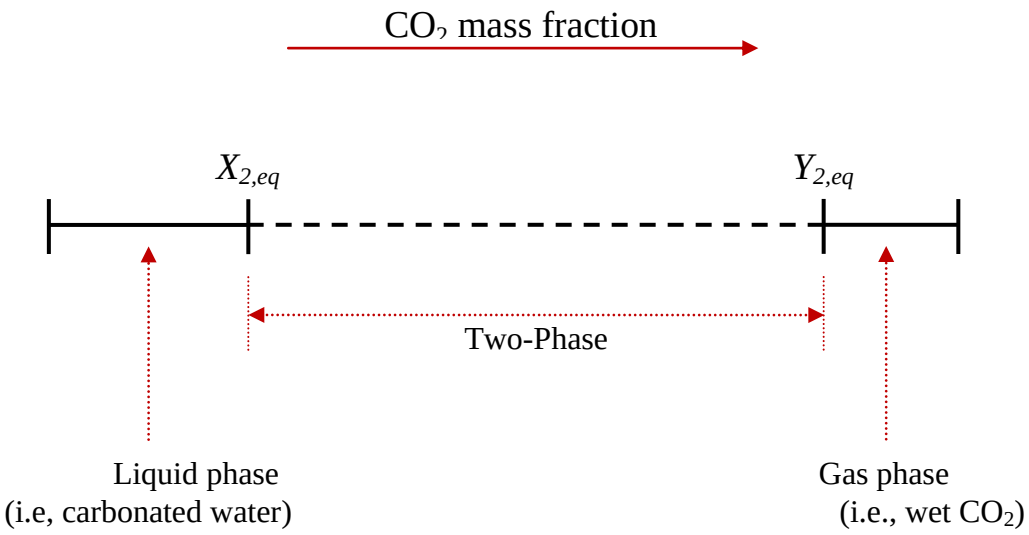

Figure 3.8: CO_2 phase partitioning in the system H_2O–NaCl–CO_2. The CO_2 mass fraction in brine–CO_2 mixtures can vary in the range from 0 (i.e., no CO_2) to 1 (i.e., no brine) (rebuilt from TOUGH2_ECO2N user guide, 2005).

3.4.1. CO_2–brine solubility measurement tests

The apparatus for measuring CO_2 solubility in brine was mainly composed of a CO_2 cylinder, a programmable syringe pump (Teledyne ISCO, 500D series), an air bath with a heater with temperature controller, a digital pressure gauge (Heise Inc.), a piston accumulator, a back pressure regulator (BPR) with maximum operating pressure of P_{max} = 34.5 MPa (Temco Inc.), and effluent fluid (CO_2 and water) collectors. The temperature of the air bath was maintained by a temperature controller (Love Controls Co.). **Figure 3.9** shows the detailed schematic of the solubility experiment setup utilized to measure CO_2 solubility in brine. The accuracy of the pressure gauges and temperature controller were $\pm$0.7 kPa for the pressure range of 0–34.5 MPa and $\pm$0.1 °C for the temperature range of 0–100 °C, respectively.

The process of mixing CO_2 with brine was conducted at the pre-determined experimental temperature and pressure. CO_2 was injected from a high pressure cylinder into the piston accumulator which contained synthetic brine. The mixture was homogenized for 48 hours inside the air bath at the experimental temperature while the outlet pressure of the CO_2 cylinder was kept constant. During the equilibration process, a ball vibrator has been attached to the cell to provide mechanical vibration in order to expedite the homogenization process. In addition, the cylinder was kept connected to the CO_2 cylinder in order to provide the pressure support of the mixture. The mixture was then oriented vertically and connected to the BPR, set at the same pressure, to release the free gas remaining on the top of the CO_2-saturated brine. The mixture was pushed upward using the hydraulic piston accumulator until the water exited from the BPR,

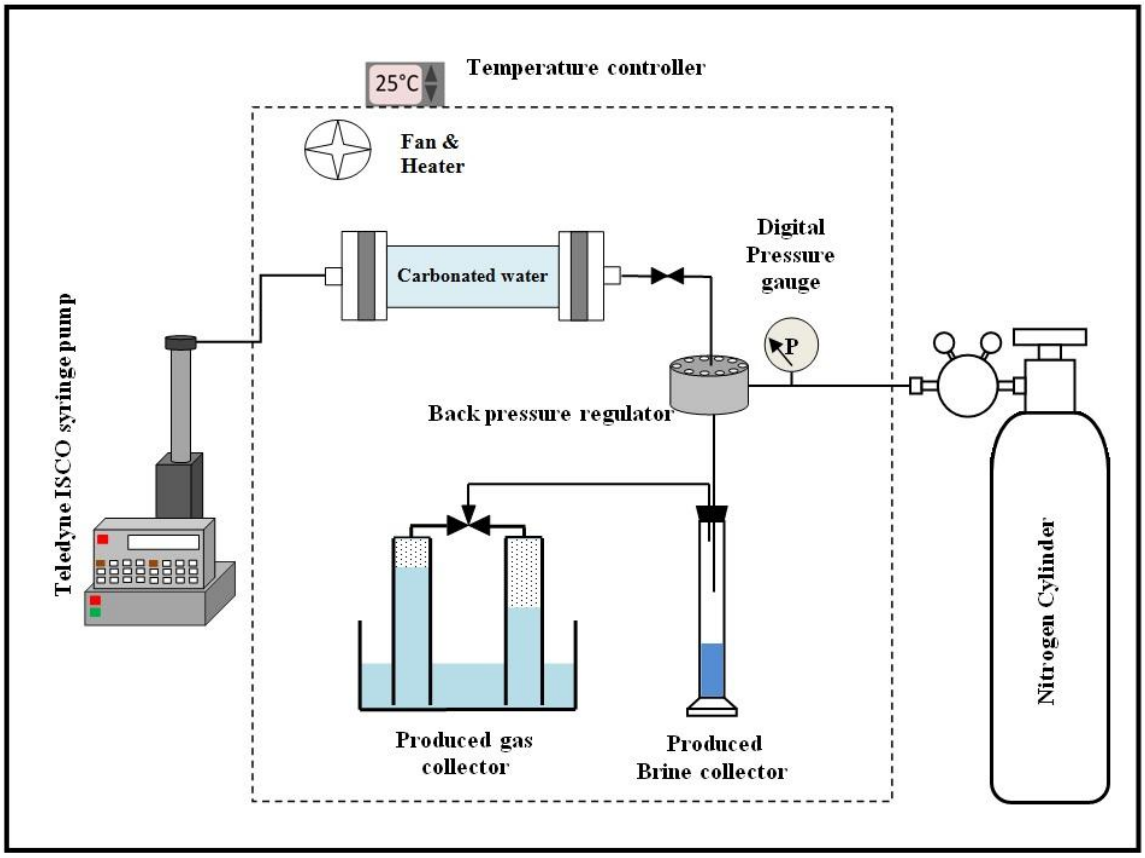

Figure 3.9: Schematic diagram of the experimental setup used to measure CO_2 solubility in brine at various pressures and constant temperature of T = 25 °C.

indicating that the free CO_2 was removed and the CO_2–brine mixture was in a saturated liquid phase.

When the CO_2-saturated brine was prepared and stabilized, a subsample was taken from the BPR. By measuring the volumes of the produced CO_2 and brine in the collectors, the gas to water ratio (GWR) was calculated to determine the CO_2 solubility in brine, as given in Equations 1 and 2.

$$GWR = \frac{Produced \;\; CO_2, cm^3\left(P_{atm}, T_{\exp}\right)}{Produced \;\; Water, cm^3\left(P_{atm}, T_{\exp}\right)} \quad \text{.....} \quad (3.2)$$

$$\chi_b = GWR \times \frac{\rho_{CO_2}}{\rho_b} \times \frac{1000}{MW_{CO_2}} \quad \text{.....} \quad (3.3)$$

The CO_2 solubility in brine was measured at different experimental conditions (pressures and temperatures) when the CW was prepared and stabilized. This was accomplished by taking a subsample of the CO_2–brine mixture in the BPR (set at the test pressure) using a syringe pump (to force the mixture out). The gas to water ratio (GWR) was measured prior to the start of each test The value was compared with previously published experimental data (Cramer, 1982; Rumpf *et al.*, 1994) for the same operating conditions to validate the obtained solubility. Otherwise, the CW was re-prepared.

Additionally, the measured solubility values were compared with the model developed by Duan *et al.* (2006) to validate the experimentally measured data. The model is capable of accurately predicting CO_2 solubility in a wide temperature–pressure–ionic strength range (i.e., from T = 0 to 260 °C, from P = 0 to 200 MPa, and salinity from s = 0 to 4.5 mole/kg water) in the aqueous solutions containing Na^+, K^+, Ca^{2+}, Mg^{2+}, Cl^-, and

$SO4^{2-}$ with experimental accuracy. It was found that the experimental data obtained for CO_2 solubility in this study was in a good agreement with the calculated values, indicating that the apparatus and experimental procedures used in this study were reliable.

3.4.2. Results of CO_2–brine solubility tests

In this experiment, the solubility of CO_2 in brine (with the salinity of s = 0.3492 mole NaCl/kg water) at different pressures and two constant temperatures were determined. **Figure 3.10** presents the measured CO_2 solubility in brine for various pressures at constant temperatures of T = 25 °C and 40 °C. The experimental data for CO_2 solubility in brine showed good agreement with calculated values based on an improved model introduced by Duan *et al.* (2006). The comparison of the experimental data with the model revealed the average relative deviation of the solubility data to be estimated at about 11.5 %. Calculated absolute and relative deviations are summarized in **Table 3.4**.

Figure 3.10 also shows that the CO_2 solubility in brine increases remarkably with equilibrium pressure up to a certain point. Further increases in the equilibrium pressure did not result in noticeable increases in CO_2 solubility in brine. This behaviour was mainly due to the CO_2 phase change from gas to liquid, which occurs near CO_2 liquefaction pressure, P_{liq}. Since molecular diffusion is the main mechanisms leading to CO_2 dissolution, and the diffusion coefficient of gaseous CO_2 in brine is significantly higher than that of liquid CO_2, further dissolution of CO_2 in brine is very limited at pressures higher than the CO_2 liquefaction pressure. However, it was observed that at a constant temperature (e.g., T = 25 °C), the CO_2 solubility in brine becomes less sensitive to pressure at higher pressures (e.g., P > 6.9 MPa). As Figure 3.10 shows, the

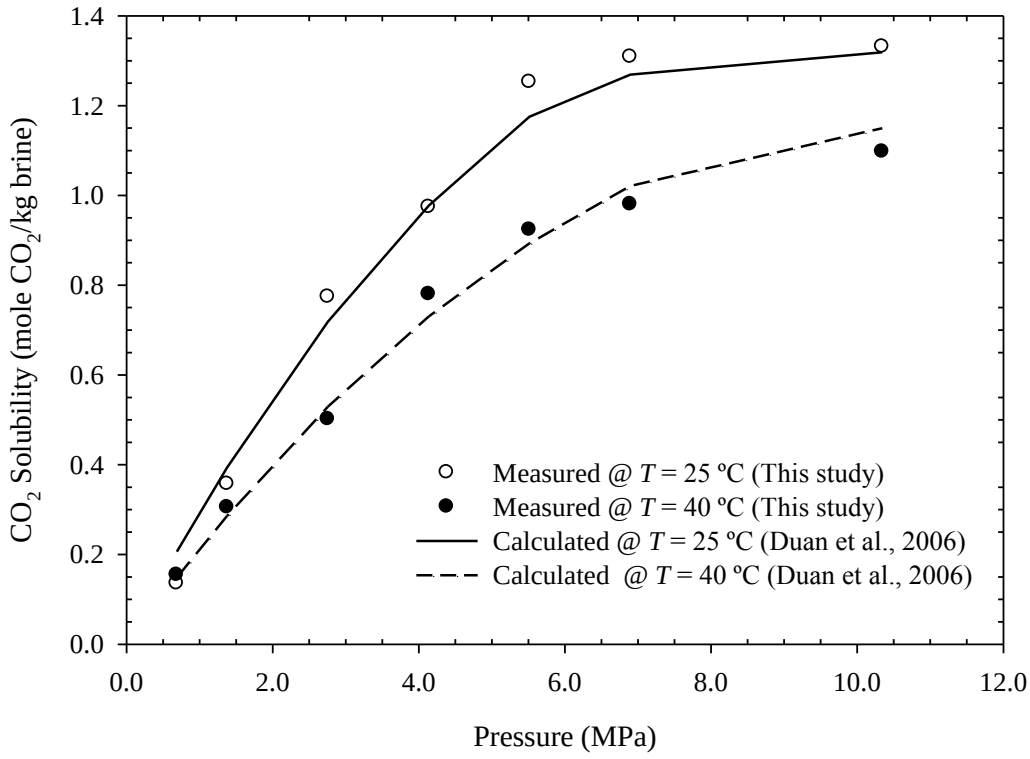

Figure 3.10: Comparison of measured and calculated CO_2 solubility in brine at 25 °C and 40 °C and different pressures.

Table 3.4: Calculated average absolute and relative deviations for the CO_2 solubility values in brine and oil at experimental temperatures of T = 25 and 40 °C.

	Temperature, °C	Average Absolute Deviation	Average Relative Deviation
CO_2 Solubility in Brine	25	0.04 Mole CO_2/kg brine	11.5 %
	40	0.03 Mole CO_2/kg brine	4.9 %
CO_2 Solubility in Oil	25	1.30 gr CO_2/100gr Oil	14.8 %
	40	1.03 gr CO_2/100gr Oil	11.5 %

experimental data of CO_2 solubility in brine was also in fair agreement with values predicted using the model developed by Duan *et al.*. However, even small differences in CO_2 solubility values might result in significant consequences when a field scenario is considered.

CO_2 solubility in pure water was also measured at equilibrium pressure of P = 4.1 MPa and various experimental temperatures of T = 25 and 40 °C in order to determine the salinity effect on CO_2 solubility. The results are compared in **Figure 3.11**. It was found that at each constant temperature, the solubility of CO_2 was reduced by adding NaCl to the pure water. For example, at temperature of T = 25 °C, solubility of CO_2 dropped from χ_w = 1.1029 mole/kg in pure water to χ_b = 0.9738 mole/kg in 2 wt.% NaCl brine. This was attributed to the solubility of CO_2 in aqueous solutions usually decreasing after the addition of inorganic salts. When NaCl concentration was increased, some of the water molecules were attracted by the Na^+ and Cl^- ions, decreasing the number of water molecules available to interact with CO_2. This phenomenon is called the salting-out effect (Liu *et al.*, 2011).

Overall, CO_2 solubility in each experiment was found to be consistent with previously reported maximum CO_2 solubility values at the same operating conditions (King *et al.*, 1992; Chapoy *et al.*, 2004; Duan *et al.*, 2006). Thus, it was concluded that CO_2 solubility in brine reached its maximum value for each test and the CW as fully saturated with CO_2 (i.e., CL = 100%).

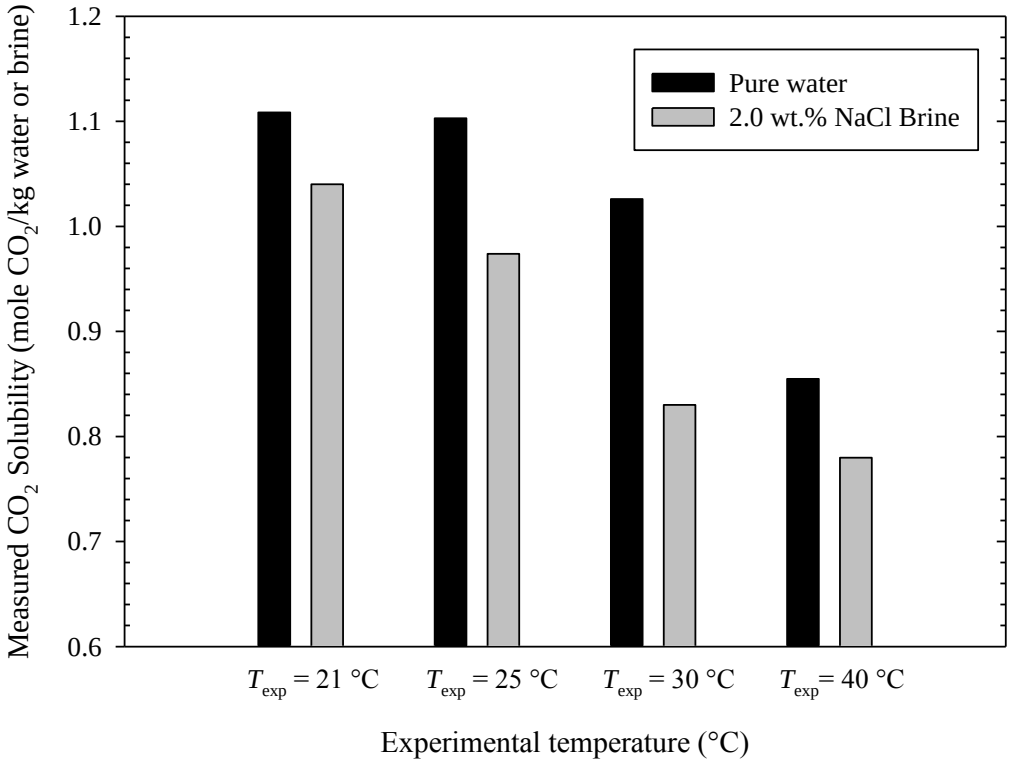

Figure 3.11: CO_2 Solubility in pure water and 2.0 wt.% brine samples at equilibrium pressure of P = 4.1 MPa and various experimental temperatures.

3.5. CO_2–oil system

3.5.1. K-value and EOS

All phases in the reservoir are initially in a thermodynamic equilibrium condition. Equilibrium K-value is defined as the ratio of equilibrium gas composition, y_i, to the equilibrium liquid composition, x_i:

$$K_i = \frac{y_i}{x_i} \quad \text{.....} \quad (3.4)$$

The equilibrium K-value for each component can be estimated from correlations (e.g., Raoult's and Dalton's laws, Hoffman *et al.* (1953) method, Wilson (1968) equation, and Standing (1979) equation) or by satisfying the equal-fugacity constraint with an Equation of State (EOS) model. An EOS model which relates pressure, volume and temperature (PVT) accurately describes the multi-phase thermodynamic equilibrium of a multi-component system. Combined with a mass-balance equation the EOS model gives the equilibrium phase split of a multi-component fluid mixture. Given a system with an overall fluid composition at specific pressure and temperature, the EOS will determine the relative amount of equilibrium oil and gas, K-values and essential fluid phase properties.

The Peng–Robinson (PR) and Soave–Redlich–Kwong (SRK) EOS are available in CMG Winprop to estimate phase equilibrium of gas–liquid and liquid–liquid at surface and reservoir conditions. PR EOS is the most well-known and widely used EOS in industry as it provides a high degree of accuracy in predicting liquid density and vapour pressure of a multi-component system. However, it tends to under-predict saturation pressure of reservoir fluids. Meanwhile, SRK improves Vapour–Liquid Equilibrium

(VLE) and saturation pressure predictions. The only disadvantage is that the SRK EOS yields a less accurate prediction in liquid density than the PR EOS. Both EOS models provide the same accuracy for VLE predictions and satisfactory volumetric predictions for vapour and liquid phases when used with volume translation.

3.5.2. CO_2 solubility, oil swelling, and viscosity reduction

CO_2 solubility in oil

CO_2 solubility in crude oil is a function of saturation pressure, temperature, and oil API gravity (Simon and Graue, 1965; Jamaluddin *et al.*, 1991; Srivastava *et al.*, 1995; Costa *et al.*, 2012). Solubility increases with the pressure and oil API gravity, while the value decreases with the temperature. The literature shows other factors affect CO_2 solubility in oil such as the oil composition and CO_2 liquefaction pressure (Emera and Sarma, 2006). It is also believed that gaseous CO_2 is more soluble in oil than the liquid CO_2, mainly due to the greater diffusion coefficient. This can be attributed to the fact that the molecular motion amplitude (i.e., moving distance) in gaseous CO_2 is much higher than in liquid CO_2 molecules. Therefore, the gaseous CO_2 molecules can more easily move from place to place, collide with the oil interface, and move into the oil phase causing a faster diffusion rate.

Emera and Sarma (2006) developed a model based on genetic algorithm to predict the CO_2 solubility in oil as a function of the saturation pressure, temperature, oil specific gravity, oil composition (through oil molecular weight), and CO_2 liquefaction pressure. **Figure 3.12** represents the graph of CO_2 solubility in different oil samples at various operational conditions using this model. It was observed that at the same saturation pressure, the CO_2 solubility in crude oils increased with decreasing temperature.

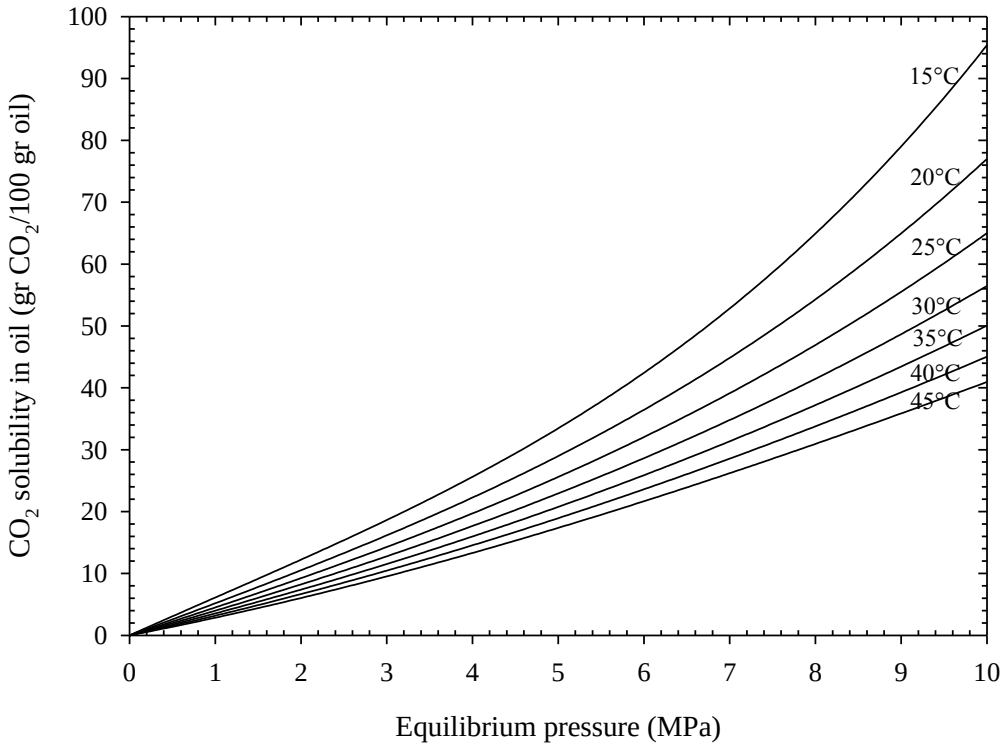

Figure 3.12: The solubility of CO_2 in an oil sample with molecular weight of MW_o = 223 gr/mole at various operating pressures and temperatures, calculated by the correlation developed by Emera and Sarma (2006).

Oil swelling factor

The swelling factor (SF) is expressed as the ratio of CO_2-saturated oil volume at reservoir pressure and temperature divided by the oil volume at reservoir temperature and atmospheric pressure.

$$SF = \frac{V_{CO_2-Oil}(P_R, T_R)}{V_{Oil}(P_{atm}, T_R)} \quad \text{.....} \quad (3.5)$$

where: SF is the swelling factor and $V_{CO2-Oil}$ and V_{Oil} are volume of the mixture and oil, respectively. The swelling factor is, mainly, a function of the CO_2 solubility (Welker and Dunlop, 1963; Simon and Graue, 1965; Sankur *et al.*, 1986; Emera and Sarma, 2006). Swelling increases with increasing CO_2 solubility. Furthermore, as the CO_2 solubility in light oil is higher than that in heavy oil, the lighter oil swells more than heavier oil. In addition to CO_2 solubility, the swelling factor is a function of the molecular size of oil molecules (Simon and Graue, 1965). It is believed that oil swelling due to CO_2 dissolution reduces the amount of residual oil saturation in the reservoir, and therefore, increases the oil recovery.

Oil viscosity reduction

Oil viscosity decreases significantly with increasing CO_2 solubility, resulting in increased oil mobility, and consequently causing an increase in oil recovery (Emera and Sarma, 2006). As depicted in **Figure 3.13**, at temperatures less than $T_{c,CO2}$, CO_2–oil viscosity noticeably decreases with increasing pressure up to the CO_2 liquefaction pressure. At pressures greater than the CO_2 liquefaction pressure, the CO_2-saturated oil viscosity flattens off and then decreases slightly. Since the oil viscosity reduction is finite and related to the maximum CO_2 solubility, at higher pressures the viscosity begins to

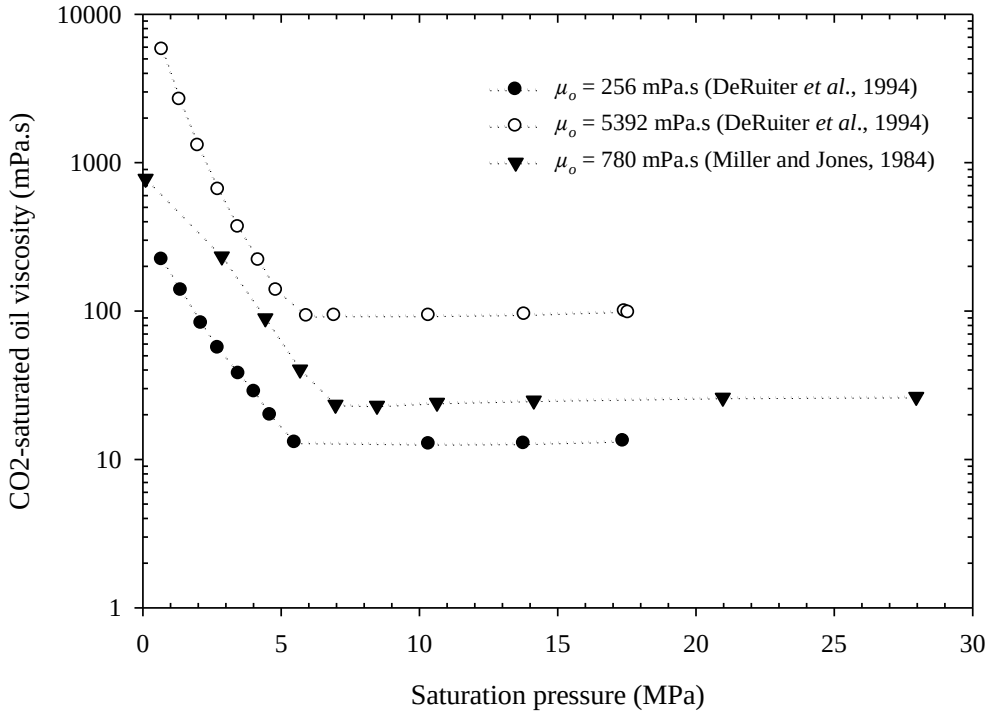

Figure 3.13: oil viscosity reduction due to CO_2 dissolution at various saturation pressures at constant temperatures of: T = 18.3 and 24 °C for three different oil samples at constant temperature.

increase marginally, mainly due to the oil compressibility (Miller and Jones, 1981; Miller and Jones, 1984; DeRuiter *et al.*, 1994). Moreover, CO_2-saturated oil viscosity reduction is higher at lower temperatures than at higher temperatures. Additionally, the viscosity reduction is higher for more viscous oil (i.e., heavier oil) than for less viscous oil (i.e., lighter oil).

3.5.3. CO_2 solubility measurement and oil swelling/extraction tests

In this study, a high pressure–high temperature visual cell was used to determine the CO_2 solubility for the CO_2–oil system at various operating pressures and at two different temperatures of T = 25 °C and 40 °C. **Figure 3.14** shows the schematic diagram of the experimental apparatus for measuring the CO_2 solubility in the crude oil. The apparatus consisted of a see-through-windowed high-pressure cell (Jerguson Co.), a magnetic stirrer (Fisher Scientific Co.), and a high pressure CO_2 cylinder. This setup was placed in an air bath so that constant temperature was maintained using temperature controller (Love Controls Co.) during the solubility measurement tests. The magnetic stirrer was placed underneath the visual cell in which the crude oil sample and a magnet were placed. Stirring the oil sample greatly accelerated the CO_2 dissolution in the crude oil by creating convective mass transfer (Abedini *et al.*, 2012; Kavousi *et al.*, 2013). The pressure inside the pressure cell was measured by using a digital pressure gauge.

The CO_2 solubility in crude oil was measured at different equilibrium pressures and four constant temperatures in the range of T = 21–40 °C. The temperature of the air bath was set at the desired test value, T, prior to each solubility measurement. The high-pressure cell was charged with $V_{o,i}$ = 25 cm^3 of the crude oil sample. The pressure cell

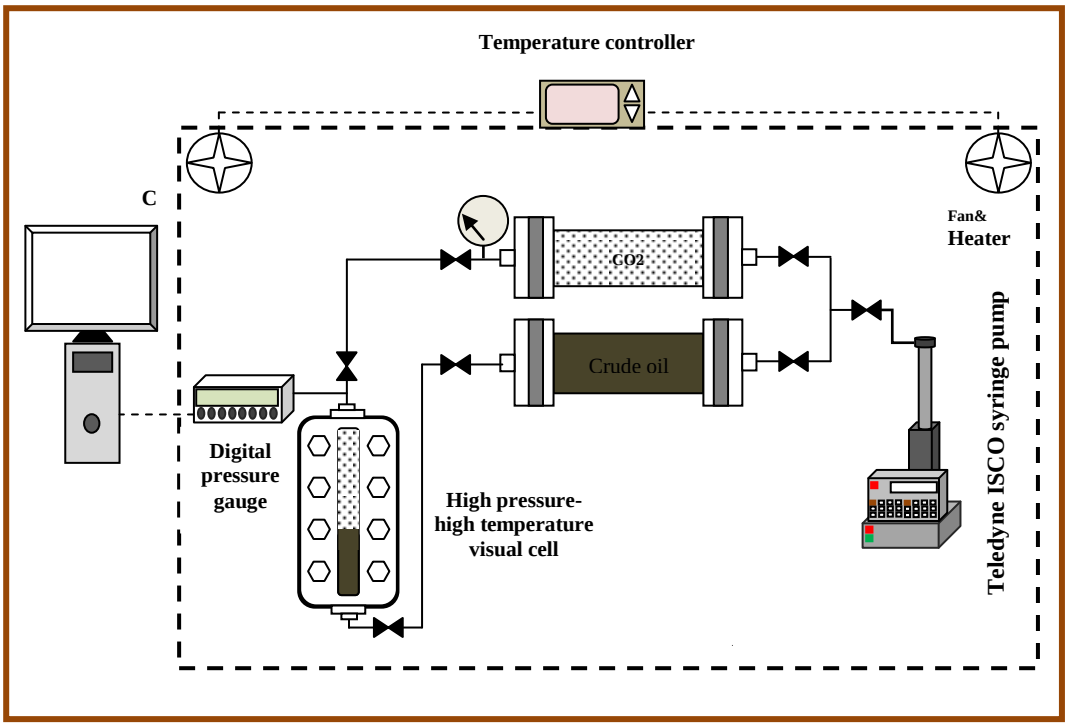

Figure 3.14: Schematic diagram of the experimental setup used for measuring the solubility for CO_2–oil mixture at various pressures and constant temperatures of T = 25 °C and 40 °C.

was pressurized with CO_2 to a pre-specified pressure, P_i. The pressure of the cell was allowed to stabilize while CO_2 was dissolving into the crude oil. The test was terminated when the pressure inside the cell reached its stable value and no further pressure drop was observed ($\Delta P \leq 0.7$ kPa/day), i.e., the final CO_2 pressure, P_f. Finally, initial and final volumes of CO_2 in visual cell, $V_{CO2,i}$ and $V_{CO2,f}$, respectively, were determined by taking photos and utilizing image analysis technique. Throughout this study, the solubility was defined as the ratio of the total mass of dissolved CO_2 in 100 gr of the original crude oil sample. It was calculated using the mass balance and ideal gas equations for the dissolution process. The detailed derivation of the CO_2 solubility formulation is as follow:

$$\begin{aligned} m_{dis} &= m_{CO_2,i} - m_{CO_2,f} \\ &= \left(\frac{PV_{CO_2}M_{CO_2}}{ZRT}\right)_i - \left(\frac{PV_{CO_2}M_{CO_2}}{ZRT}\right)_f \\ &= \frac{M_{CO_2}}{RT}\left[\left(\frac{PV_{CO_2}}{Z}\right)_i - \left(\frac{PV_{CO_2}}{Z}\right)_f\right] \end{aligned} \quad \text{..... (3.6)}$$

$$m_{oil} = \left(\rho_o V_{o,i}\right)_{@T_{\exp}} \quad \text{..... (3.7)}$$

$$\begin{aligned} \chi_{CO_2} &= \frac{m_{dis}}{m_{oil}} \times 100 \\ &= \frac{M_{CO_2}}{RT\rho_{oil}V_{o,i}}\left[\left(\frac{PV_{CO_2}}{Z}\right)_i - \left(\frac{PV_{CO_2}}{Z}\right)_f\right] \end{aligned} \quad \text{..... (3.8)}$$

The swelling factor, *SF*, is determined by measuring the final volume of the crude oil in the cell, $V_{o,f}$, as a result of two factors: CO_2 dissolution in the oil and light to medium hydrocarbon groups extraction from the oil to the CO_2 phase. *SF* is expressed as the ratio of final CO_2-saturated oil volume, $V_{o,f}$, at experimental pressure and temperature

divided by the original oil volume, $V_{o,i}$, at experimental temperature and atmospheric pressure.

$$SF = \frac{V_{o,f}(P,T)}{V_{o,i}(P_{atm},T)} \quad \text{.....} \quad (3.9)$$

CO_2 solubility values were also calculated, based on the correlations developed by Emera and Sarma (2006) which were found to be more accurate, compared to other correlations available in the literature (Al-Jabra and Al-Anazi, 2009). The models, based on a genetic algorithm, were proposed as a function of the saturation pressure, temperature, oil specific gravity, and oil molecular weight.

Swelling factor was determined by measuring the change of the interface level as a result of two factors: CO_2 dissolution in the oil and light-hydrocarbon extraction into the CO_2-rich vapour phase.

3.5.4. CO_2 solubility in the oil phase

The CO_2 solubility in the crude oil was measured at seven different pressures and two temperatures (T = 25 °C and 40 °C). The measured CO_2 solubility in the crude oil versus equilibrium pressure data at T = 25 °C and 40 °C are shown in **Figure 3.15**. It was observed that the measured CO_2 solubility in the crude oil sample increased with the equilibrium pressure. Based on Henry's Law, the concentration of dissolved CO_2 depends on the partial pressure of the CO_2. The partial pressure controls the number of CO_2 molecule collisions with the surface of the crude oil sample. If the partial pressure increases (i.e., higher experimental pressure) the number of collisions with the surface increases as well. Thus, the increased number of collisions enabled greater dissolved CO_2

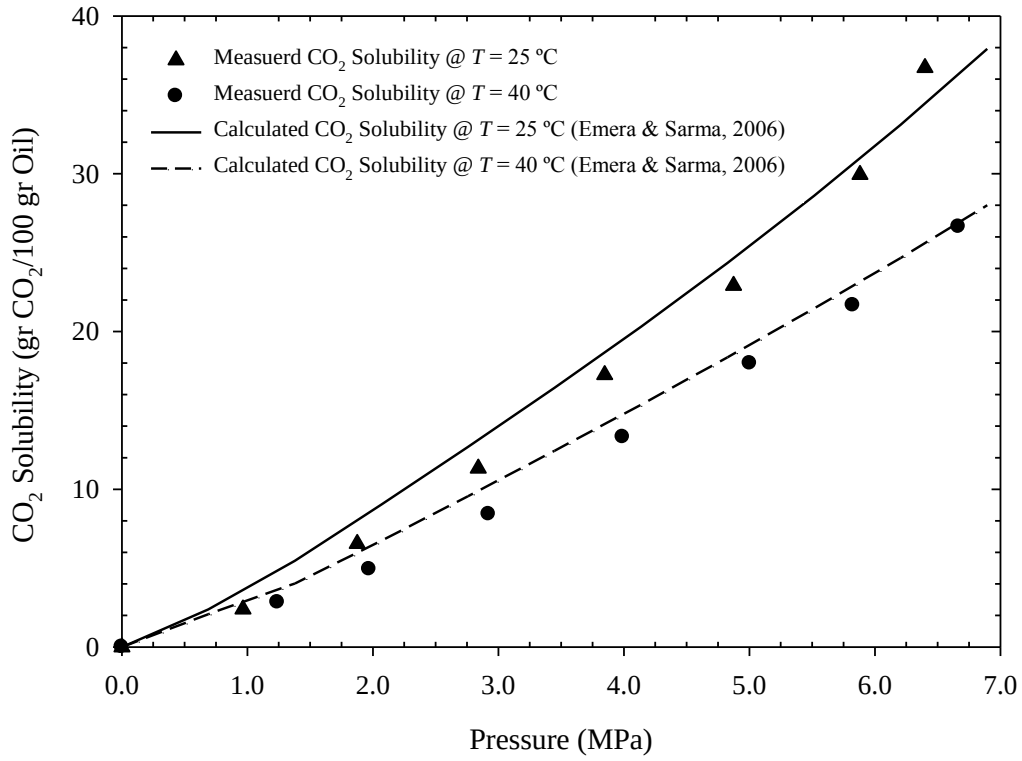

Figure 3.15: Measured and calculated CO_2 solubility in crude oil sample at different equilibrium pressures and two constant temperatures of T = 25 and 40 °C.

and higher CO_2 solubility values. Moreover, it was noted that increasing the temperature led to a reduction in the solubility of CO_2 in the crude oil. For example, at equilibrium pressures close to P = 5.8 MPa, the solubility of CO_2 reduces from χ_b = 29.95 gr CO_2/100 gr of oil to χ_b = 21.65 gr CO_2/100 gr of oil when experimental temperature increased from T = 25 °C to 40 °C.

The measured CO_2 solubility values in crude oil were also calculated using the correlation developed by Emera and Sarma (2006). Figure 3.15 presents the calculated CO_2 solubility values in the crude oil samples. It was observed that the calculated CO_2 solubility data was in a fair agreement with the measured data within the range of experimental conditions of this study.

3.5.5. Oil swelling factor and extraction pressure

Figure 3.16 depicts the oil swelling factor, *SF*, as a result of CO_2 dissolution in the oil phase at experimental temperatures in the range of T = 21 to 40 °C. Swelling factor was equal to one at atmospheric pressure and experimental temperature. By increasing the equilibrium pressure, the oil phase swelled and swelling factor gradually became greater than one, mainly due to higher solubility of CO_2 in the crude oil. As an example, at the experimental temperature of T = 25 °C, maximum swelling occurred at the pressure of 6.4 MPa, at which maximum swelling factor and CO_2 solubility of SF = 1.3571 and $\chi_{o,max}$ = 33.11 gr CO_2/100 gr of oil were achieved, respectively. It was also found that during the swelling/extraction tests, the oil swelling factor curves exhibited a sharp decline at a pressure known as extraction pressure, P_{ext}. At this pressure, the majority of light to medium hydrocarbon groups of the crude oil were extracted by CO_2 and vaporized into the CO_2-rich phase. Maximum CO_2 solubility, $\chi_{o,max}$, maximum oil

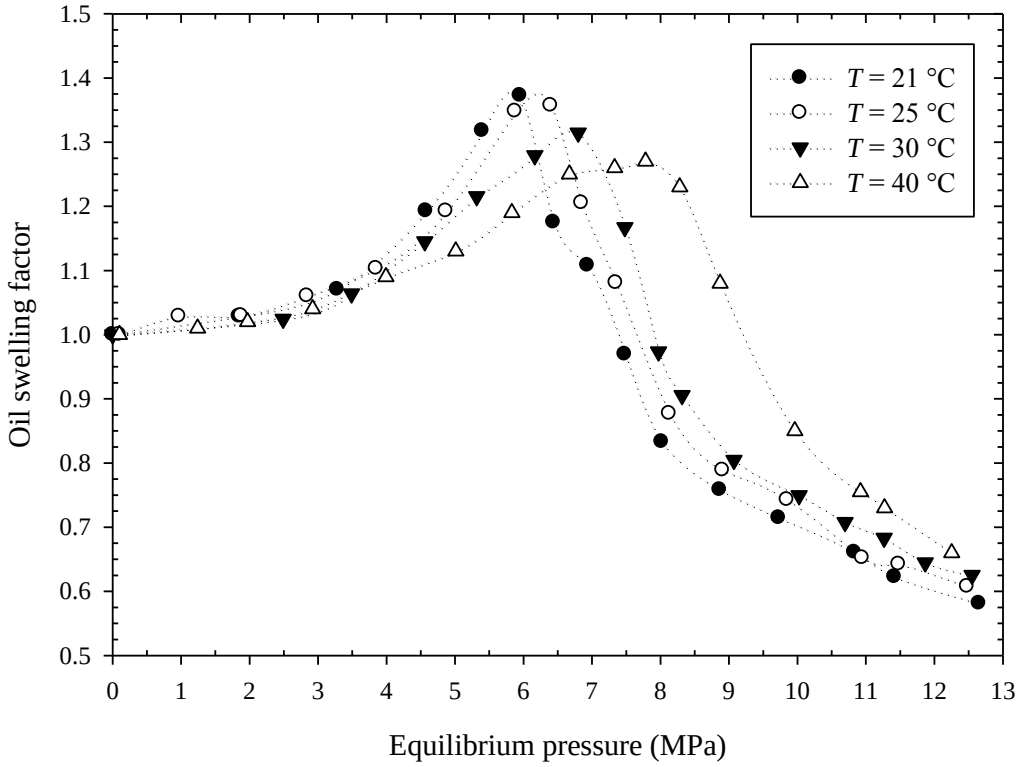

Figure 3.16: Measured oil swelling factor of the crude oil–CO_2 system versus equilibrium pressure at various experimental temperatures.

Table 3.5: Measured extraction pressure, maximum CO_2 solubility, and oil swelling factor for swelling/extraction tests conducted at various experimental temperatures.

Experimental Temperature, T_{exp} (°C)	Measured extraction pressure, P_{ext} (MPa)	Maximum CO_2 solubility, $\chi_{o,max}$ ($grCO_2/100grOil$)	Maximum oil swelling factor, SF_{max}
21	6.0	33.8	1.37
25	6.4	34.2	1.36
30	6.8	31.4	1.31
40	7.8	33.45	1.27

swelling factor, SF_{max}, and extraction pressure, P_{ext}, obtained at various operating temperatures are summarized in **Table 3.5**. At equilibrium pressures beyond the extraction pressure, the CO_2–oil interaction is primarily governed by extraction of the remaining light to medium hydrocarbon rather than the oil swelling. Thus, the oil phase started to shrink and the oil swelling factor was reduced. The reduction in the swelling factor was observed to be continuous as the equilibrium pressure was further increased. This was attributed to the formation of a high-density CO_2-rich phase which had a higher capability to extract light to medium hydrocarbon components of the crude oil (Tsau *et al*., 2010; Bui *et al*., 2010). The impact of experimental temperature on the swelling/extraction curve is presented in Table 4 and the results revealed that the maximum swelling factor decreased with increased experimental temperatures. In addition, the extraction pressures of the CO_2–oil system were greater at higher temperatures than at lower temperatures. For example, the extraction pressure of P_{ext} = 6.8 MPa at T = 30 °C reduced to P_{ext} = 6.0 MPa at T = 21 °C.

Figure 3.17 illustrates the CO_2 solubility along with the swelling factor for the CO_2–oil system at various equilibrium pressures and experimental temperatures of T = 21 to 40 °C. This study showed the solubility of CO_2 in the oil sample and the oil swelling factor increased noticeably as the pressure increased upward to the extraction pressure, P_{ext}. This figure depicts direct relationship between the CO_2 solubility in the crude oil sample and the oil swelling factor. For the pressures higher than P_{ext}, light to medium hydrocarbon group extraction is a dominant process, and the chemical composition of both liquid and vapour phases change frequently.

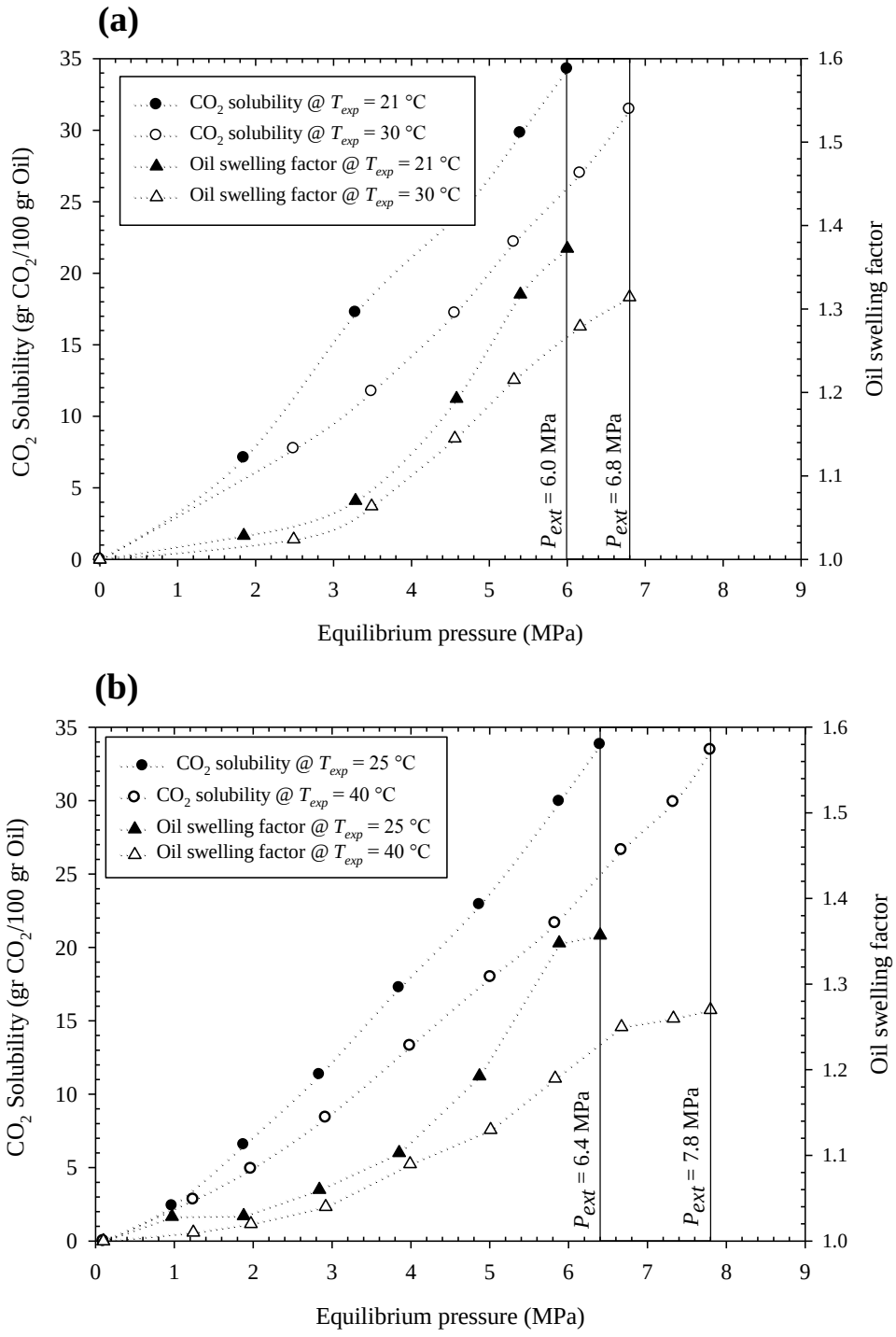

Figure 3.17: CO_2 solubility in crude oil and oil swelling factor at various operating pressure and four constant temperatures: (a) T_{exp} = 21 °C and 30 °C and (b) T_{exp} = 25 °C and 40 °C.

The maximum CO_2 solubility values in oil, which existed at extraction pressures for the different swelling/extraction tests conducted at different experimental temperatures, are shown in Figure 3.17. The results showed that the maximum CO_2 solubility values required to initiate the extraction of major light to medium hydrocarbon groups are approximately the same for different experimental temperatures. Therefore, it can be concluded that light to medium hydrocarbon extraction occurs when a definite amount of CO_2 is dissolved into the oil, which is called the threshold CO_2 solubility, χ_{th}. The threshold CO_2 solubility for the CO_2–oil system of this study was found to be χ_{th} = 33.21 gr CO_2/100 gr of oil. **Figure 3.18** depicts the extraction pressures of the CO_2–oil system at different experimental temperatures. Since CO_2 solubility in oil is directly proportional to equilibrium pressure and inversely proportional to experimental temperature, higher pressure was required to reach the threshold CO_2 solubility as the experimental temperature increases. This resulted in higher extraction pressures observed at higher experimental temperatures. The threshold CO_2 solubility parameter defined in this study has a unique value for each CO_2–oil mixture and depending on the composition of the crude oil. For a particular crude oil composition saturated with CO_2, this parameter can be used to estimate the extraction pressure at various temperatures. Moreover, the experimental data obtained for the extraction pressure showed a linear behaviour with experimental temperature as indicated in **Figure 3.19**. The extraction pressure was observed to increase linearly from P_{ext} = 6.0 MPa at T = 21°C to P_{ext} = 7.8 MPa at T = 40°C.

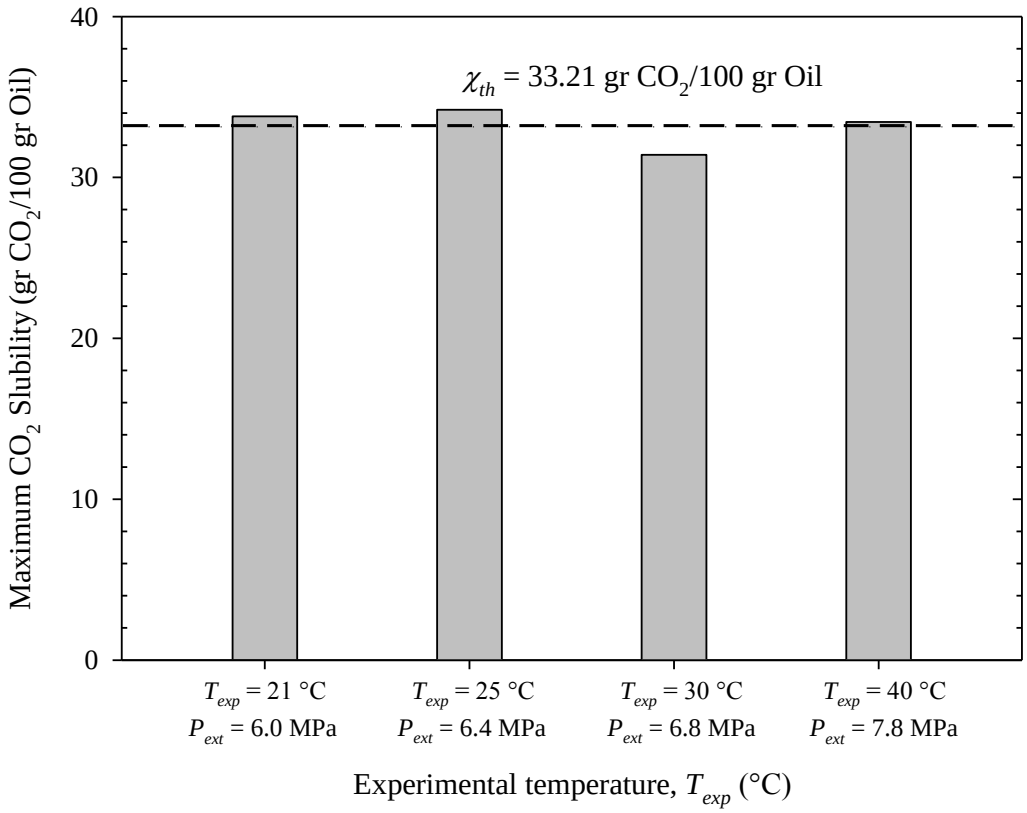

Figure 3.18: Threshold CO_2 solubility values and extraction pressures for different experimental temperatures.

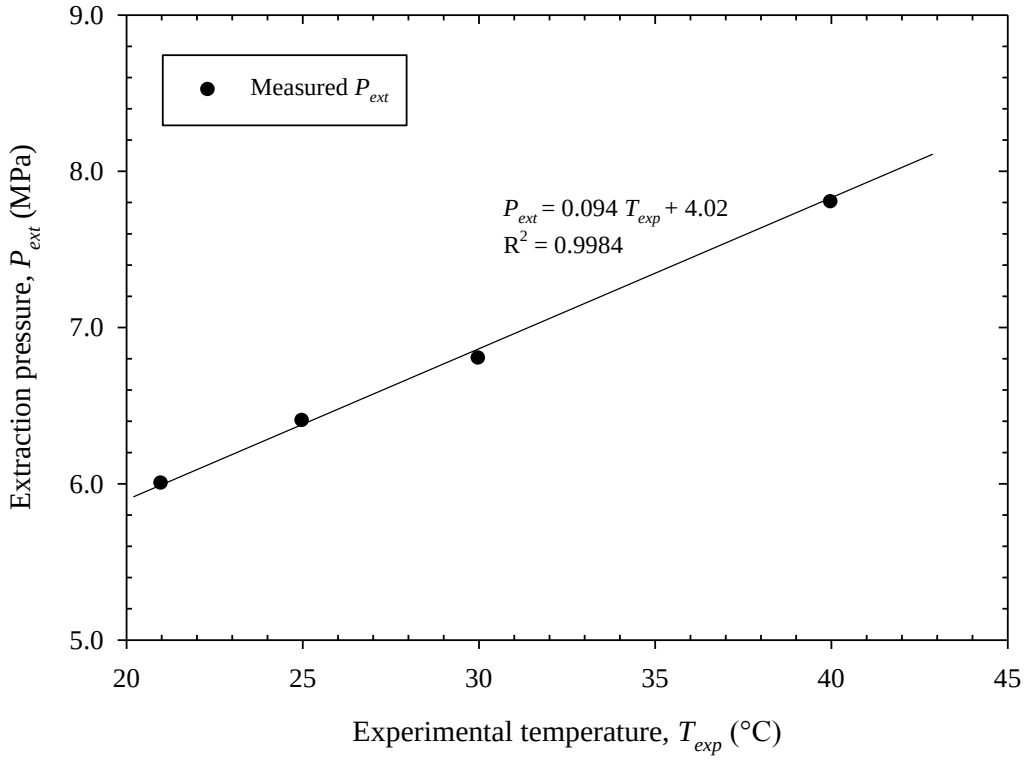

Figure 3.19: Measured extraction pressure, P_{ext}, for the CO_2–oil system at various experimental temperatures and the linear equation fitted to the experimental data points.

3.6. Chapter summary

In this chapter, a detailed phase behaviour study on the CO_2–water, CO_2–brine, and CO_2–oil systems was conducted through carefully-designed laboratory experiments. CO_2 solubility measurements in water, brine, and oil phases were conducted at various experimental conditions. Afterward, swelling/extraction tests were carried out for the CO_2–oil system to examine the oil swelling and light component extraction during various equilibrium pressures in the range of P = 0.7–10.3 MPa and experimental temperatures in the range of T = 21–40 °C. It is believed that the findings of this study are of significance to any CO_2 EOR and storage project.

The solubility of CO_2 in brine increases with increased pressure at constant temperature and salinity. In addition, the impact of pressure on CO_2 solubility diminishes as the pressure of the system increases. Moreover, the solubility of CO_2 in brine decreases at higher temperatures. The comparison of the CO_2 solubility in pure water and synthetic brine (2.0 wt.% NaCl) also indicated that the addition of salt leads to a reduction in CO_2 solubility in water.

The CO_2 solubility in the oil phase is directly proportional to pressure while inversely proportional to the operating temperature. The CO_2 solubility increases steadily with pressure at any constant experimental temperature. However, the increase was noticeably higher for the solubility measurement tests carried out at lower experimental temperatures.

At a constant temperature, the swelling factor increased with pressure until extraction pressure, P_{ext}, was reached at which point most of the light to medium hydrocarbon groups of the oil were extracted and vaporized into the CO_2-rich phase. For

the pressures higher than extraction pressure, the oil shrinks and the oil swelling factor decreases substantially. Furthermore, the maximum oil swelling factor was found to be higher for swelling/extraction tests conducted at lower temperatures.

The existence of threshold CO_2 solubility, χ_{th}, in the oil phase is the prominent condition affecting the extraction of major light to medium hydrocarbon groups. This threshold CO_2 solubility was found to be approximately χ_{th} = 33.21 gr CO_2/100 gr of oil for the oil sample used in this study. In addition, the threshold CO_2 solubility was found to be independent of temperature and was the same for all swelling/extraction tests performed at different experimental temperatures.

CHAPTER FOUR: CWI: experiments, results, and discussion

A series of sand-pack flooding tests including a base case conventional WF and 16 subsequent CWI tests were carried out at various operating conditions. Flooding experiments were performed on an artificial porous medium, which was made of unconsolidated silicon sands that were carefully packed by following a thorough procedure. The effects of operating pressure, temperature, CW injection rate, and carbonation level of the injected CW on the performance of secondary and tertiary CWI were systematically investigated through this study. The operating pressures ranged from P = 0.7 MPa to 10.3 MPa and the tests were carried out in an air bath set to a constant temperatures of T = 25 °C and 40 °C. CO_2 storage capacity of each CWI test was investigated by measuring injected and produced volumes of CO_2 and the amount of stored CO_2 was calculated using a mass balance equation.

4.1. Porous medium

The flooding experiments were performed in a sand-pack flooding apparatus. The length and internal diameter of the sand-pack vessel were L_{sp} = 30.48 and D_{sp} = 2.54 cm, respectively. The sand used in this study was purchased from Bell and Mackenzie Company Limited, with 99.88% of its composition as silicon dioxide (SiO_2). The particle mesh size ranged from ASTM 40 to 270 as presented in **Table 4.1** and the average (by weight) diameter of the sand was calculated to be 0.214 mm.

Table 4.1: Properties of the sand used for flooding experiments conducted in this study.

U.S. Sieve	Approximate Diameter (mm)	Percent Retained
40 Mesh	0.422	2 %
50 Mesh	0.297	28 %
70 Mesh	0.211	38 %
100 Mesh	0.152	21 %
140 Mesh	0.104	8 %
200 Mesh	0.075	2 %
270 Mesh	0.053	1 %

4.2. Fluid samples

Synthetic brine of 20,000 ppm NaCl was prepared using deionized water. The density and viscosity of the brine were measured to be ρ_b = 1010.2 kg/m^3 and μ_b = 0.90 mPa.s, respectively, at a temperature of T = 25°C and atmospheric pressure (i.e., P_{atm} = 101.1 kPa). The reason for choosing simple NaCl brine was that since different seawaters are having different salinities and ion characteristics in different areas, it is time consuming and difficult to prepare the exact seawater or brine composition for laboratory studies. Additionally, the injected brine in water flood projects is obtained from the most convenient source and is usually of different composition than the connate water. Therefore, synthetic NaCl brine was commonly considered as representative of typical water flooding injectant and is used widely in petroleum laboratory studies.

The study used a light stock tank oil sample from the Bakken oil reservoir, with API gravity of 44.1 and composition presented in **Figure 4.1**. The density and viscosity of the stock tank oil sample were ρ_o = 799.0 kg/m3 and μ_o = 2.76 mPa.s at 25 °C and atmospheric pressure of 101.1 kPa. The asphaltene content (*n*-Pentane insoluble) of the stock tank oil sample was also measured to be 1.23 wt.%. The MMP of the CO_2–oil mixture was calculated by Emera and Sarma's correlation to be 8.3 MPa at the constant temperature of 25°C. **Table 4.2** summarizes different characteristics of the stock tank oil sample used in this study.

4.3. Experimental setup and methodology

The flooding apparatus used in this study is a typical setup used for sand-pack experiments. The complete schematic of the setup is shown in **Figure 4.2**. A syringe

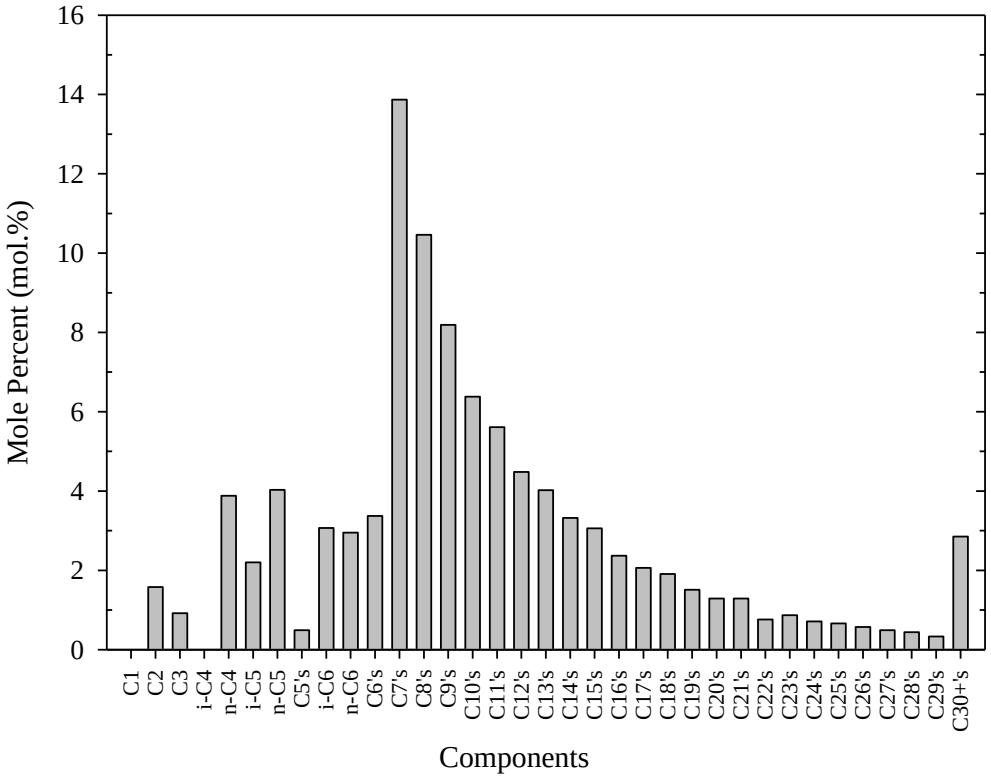

Figure 4.1: Gas Chromatography (GC) compositional analysis result for Bakken stock tank oil sample used in this study.

Table 4.2: Physical properties of the oil sample used in this study at P_{atm} = 101.1 kPa and T = 25°C.

Property	Value
Molecular weight	223 gr/mol
Density at 101.1 kPa & 25 °C	799 kg/m^3
API Density	44.1 °API
Viscosity at 101.1 kPa & 25 °C	2.76 mPa.s
n-C5 insoluble asphaltene	1.23 wt.%

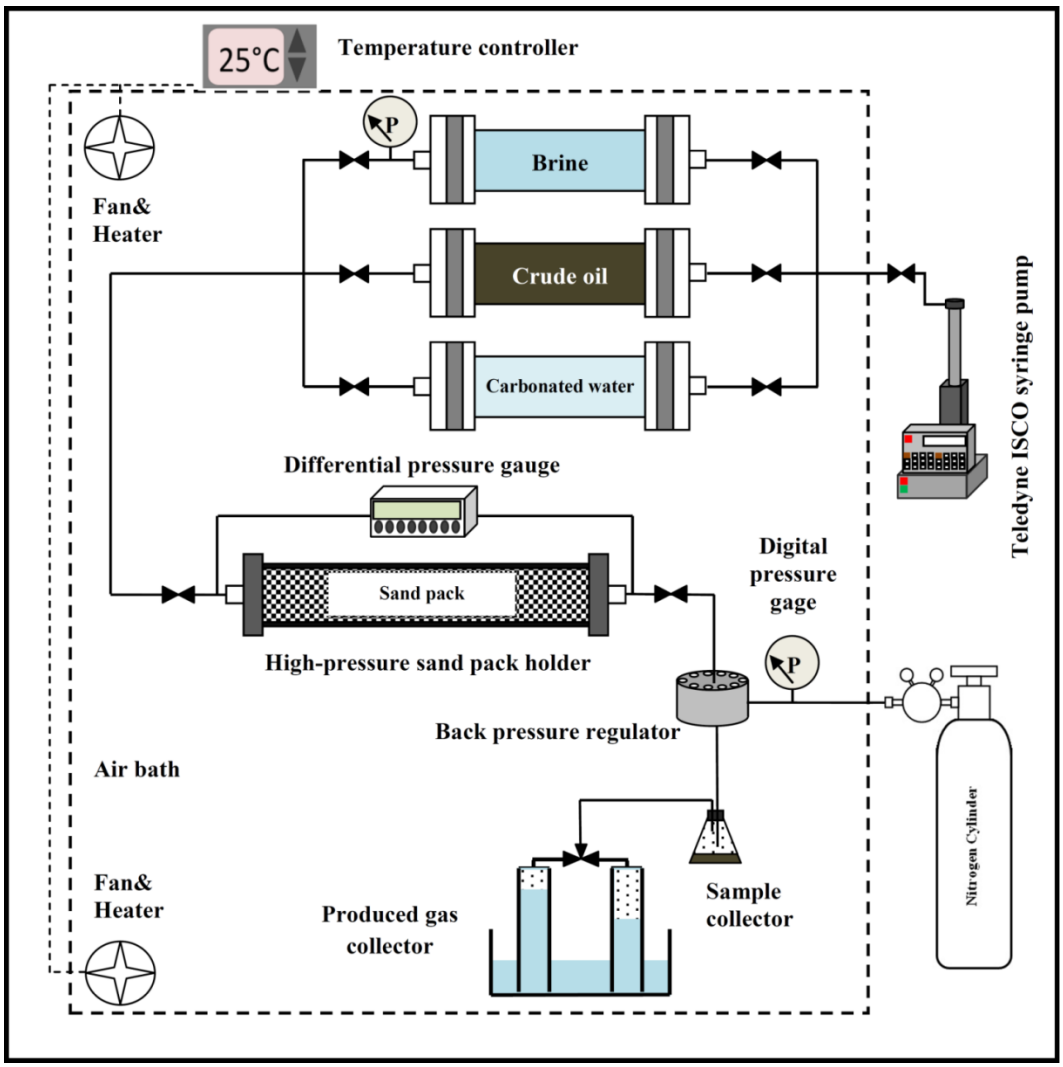

Figure 4.2: Schematic diagram of the sand-pack flooding apparatus used in this study.

pump (Teledyne ISCO, 500D series) was used to push the injection fluids (i.e., brine, crude oil, and carbonated brine) into the sand-pack. Three piston accumulators were used to hold brine, crude oil, and carbonated brine. Produced liquids (i.e., water and oil) and gas collected using a precisely graduated cylinder and a carefully designed gas bubbler, respectively, at atmospheric pressure (P_{atm} = 101.1 kPa) and experimental temperature. The setup, accumulators, produced fluid collectors, and connection lines were kept inside an air bath (temperature controlled) to maintain constant temperature during the experiment. The complete setup for controlling the temperature inside the air bath included a temperature controller, a temperature probe (sensor), a heater, and industrial fans. The fans were used to circulate the air and provide uniform temperature for the entire air bath.

A back pressure regulator (Temco Inc), a precisely graduated cylinder, a carefully designed gas bubbler along with the valves, joints and tubing formed the production system. Produced liquids (i.e., water and oil) and gas were collected at atmospheric pressure (i.e., P_{atm} = 101.1 kPa) and experimental temperature (i.e., T = 25 or 40 °C). The back pressure regulator was a dome-type nitrogen-loaded actuator set to maintain a constant system pressure (rated to 17.2 MPa with an accuracy of 1%). It was connected at the outlet of the sand-pack to maintain the desired system pressure. The outlet of the back pressure regulator was connected to the graduated cylinder to collect the produced fluids (i.e., oil, water and gas phases). The gas collected in the burette was allowed to flow through the gas bubbler.

The challenge was to pack the sand thoroughly so that the sand-pack would behave as close to a homogeneous porous media without layers of varying particle sizes

in either a horizontal or vertical direction (known as sorting), which could result in permeability variations or trends from one segment/direction to another. Therefore, the following detailed procedure was used to prevent any artificially induced heterogeneity inside the sand-pack. Before packing, the inner wall of the stainless steel pipe (25.4 mm ID) used in this study was carefully coated with a very thin layer of water- and hydrocarbon-proof resin (Bluemagic Inc.) and sand to make the inside surface of the sand-pack vessel rough enough to prevent fluid channelling through the porous medium boundary near the pipe wall. To fill the stainless steel pipe with sand, a wet packing procedure (using methanol) was implemented. During the packing process, a ball vibrator (Deca Vibrator Industries, Inc.) was attached to the pipe to provide a uniform tight packing. The reason for choosing methanol as a packing fluid was to use a volatile liquid so that the remained liquid inside the sand-pack could be removed easily through a drying process. The drying process involved injecting air to the sand-pack for 2 hours. After that, the sand-pack was vibrated using the ball vibrator for 1 hour to pack the sand as much as possible. The free space on top of sand was filled by adding more dry sand to the system. Finally the sand-pack was vacuumed for 3 hours to remove the air inside the pores.

The pore volume of the sand-pack was measured by allowing injected brine to imbibe into the sand-pack for 2 hours and recorded. Absolute permeability measurement was also carried out for each test by brine injection at different flow rates and the slope for a differential pressure versus flow rate curve was calculated using Darcy's Law. The measured porosity and absolute permeability values for each run were summarized in **Table 4.3**. Absolute permeability values varied from one sand-pack to another, likely

Table 4.3: Experimental conditions, characteristics of the unconsolidated sand-packs, and flooding specifications for the conventional WF and ten CWI tests conducted in this study.

Test	Mode	CL (%)	P (MPa)	T (°C)	q_{inj} (cm^3/min)	χ_b (mole/kg)	k_{abs} (mD)	ϕ (%)	S_{wi}	S_{or}
#1	WF	-	4.1	25	1.0	-	5608	27.84	0.384	0.248
#2	SCWI	100	0.7	25	1.0	0.1354	6715	27.91	0.365	0.238
#3	SCWI	100	1.4	25	1.0	0.3572	7190	27.32	0.363	0.226
#4	SCWI	100	2.8	25	1.0	0.7737	7047	27.39	0.371	0.201
#5	SCWI	100	4.1	25	1.0	0.9738	7184	27.58	0.365	0.181
#6	SCWI	100	5.5	25	1.0	1.2523	4320	28.84	0.385	0.155
#7	SCWI	100	6.9	25	1.0	1.3084	4487	27.13	0.365	0.150
#8	SCWI	100	10.3	25	1.0	1.3188	4322	26.61	0.373	0.136
#9	SCWI	100	4.1	40	1.0	0.7797	4320	27.13	0.385	0.186
#10	SCWI	100	4.1	25	0.5	0.9738	7105	27.65	0.372	0.177
#11	SCWI	50	4.1	25	1.0	0.4869	4011	26.54	0.368	0.207
#12	TCWI	100	1.4	25	1.0	0.3572	4136	28.15	0.376	0.223
#13	TCWI	100	4.1	25	1.0	0.9738	4037	26.83	0.370	0.197
#14	TCWI	100	6.9	25	1.0	1.3084	4053	27.14	0.384	0.178
#15	TCWI	100	10.3	25	1.0	1.3188	4106	26.92	0.372	0.174
#16	TCWI	100	4.1	40	1.0	0.7797	4074	27.44	0.380	0.208
#17	TCWI	50	4.1	25	1.0	0.3896	4282	27.33	0.361	0.212

because of unexpected variations in pore structures in different packs. However, porosities and consequently pore volumes were relatively more consistent for all sand-packs. After every test, the sand was discarded and the cylinder was thoroughly cleaned. Then, a new sand-pack was prepared for the next run.

Accumulators were filled with stock tank oil, water and CW and then they were placed into the air bath and equilibrated at the experimental temperature for 48 hours before the injection process started. The brine saturated sand-pack was flooded with stock tank oil afterwards. The effluent fluids were gathered using precisely graduated collectors. Visual indication through transparent collectors provided monitoring of the water and/or gas breakthrough and the pressure response. All sand-packs were saturated with oil and throughout the oil saturation process, irreducible water saturation was measured. Then, CWI was carried out at different operating conditions. Current performance analysis of secondary CWI focused on the effect of operating pressure on the oil recovery improvement while keeping other parameters unchanged. In this study, the influences of operating temperature, injection flow rate, and saturation level of CW were studied individually.

The apparatus and experimental procedures for preparation of CW at pre-specified pressure and temperature were similar to that reported in the CO_2 solubility determination in brine. The aforementioned procedure was followed to prepare CW with the maximum CO_2 saturation at the specified pressure and temperature. However, for test number 11, partially saturated CW at the pressure of P = 4.1 MPa was required. Therefore measured maximum CO_2 saturation (CL = 100%) in brine at 4.1 MPa ($\chi_{b,max}$ = 0.9738 moles/kg) was divided by two to get CO_2 saturation for a partially (CL = 50%)

saturated CW. Calculated CO_2 saturation (which was calculated to be χ = 0.4869 mole/kg) was incorporated into the model developed by Duan *et al*. (2006) to find the corresponding pressure at which maximum CO_2 solubility in brine was $\chi_{b,max}$ = 0.4869 mole/kg. The pressure was calculated to be P = 1.7 MPa. Therefore fully saturated CW was prepared at the pressure of P = 1.7 MPa and then the mixture pressure was raised to the pressure of P = 4.1 MPa to prepare a partially saturated (i.e., CL = 50%) CW at P = 4.1 MPa.

It is believed that four principal forces involved in fluid flow through porous media are: viscous, gravity, hydrodynamic, and capillary forces. In order to investigate the relative importance of each force during an immiscible displacement, different dimensionless numbers have been formulated by dividing any two of those forces. Capillary number is an important dimensionless number which is defined as the ratio of viscous force to the capillary force. During the CWI tests with two immiscible fluids (i.e., carbonated water and stock tank oil), the complete capillary number could be defined as (Mosavat *et al.*, 2013):

$$N_{CA} = \frac{\sqrt{2} v_L \mu_L l_{sp}}{\sigma_{eq} \sqrt{k_{abs} \phi}} \quad \ldots\ldots\ldots\ldots\ldots\ldots\ldots\ldots\ldots\ldots\ldots\ldots\ldots\ldots\ldots\ldots\ldots\ldots\ldots\ldots\ldots\ldots \quad (4.1)$$

where v_L and μ_L are displacing liquid (i.e., carbonated water) velocity and viscosity, respectively, ϕ is porosity of the porous medium, σ_{eq} is the equilibrium interfacial tension between displacing (i.e., carbonated water) and displaced liquid (i.e., stock tank oil), k_{abs} is the permeability, and l_{sp} is the length of sand-pack. σ_{eq} between the carbonated water and the stock tank oil sample was obtained from literature (Yang *et al.*, 2005). Using Equation 4.1, with known permeability, porosity, length, viscosity of displacing fluid,

cross-sectional area of the porous medium, and carbonated water injection rate, the complete capillary number, N_{CA}, for each of the flooding tests conducted in this study was calculated to be about $N_{CA} = 0.01$. Therefore, based on the flow region identifications proposed by Cinar *et al.* (2006), it can be concluded that the flow characteristics of the flooding tests in this study were viscous-dominated flow.

The Reynolds number represents the ratio of the importance of inertial effects to viscous effects in fluid flow calculations. The critical value of $Re = 1$ has been considered to differentiate between laminar (i.e., Darcian) and turbulent (i.e., Non Darcian) flows (Mosavat *et al.*, 2013). For the purpose of this study, Reynolds number was calculated using the following equation proposed by Zendehboudi *et al.* (2011).

$$Re = \frac{\rho_L v_L D}{\mu_L} \qquad \text{(4.2)}$$

where ρ_L is the liquid density, v_L is the liquid velocity, D is a representative grain diameter, and μ_L is the liquid viscosity. The diameter, D, was calculated based on the following equation (Dullien, 1992):

$$D = \sqrt{\frac{32 k_{abs}}{\phi}} \qquad \text{(4.3)}$$

Reynolds number was calculated for all flooding tests in this study and the results indicated a laminar (i.e., Darcian) flow regime in the sand-pack tests performed in this study. For instance, the Reynolds number of $Re = 0.3$ was calculated for the reference water flooding test.

It is also believed that in immiscible two-phase flow through porous media, capillary phenomenon is a concern. The capillary pressure (the difference between

wetting and non-wetting phase pressures) depends on curvature of the interface between the two fluids, the wettability, and the pore geometry (Amyx *et al.*, 1960). Laboratory displacement processes are almost always affected by viscous instabilities and end effects. These effects are minimized using the Rapoport and Leas (1953) scaling criterion for stabilized floods. The scaling criterion used was found to minimize the dependence of oil recovery on the injection rate and length of the porous medium.

$$L_{sp} v_L \mu_L \geq 1 \qquad \text{.....} \qquad (4.4)$$

where, L_{sp} is the length of the sand-pack (cm), v_l is Darcy velocity (cm^3/min) and μ_L is the viscosity of displacing fluid (mPa.s). The immiscible floods in this work were designed to operate at a scaling criterion of approximately 5.41 to ensure the stability of the floods. A Rapoport and Leas scaling coefficient of greater than one would minimize the capillary end effects (Rapoport and Leas, 1953).

4.4. Secondary displacement test results

A total of eleven sand-pack flooding experiments were carried out throughout this study. All the characteristics of the displacement tests are listed in **Table 4.4**. During the tests, the end product water, oil, and gas and the differential pressure (*dP*) across the sand-pack were monitored and recorded. **Figure 4.3** portrays measured cumulative products (i.e., oil and brine) and the differential pressure across the sand-pack for the base WF scenario. The base WF was conducted at a pressure and temperature of P = 4.1 MPa and T = 25 °C, respectively. Since both water and oil are incompressible and immiscible fluids and there is no significant interaction between the phases, the flooding

Table 4.4: Experimental conditions, characteristics of the unconsolidated sand-packs, and flooding specifications for the conventional WF and ten CWI tests conducted in this study.

Test	Mode	*CL* (%)	*P* (MPa)	*T* (°C)	q_{inj} (cm^3/min)	χ in Brine (mole/kg)	k_{abs} (mD)	ϕ (%)	S_{wi}	S_{or}
#1	WF	-	4.1	25	1.0	-	5608	27.84	0.384	0.248
#2	SCWI	100	0.7	25	1.0	0.1354	6715	27.91	0.365	0.238
#3	SCWI	100	1.4	25	1.0	0.3572	7190	27.32	0.363	0.226
#4	SCWI	100	2.8	25	1.0	0.7737	7047	27.39	0.371	0.201
#5	SCWI	100	4.1	25	1.0	0.9738	7184	27.58	0.365	0.181
#6	SCWI	100	5.5	25	1.0	1.2523	4320	28.84	0.385	0.155
#7	SCWI	100	6.9	25	1.0	1.3084	4487	27.13	0.365	0.150
#8	SCWI	100	10.3	25	1.0	1.3188	4322	26.61	0.373	0.136
#9	SCWI	100	4.1	40	1.0	0.7797	4320	27.13	0.385	0.186
#10	SCWI	100	4.1	25	0.5	0.9738	7105	27.65	0.372	0.177
#11	SCWI	50	4.1	25	1.0	0.4869	4011	26.54	0.368	0.207

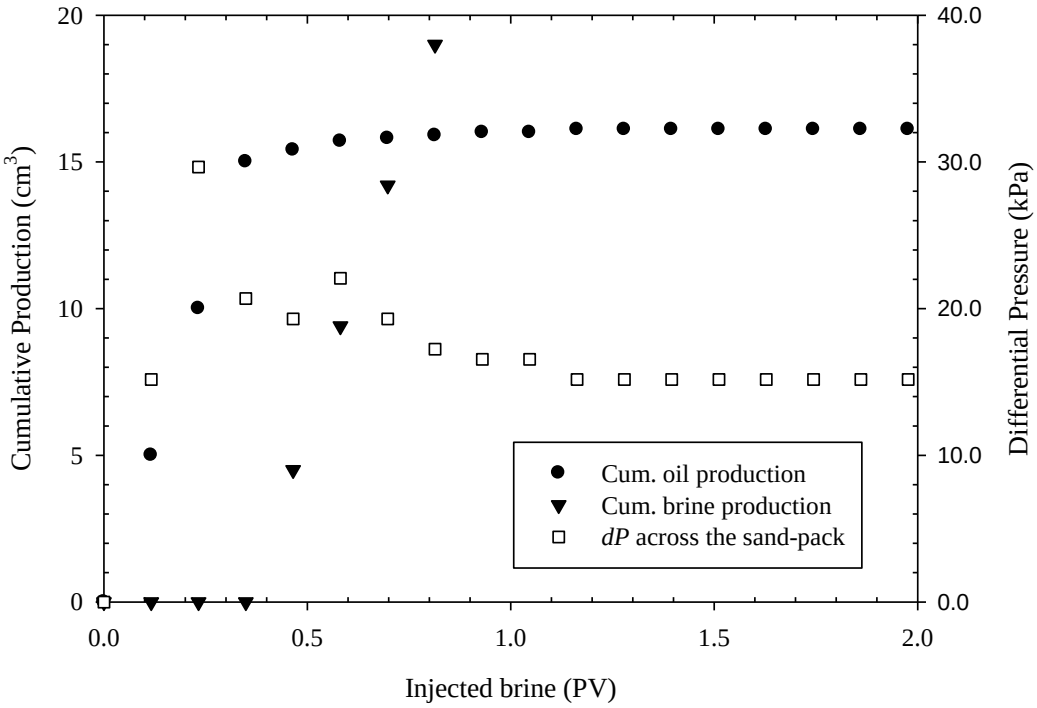

Figure 4.3: Measured cumulative produced oil and water as well as differential pressure across the sand-pack during conventional WF at pressure of P = 4.1 MPa and constant temperature of T = 25 °C.

behaviour of WF is less sensitive to the operating pressure. Therefore, the conventional WF scenario was considered as a base control comparison test for all other experiments conducted at different pressures and constant temperature of T = 25 °C.

4.4.1. Effect of operating pressure

Seven CWI tests were carried out at various operating pressures of P = 0.7–10.3 MPa and a constant temperature of T = 25 °C. **Table 4.5** summarizes the oil recovery data for the CWI tests as well as the reference WF (base case scenario). It was found that CWI under secondary mode significantly improved the ultimate oil recovery. The improvement over conventional WF ranged from 2.74% at the pressure of P = 0.7 MPa to 19.02% at the pressure of P = 10.3 MPa.

Figure 4.4 shows the oil recovery curves for base case WF and the subsequent CWI tests versus PV of CW injection at different pressures. As mentioned earlier, except for operating pressure and CW mixture, which was prepared at each operating pressure, other experimental conditions were kept constant.

As shown in Figure 4.3, a relatively small improvement in oil recovery was produced using CWI at the pressure of P = 0.7 MPa compared to conventional WF. This was attributed to the very limited solubility of CO_2 in the injected brine (or low carbonation level) and subsequent limited CO_2 mass transfer from the water into oil phase during the process. From the section of CO_2 solubility in brine, CO_2 solubility in brine at a pressure of P = 0.7 MPa is χ_b = 0.1354 mole/kg, which means that the 180 minutes of injection time for CW with a flow rate of q_{inj} = 1.0 cm^3/min, a total of 0.024 moles of CO_2 were injected into the sand-pack. When pressure was increased to P = 6.9 MPa, the total injected CO_2 during the injection period increased to 0.235 moles which is about 10

Table 4.5: Ultimate RF, RF at breakthrough time, and RF improvement for eight sand-pack flooding experiments conducted at various operating pressures and constant temperature of T = 25 °C.

Test	Mode	P (MPa)	RF at Water BT (%)	Ultimate RF (%)	RF Improvement* (%)
#1	WF	4.1	57.14	59.74	-
#2	SCWI	0.7	57.67	62.48	2.74
#3	SCWI	1.4	57.00	64.55	4.81
#4	SCWI	2.8	57.48	67.99	8.25
#5	SCWI	4.1	56.98	71.51	11.77
#6	SCWI	5.5	59.77	74.81	15.07
#7	SCWI	6.9	60.54	76.43	16.69
#8	SCWI	10.3	58.78	78.76	19.02

* RF improvement is taken as the difference between RF for base case conventional WF and that for each CWI test.

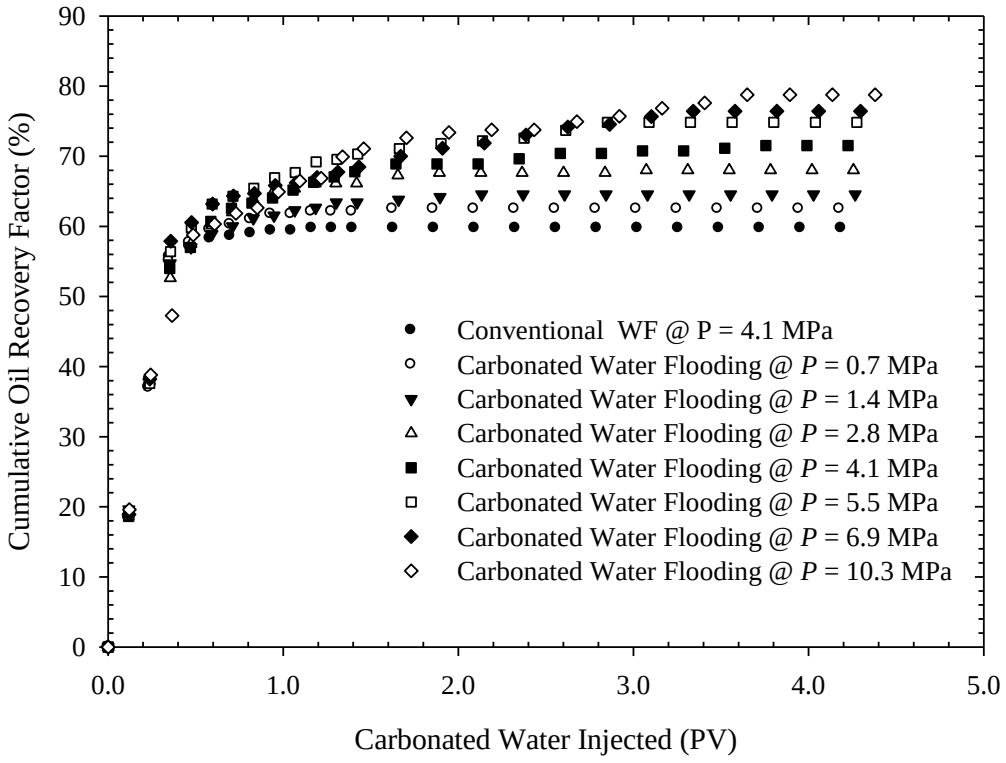

Figure 4.4: Cumulative oil recovery factors for seven CWI tests and the conventional WF (base case) at various operating pressures and constant temperature of T = 25 °C.

times higher than that at the pressure of P = 0.7 MPa. This increased the oil recovery factor from 62.5 to 76.4%.

Figure 4.5 presents the ultimate recovery together with CO_2 solubility in brine as a function of pressure and shows that at the same temperature and salinity, CO_2 solubility increased as the pressure increased. However, the rate of solubility increase slowed when the pressure approached P = 5.6 MPa. On the other hand, the ultimate recovery factor also tends to reach a plateau as the pressure increases. Comparison of the two curves indicates that there is a direct relationship between the amount of CO_2 dissolved in the injected brine and the obtained ultimate oil recovery factor.

Figure 4.6 compares the ratio of CO_2 produced to the CW injected during the CWI processes at various pressures. It was found that the breakthrough times (BT) for all tests with different pressures were almost the same and occured after injection of about 1.0 PV of CW. It was also observed that the water breakthrough occurs after injection of about 0.4 PV of CW, which is sooner than that of CO_2. However, the CO_2 production started at approximately 0.6–0.7 PV of injected carbonated water and the values were close to zero and were ignored. It is believed that the injected CW displaces the original oil in place, together with the connate water inside the porous medium. As a result, the connate water in which there was no dissolved CO_2, was produced earlier than the injected carbonated water. For all CWI tests conducted at various operating pressures, after the CO_2 breakthrough, this ratio increased gradually until it reached to a maximum value and remained constant for subsequent PVs of injected CW. This was attributed to a post-injection process where after injection of a portion of PVs of CW, the oil was completely saturated with CO_2 and majority of CO_2 remains in water phase. Thus, the CO_2 transfer

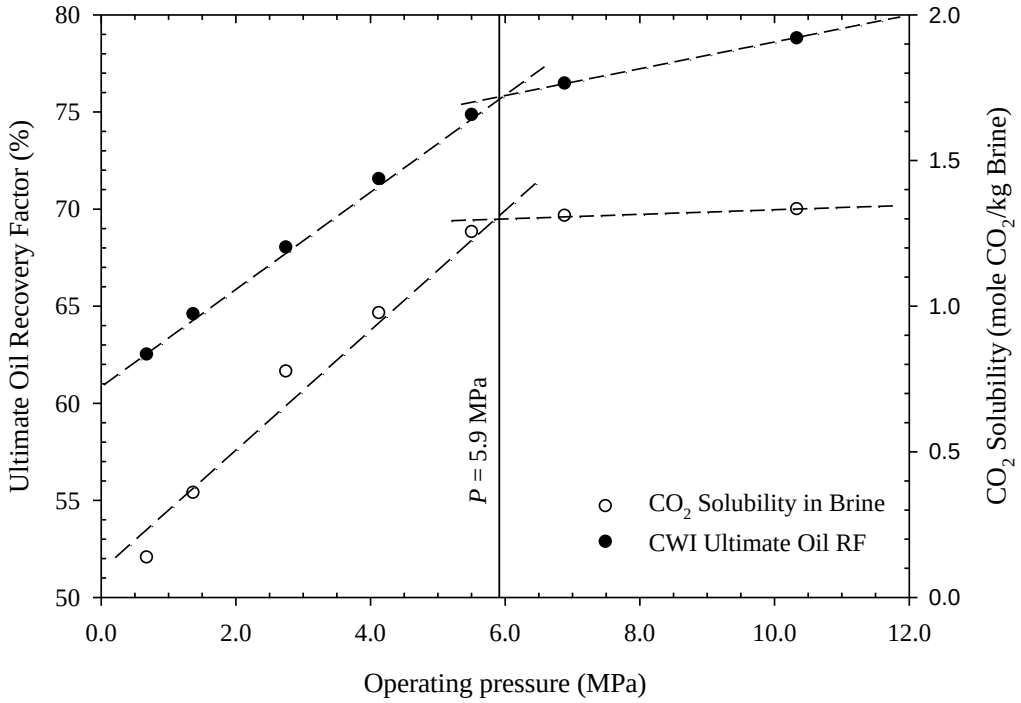

Figure 4.5: Ultimate oil recovery factor and CO_2 solubility in brine as a function of pressure for seven secondary CWI at constant temperature of T = 25 °C and various pressures.

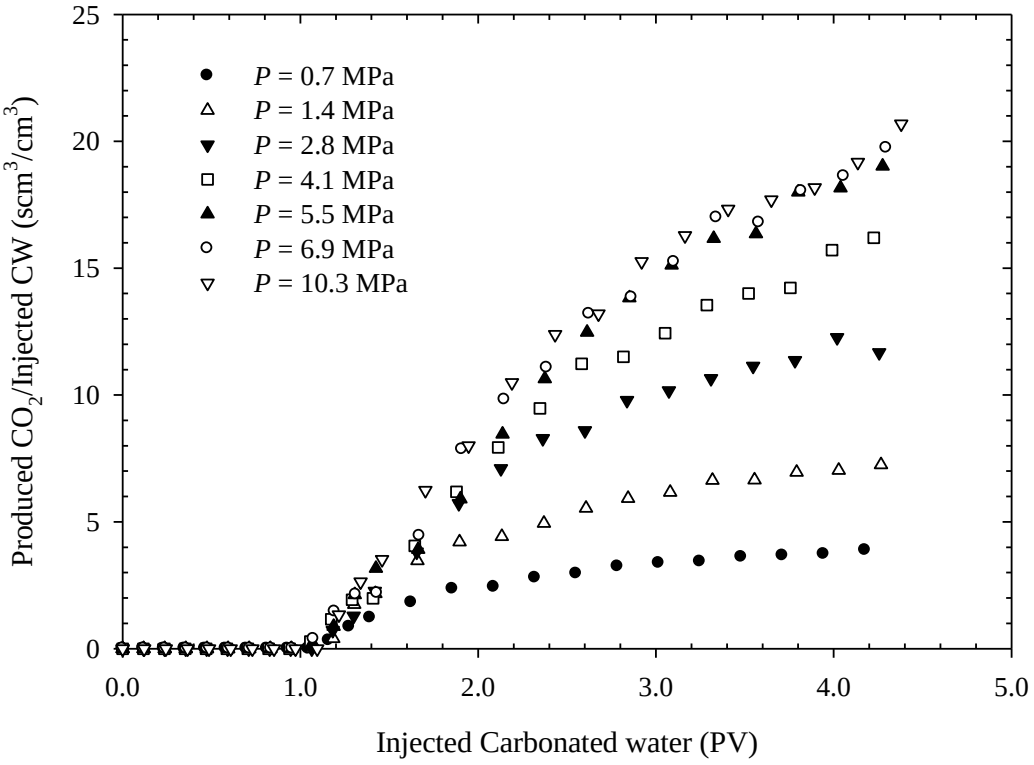

Figure 4.6: The ratio of produced CO_2 to injected CW for seven secondary CWI tests at different pressures and constant temperature of T = 25 °C.

from brine to the oil phase slowed to a very limited quantity.

The amount of CO_2 stored in the porous medium at any particular time during CWI for different operating pressures are plotted in **Figure 4.7**. This figure shows that larger amounts of CO_2 were stored in the reservoir at higher pressures and likely due to the larger CO_2 solubility values in both oil and brine. It was found that at low pressures, the plot reaches its stable values after about 1 PV of CWI. However, as the pressure increases, the stability time increases and nearly shifts to 2 PV of CWI. This was due to higher pressures, even after 1 PV injection of carbonated water, where CO_2 transfer from brine to the oil phase still continued because CW at such pressures contain a higher amount of dissolved CO_2 compared to that at lower pressures. Furthermore, it can be concluded that the CWI processes operated at higher pressures resulted in higher storage of CO_2 at the end of the flooding process.

4.4.2. Effect of temperature

To investigate the effect of operating temperature on the performance of CWI, an additional test was carried out at operating pressure of P = 4.1 MPa and constant temperature of T = 40 °C. **Figure 4.8** shows the comparison of the recovery for CWI tests implemented at T = 25 °C and 40 °C. Since at elevated temperatures, less CO_2 can be dissolved in brine, a lower amount of CO_2 could be injected in to the sand-pack and therefore a decrease in the oil recovery factor was observed. The CO_2 solubility in brine at temperature of T = 40 °C was reduced to χ = 0.7303 mole/kg compared to χ = 0.9775 mole/kg at temperature of T = 27 °C. This was a reduction of 1.8% in ultimate oil recovery using CWI when the temperature was increased to T = 40 °C from the initial value of T = 25 °C and at a constant pressure of P = 4.1 MPa. Figure 4.8 presents the

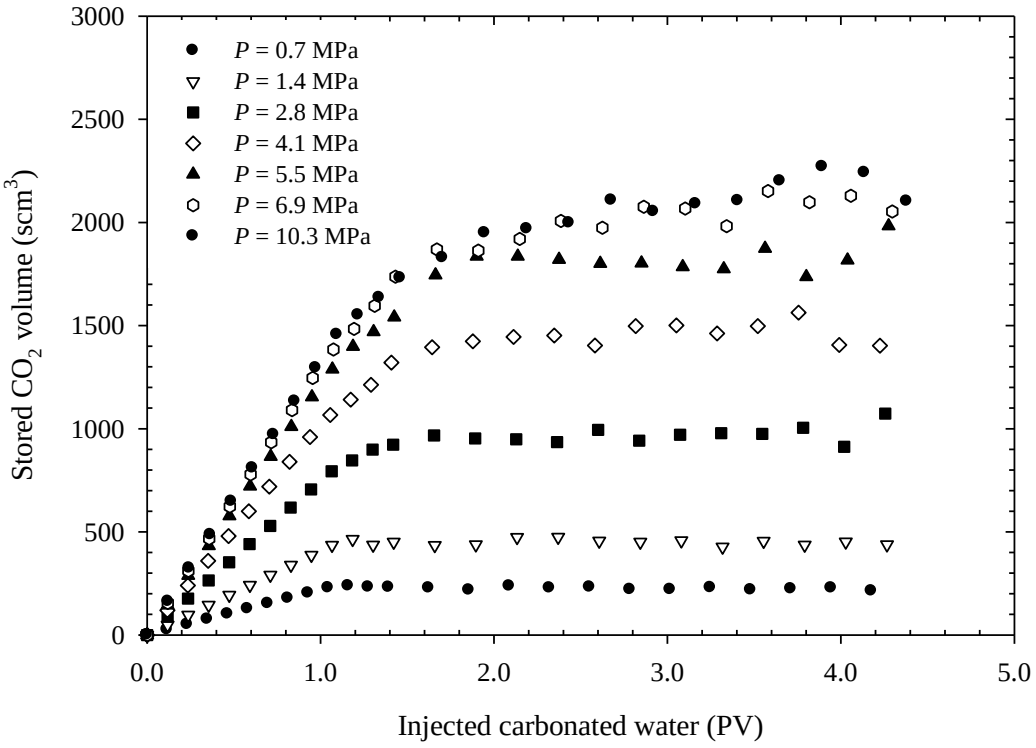

Figure 4.7: The cumulative stored CO_2 in the reservoir at different pressures and constant temperature of T = 25 °C.

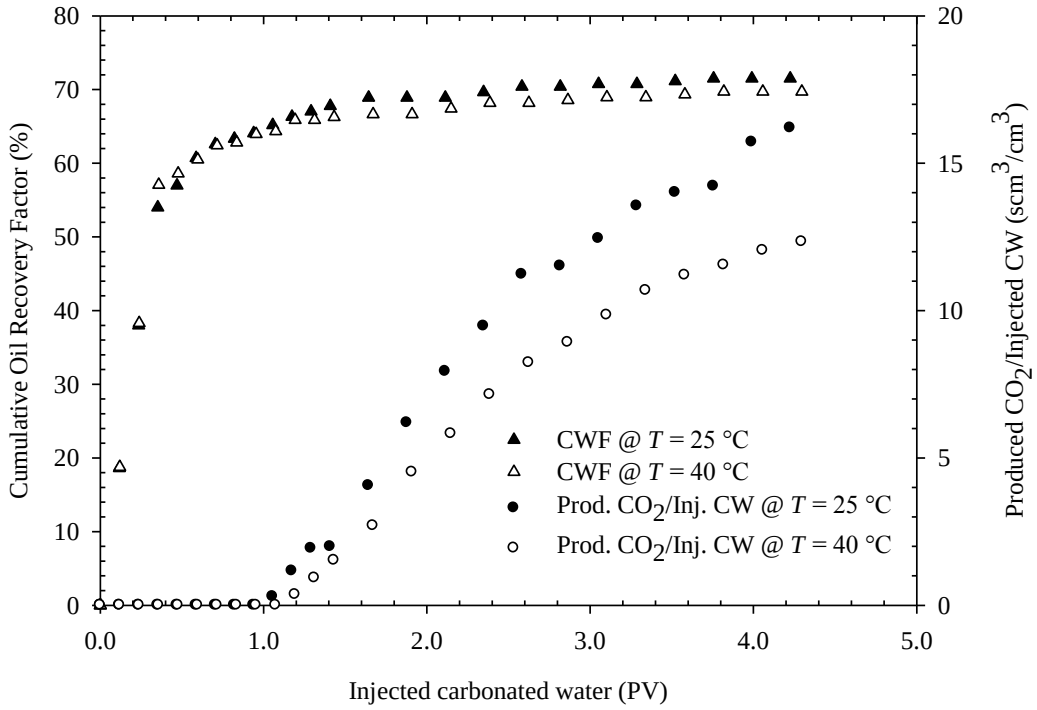

Figure 4.8: Cumulative oil recovery and the ratio of produced CO_2 to injected CW for two secondary CWI tests at constant pressure of P = 4.1 MPa and two operating temperatures of T = 25 °C and 40 °C (Tests #5 and #9).

ratio of produced CO_2 to injected CW. This plot shows the amount of produced CO_2 decreased with higher temperatures, likely due to the lower CO_2 solubility in brine and lower concentration of CO_2 injection to the sand-pack.

4.4.3. Effect of CW injection rate

The effect of CW injection rate on the performance of CWI is another parameter investigated in this study. The CW injection rate was reduced to q_{inj} = 0.5 cm^3/min (test #10) at a pressure of P = 4.1 MPa and the results were compared to those of test #5 (i.e., CW injection rate of q_{inj} = 1.0 cm^3/min and constant pressure of P = 4.1 MPa) while all other operating conditions constant for both tests. Cumulative oil recovery, as well as the ratio of produced CO_2 to injected CW, were plotted against the PV of injected CW for two injection rates of q_{inj} = 0.5 and 1.0 cm^3/min. The results are shown in Figure **4.9**. Cumulative oil recovery of CWI increased slightly to about RF = 71.91% at q_{inj} = 0.5 cm^3/min compared to RF = 71.51% at q_{inj} = 1.0 cm^3/min. The process of CWI is almost independent of CW injection rate as confirmed by the comparison of the produced CO_2 data with injected CW for the two injection rates. Since the permeability of the porous medium in this study was relatively high (k_{abs} = 4.0–7.2 D), increasing the contact time between CO_2 and the oil by reducing the CW injection rate was less effective. It is expected that for low permeability porous media, the CW injection rate plays an important role in performance of CWI.

4.4.4. Effect of carbonation level

Carbonation level, *CL*, in this study is defined as the ratio of the amount of dissolved CO_2 to the maximum amount of CO_2 that can be dissolved in water or brine at specific conditions. This parameter plays an important role in the performance of CWI as

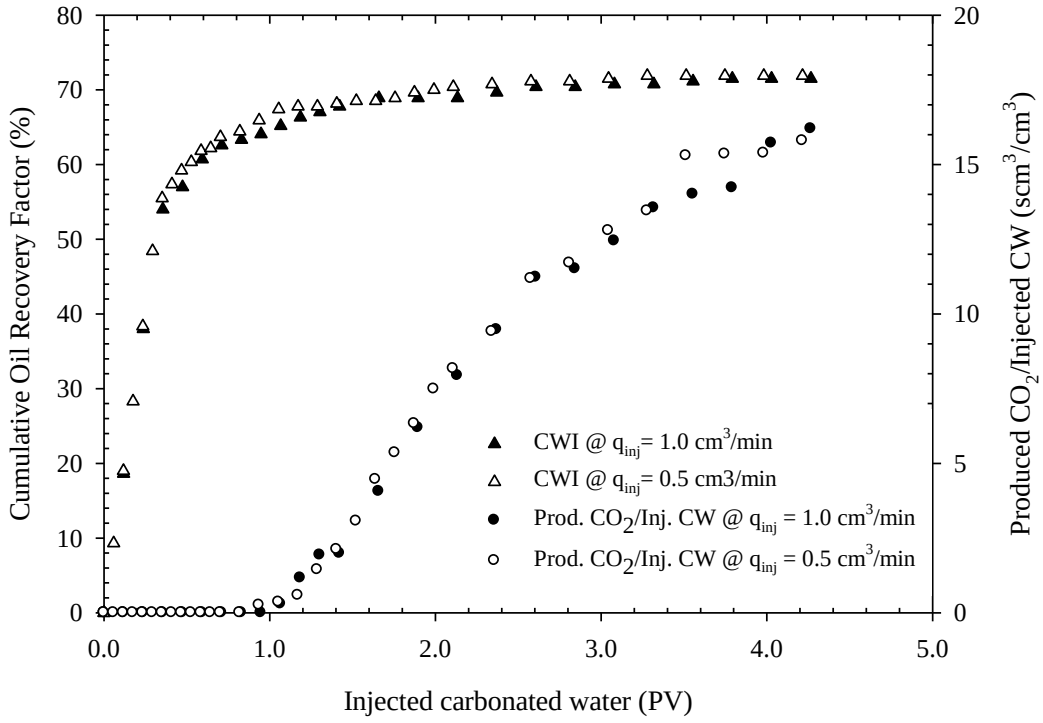

Figure 4.9: Cumulative oil recovery and the ratio of produced CO_2 to injected CW for CW injection rates of q_{inj} = 1.0 cm^3/min and 0.5 cm^3/min, operated at temperature of T = 25 °C and pressure of P = 4.1 MPa (Tests #5 and #10).

it controls the amount of CO_2 in injected brine. Under fixed experimental conditions (i.e., pressure, temperature, and brine salinity), the maximum amount of CO_2 that can be dissolved in the water or brine is a carbonation level of *CL* = 100%, which means that water or brine is completely saturated with CO_2. To study the effect of carbonation level of injected brine, test #10 was conducted with a carbonation level of *CL* = 50%. As shown in **Figure 4.10**, results clearly indicate that this parameter has a significant impact on the recovery performance of CWI and a noticeable reduction of 4.2% in ultimate oil recovery was observed when the carbonation level was reduced from *CL* = 100% to *CL* = 50%.

4.5. Tertiary displacement test results

The performance of tertiary CWI was examined through a series of sand-pack flooding experiments under equivalent operating conditions used in the secondary CWI tests and the results were compared. **Table 4.6** summarizes the experimental conditions, physical characteristics of the porous medium, and the flooding specifications for the conventional WF, secondary CWI, and six tertiary CWI test conducted in this study.

The tertiary CWI tests were carried out at different operating pressures ranging from *P* = 1.4 MPa to 10.3 MPa and two constant operating temperatures of *T* = 25 and 40 °C. Prior to each experiment, the sand-pack was water flooded for about 2 PVs of injected water. Then various tertiary flooding tests at the specific operating conditions were implemented. The objective was to comprehensively examine the effect of various parameters on the

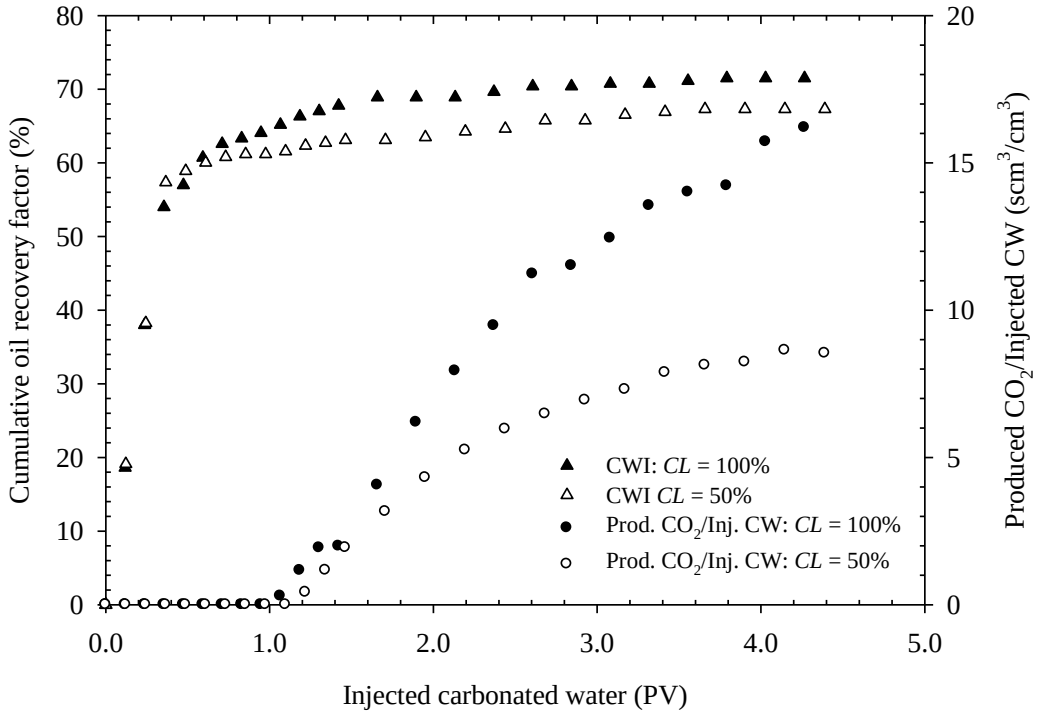

Figure 4.10: Cumulative oil recovery and the ratio of produced CO_2 to injected CW for secondary CWI tests performed with different brine carbonation levels of *CL* = 50% and *CL* = 100%, operated at temperature of *T* = 25 °C and pressure of *P* = 4.1 MPa (Tests #5 and #11).

Table 4.6: Experimental conditions, characteristics of the unconsolidated sand-packs, and flooding specifications for the conventional WF, secondary CWI, and five tertiary CWI tests conducted in this study.

Test	Mode	*CL* (%)	*P* (MPa)	*T* (°C)	q_{inj} (cm^3/min)	χ in Brine (mole/kg)	k_{abs} (mD)	ϕ (%)	S_{wi}	S_{or}
#1	WF	-	4.1	25	1.0	-	5608	27.84	0.384	0.248
#2	SCWI	100	4.1	25	1.0	0.9738	7184	27.58	0.365	0.181
#3	TCWI	100	1.4	25	1.0	0.3572	4136	28.15	0.376	0.223
#4	TCWI	100	4.1	25	1.0	0.9738	4037	26.83	0.370	0.197
#5	TCWI	100	6.9	25	1.0	1.3084	4053	27.14	0.384	0.178
#6	TCWI	100	10.3	25	1.0	1.3188	4106	26.92	0.372	0.174
#7	TCWI	100	4.1	40	1.0	0.7797	4074	27.44	0.380	0.208

tertiary CWI process and evaluate the performance of tertiary CWI compared to secondary CWI process.

4.5.1. Effect of operating pressure

Figure 4.11 shows the calculated oil recovery versus the injected PV of CW or water at four different pressures of P = 1.4, 4.1, 6.9, and 10.3 MPa and constant temperature of T = 25 °C. The oil recovery (RF) is defined as the ratio of the volume of the produced oil at any PVs of the injected fluid to that of the initial original light crude oil in the sand-pack. The tertiary CWI tests were terminated at about 6.0 PVs of injected CW as no more oil was produced and maximum RF was reached. The cumulative oil recovery at water and CO_2 breakthrough time, as well as the cumulative oil recovery for each tertiary CWI test are shown in **Figure 4.12** and summarized in **Table 4.7**. The increased oil recovery with injection pressure presented in **Figures 4.10** and **4.11** were attributed to the increased solubility of CO_2 in the injected brine and consequently in the oil phase. Hence, more CO_2 was dissolved in oil phase through larger contact area between the water and oil, ultimately leading to more favourable oil swelling and viscosity reduction.

The ratio of measured cumulative produced CO_2 to injected carbonated water versus the injected PV of CW is shown in **Figure 4.13**. It can be observed that this ratio is zero before CO_2 breakthrough. However, after CO_2 breakthrough, the ratio increased gradually due to CO_2 production. Moreover, the CO_2 production rate was higher and the plot of produced CO_2 versus PV of injected CW showed significant increases when tertiary CWI was implemented at higher pressures. This can be attributed to the higher CO_2 solubility and CO_2 content in injected CW at higher pressures.

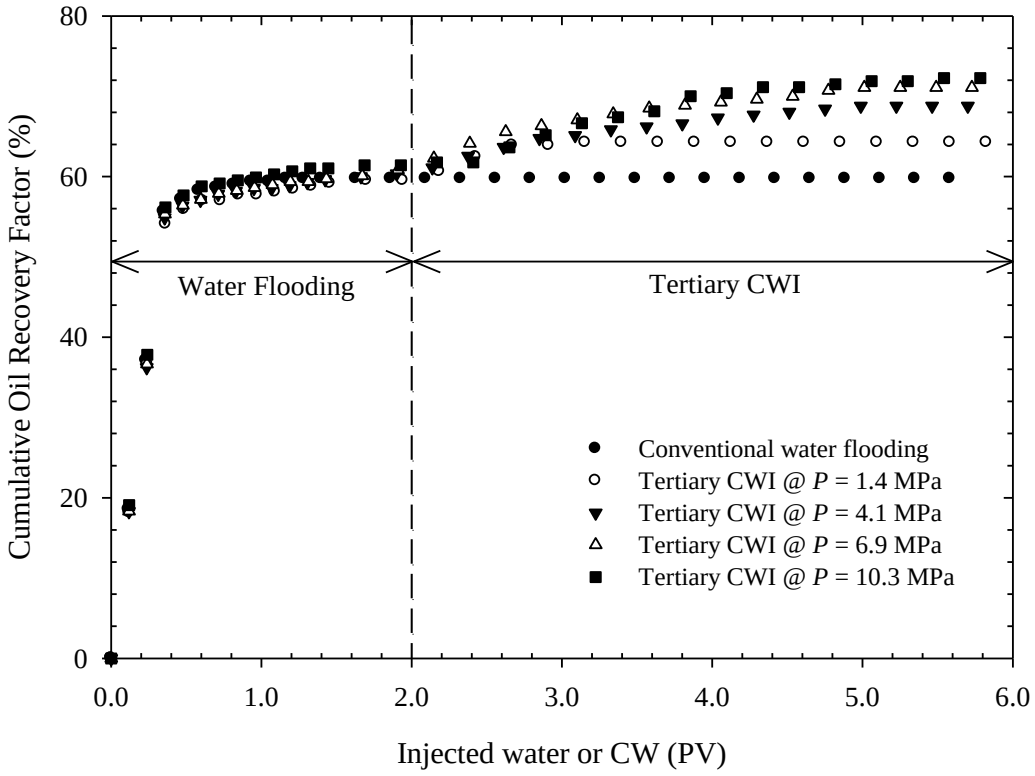

Figure 4.11: Cumulative oil recovery for four tertiary CWI tests and the conventional WF (base case) at various operating pressures and constant temperature of T = 25 °C.

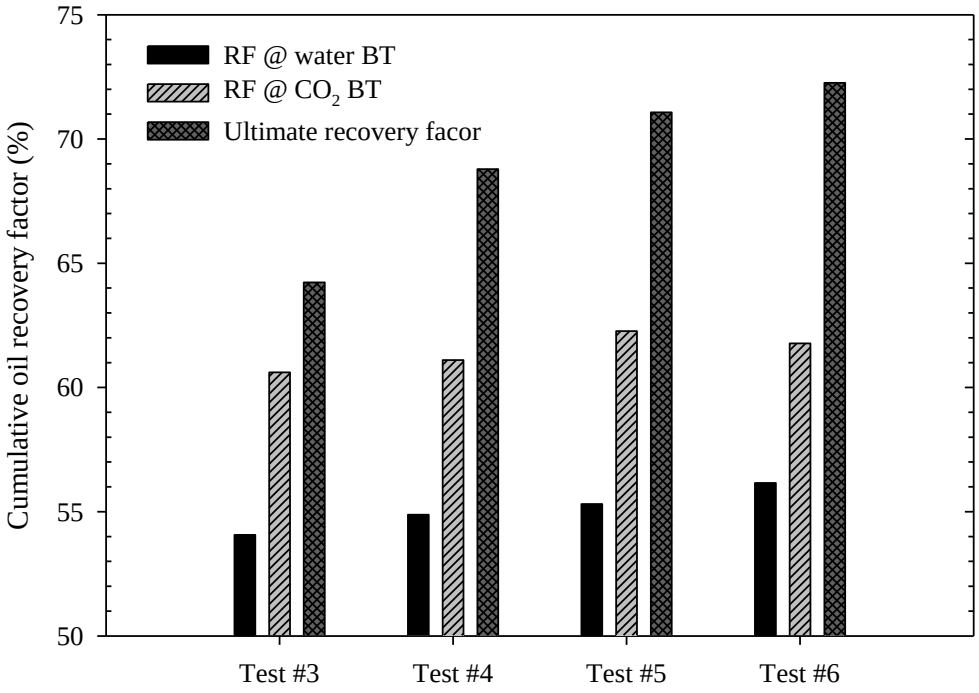

Figure 4.12: Comparison of recovery factors at water and CO_2 breakthrough times as well as ultimate recovery factor for different tertiary CWI tests conducted at constant temperature of T = 25 °C and various pressures of P = 1.4 MPa (test#3), 4.1 MPa (test#4), 6.9 MPa (test#5), and 10.3 MPa (test#6).

Table 4.7: Ultimate oil recovery factors, Recoveries at water and CO_2 breakthrough times, and recovery improvements over conventional waterflooding for the secondary CWI and five tertiary CWI conducted at various operating pressures and temperatures of T = 25 °C and 40 °C.

Test	Mode	P (MPa)	T (°C)	Oil RF at Water BT (%)	Oil RF at CO_2 BT (%)	Ultimate oil RF (%)	RF Improvement* (%)
#1	WF	4.1	25	57.14	-	59.74	-
#2	SCWI	4.1	25	56.98	64.06	71.51	11.77
#3	TCWI	1.4	25	54.07	60.61	64.23	4.49
#4	TCWI	4.1	25	54.88	61.10	68.79	9.05
#5	TCWI	6.9	25	55.31	62.27	71.07	11.33
#6	TCWI	10.3	25	56.16	61.77	72.26	12.52
#7	TCWI	6.9	40	54.86	59.58	66.48	6.74

* RF improvement is taken as the difference between RF for base case conventional WF and that for each CWI test.

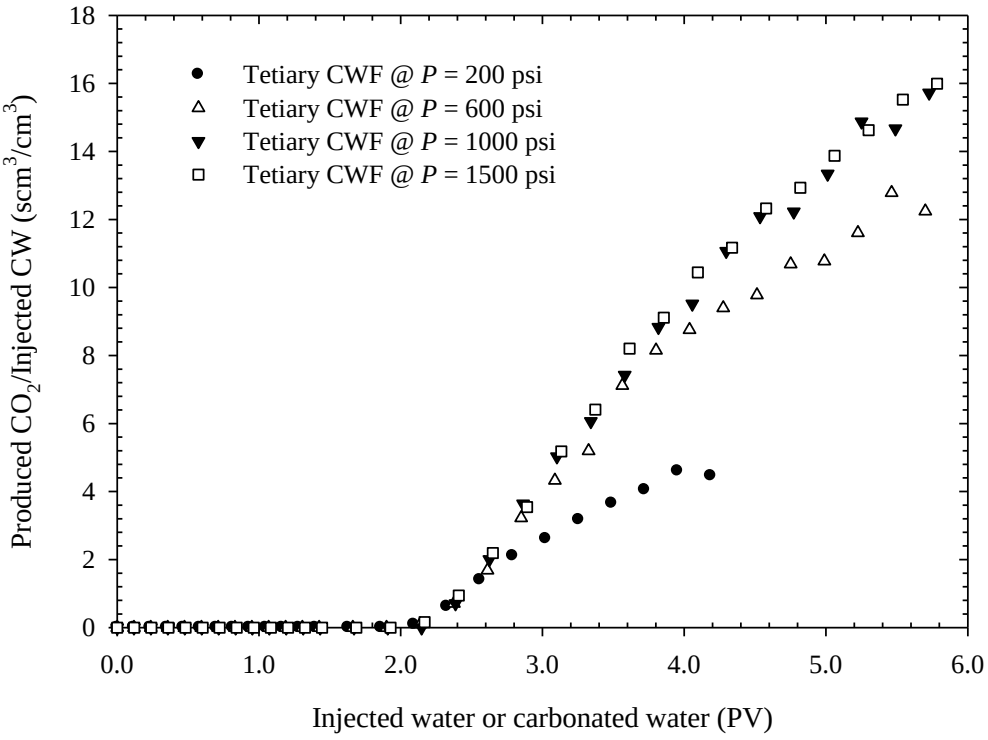

Figure 4.13: The ratio of produced CO_2 to injected CW for four tertiary CWI tests at different pressures and constant temperature of T = 25 °C.

Cumulative oil recovery and CO_2 solubility in brine as a function of experimental pressure are plotted simultaneously in **Figure 4.14**. This graph depicts that when the injection pressure was less than about P = 5.6 MPa, the ultimate oil RF increased considerably because of reduced oil viscosity and oil swelling as a result of an increased CO_2 solubility in the injected brine and subsequently in the oil phase. Furthermore, the oil RF increased marginally when the injection pressure exceeded the pressure of P = 5.6 MPa. This is a consequence of the insignificant increase in CO_2 solubility when pressure nears $P > 5.6$ MPa.

In addition, the sand particles were analysed under microscope camera in order to observe possible evidence of asphaltene precipitations. The observation has been performed for each of the CWI sand-pack flooding tests and no indication of asphaltene precipitation were observed. Therefore, it has been concluded that for the experimental conditions and fluid characteristics of this study, the CWI process has been proceed without any asphaltene precipitations.

4.5.2. Effect of operating temperature

Figure 4.15 shows the measured oil RF for tertiary CWI versus PV of injected CW at the pressure of P = 4.1 MPa and two different temperatures of T = 27 °C and 40 °C. It was found that tertiary CW flooding performed at a temperature of T = 40 °C resulted in a lower ultimate oil RF of 66.48% compared to RF of 68.79% at the temperature of T = 25 °C. This was because at a constant pressure, a relatively smaller amount of CO_2 dissolved in the brine at T = 40 °C (i.e., χ_b = 0.7303 mole/kg) compared to the solubility of χ_b = 0.9775 mole/kg at temperature of 25°C, resulting in a difference in CO_2 transfer to the oil phase in the sand-pack. In addition, the ratio of produced CO_2

to injected CW for two operating temperatures of T = 25 °C and 40 °C is presented in Figure 4.15.

4.5.3. Effect of carbonation level

Carbonation level, *CL*, in this study is defined as the ratio of the amount of dissolved CO_2 to the maximum amount of CO_2 that can be dissolved in water or brine at specific conditions. Under constant experimental conditions (i.e., pressure, temperature, and brine salinity), the maximum amount of CO_2 that can be dissolved in the water or brine is a carbonation level of *CL* = 100%. **Figure 4.16** presents the plot of cumulative oil recovery together with the ratio of produced CO_2 to injected CW for two different carbonation levels of *CL* = 50% and 100% at constant operating pressure and temperature of P = 4.1 MPa and T = 25 °C, respectively. As observed, the ultimate recovery was reduced from 68.8% to 66.8% when the carbonation level was decreased from *CL* = 100% to 50%.

This reduction in RF was attributed to the lower amount of CO_2 delivered to the sand-pack when the maximum CO_2 solubility was reduced to half in the In addition, the amount of produced CO_2 is almost double for the carbonation level *CL*=100% compared to that at the lower carbonation level of *CL* = 50%.

4.6. Tertiary vs. secondary CWI

Figures 4.17 and **4.18** compare oil recovery of CWI in secondary and tertiary modes at a pressure of P = 4.1 MPa and temperature of T = 25 °C. Since the secondary CWI tests were conducted up to about 4 PVs, the recovery factor curve was extended by a dashed line allow comparison with the tertiary CWI.

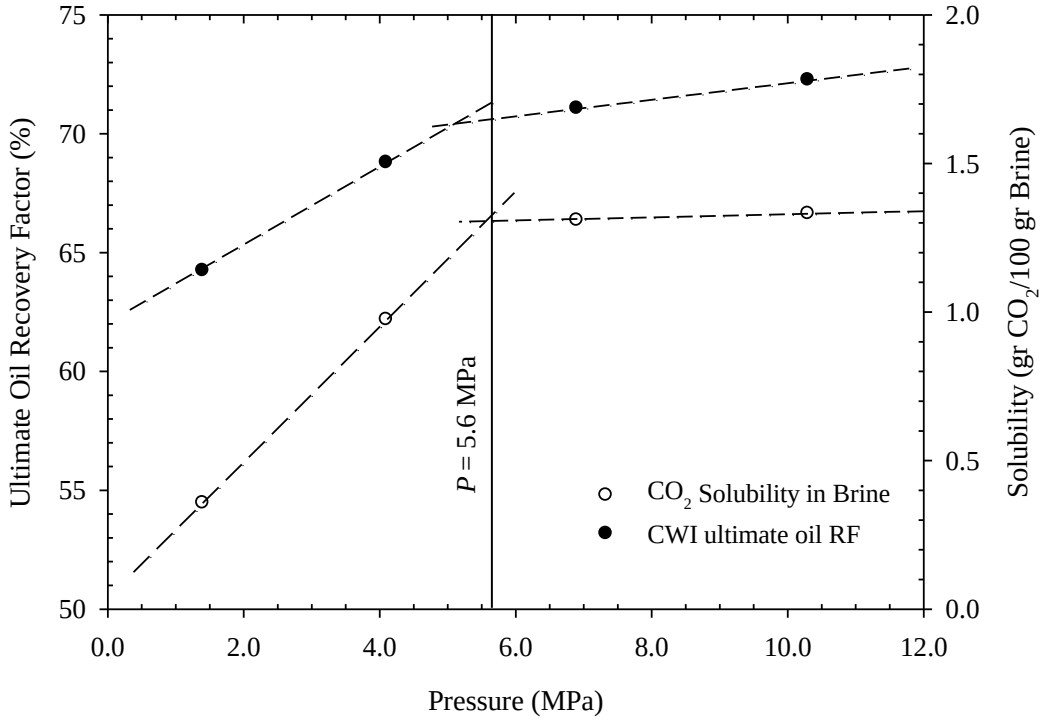

Figure 4.14: Cumulative oil recovery and CO_2 solubility in brine as a function of pressure for four tertiary CWI at constant temperature of T = 25 °C and various pressures.

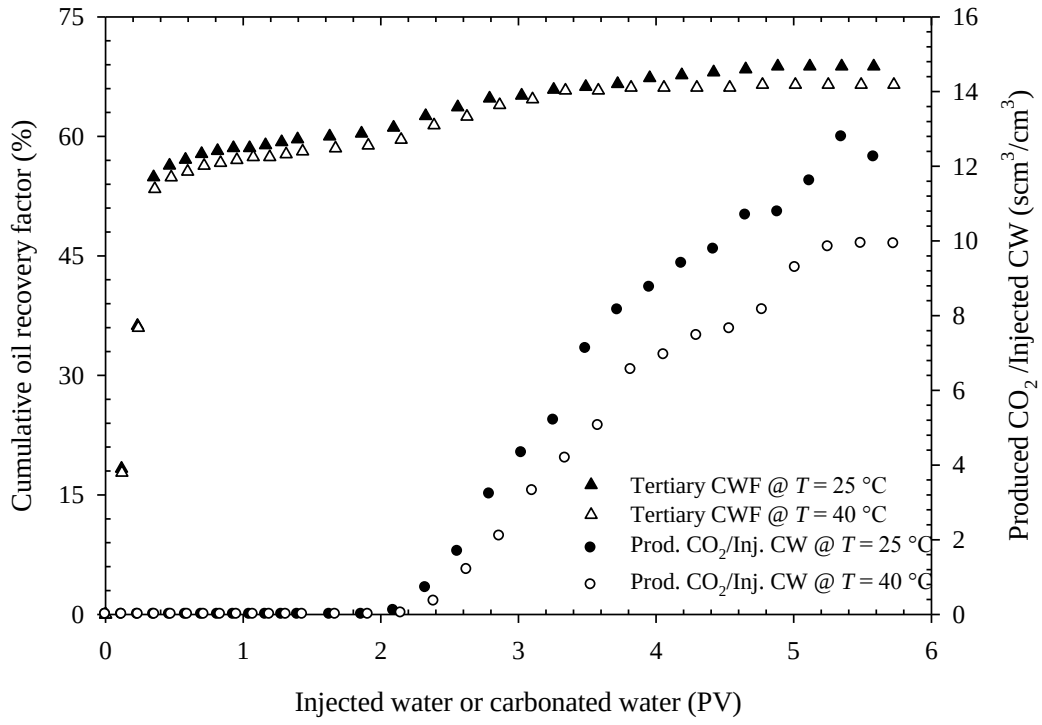

Figure 4.15: Cumulative oil recovery and the ratio of produced CO_2 to injected CW for two tertiary CWI tests at constant pressure of P = 4.1 MPa and two operating temperatures of T = 25 and 40 °C.

It was observed that CWI in the secondary mode resulted in higher oil recovery of about 2.7% compared to the tertiary mode. This was because in the tertiary CWI, the injected CW followsed the previously flooded water path (initial water flooding) due to more a favourable mobility ratio. Therefore, a lower contact area between the CW and the oil phase was obtained when CW was injected in tertiary mode and a higher in-situ water saturation.Hence, according to Fick's Law of diffusion, with less contact area, less CO_2 is conveyed to the originally in-place oil, from the injected CW. This resulted in lower oil swelling and viscosity reduction which are two main mechanisms of oil recovery in CWI process.

In addition, the time of interface contact is higher in secondary CWI because the injection of carbonated water started from the beginning of the flooding tests. Thus, CO_2 mass transfer from brine to the oil phase lasted longer and more CO_2 diffuses to the oil layer, therefore the oil swelling effect and viscosity reduction are more noticeable in secondary CWI compared to the tertiary CWI.

4.7. CO_2 storage during CWI

It is obvious that the amount of CO_2 that have been stored inside the reservoir might not be substantial compared to CO_2 flooding. However, in large scales, it would be beneficial to enhance the oil recovery while storing even a portion of injected CO_2. It is believed that applying CWI as a means of improved secondary oil recovery is also valuable in terms of a solution to climate change and global warning issues. Moreover, in some areas the amount of captured CO_2 is very limited and it is not economically feasible to transport it to other CO_2 injection sites. Therefore, improving the oil recovery together

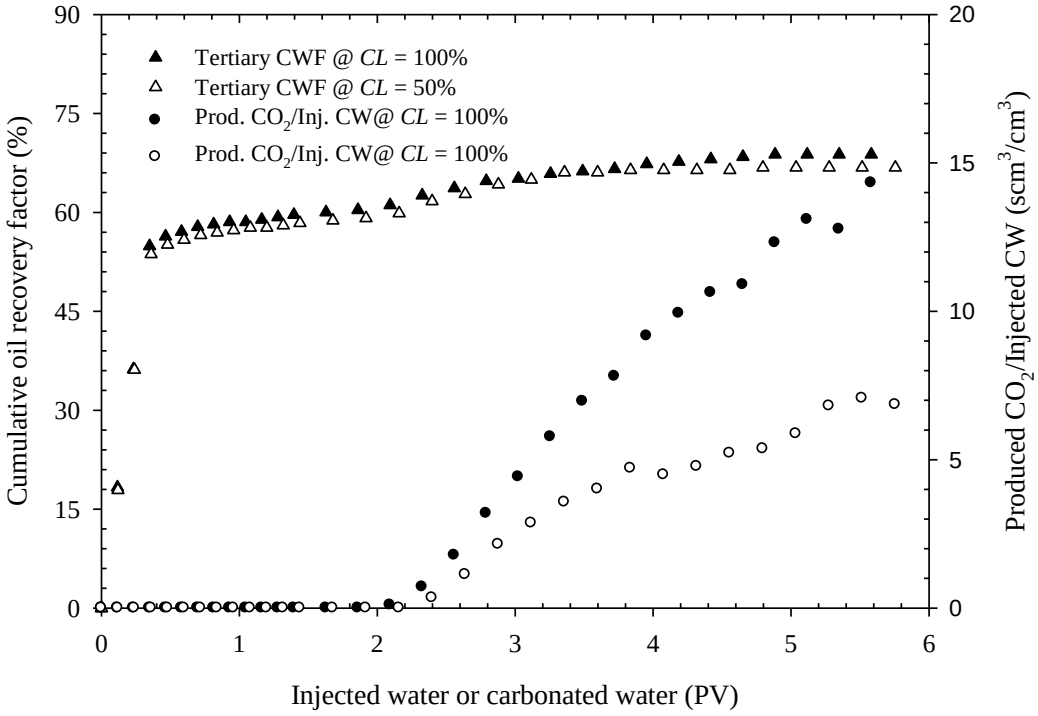

Figure 4.16: Cumulative oil recovery and the ratio of produced CO_2 to injected CW for tertiary CWI tests performed with different brine carbonation levels of *CL* = 50% and *CL* = 100%, operated at temperature of *T* = 25 °C and pressure of *P* = 4.1 MPa.

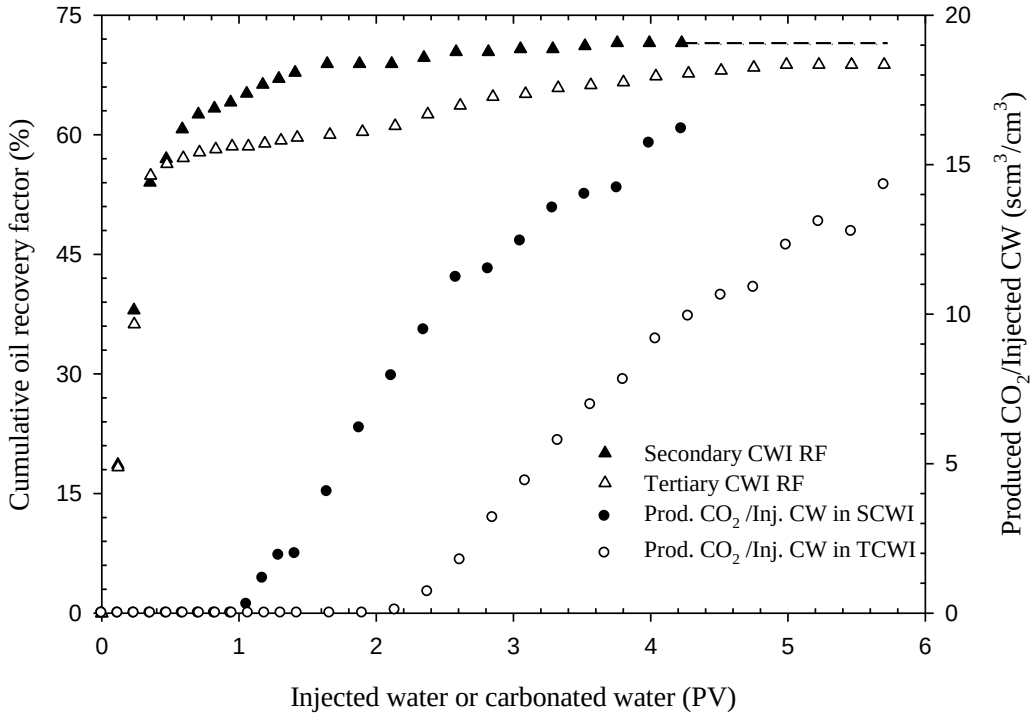

Figure 4.17: Cumulative oil recovery and the ratio of produced CO_2 to injected CW for secondary and tertiary CWI operated at temperature of T = 25 °C and pressure of P = 4.1 MPa.

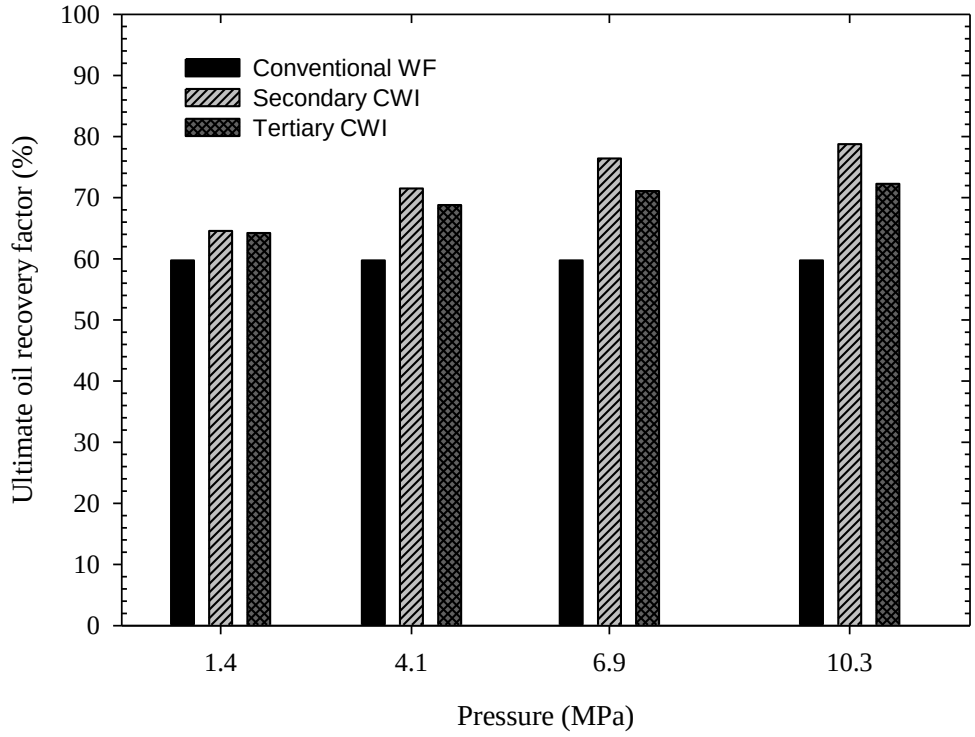

Figure 4.18: Comparison of the ultimate oil recovery factors for conventional water flooding, secondary CWI, and tertiary CWI tests conducted at various operating pressures and constant temperature of T = 25 °C.

with storing the locally accumulated CO_2 is considered as the key advantage of utilizing CWI.

In this study, CWI process was found to have great potential to permanently store injected CO_2 in oil reservoirs while substantially improving oil recovery. **Figure 4.19** shows graphs of the amount of CO_2 that was stored in the reservoir during the tertiary CWI process for different operating pressures. It was observed that the CO_2 storage process initiates at about 1 PV when carbonated water was injected and the amount of stored CO_2 increased considerably for a while and then remained the same for the rest of the CWI process. At this point, both the oil recovery and CO_2 storage flattened because no more CO_2 could be dissolved into the residual oil and the entire injected CO_2 from CW flows to the production side because the porous medium had accepted its maximum CO_2 capacity. It was also observed that the experimental pressure increased with higher CO_2 solubility in both the oil and brine phases as depicted in **Figure 4.20**. This figure clearly shows that cumulative amount of injected, produced, and stored CO_2 increased as the experimental pressure increased. However, the improvement in CO_2 storage capacity was less effective when the operating pressure was increased from P = 6.9 to 10.3 MPa, as discussed earlier, the solubility of CO_2 in brine increased only slightly at higher pressures. **Table 4.8** summarizes the total amount of CO_2 that was injected, produced, stored, and the CO_2 stored to injected ratio (SIR) for all CWI tests conducted in this study. CO_2 SIR is defined as the fraction of injected CO_2 that has been stored in the reservoir. The CO_2 SIR values were recorded when no more oil was produced for each CWI test. It is found that the SIR values are in the range of 40.7–47.1% for all CWI tests

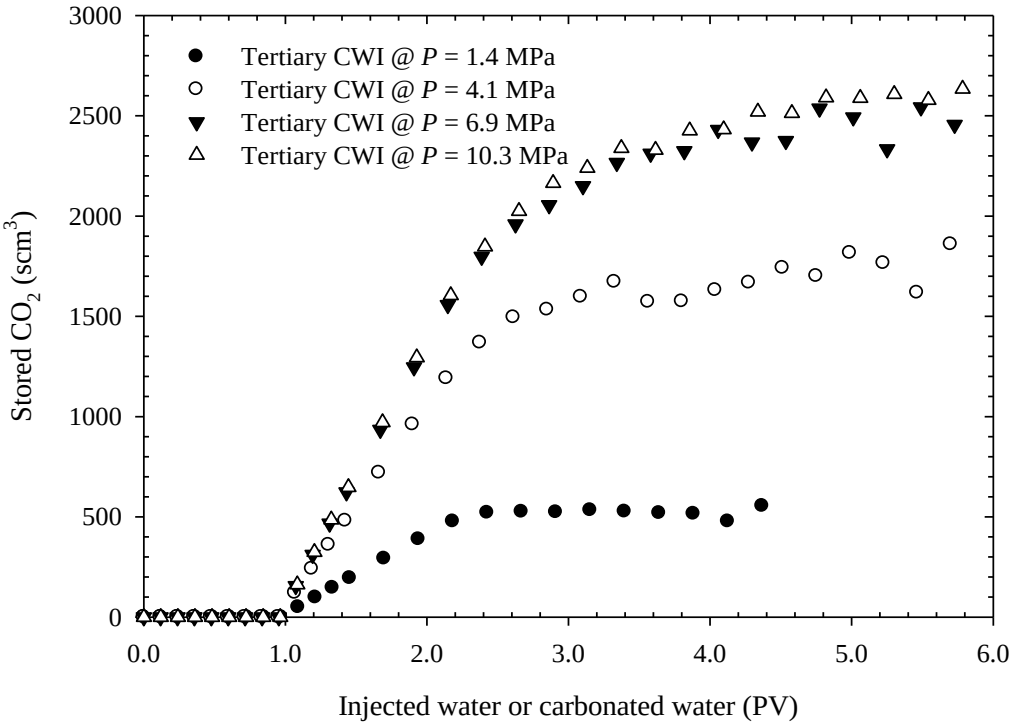

Figure 4.19: The cumulative volume of the stored CO_2 in the reservoir at the end of four tertiary CWI tests at various pressures and constant temperature of T = 25 °C.

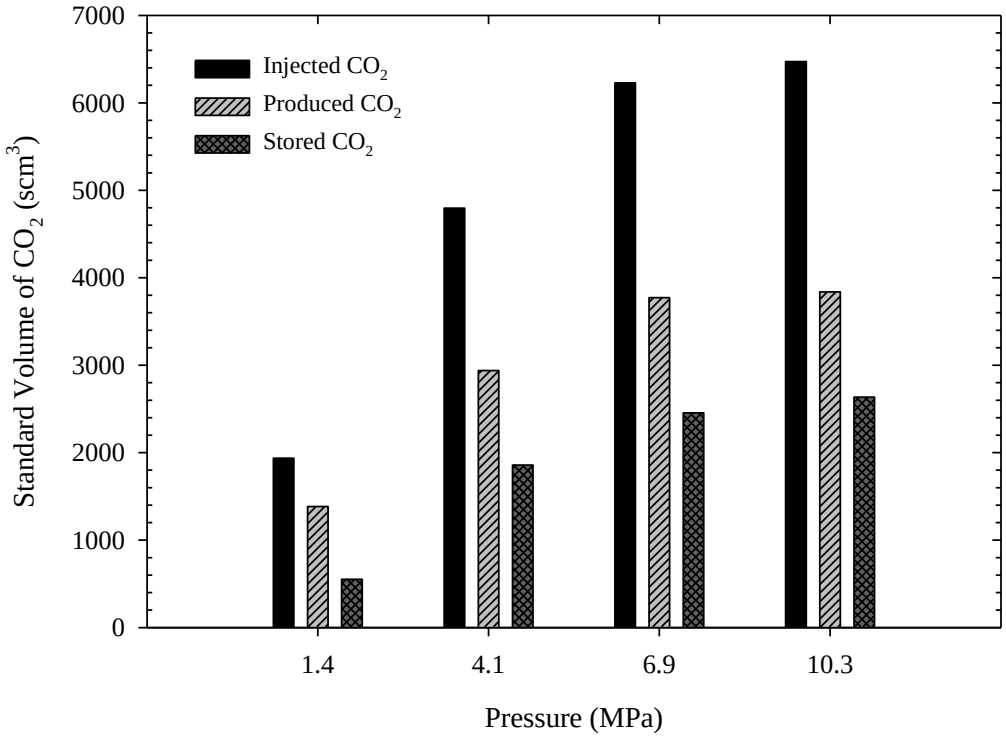

Figure 4.20: Total volume of CO_2 injected, produced, and stored at the end of tertiary CWI (approximately 5.7 PV of brine was injected) at various operating pressures and constant temperature of T = 25 °C.

Table 4.8: Total amount of injected, produced, and stored CO_2 as well as the CO_2 SIR ratio for seven CWI tests carried out in this study.

Test	Mode	*CL* (%)	*P* (MPa)	*T* (°C)	Injected CO_2 (cm^3)	Produced CO_2 (cm^3)	Stored CO_2 (cm^3)	CO_2 SIR (%)
#2	SCWI	100	4.1	25	3838	2275	1563	40.7
#3	TCWI	100	1.4	25	871	339	532	61.1
#4	TCWI	100	4.1	25	4077	2262	1815	44.5
#5	TCWI	100	6.9	25	5294	2801	2493	47.1
#6	TCWI	100	10.3	25	6148	3571	2577	41.9
#7	TCWI	100	6.9	40	2867	1631	1236	43.1
#8	TCWI	50	6.9	25	1799	991	808	44.9

except tertiary CWI conducted at P = 1.4 MPa and T = 25 °C which was found to be 61.1%. This was be attributed to the very limited amount of CO_2 in the injected water because of low CO_2 solubility at the pressure of P = 1.4 MPa (i.e., χ = 0.3572 mole/kg). Therefore, the residual oil and brine in the reservoir were able to maintain most of the injected CO_2 and consequently higher CO_2 SIR was recorded.

4.8. Chapter summary

In total, seventeen sand-pack flooding tests, including the base case conventional WF, ten secondary CWI, and six tertiary CWI tests were carried out at various operating pressures, two operating temperatures, two CW injection rates, and two CW carbonation levels. A mixture of light crude oil samples from the Bakken formation with viscosity of μ_o = 2.76 and 2.0 wt.% NaCl brine were prepared as test fluids. Flooding experiments were performed on an artificial porous medium which was unconsolidated silica sands that were carefully packed by following a prescribed procedure. The effects of operating pressure, temperature, CW injection rate, and carbonation level of the injected CW on the performance of both secondary and tertiary CWI were systematically investigated throughout this study. Furthermore, the performance of secondary CWI was compared with that of tertiary CWI under consistent operating conditions. The operating pressures ranged from P = 0.7 MPa to 10.3 MPa and the tests were carried out in an air bath set to constant temperature of T = 25 °C or 40 °C. Moreover, the tests were conducted in both secondary and tertiary modes to investigate the effect of injection scheme on the performance of CWI on oil recovery and CO_2 storage. The flooding test results obtained

in this study revealed that CWI could be used to significantly improve oil recovery techniques in light oil systems as well as permanently store CO_2 underground.

CHAPTER FIVE: Numerical simulation of CWI

In this chapter, a comprehensive and systematic numerical simulation approach was taken to provide historical models to verify the actual sand-pack flooding tests that studied various parameters affecting the performance of carbonated water injection (CWI) in a light oil system. During this study, two groups of laboratory CWI sand-pack flooding experiments were conducted for secondary and tertiary scenarios. The experimental temperatures were T = 25 and 40 ºC and the operating pressure was ranged from P = 0.7–10.3 MPa. The objectives of this chapter are primarily to provide EOS-base data for the lab-scale PVT tests, including oil and brine characteristics, solubility, and saturation pressure parameters. Thereafter, the PR-EOS was used as to construct a fluid model for incorporation into the compositional simulation model in order to simulate/verify the lab-scale sand-pack flooding tests.

5.1. Introduction

An equation representing a compositional phase reservoir simulation was constructed to reproduce and evaluate the recovery performance of the experimental carbonated water injection test results. A sand-pack model was developed to simulate the parameters of the phase flooding system used to investigate the fluid characterization and rock-fluid properties, and inlet and outlet placement design representing the respective model parameters used in the CWI test studies. These are discussed in detail in this chapter, leading to the complete compositional simulation model for evaluation of the performance of the CWI process and sensitivity studies investigated in this study.

5.2. Reservoir model construction

The first step in the development of a numerical simulation model was to construct the reservoir grid system, which was a 3-dimensional cylindrical model. The model was constructed using geometry representative of the cylindrical laboratory sand-pack physical model used in this study. The model construction tool, BUILDER, from CMG, together with the equation-of-state (EOS) compositional simulator, GEM, was utilized for this purpose. For simplification, the conventional Cartesian grid system was established without corner point geometry or local grid refinement. The model was constructed with 100 blocks in the X-direction, 10 blocks in the Y-direction and the 10 layers in the Z-direction (depth) to constitute a total of 10,000 blocks. As illustrated in **Figure 5.1**, some of the blocks were eliminated by using the NULL option so that an approximated circular cross section was constructed. The final grid block model contained a total of 8,800 active grid blocks with dimensions of 30.48 cm (length) and 2.54 cm (diameter) in the I-direction and JK-plane, respectively.

Both general and test-specific properties during development of the homogeneous anisotropic reservoir model were adapted from preliminary laboratory measurements and sand-pack flooding characteristics corresponding to each test and are summarized in **Tables 5.1 and 5.2**. Since the ratio of diameter (d_{sp}) to length (l_{sp}) of the sand-pack was relatively small (i.e., d_{sp}/l_{sp} = 0.83) compared to actual reservoir scales and the sand-packing procedure was carried out in the same manner for all directions, it was assumed that the sand-pack was a homogeneous porous medium in all spatial directions. Hence, a constant absolute permeability was assigned for I, J, and K-directions. This was done by implementing equal I- and J-direction permeability values and assigning a factor of one

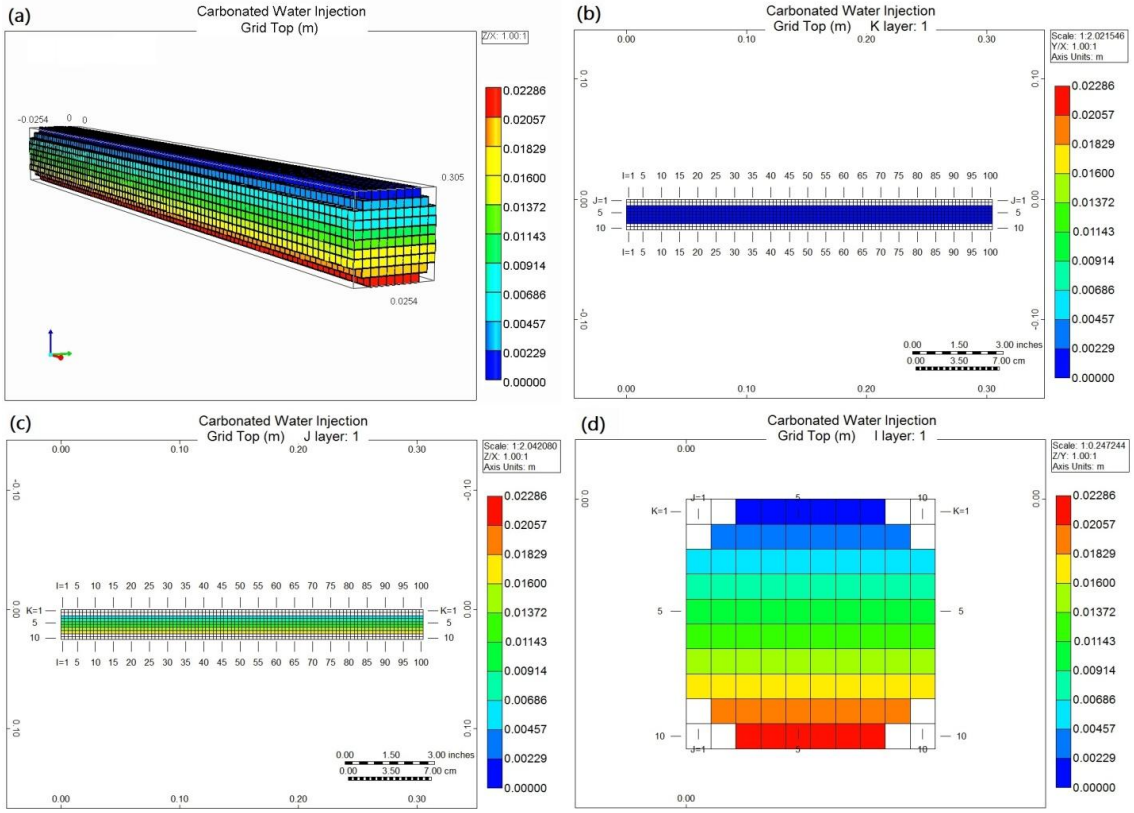

Figure 5.1: 3-Dimentional sand-pack simulation model: (a) 3D view, (b) top view or IJ-plane, (c) side view or IK-plane, and (d) cross-section or JK-plane.

Table 5.1: Experimental conditions, characteristics of the unconsolidated sand-packs, and flooding specifications for the conventional WF and ten secondary CWI tests conducted in this study.

Test	Mode	CL (%)	P (MPa)	T (°C)	q_{inj} (cm^3/min)	χ in Brine (mole/kg)	k_{abs} (mD)	ϕ (%)	S_{wi}	S_{or}
#1	WF	-	4.1	25	1.0	-	5608	27.84	0.384	0.248
#2	SCWI	100	0.7	25	1.0	0.1354	6715	27.91	0.365	0.238
#3	SCWI	100	1.4	25	1.0	0.3572	7190	27.32	0.363	0.226
#4	SCWI	100	2.8	25	1.0	0.7737	7047	27.39	0.371	0.201
#5	SCWI	100	4.1	25	1.0	0.9738	7184	27.58	0.365	0.181
#6	SCWI	100	5.5	25	1.0	1.2523	4320	28.84	0.385	0.155
#7	SCWI	100	6.9	25	1.0	1.3084	4487	27.13	0.365	0.150
#8	SCWI	100	10.3	25	1.0	1.3188	4322	26.61	0.373	0.136
#9	SCWI	100	4.1	40	1.0	0.7797	4320	27.13	0.385	0.186
#10	SCWI	100	4.1	25	0.5	0.9738	7105	27.65	0.372	0.177
#11	SCWI	50	4.1	25	1.0	0.4869	4011	26.54	0.368	0.207

Table 5.2: Experimental conditions, characteristics of the unconsolidated sand-packs, and flooding specifications for the six tertiary CWI tests conducted in this study.

Test	Mode	*CL* (%)	*P* (MPa)	*T* (°C)	q_{inj} (cm^3/min)	χ in Brine (mole/kg)	k_{abs} (mD)	ϕ (%)	S_{wi}	S_{or}
#12	TCWI	100	1.4	25	1.0	0.3572	4136	28.15	0.376	0.223
#13	TCWI	100	4.1	25	1.0	0.9738	4037	26.83	0.370	0.197
#14	TCWI	100	6.9	25	1.0	1.3084	4053	27.14	0.384	0.178
#15	TCWI	100	10.3	25	1.0	1.3188	4106	26.92	0.372	0.174
#16	TCWI	100	4.1	40	1.0	0.7797	4074	27.44	0.380	0.208
#17	TCWI	50	4.1	25	1.0	0.3896	4282	27.33	0.361	0.212

ratio for vertical to horizontal permeability ratio (k_v/k_h = 1). In addition, compressibility of the sand-pack was assumed to be 5×10^{-8} $Psia^{-1}$.

5.3. Reservoir fluids model

Oil recovery through a CO_2-based process proceeds with the involvement of two or more phases (e.g., oil, water, and gas phases) along with the physiochemical interactions within the phases, which are due to mutual interactions of the number of components existing within them. Fluid phases inside the porous medium include crude oil, which typically contain light (e.g., C_1-C_5), intermediate (e.g., C_5-C_{12}) and heavier fractions (e.g., C_{12+}); formation or injection water; and free gas phase, if it exists. For conventional reserves, the extent of various hydrocarbon fractions in the reservoir oil determines the choice of recovery process. From simulations, a larger number of these components (real and/or pseudo-components) require more computational time and data storage capacity. The procedure of combining the components, which constitute the reservoir oil, along with their interaction with CO_2, form an integral part of any reservoir fluid study, especially in the case of solvent-based EOR. Simulation of the compositional phase behaviour of the reservoir fluid allows for variations on the incorporation of the oil components and their interaction coefficients, while providing options for the user to control the combinations considered in the study.

In this study, complex phase equilibria of a Bakken reservoir sample of recovered oil using carbonated water flooding were studied to produce their PVT properties which were compared to the Peng-Robinson Equation of State (PR-EOS). **Table 5.3 and 5.4** summarizes the physical properties of the fluids used in this study: crude oil, synthetic

brine, and high purity CO_2. WinProp^{TM}, a CMG equation of state multiphase equilibrium property software was used to reproduce the observed fluid behaviour and production characteristics, to predict phase behaviour of CO_2/brine and CO_2/oil mixtures and minimum miscibility pressure (MMP) between pure CO_2 and the crude oil sample.

5.4. History matching approach and procedure

The history matched EOS modelwas obtained through the following steps:

- Conducting a gas chromatography test as well as various laboratory PVT experiments using both crude oil and brine samples in order to gather reliable PVT data.
- Incorporationof this compositional and experimental PVT data into CMG's WINPROP^{TM} and adjusting the numerical parameters in order to achieve convergence.
- Tuning of the PR-EOS model by following detailed procedures in order to match the PVT model to the obtained experimental data.
- Exporting the verified EOS model in CMG's GEM^{TM} in order to perform CWI sand-pack flooding simulations.

The experimental data used for carrying out the equation of state modeling consisted of the results from the following laboratory tests:

- Compositional analysis of the Bakken crude oil sample.
- CO_2 solubility measurements at different pressures and temperatures.
- CO_2/oil saturation pressure tests at different temperatures.
- Swelling/extraction test at different temperatures.

Table 5.3: Physical properties of the oil sample used in this study at P_{atm} = 101.1 kPa and T = 25°C.

Property	Value
Molecular weight	223 gr/mol
Density at 101.1 kPa & 25 °C	799 kg/m^3
API Density	44.1 °API
Viscosity at 101.1 kPa & 25 °C	2.76 mPa.s
n-C5 insoluble asphaltene	1.23 wt.%

Table 5.4: The physical properties of the brine sample and CO_2 used in this study at atmospheric pressure (i.e., P_{atm} = 101.3 MPa) and two temperatures of T = 25 °C and 40 °C.

Fluid	Density P_{atm}, 25 °C (kg/m^3)	Density P_{atm}, 40 °C (kg/m^3)	Viscosity P_{atm}, 25 °C (mPa.s)	Viscosity P_{atm}, 40 °C (mPa.s)
Brine	1010.2	1008.2	0.90	0.70
CO_2	1.8093	1.7205	0.0149	0.0156

- CO_2/oil pendant drop IFT test at different temperatures.

Reservoir fluid characterization or EOS tuning for the reproduction of PVT properties was conducted by following a multi-step described in the following sections.

5.4.1. Splitting heavy components (C_{30+}) into the pseudo-components

Since a single heavy fraction lumps thousands of compounds with a carbon number higher than seventeen, the properties of the heavy component C_{30+} were not known precisely, representing the main source of error in the EOS model's predictive accuracy. Therefore, C_{30+} fractions were split into pseudo-components to enhance EOS predictions, as per the procedure suggested by Whitson (1983). Whitson's method used a three-parameter gamma probability function to characterize the molar distribution (mole fraction/molecular weight relation) and physical properties (e.g. specific gravity) of petroleum fractions such as C_{30+}, preserving the molecular weight of the plus fraction.

5.4.2. Lumping or pseudoization of components into a lower number of pseudo-components

This step was performed primarily to minimize the number of components and speed up the simulation run time. The lumping procedure for combining components was carried out in such a way that pseudo-components with similar properties and molecular weight were combined. Several trial regressions were carried out in order to select the best grouping scheme to correspond to the laboratory experiments.

5.4.3. History matching of PVT properties through regression

Experimental data from laboratory measurements, including density and viscosity measurements, gas chromatography analysis, swelling/extraction test, solubility measurement, and minimum miscibility pressure measurement were used in this step. Regression for the corresponding viscosity was based on the Jossi-Stiel-Thodos (JST) correlation and was carried out in a separate regression block. Other experimental data were excluded in this regression run. Several regression runs were necessary to achieve match to the experimental data. Regression variables were chosen to exclude any regression parameters that, judged by inspection and previous experience, could not significantly affect the calculated value of the regression data. Parameters of components used in the regression runs included the following:

a. Critical pressure (P_c)
b. Critical temperature (T_c)
c. Critical volume (V_c)
d. Accentric factor (ω)
e. Volume shifts
f. Interaction parameters between CO_2 and plus components (BIC)

5.5. Initial compositional fluid model

The composition of each of the components that constitute the reservoir fluid, including the mole fraction, molecular weight, and specific gravity of the components, are summarized in **Figure 5.2** and **Table 5.5**. The objective was to numerically reproduce

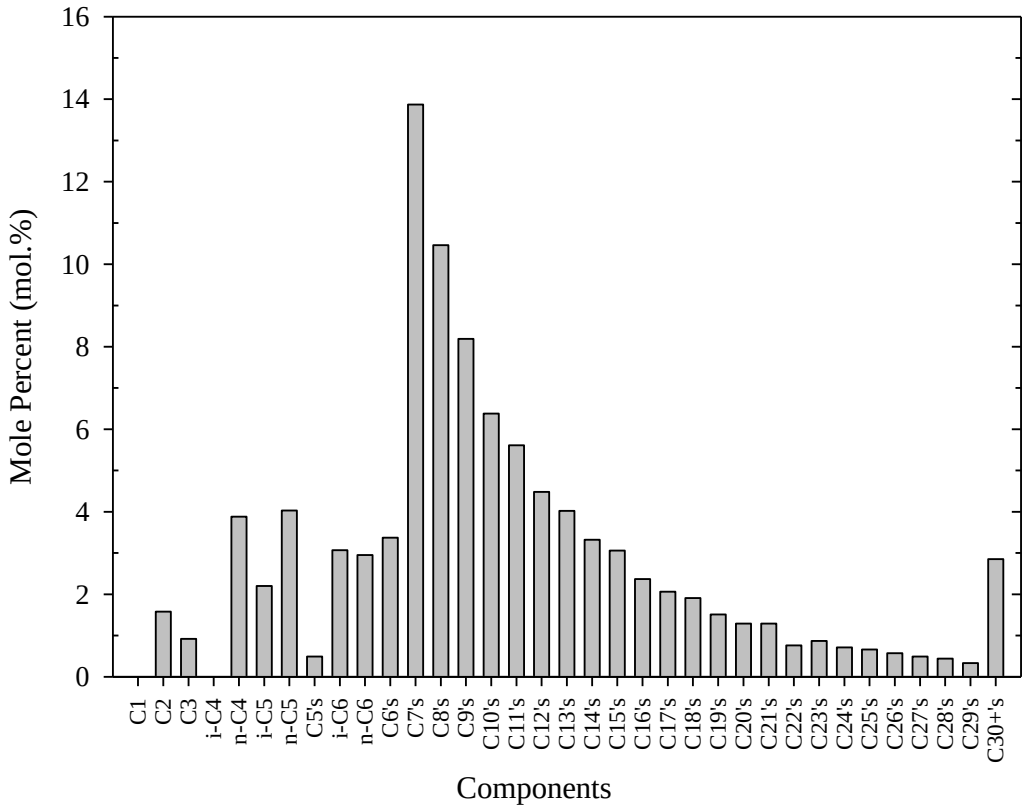

Figure 5.2: Gas Chromatography (GC) compositional analysis result for the Bakken stock tank oil sample used in this study.

Table 5.5: Gas chromatography (GC) compositional analysis of the light crude oil under study at 21°C and atmospheric pressure.

Carbon number	Mole %	Carbon number	Mole %	Carbon number(s)	Mole %
C_1	0	C_{12}'s	4.48	C_{28}'s	0.44
C_2	1.58	C_{13}'s	4.02	C^{29}'s	0.33
C_3	0.92	C_{14}'s	3.32	C_{30+}'s	2.85
i-C_4	0	C_{15}'s	3.06		
n-C_4	3.88	C_{16}'s	2.37	C_1–C_6	22.48
i-C_5	2.20	C_{17}'s	2.06	C_{7+}	77.52
n-C_5	4.03	C_{18}'s	1.91		
C_5's	0.49	C_{19}'s	1.51	C_1–C_{14}	78.82
i-C_6	3.07	C_{20}'s	1.29	C_{15+}	21.18
n-C_6	2.95	C_{21}'s	1.29		
C_6's	3.37	C_{22}'s	0.76	C_1–C_{29}	97.14
C_7's	13.87	C_{23}'s	0.87	C_{30+}	2.86
C_8's	10.46	C_{24}'s	0.71		
C_9's	8.19	C_{25}'s	0.66		
C_{10}'s	6.38	C_{26}'s	0.57	MW (C_{30+})	674.4
C_{11}'s	5.61	C_{27}'s	0.49	SG (C_{30+})	1.212

the PVT properties of the crude oil using thermodynamic multiphase flash calculations and incorporate the corresponding correlations in the CMG's equation of state phase behaviour and fluid property program, WinProp software, to calculate the multi-phase multi-component equilibrium properties. The associated synthetic brine properties, including the salinity, compressibility, viscosity and the density were also simulated using WinProp at the atmospheric reference pressure (i.e., P_{atm} = 101.1 kPa). The CO_2 properties, including density, viscosity, and the various components in oil which are responsible for the solubility and miscibility, were determined using various databases of WinProp (Table 2). Furthermore, minimum miscibility pressure (MMP) between the crude oil sample and CO_2 was simulated at various operating temperatures. **Figure 5.3** depicts the phase envelope of the Bakken crude oil.

5.6. History matching: EOS tuning results

Each of the laboratory experiments used to obtain the fluid properties was first simulated with the PR-EOS without regression analysis. Peng-Robinson (PR) EOS was chosen because it is widely accepted in the industry and it generally yields more accurate and satisfactory volumetric predictions for vapour and liquid phases, rather than using the comparable Soave-Redlich-Kwong (SRK) equation. Afterward, the physical properties obtained from the numerical simulation model without regression were compared with the laboratory PVT data. The comparisons of the laboratory density and viscosity data and the values attained by the preliminary simulation model from WinProp are given in **Figure 5.4**. Saturation pressure, together with the swelling factor curves were also included in the EOS comparisons and the initial simulation results along with

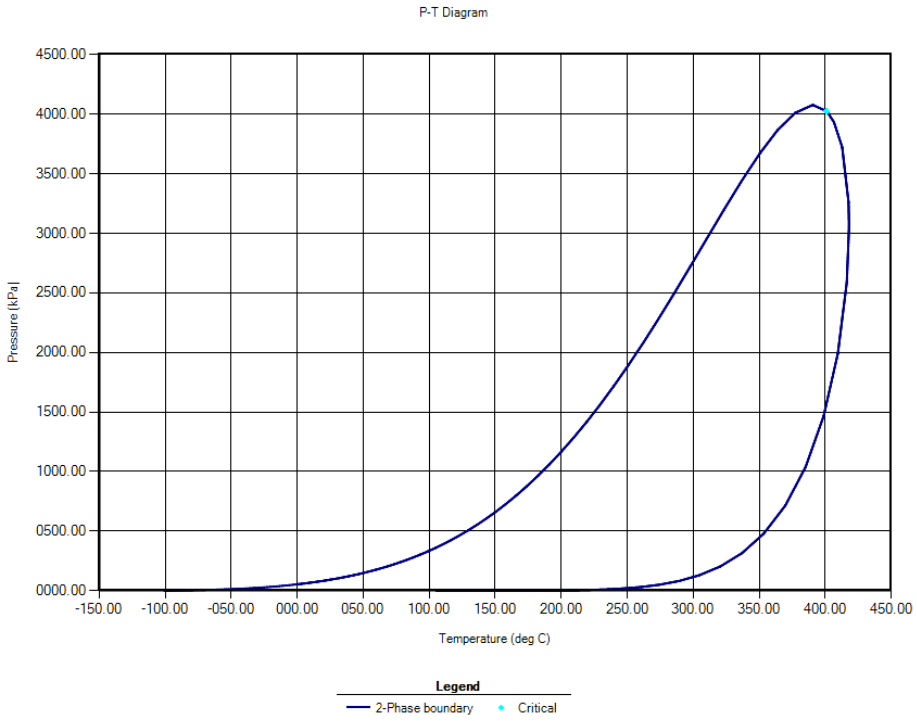

Figure 5.3: initial phase diagram of the Bakken crude oil sample based on the original un-tuned PR-EOS from the WINPROP's database

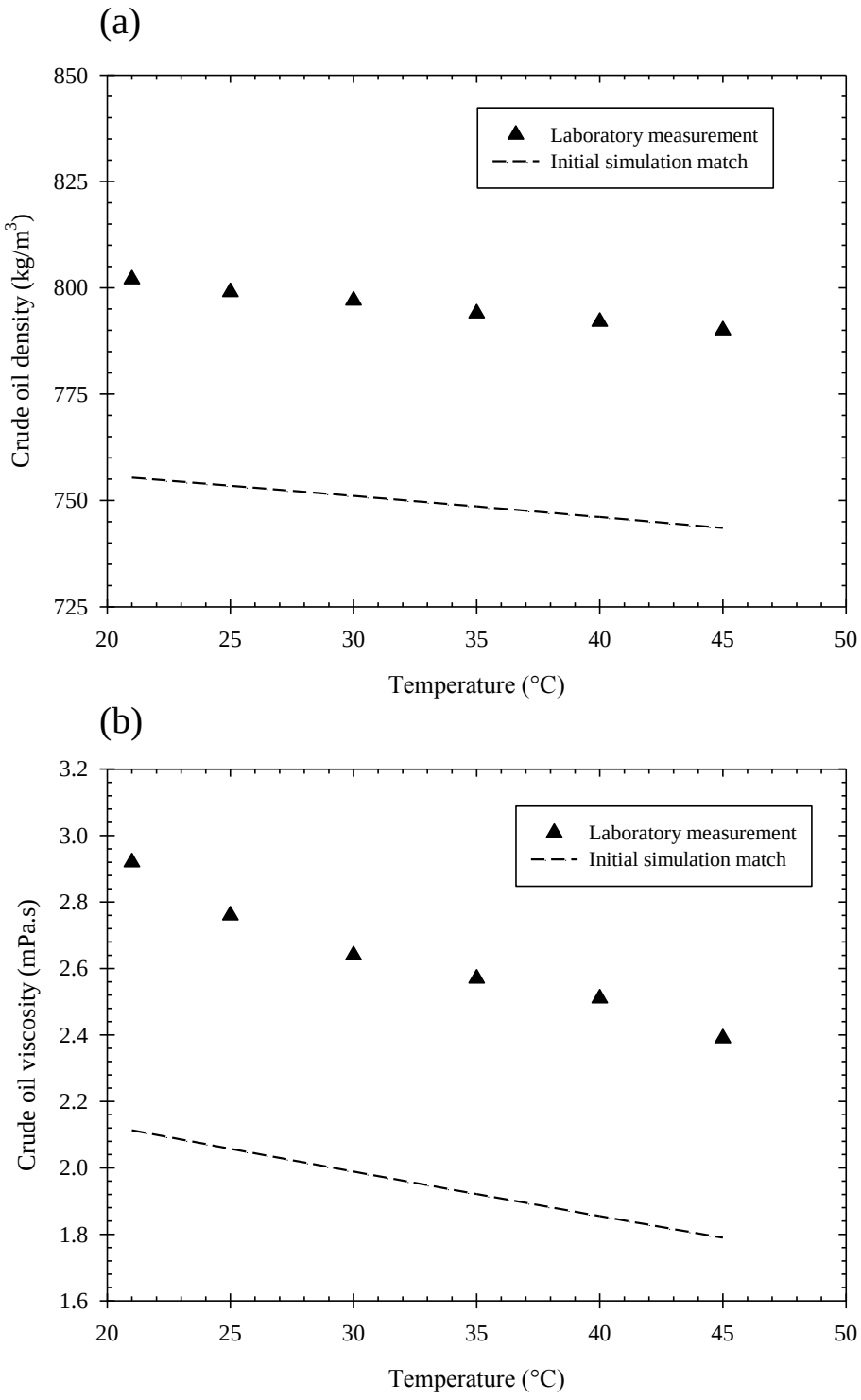

Figure 5.4: Preliminary matches of the crude oil properties: (a) dead oil density (b) dead oil viscosity

the experimental values are depicted in **Figures 5.5 and 5.6**. It is believed that the swelling factor was not only a function of the amount of CO_2 dissolved (i.e., CO_2 solubility), and the size of the oil molecules (Simon and Graue, 1965). Molar weight was also used as a regression parameter to obtain a confidence level in the swelling and saturation pressure calculation. These preliminary results demonstrated that the behaviour of the simulated fluid was being inaccurately reproduced with the basic (i.e., un-tuned) EOS, and the predictions were in poor agreement with the laboratory data. Thus, the EOS parameters needed to more accurately reproduce the behaviour of the reservoir fluid. The next step was adjust and characterize the EOS to more accurately reproduce the PVT experimental results through the previously mentioned multi-step procedure. In order to improve the EOS predictions, the initial fluid model that was constructed with extended composition up to C_{29}, was used and the remaining heavy components were combined as one heavy component (i.e., C_{30+}). Based on the nature of the light crude oil sample used in this study and the relatively low mole percent of C_{30+} (2.86 mol.%), it was decided to keep this fraction as a single component and not split it into pseudo-components. Therefore, by keeping the heavy components, the total number of components of the reservoir fluid remained at 30 components. The properties of this 30-component mixture were used to adjust the EOS by various regression analyses to better fit the PVT experiments. Several regressions were required to achieve reasonable accuracy during the EOS tuning process. For each regression, an appropriate set of parameters was selected to be changed based on previous simulation experiences, along with the corresponding uncertainties for each property. Finally, 21 parameters were selected for adjustment, including critical pressure (P_c), critical temperature (T_c), critical volume (v_c), and

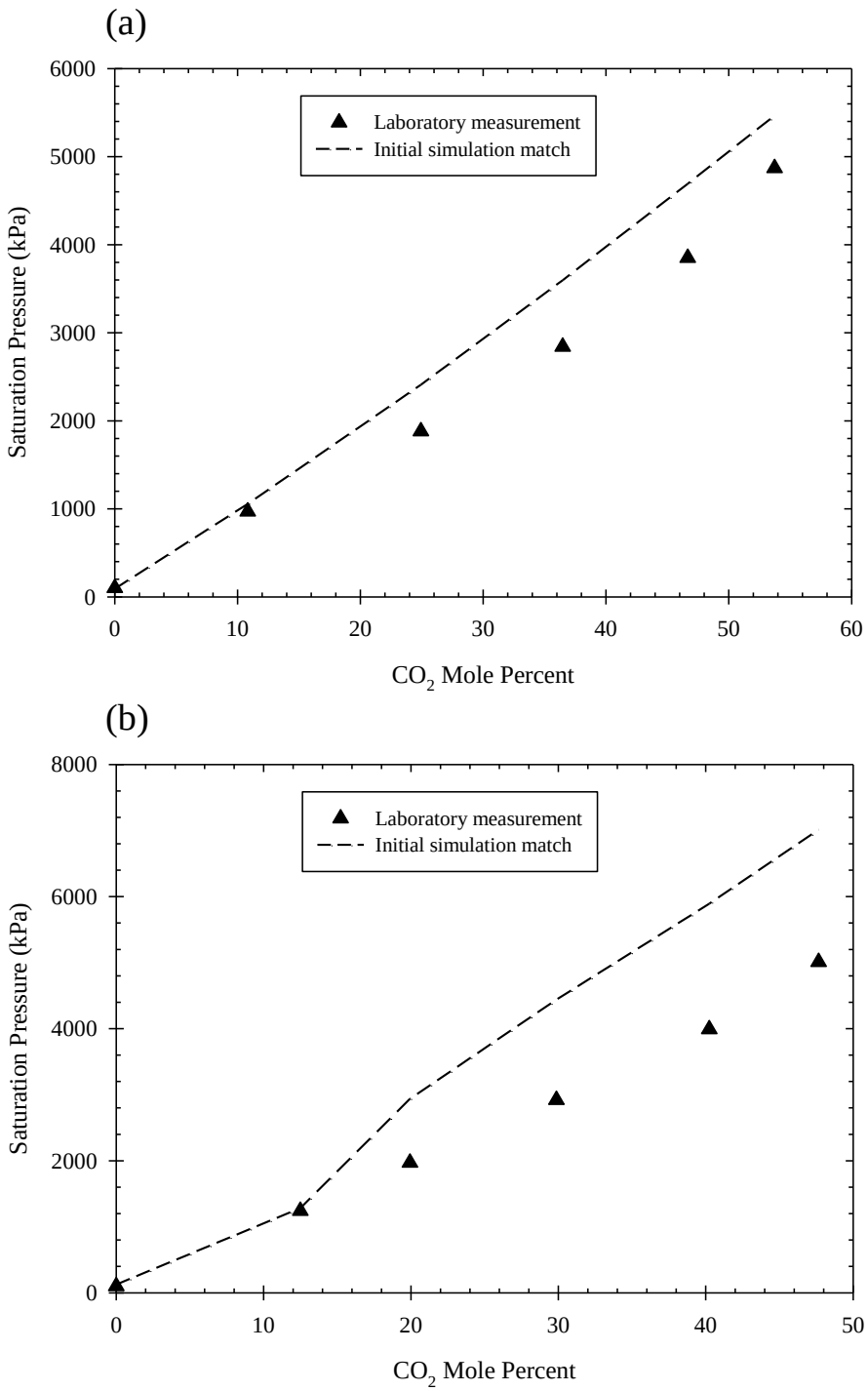

Figure 5.5: Preliminary matches of the saturation pressure of the crude oil–CO_2 mixture: (a) T = 25 °C (b) T = 40 °C

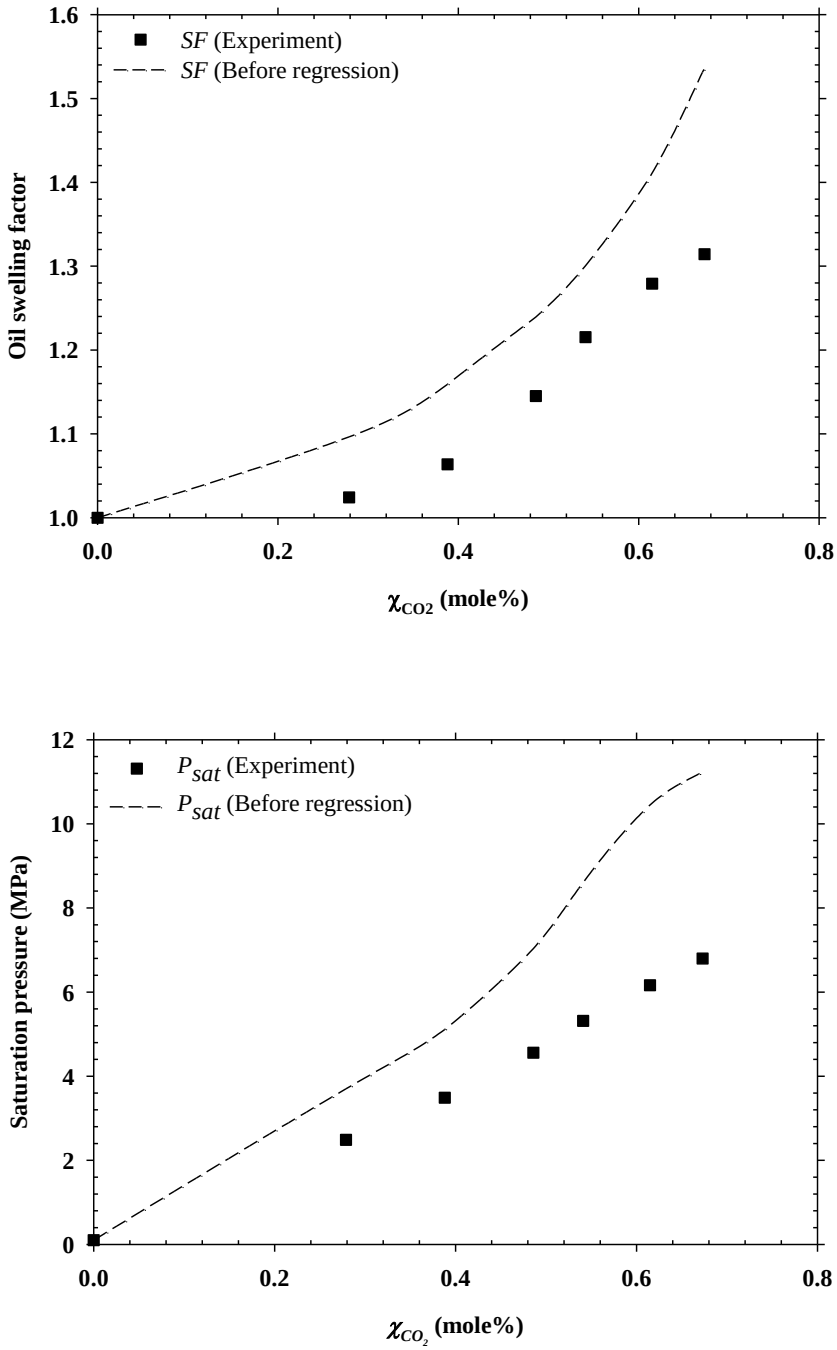

Figure 5.6: Preliminary matches of the oil swelling factor and saturation pressure at T = 25 °C

molecular weight (MW) of the heavy pseudo-components. Also, binary interaction coefficients (BICs) between the carbon dioxide and the heavier hydrocarbon fraction were modified.

As a final step, regression analyses were performed against both the oil and gas viscosity to ensure an accurate estimation of reservoir fluid viscosity. The mixing rule exponent parameters, polynomial coefficients and the v_c properties of the plus components and the C_1 of the JST correlation were used in the viscosity regression.

Once a satisfactory match of all the experimental data was obtained, the 30-component EOS model required grouping into a reduced pseudo-component EOS model to be acceptable for a compositional reservoir simulation. Performing these steps minimizes the computational time required to solve the numerical equations through iterations, and hence, the numerical complexity of the simulation. The existing components were lumped to form new pseudo-components. Using the regression parameters, these newly-formed pseudo-components were then fine-tuned for the more accurate matching to the EOS properties. This process was repeated a number of times to select the best groupings at each stage in the pseudoization process and the final properties are summarized in **Table 5.6**.

HC–HC and CO_2–HC interaction coefficients of the final fluid model are shown in **Table 5.7**. **Figures 5.7-5.10** shows very reasonable and accurate matches of the EOS model with the laboratory experimental properties obtained. They represent the tuned EOS model for use in the compositional reservoir simulation. As can be seen, the results provided very good predictions when compared against the test observations. This EOS was accepted for use in the simulation.

Table 5.6: Final simulation output for major properties of the six pseudo-components of the crude oil under study.

C_p	C_1–C_3	C_4–C_8	C_9–C_{15}	C_{16}–C_{21}	C_{22}–C_{29}	C_{30+}
Composition (mole %)	2.5	44.3	35.1	10.4	4.84	2.85
P_c (MPa)	4.646	3.216	2.313	1.581	1.214	1.698
T_c (K)	330.780	522.356	650.857	761.420	831.067	805.504
ω	0.11787	0.29143	0.49354	0.75936	0.96131	1.12992
MW (gr/mol)	35.23	89.54	152.78	251.30	334.78	674.40
Volume shift	0.00000	0.00255	0.04699	0.11797	0.19314	-0.77194
SG	0.413	0.702	0.799	0.857	0.888	1.212
δ_{CO2}	0.122667	0.111421	0.152121	0.15	0.15	0.059167

Table 5.7: Binary interaction coefficients (BICs) between different hydrocarbon psoudo-components and CO_2.

Interaction Coefficients							
Component	CO_2	C_1–C_3	C_4–C_8	C_9–C_{15}	C_{16}–C_{21}	C_{22}–C_{29}	C_{30+}
CO_2	-	0.122	0.111	0.152	0.15	0.15	0.0592
C_1–C_3	0.122	-	0.113	0.225	0.349	0.451	0.503
C_4–C_8	0.111	0.113	-	0.008	0.020	0.030	0.035
C_9–C_{15}	0.152	0.225	0.008	-	0.004	0.008	0.011
C_{16}–C_{21}	0.15	0.349	0.020	0.004	-	0.001	0.002
C_{22}–C_{29}	0.15	0.451	0.030	0.008	0.001	-	0.0002
C_{30+}	0.059	0.503	0.035	0.011	0.002	0.0002	-

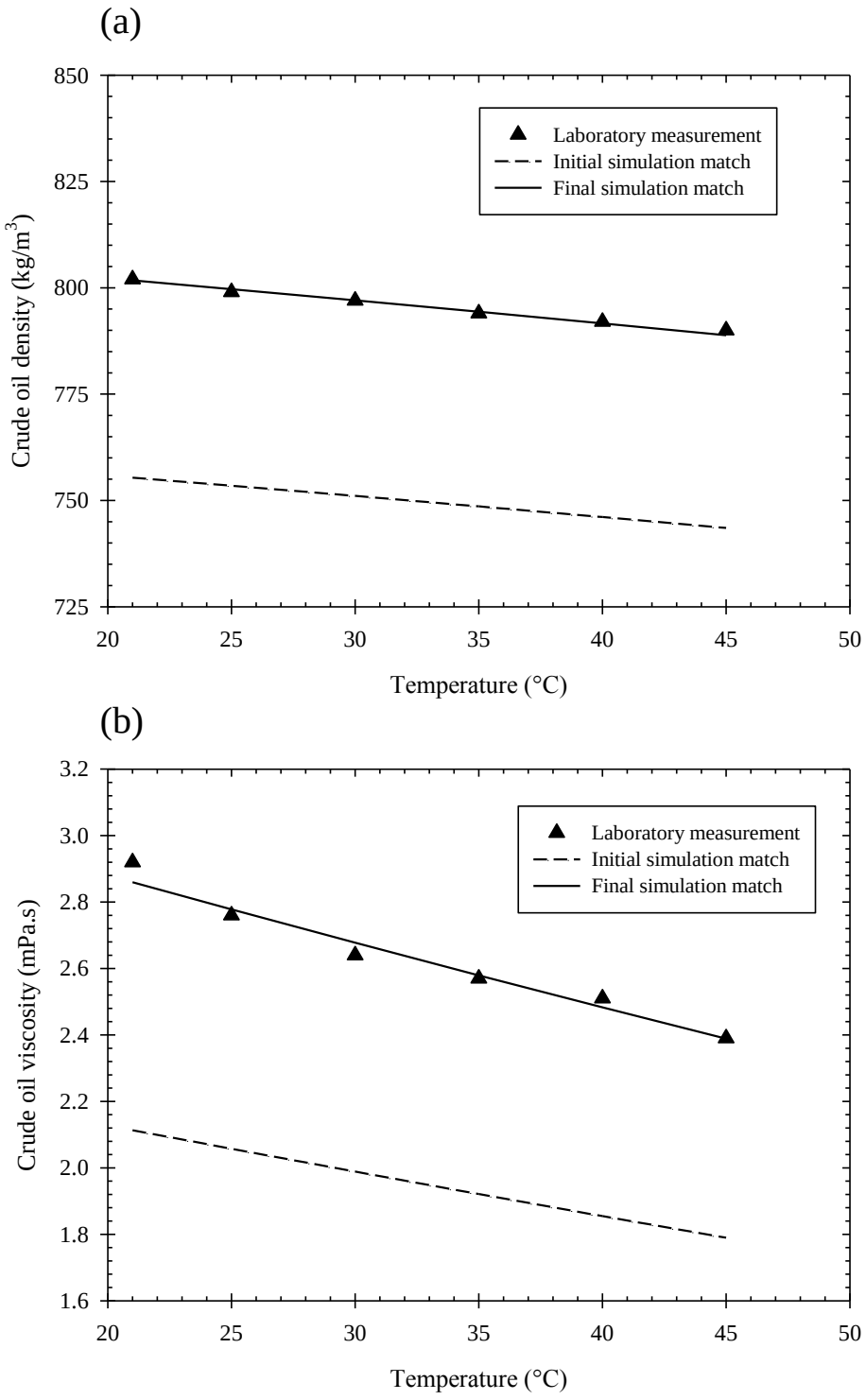

Figure 5.7: Final matches of the crude oil properties: (a) dead oil density (b) dead oil viscosity.

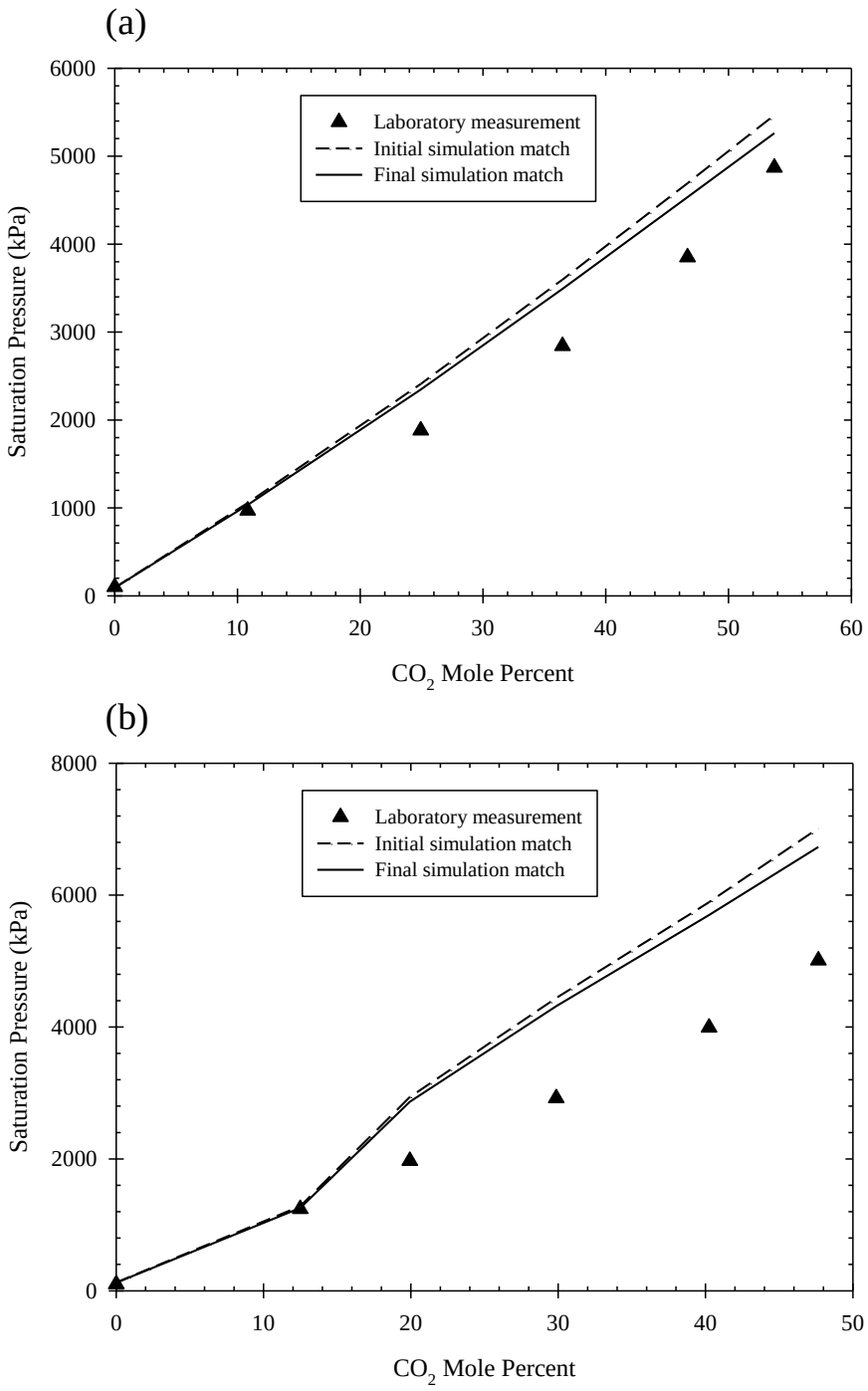

Figure 5.8: Final matches of the saturation pressure of the crude oil–CO_2 mixture: (a) T = 25 °C (b) T = 40 °C.

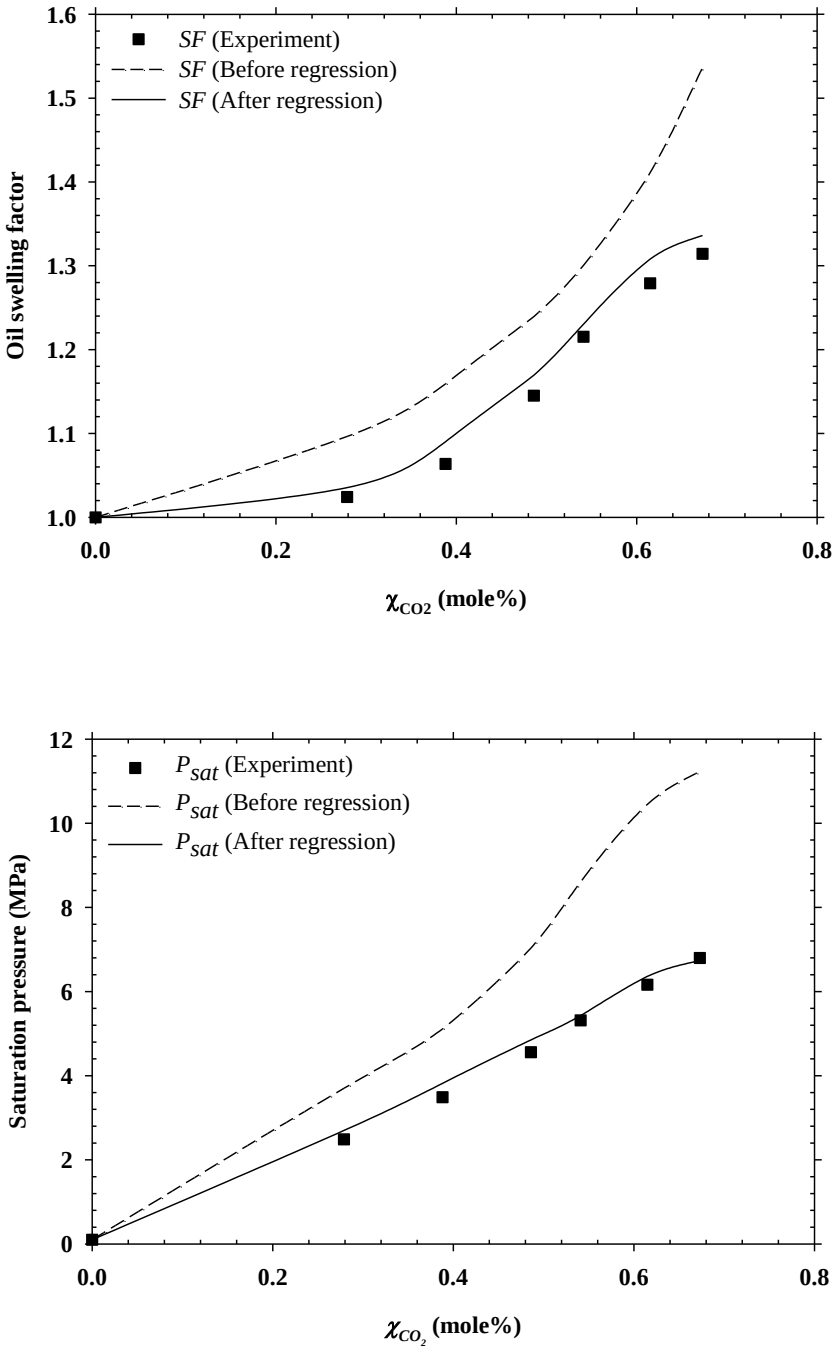

Figure 5.9: Final matches of the oil swelling factor and saturation pressure at T = 25 °C.

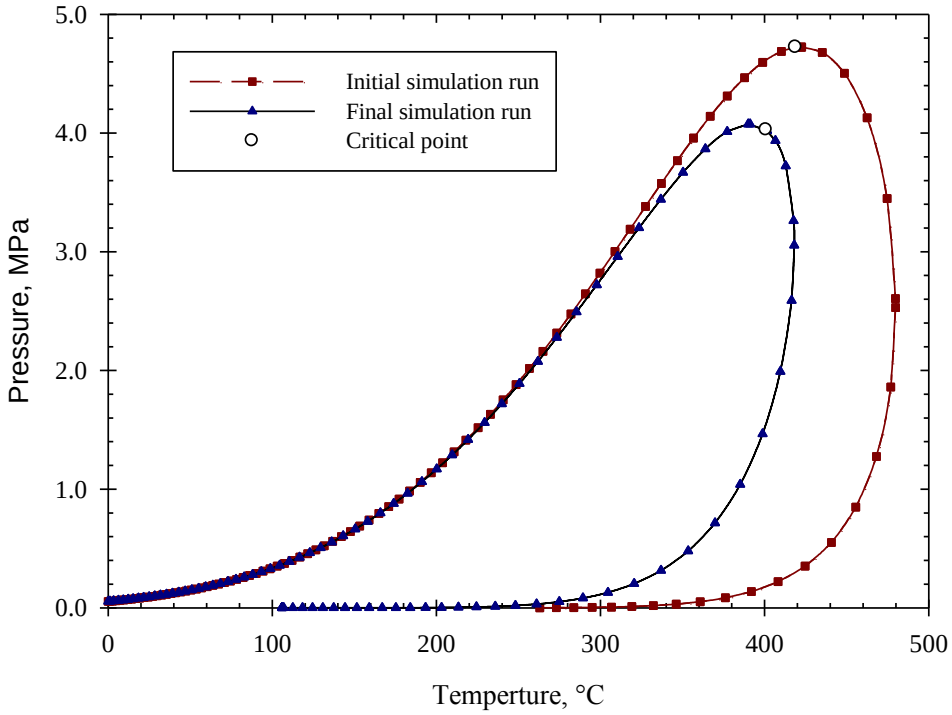

Figure 5.10: Initial and final two-phase envelope corresponding to the oil sample of this study.

5.7. Minimum miscibility pressure (MMP)

By definition, minimum miscibility pressure (MMP) is the lowest pressure at which injectant fluids, such as CO_2, are completely soluble in the reservoir oil Interfacial tension (IFT) between the two fluids reduces to zero and therefore no interface exists between the two fluids in the porous medium. In other words, miscibility is achieved when the crude oil and injected fluids can be mixed together in all proportions and all resultant mixtures remain in a single phase region of the phase envelope. It is believed that there are no interfaces between the fluid phases because only one phase exists in mixtures of miscible fluids, and, therefore, interfacial tension between the fluids reduced to zero. In a miscible flooding process, the reservoir pressure is maintained at or higher than the MMP to ensure the miscibility condition is reached inside the reservoir. The value of MMP is used to determine whether a CO_2-based EOR process proceeds in a immiscible or miscible condition. In this study, MMP was determined through applying a vanishing interfacial tension (VIT) technique on equilibrium IFT data (Abedini *et al.*, 2014; Orr and Jessen, 2007). Moreover, different available correlations (Bon and Sarma, 2004; Emera and Sarma, 2005) and CMG's WinProp software were utilized to estimate the MMP between CO_2 and the Bakken crude oil sample of this study. **Table 5.8** presents the MMP values obtained from both laboratory measurements and mathematical correlations selected from the literature. As an example, it was seen that the estimated MMP values ranged from 8.96 MPa (Swelling/extraction tests) to 9.61 MPa (Correlation) at an experimental temperature of T = 30 °C. The relative deviations of the approximated values were calculated based on the **Equation 5.1** and the results are illustrated in **Figure 5.11**. The result of the tuned EOS effectively show the efficacy of the correlation and

Table 5.8: Comparison of the MMP between CO_2 and Bakken crude oil obtained by various experimental and numerical techniques.

MMP (MPa)					
Temperature (°C)	Swelling/ extraction	VIT technique	Correlation	Simulation	
				Initial run	After tuning
21	8.07	N/A	7.53	8.65	8.17
25	8.34	N/A	8.44	10.51	8.40
30	8.96	9.18	9.61	12.79	9.01
40	10.22	N/A	11.98	17.29	10.62

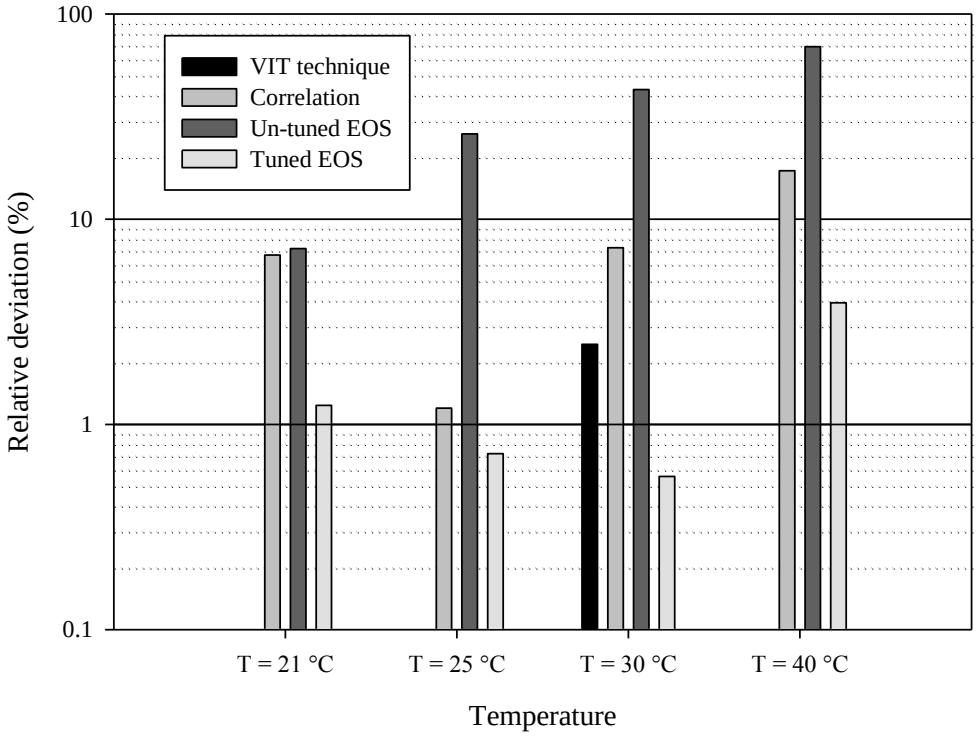

Figure 5.11: Relative deviation of the approximated MMP values obtained from various methods against the actual MMP values obtained by swelling/extraction test.

tuning procedure that was employed in this study by reducing the relative deviation by one or two orders.

$$Relative\ Deviation\ (\%) = \frac{\left|MMP_{approx} - MMP_{actual}\right|}{MMP_{actual}} \times 100 \quad \text{..... (5.1)}$$

5.8. Rock–fluid properties

Initial two-phase relative permeability curves were incorporated into the simulation model using available correlations in GEM. Three-phase relative permeability was obtained using Stone's Second Model by assuming end point saturations accordingly. The assigned initial water and residual oil saturations, experimental conditions, sand-pack characteristics, and flooding specifications are given in **Table 5.9**. The assigned Corey exponents were consistent for all simulation runs and are presented in **Table 5.10**.

In this study, particular relative permeability curves were constructed for each experiment. The general characteristics of the curves for different runs were kept identical while the end point saturations were modified to match the experimental values for each run. For example, relative permeability curves shown in **Figure 5.12** were constructed using the corresponding values for test #5 conducted at P = 4.1 MPa and T = 25 °C. Other assumptions for the rock–fluid properties in the simulation model are as follows:

- The sand-pack system is a water-wet system.
- Hysteresis has no effect on relative permeability curves.
- Relative permeability curves are independent of temperature.

- Capillary pressure is neglected during simulation runs.

5.9. Injection/production configurations

The sand-pack model was developed by considering a double injection/single production well pattern which were perforated in the first (J = 1) and last (J = 100) layers in the longitudinal direction (i.e., J-direction). As shown in **Figure 5.13**, perforations were completed according to hole patterns on the inlet and outlet metal caps of the physical sand-pack cylinder. **Figure 5.14** shows the location of the injection and production sides in the actual sand-pack experiment as well as the simulation model. The CO_2 injection rates were incorporated in the model based on the CO_2 solubility value in brine at corresponding operating pressure and temperatures, considering the desired carbonation level for each run. **Table 5.11** summarizes the assigned values of water and CO_2 injection rates for each experiment, together with the separator conditions at the production side.

5.10. Model initialization

Reservoir initial conditions before production start-up and water flooding, together with the typical characteristics of the homogeneous sand-pack, were used for the initialization of the simulation model. Since the entire CWI process proceeds without free gas generation, a two-phase water-oil fluid system was selected in the CMG GEM simulator. The fluid compositions were also assigned for both water and oil phases in the initialization section by importing the tuned EOS characteristics from CMG WINPROP

Table 5.9: Experimental conditions, characteristics of the unconsolidated sand-packs, and flooding specifications for various flooding tests conducted in this study.

Test	Mode	*CL* (%)	*P* (MPa)	*T* (°C)	q_{inj} (cm^3/min)	χ in Brine (mole/kg)	k_{abs} (mD)	ϕ (%)	S_{wi}	S_{or}
#1	WF	-	4.1	25	1.0	-	5608	27.84	0.384	0.248
#2	SCWI	100	0.7	25	1.0	0.1354	6715	27.91	0.365	0.238
#3	SCWI	100	1.4	25	1.0	0.3572	7190	27.32	0.363	0.226
#4	SCWI	100	2.8	25	1.0	0.7737	7047	27.39	0.371	0.201
#5	SCWI	100	4.1	25	1.0	0.9738	7184	27.58	0.365	0.181
#6	SCWI	100	5.5	25	1.0	1.2523	4320	28.84	0.385	0.155
#7	SCWI	100	6.9	25	1.0	1.3084	4487	27.13	0.365	0.150
#8	SCWI	100	10.3	25	1.0	1.3188	4322	26.61	0.373	0.136
#9	SCWI	100	4.1	40	1.0	0.7797	4320	27.13	0.385	0.186
#10	SCWI	100	4.1	25	0.5	0.9738	7105	27.65	0.372	0.177
#11	SCWI	50	4.1	25	1.0	0.4869	4011	26.54	0.368	0.207
#12	TCWI	100	1.4	25	1.0	0.3572	4136	28.15	0.376	0.223
#13	TCWI	100	4.1	25	1.0	0.9738	4037	26.83	0.370	0.197
#14	TCWI	100	6.9	25	1.0	1.3084	4053	27.14	0.384	0.178
#15	TCWI	100	10.3	25	1.0	1.3188	4106	26.92	0.372	0.174
#16	TCWI	100	4.1	40	1.0	0.7797	4074	27.44	0.380	0.208
#17	TCWI	50	4.1	25	1.0	0.3896	4282	27.33	0.361	0.212

Table 5.10: Incorporated Corey exponents to estimate the water/oil and oil/gas relative permeability values obtained by history matching.

Relative permeability	System	Exponent
k_{rw}	Water/oil	4.0
k_{ro}	Water/oil	2.6
k_{ro}	Oil/gas	2.5
k_{rw}	Oil/gas	2.0

modulus. Finally, initialization of the reservoir model yields the relative in-place distribution of oil and water as summarized in **Table 5.12**.

5.11. Simulation results

The details of the technique to reproduce historical fluid production of primary water flooding and different carbonated water injection tests were presented. As mentioned earlier, the relative permeability curves were considered as the most uncertain parameter in the numerical simulation for the carbonated water flooding tests. Since, each test was conducted using the fresh sand, following identical packing procedures, the Corey exponents for relative permeability correlations were held constant for each flooding test. These exponents were utilized in order to construct the relative permeability curves for both water-oil and liquid-gas systems. The appropriate initial, critical, and residual saturations were originated from preliminary experimental results and incorporated to the relative permeability curves. However, the liquid-gas relative permeability curve was adjusted in each test because the gas relative permeability varied with operating conditions such as pressure and temperature.

Compositional simulation runs were completed using GEM modulus from CMG software. The results of the numerical simulation for 17 flooding experiments included conventional water flooding, secondary CWI, and tertiary CWI are presented in **Figures 5.15 and 5.16** as well as **Appendix A**, where the oil recovery, produced water to oil ratio (WOR), and gas to water ratio (GOR) are plotted versus injection time. The results showed that the model created CWI in sand-pack using the CMG simulator returned satisfactory results and laboratory production data were acceptably matched. The

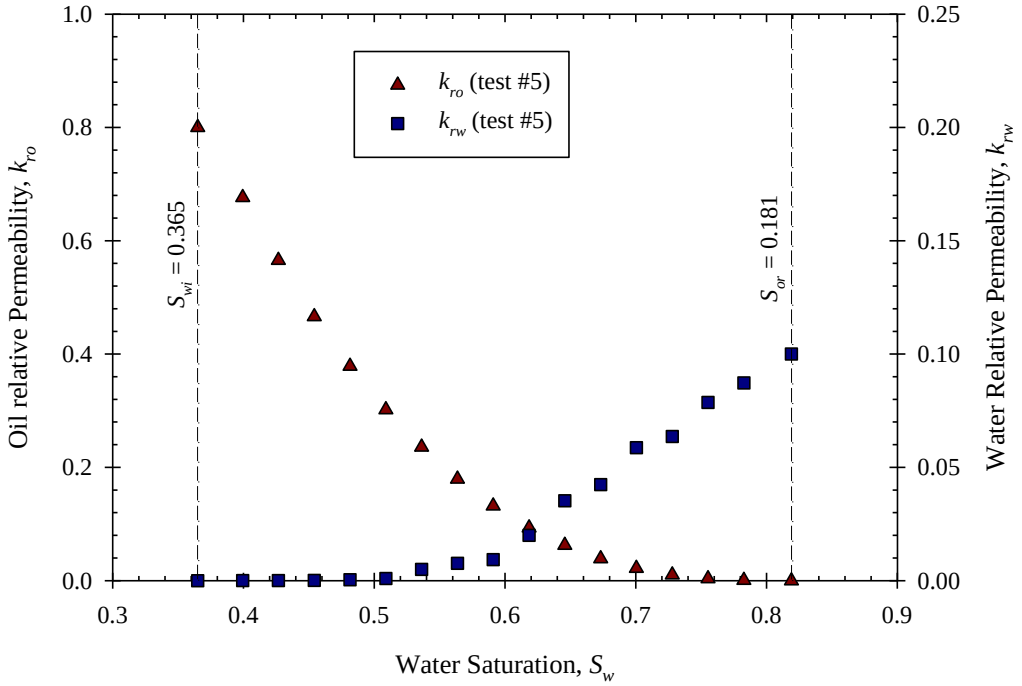

Figure 5.12: Final relative permeability curves to match the production dada of test #5 conducted at P = 4.1 MPa and T = 25 °C.

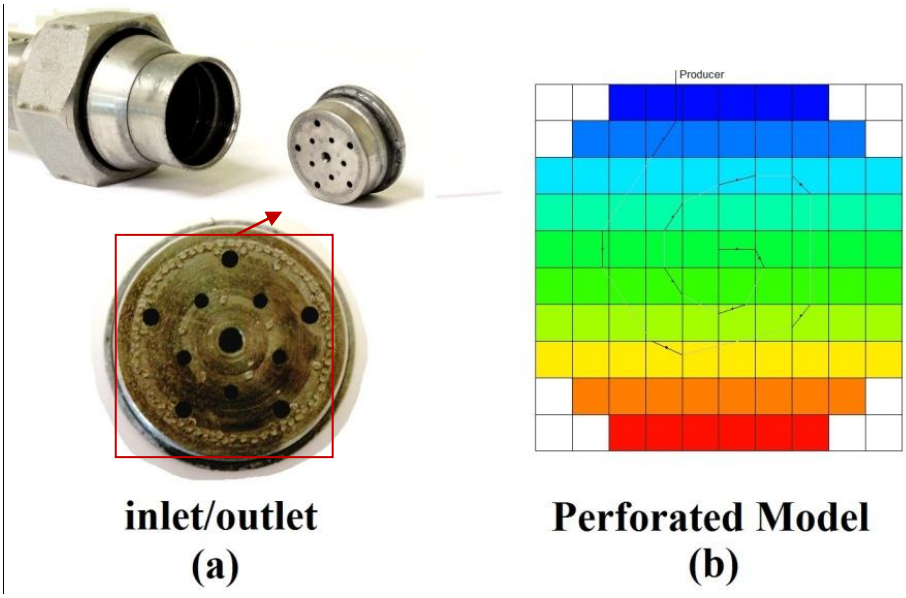

Figure 5.13: Hole pattern on the injection and production caps of the physical sand-pack cylinder (a) and the perforated model (b).

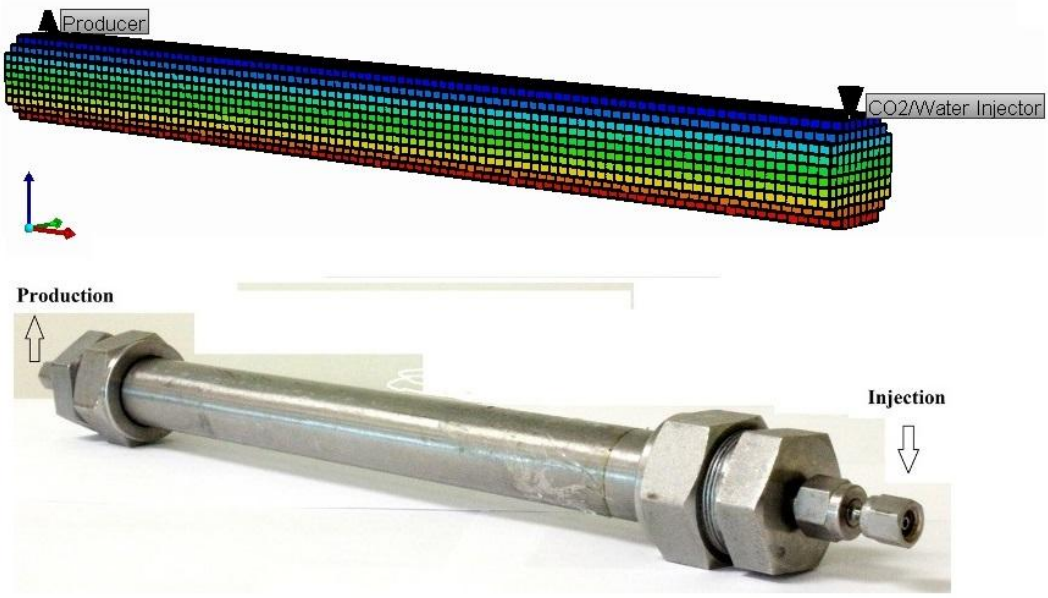

Figure 5.14: Injection and production well locations: actual sand-pack vs. simulation model.

Table 5.11: Simulation inputs for injection rate and separator conditions at the production side.

Run	*Mode*	*CO_2 Injection rate* (standard m^3/day)	*Water Injection rate* (m^3/day)	*Separator Pressure (kPa)*	*Separator Temperature (°C)*
#1	WF	-	0.00144	4100	25
#2	SCWI	0.004784123	0.00144	700	25
#3	SCWI	0.012621038	0.00144	1400	25
#4	SCWI	0.027337338	0.00144	2800	25
#5	SCWI	0.034407522	0.00144	4100	25
#6	SCWI	0.044247833	0.00144	5500	25
#7	SCWI	0.046230029	0.00144	6900	25
#8	SCWI	0.047028561	0.00144	10300	25
#9	SCWI	0.027549338	0.00144	4100	40
#10	SCWI	0.017203761	0.00144	4100	25
#11	SCWI	0.017203761	0.00072	4100	25
#12	TCWI	0.012621038	0.00144	1400	25
#13	TCWI	0.034407522	0.00144	4100	25
#14	TCWI	0.046230029	0.00144	6900	25
#15	TCWI	0.047028561	0.00144	10300	25
#16	TCWI	0.027549338	0.00144	4100	40
#17	TCWI	0.017203761	0.00144	4100	25

Table 5.12: Reservoir volumetric distribution resulting from the initialization of the in the simulation model.

Run	Mode	Total Pore volume, cm^3	Original oil in-place, cm^3	Connate water in-place, cm^3	Initial oil saturation, %	Connate water saturation, %
#1	WF	43.06	27.04	16.02	0.628	0.372
#2	SCWI	43.05	27.34	15.71	0.635	0.365
#3	SCWI	42.13	26.84	15.29	0.637	0.363
#4	SCWI	42.29	26.60	15.69	0.629	0.371
#5	SCWI	42.60	27.05	15.55	0.635	0.365
#6	SCWI	41.67	25.63	16.04	0.615	0.385
#7	SCWI	41.83	26.56	15.27	0.635	0.365
#8	SCWI	41.07	25.75	15.32	0.627	0.373
#9	SCWI	41.82	25.72	16.10	0.615	0.385
#10	SCWI	42.75	26.85	15.90	0.628	0.372
#11	SCWI	40.90	25.85	15.05	0.632	0.368
#12	TCWI	43.52	27.15	16.37	0.624	0.376
#13	TCWI	41.36	26.06	15.30	0.630	0.370
#14	TCWI	41.83	26.02	15.81	0.622	0.378
#15	TCWI	41.53	26.16	15.37	0.630	0.370
#16	TCWI	42.29	26.22	16.07	0.620	0.380
#17	TCWI	42.13	26.54	15.59	0.630	0.370

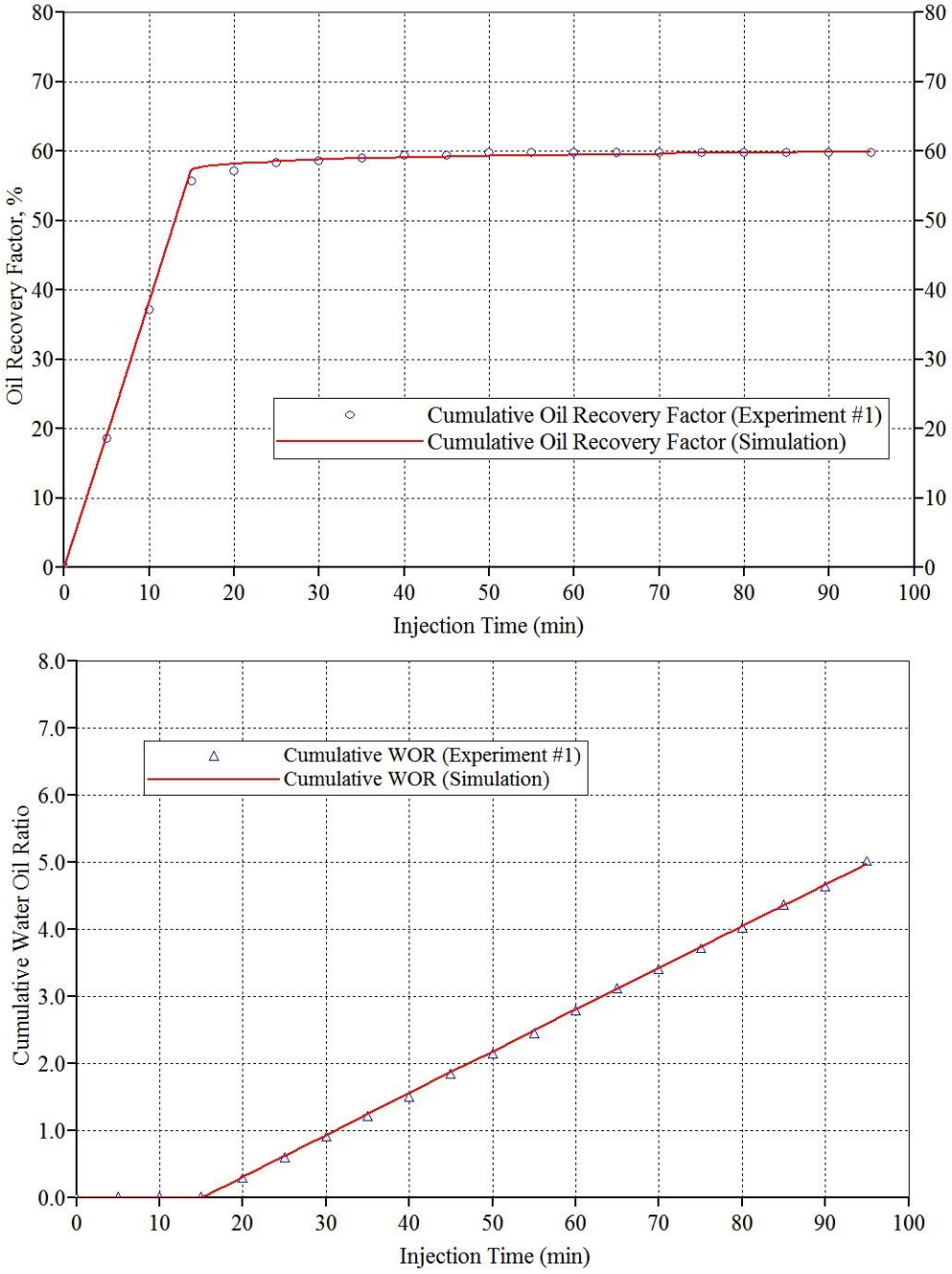

Figure 5.15: Comparison of the simulated and measured cumulative oil recovery (a) and water oil ratio (b) for Test #1 (WF, P = 4.1 MPa, T = 25 °C, q_{inj} = 1.0 cm^3/min).

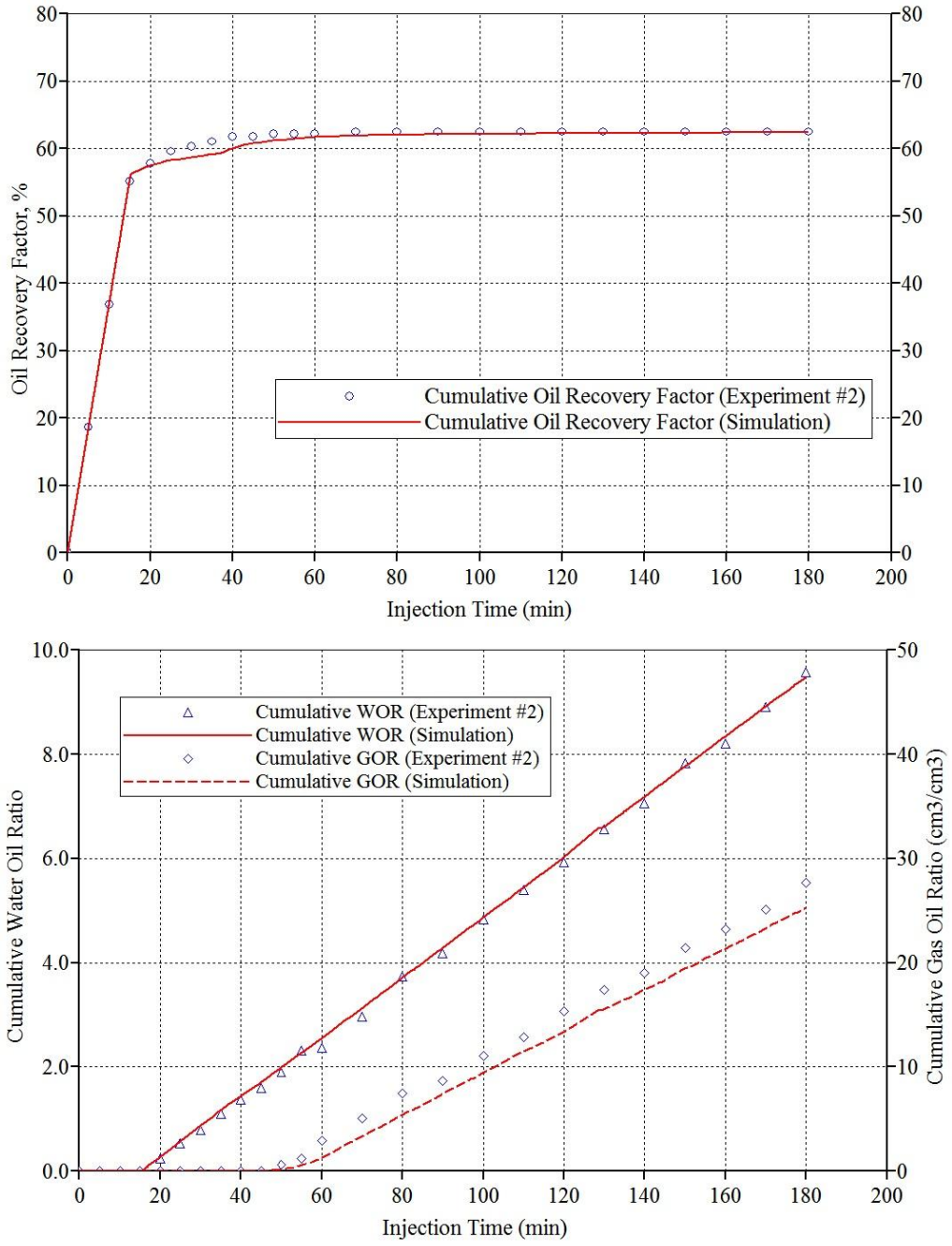

Figure 5.16: Comparison of the simulated and measured cumulative oil recovery (a) and water oil ratio (b) for Test #2 (SCWI, P = 0.7 MPa, T = 25 °C, q_{inj} = 1.0 cm^3/min, CL = 100%).

comparison of the experimental results with those obtained by numerical simulation favourably showed that the simulation model was capable of reproducing the experimental observations with reasonable agreement. Based on these results, it was concluded that the simulation model has been properly calibrated and it could be used in future scale-up scenarios.

5.12. Chapter summary

Procedures for reservoir model development using the CMG's WINPROP and GEM, the Equation of State and compositional simulators, were briefly presented in this chapter. Compositional reservoir fluid of a Bakken crude oil sample was developed using CMG's WinProp program. Rigorous reservoir fluid characterization procedures were followed to obtain the final EOS matched compositional reservoir model are described in detail. Minimum miscibility pressures of both the reservoir fluid models are predicted using CMG's WinProp program. Rock-fluid properties, injection/production well placements and the model initialization procedures were also presented. The results of the sand-pack flooding simulation were found to demonstrate a good match with the experimental flooding results.

CHAPTER SIX: Micro-model study

In this chapter, the performance of carbonated water injection was investigated through various precisely-designed flooding experiments using a visual 2-dimensional porous pattern called a micro-model. Visual micro-models are considered to be a powerful tool to investigate the mechanisms of oil recovery from porous media at pore scale. In this study, a thorough procedure was followed to design the 2-dimensional flow network patterns with pre-specified characteristic properties in order to be representative of the porous media. The micro-model was constructed by implementing various state-of-the-art facilities, equipment, and procedures, which are explained in detail throughout this chapter. In addition, the experimental procedures and the fluid system used for performing micro-model tests are introduced. Image analysis technique was employed to quantify the results depicted by high quality photos during the flooding experiments.

Viscous fingering was found to be the dominant displacement mechanism up to solvent breakthrough in all the flooding tests. In tertiary CWI, subsequent growth of the fingers was observed due to the more beneficial dispersion-type CO_2 mass transfer from the brine to the oil phase.

This chapter begins with explanation of the implemented methods for the design of the flow network pattern. This is followed by a description of the laser engraving procedure and the experimental apparatus for carrying out the visual micro-model flooding tests. These tests were designed to systematically observe the details of the oil recovery process and related fluid-fluid and solid-fluid interactions. The results of 5 micro-model floods are presented and discussed in this chapter. Obtained high quality

images were analysed to understand the dynamics of the carbonated water injection process. Finally, a number of conclusions are presented in order to understand the pore-scale mechanisms during CWI and practical applications for future and current field scale projects.

6.1. Introduction

Visual micro-models used in this study can be defined as a flooding apparatus that enable visual observation of multiphase flow behaviour in porous media at the pore level. The glass micro-models are essentially a micro-scale flow network engraved onto the surface of an appropriate type of glass plate. The first step in construction of a micro-model the generation of a high contrast diagram of a flow network pattern. The flow network pattern is then etched onto a glass plate to produce very thin micro channels with an engraving depth on the order of 10^{-5} m. This plate is then sandwiched with another matching glass plate to seal the micro channels. This assembly generates a thin 3-dimensional path through which various flow phenomena may be visually observed and consequently analysed. Since the thickness of the resultant 3-dimentional pattern is negligible compared to the network area, these models are well known in the petroleum industry as a 2-dimesional micro-model.

In the petroleum industry, transparent micro-models have been utilized as a representative geometric structure of a typical reservoir rock pore network that permits direct visualization of different multi-phase fluid flow phenomena in a porous media. The literatures shows that the application of micro-models is growing in petroleum sector for observing pore-scale processes of fundamental and practical concepts in porous media

(Sayegh and Fisher, 2008). Various researchers utilized micro-models to analyze the detailed mechanisms and investigate the performance of different oil recovery techniques at pore-scale. Micro-models have proven to be very practical and functional for performing fundamental examinations of different oil recovery processes including waterflooding (Wang *et al.*, 2006), gels for conformance control (Bai *et al.*, 2007), immiscible displacements (Chatzis and Dullien, 1983; Mahers and Dawe, 1985; Touboul *et al.*, 1987), surfactant floods (Paterson *et al.*, 1984; Hornof and Morrow, 1988), foam injection (Owete and Brigham, 1987; Armitage and Dawe, 1989; Chang *et al.*, 1994; Romero *et al.*, 2002), foamy oil flow (Bora *et al.*, 2003), microbial EOR (Soudmand-asli *et al.*, 2007), solution gas drive (Lago *et al.*, 2002; Grattoni and Dawe, 2003; George *et al.*, 2005), and carbonated water flooding (Sohrabi *et al.*, 2008; kechut *et al.*, 2010; Riazi, 2011; Sohrabi *et al.*, 2012). Micro-models have also been used to study specific essential and basic aspects of multi-phase flow through porous media such as wettability (Morrow *et al.*, 1986; Laroche *et al.*, 1999; Grattoni and Dawe, 2003; Romero-zeron and Kantzas, 2007), capillary pressure (Smith *et al.*, 2005); interfacial tension (Mackay *et al.*, 1998), asphaltene deposition (Danesh *et al.*, 1988), heterogeneity (Bahralolom *et al.*, 1988a), mass transfer (Mahers and Dawe, 1982; Mahers and Dawe, 1984), scaling (Ren *et al.*, 2006), multiple-contact miscibility (Campbell and Orr, 1985; Bahralolom and Orr, 1988), and gravity drainage (Ren *et al.*, 2005).

6.2. Fluids

The same mixture of Bakken crude oil sample was used in the micro-model study. Also, identical synthetic brine was used, which was distilled water with 2.0 wt.% NaCl.

In order to differentiate between the phases in the micro-model to classify the in-place fluid phases during image analysis, a blue water-soluble liquid dye was used to alter the colour of the water phase. In addition, the colour of the oil was changed to dark red using hydrocarbon-soluble red dye. Density and viscosity of the blue dye liquid were calculated to be ρ_d = 1090.7 gr/cm^3 and μ_d = 1.75 mPa.s, respectively. The concentration of the dye liquid was 0.1 ml of dye dissolved in 1000 ml of brine.

6.3. Manufacturing of the glass micro-model

After the flow pattern was generated and the fluid inlet and outlet added to the drawing, the micro-model is ready to be transferred to a computer which was loaded with the interface program, LaserCut 5.3, to contorl operation of the high-precision laser machine (BossLaser, LLC). The physical dimensions of the flow area on the glass were w_p = 39.81 mm wide and l_p = 123.79 mm long. The next step was to engrave the designed pattern onto a piece of plate glass which was w_g = 101.6 mm wide and l_g = 203.2 mm long. The etching procedure used here was different than the conventional etching procedure in which the various chemicals, masks, and films were used. The new laser-based procedure provided a high-precision fine pattern (400 dpi) enabling every specific channel, pore, or grain to be accurately designed before the laser engraving process is initiated. The conventional chemical etching procedure does not allow the required level of accuracy or reliability in the engraving depth provide by the laser method. The process of image analysis and the physical accuracy of the entire process is enhanced when the laser machine is used to engrave the micro pattern on the glass surface. The detailed procedure of constructing the glass micro-model is summarized below:

- A thick glass plate was cut with appropriate dimensions.
- Inlet and outlet holes were drilled in predefined locations.
- The glass plate was chemically cleaned to avoid any contamination.
- The glass plate was placed on the working platform of the laser machine.
- Appropriate laser power and machine speed were chosen.
- The loaded micro pattern was then engraved onto the surface of the glass plate.
- The engraved glass was cleaned again to remove any glass dust.
- The engraved and plain glass plates were bonded together in a high temperature fusion furnace. A predetermined temperature profile up to 690 °C was followed during the thermal fusion process.

6.4. Micro-model flooding procedures

6.4.1. Experimental apparatus

A schematic diagram of the high pressure micro-model flooding setup is shown in **Figure 6.1**. The basic elements of the setup are a pumping system, micro-model, effluent fluid collectors, the associated flow lines, and the photography equipment. Crude oil, brine, carbonated water, and the cleaning solvents were pumped through the micro-model using corresponding piston accumulators, a double piston Quizix pump (Chandler Engineering, QX series), and a high pressure accurate syringe pump (Teledyne ISCO, 500D series). The produced fluids passed through a back pressure regulator set at constant pressure and eventually stored in the appropriate fluid collectors. Additionally, an in-house precise bubbler system was designed and utilized to collect the produced gas. Most of the components of the micro-model flooding apparatus were made of stainless

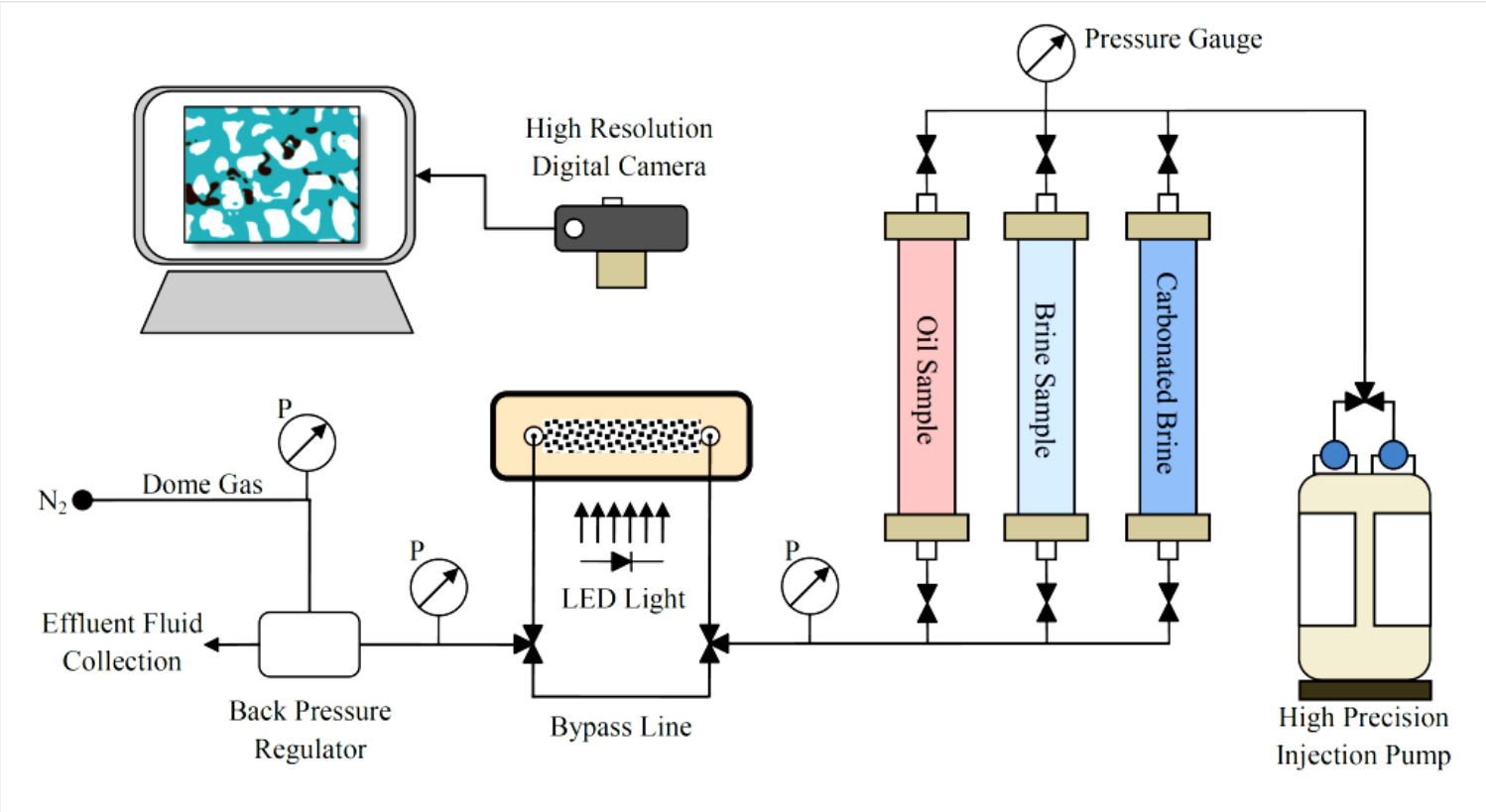

Figure 6.1: Schematic of the micro-model flooding apparatus used in this study.

steel to provide minimum corrosion caused by CO_2 and the brine. Because the volumes of the fluids used in any micro-model flood are very small, 1/16" stainless steel tubing was used to minimize the dead spaces and associated error in fluid volume calculations.

In order to avoid the effects of gravity on the fluid flow, the micro-model plate was oriented horizontally. A light source was placed below the micro-model with a rectangular white plexy-plastic sheet to diffuse the light and provide constant light intensity. High quality video and microscope cameras were positioned above the micro-model in order to take still and video images during the flooding process. The microscope camera was used to take high resolution images that could be used in order to visualize and analyze the fluid-fluid interfaces, interfacial tension, contact angle, and trapping mechanisms, while a video camera was employed to observe some dynamic effects such as dissolution process, frontal advance, and breakthrough time.

The pressure of the back-pressure regulator and the micro-model's inlet and outlet were monitored during each CWI test. The temperature inside the room was monitored and kept constant using a wall-mounted temperature control.

6.4.2. Experimental procedure

The procedure to carry out the CWI micro-model experiments was similar to that used in the CWI sand-pack flooding tests and consisted of:

- cleaning the model,
- saturating with water,
- oil flooding to establish the connate water saturation,
- water flooding (in case of tertiary CWI), and
- carbonated water injection.

The injected fluids (i.e., brine, carbonated water, and oil) were induced in a way that they would pass through the bypass loop for a time before directing the flow into the micro-model. This was to ensure that the inlet lines were properly flushed from the previously injected fluid(s) and to allow enough time for the pressures to stabilize.

6.5. Experimental results and observations

6.5.1. Micro-model specifications and fluid properties

Figure 6.2 illustrates the micro-model pattern generated in this study. The characteristics of the pattern are summarized in **Table 6.1**. **Figure 6.3** shows the grain area histograms for the designed pattern. The histogram of the pattern engraved on the glass plate was very similar to that of the original pattern, indicating that the characteristics of the pattern were preserved through the laser engraving process. The properties of the resultant glass micro-model are summarized in **Table 6.2**. One unanticipated result that added to the realism of the resultant pattern was that few grains that were too close to each other were fused together because of the limits of the resolution of the laser machine. This was considered as the cementing of the grains as observed in real reservoir rock. Therefore, the appearance of the grain fusion during the laser engraving process was considered beneficial because the achieved micro porous structure is more similar to the real rock-type porous medium in terms of pattern heterogeneity.

Various properties of CO_2, brine, prepared carbonated water, and light crude oil samples were measured or calculated during this study. **Table 6.3** summarizes the fluid

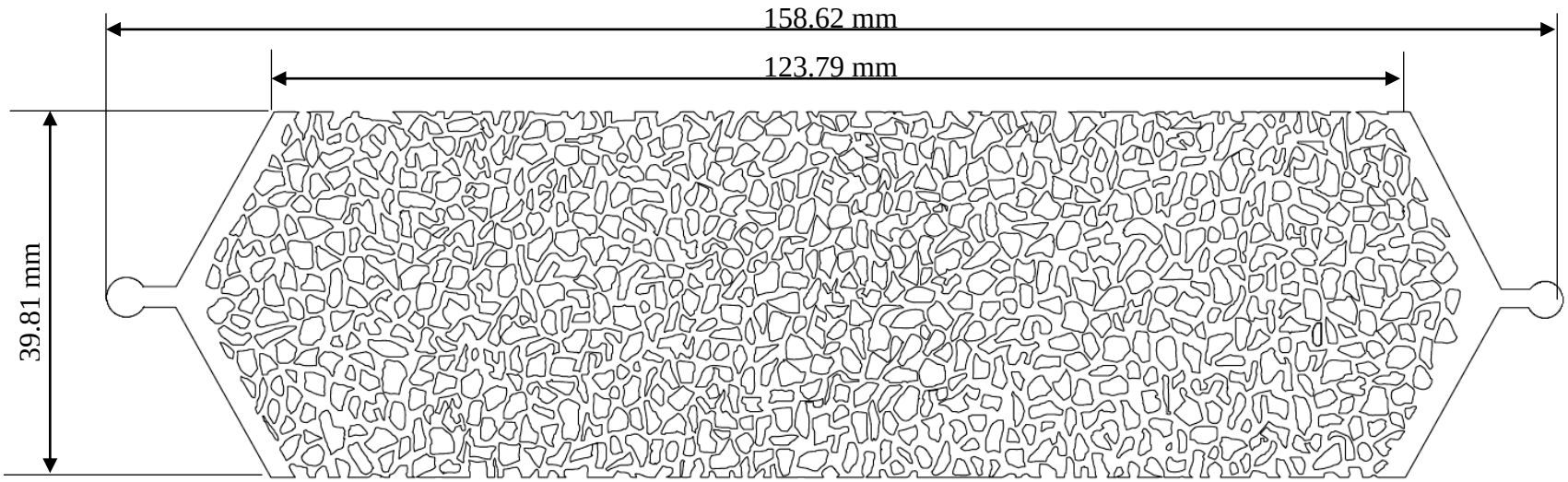

Figure 6.2: The micro porous pattern used by the laser machine to engrave a piece of flat glass.

Table 6.1: Characteristics of the constructed micro pattern used in this study.

Property	Value
Number of grains	689
Max throat size	1.540 mm
Min throat size	0.115 mm
Average grain size	0.298 mm^2
Max grain size	10.854 mm^2
Min grain size	0.002 mm^2

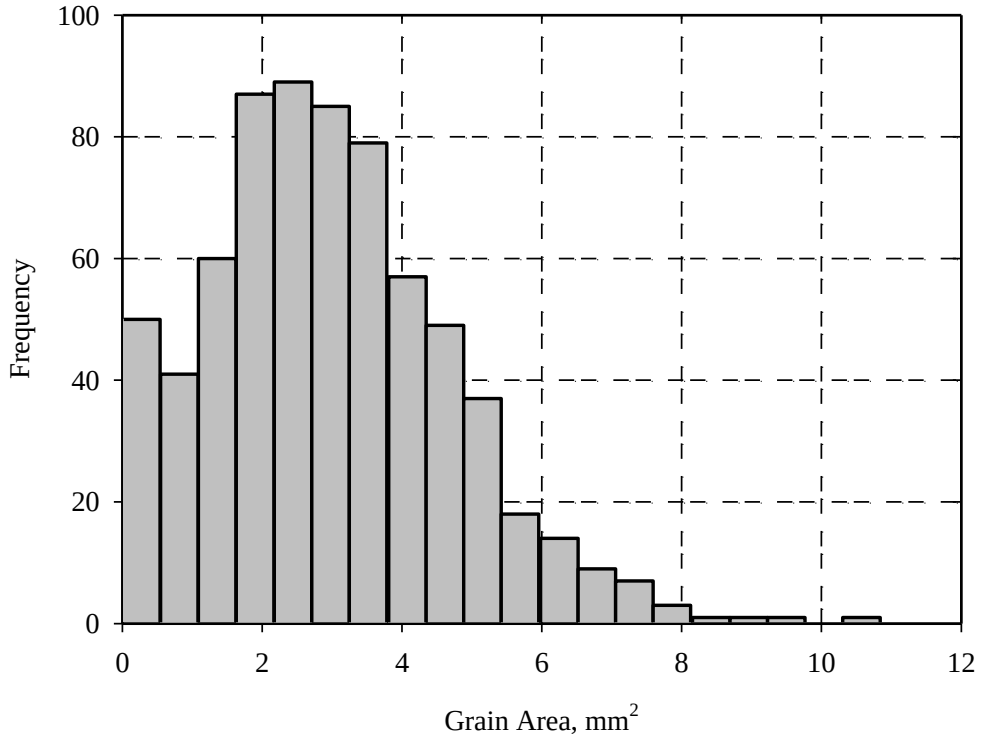

Figure 6.3: Grain data histogram for the designed micro-pattern engraved on a glass plate in this study.

properties used in the micro-model experiments including density and viscosity of different fluids at two experimental temperatures.

6.5.2. Flooding tests

Figure 6.4 provides a conceptual model of how the residual oil saturation may decrease over time when CWI is injected as a tertiary oil recovery technique: (a) the pore space is fully saturated with the reservoir oil, (b) residual oil saturation after primary water flooding, (c) during CWI, injected CO_2 diffuses into the residual oil from carbonated the water phase due to the CO_2 concentration gradient between the two phases. Therefore, the oil ganglion swells, its viscosity reduces and consequently forces some previously immobile oil to become mobile (d). The residual oil saturation in this frame is much less than the residual oil saturation after primary water flooding (i.e., frame b). Three types of flooding modes were implemented: i) conventional water flooding, ii) secondary CWI, and iii) tertiary CWI. The objective was to investigate the effect of various pore-scale parameters and processes on the oil recovery and analyse the details of the recovery mechanisms during CWI. The water and carbonated water injection flow rate was constant for all flooding tests and was set at q_{inj} = 0.05 cm^3/min. It should be noted that the micro-model construction technique, flooding apparatus, and procedures were relatively new during this study. Therefore, a number of micro-models were damaged during laser engraving, thermal fusion, connecting of the stainless steel fittings and conducting flooding tests. It took more than a year to finalize all the procedures and achieve successful micro-model runs. Some of the runs, specifically

Table 6.2: Dimensional characteristics and pore properties of the glass micro-model constructed in this study.

Property	Value
Pattern length	123.79 mm
Pattern breadth	39.81 mm
Engraving depth	0.0123 cm
Pore area	25.64 cm^2
Pore volume	0.315 cm^3
Porosity	52.0 %

Table 6.3: Properties of the fluids used in the micro-model study of CWI process.

Property	Fluid		
	CO_2	Brine	Crude Oil
Viscosity at 25 °C (mPa.s)	0.0149	0.90	2.76
Density at 25 °C (kg/m^3)	1.8093	1010.2	799.0
Viscosity at 40 °C (mPa.s)	0.0156	0.70	2.512
Density at 40 °C	1.7205	1008.2	792.0

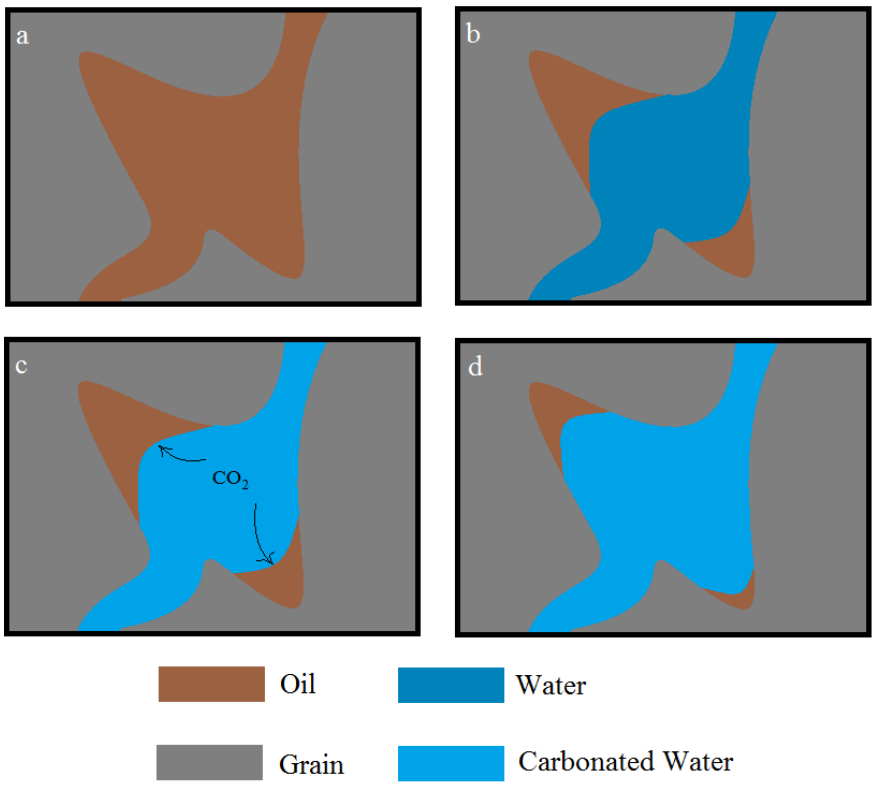

Figure 6.4: Schematics showing the reduction in residual oil saturation over the time.

those carried out at the beginning of the study, were replicated to ascertain the reproducibility of the observed results.

6.5.3. Image processing

Three essential objectives were sought during the micro-model flooding experiments: 1) to achieve visualized qualitative information about multi-phase fluid flow mechanisms in the porous media, 2) to study the residual oil trapping mechanisms during various stages of carbonated water injection, and 3) to process the visualization results using image processing techniques to obtain quantitative analysis of the performance of various carbonated water injection scenarios.

Various distributions of fluids in the micro-model were captured using a high quality camera as well as a laboratory microscope camera. Afterwards, the saturation distributions were imported to the image processing software to achieve quantitative analysis of the saturation distributions. The saturation of the oil, water, and carbonated water phases existing inside the micro-model were calculated using the image processing toolbox of MATLAB.

Using this image processing toolbox, an m-file was constructed to examine the grain size distribution, pore space, and fluid saturations, based on the number of pixels representing each section (i.e., grain and pore) and phase (i.e., water, oil, and carbonated water). The accuracy of the implemented technique was investigated when the micro-model was fully saturated with water and crude oil. It was found that the procedure was reasonably accurate in estimating the fluid saturations. As an example **Figure 6.5** illustrates the MATLAB interface containing the original m-file and the analysed image of the micro-model when carbonated water was injected in the tertiary phase.

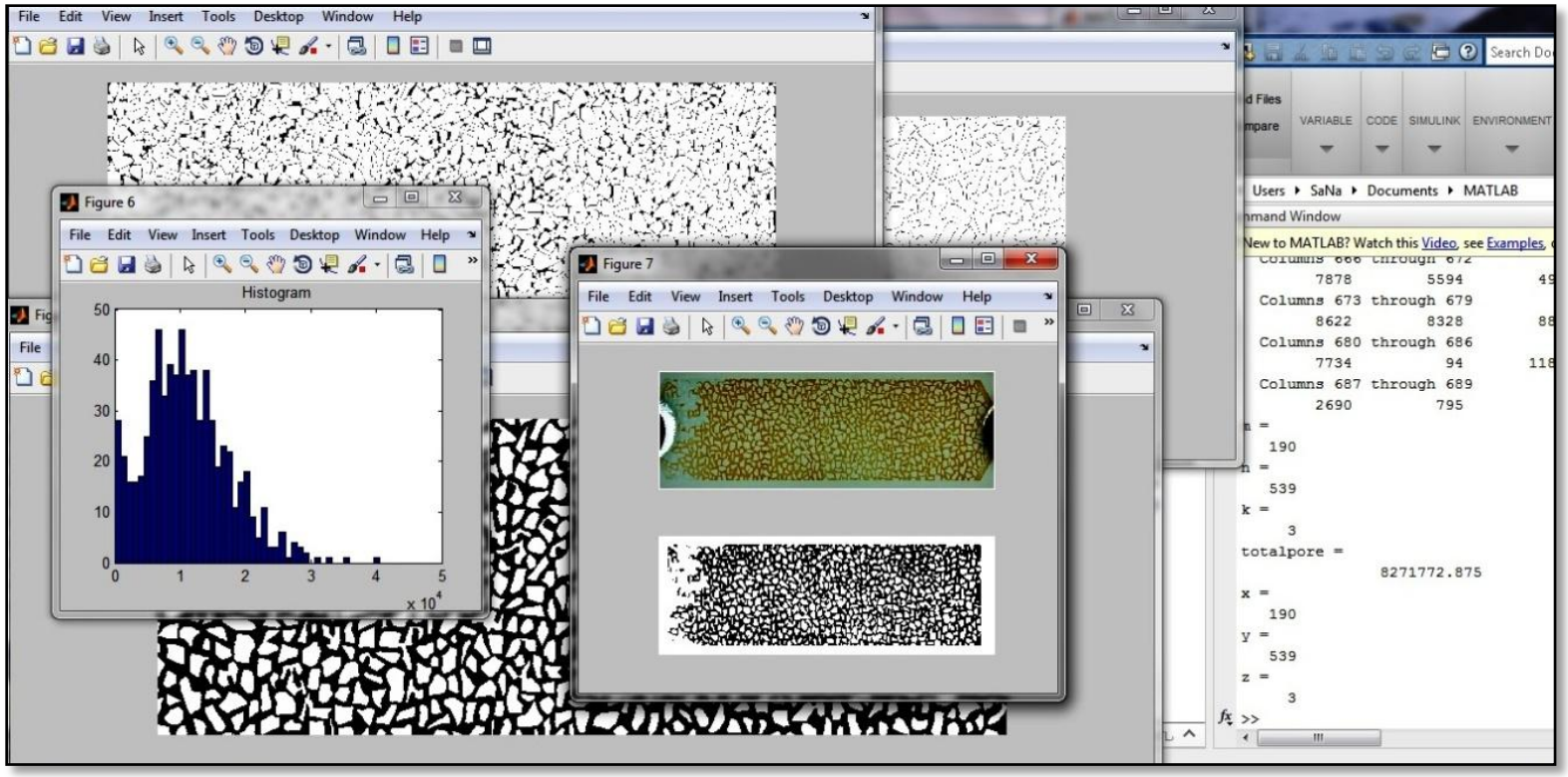

Figure 6.5: Sample snapshot of the MATLAB interface used for image analysis in this study.

The specific MATLAB code was capable of automatically reading the source image file and calculating the number of pixels for each phase presented in micro-model and finally, calculates the saturation of each phase. The complete MATLAB code for image processing of the captured images in this study is available in **Appendix B**. An Identical image processing technique was implemented to observe the fluid trapping and oil swelling mechanisms during the CWI micro-model experiments.

6.5.4. Run #1: Initial waterflooding without connate water saturation

In this run, the model was fully saturated with oil at initial oil saturation of 100%, as illustrated in **Figure 6.6**. As was previously mentioned, the study attempted to minimize the air bubbles inside the micro-model by multi-stage vacuuming. However, a few air bubbles still remained in the model. Some of these areas are magnified and presented in **Figure 6.7** and the volume of these air bubbles were calculated using image processing tools. The volume of air bubbles was negligible compared to the volume of the liquid phase inside the micro-model, however, appropriate changes were incorporated in the image analysis and saturation calculations.

After saturating the micro-model with oil, water injection process was implemented at a low flow rate of q_{inj} = 0.05 cm^3/min. **Figure 6.8** illustrates the sequences of the water flooding process during 5 pore volume injections of the brine sample.

As noted in Figure 6.8(c), the water breakthrough time was observed to be t_{BT} = 281 s. The cumulative oil recovery is depicted in **Figure 6.9** and can be seen that oil recovery increases substantially up to breakthrough time and tends to flatten of after t_{BT}.

Figure 6.6: A fully saturated micro-model with the oil phase, ready for the water flooding stage.

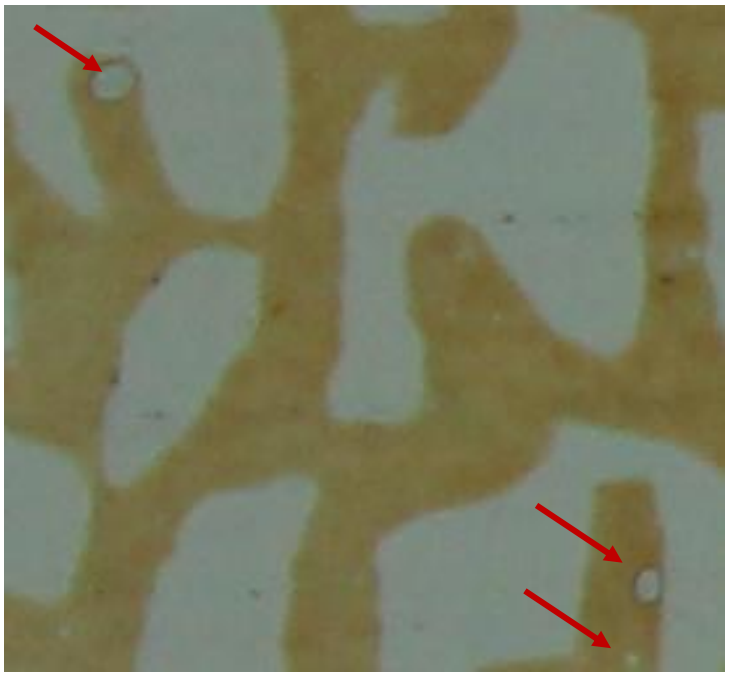

Figure 6.7: Magnified micro-model and the air bubbles inside the pore space.

a: (t = 60 s)

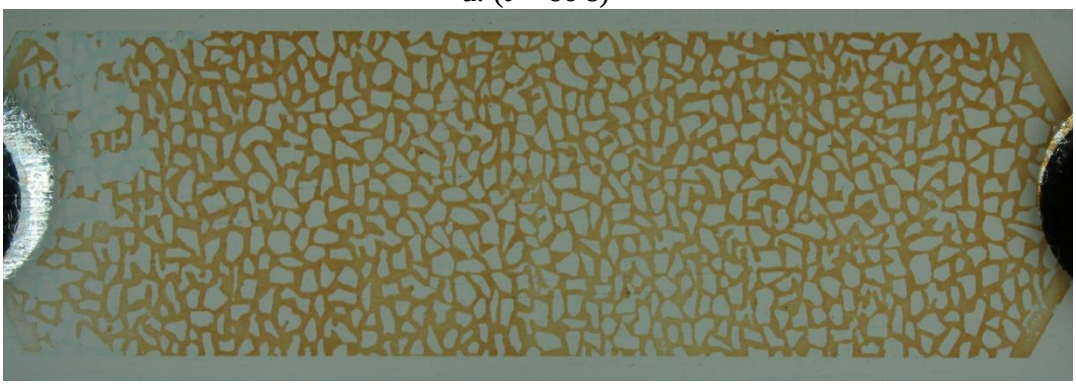

b: (t = 90 s)

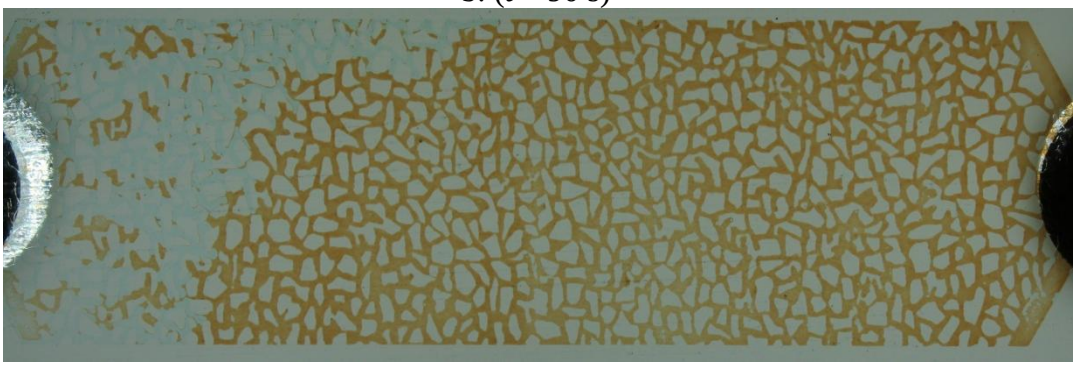

c: (t_{BT} = 281 s)

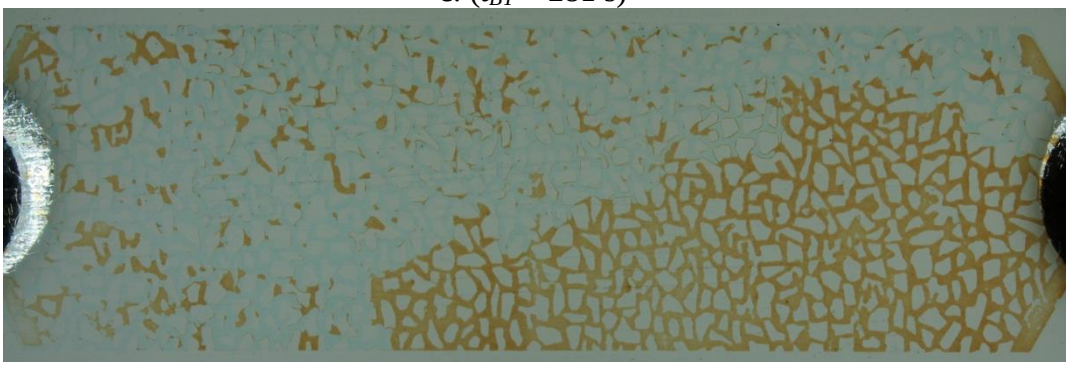

(Continued on next page …)

d: (t = 372 s)

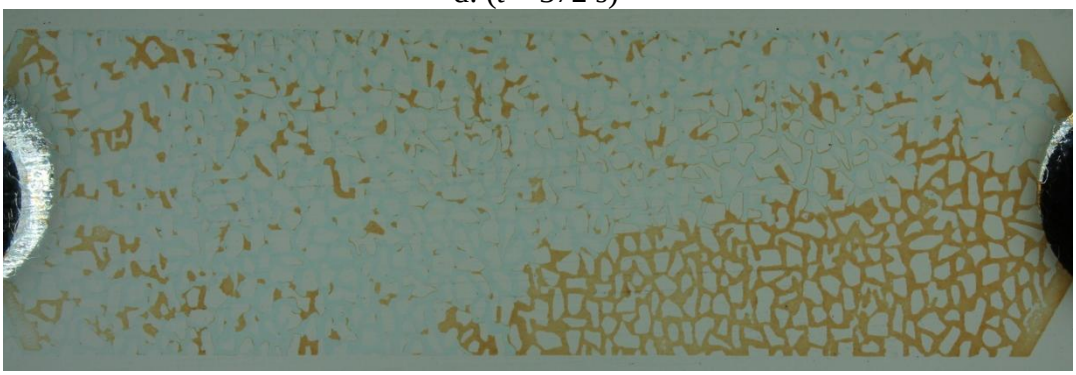

e: (t = 1800 s)

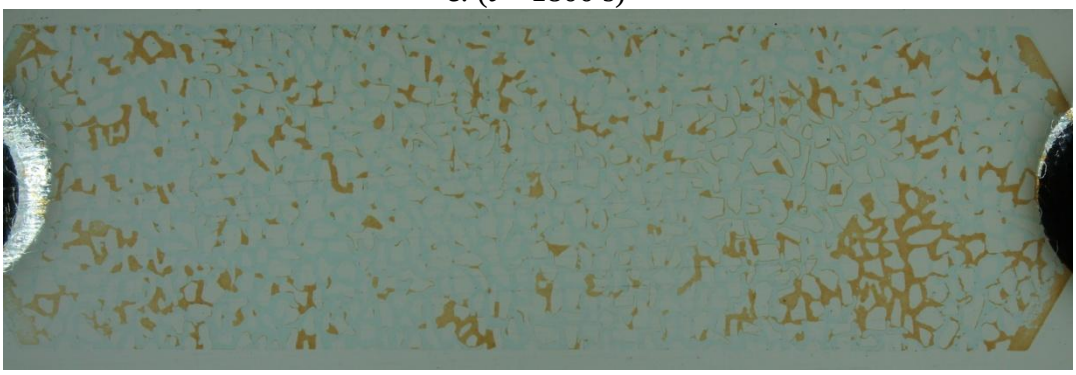

Figure 6.8: Water front advance in water flooding process: a) t = 60 s b) t = 90 s c) $t = t_{BT}$ = 281 s d) t = 372 s e) t = 1800 s.

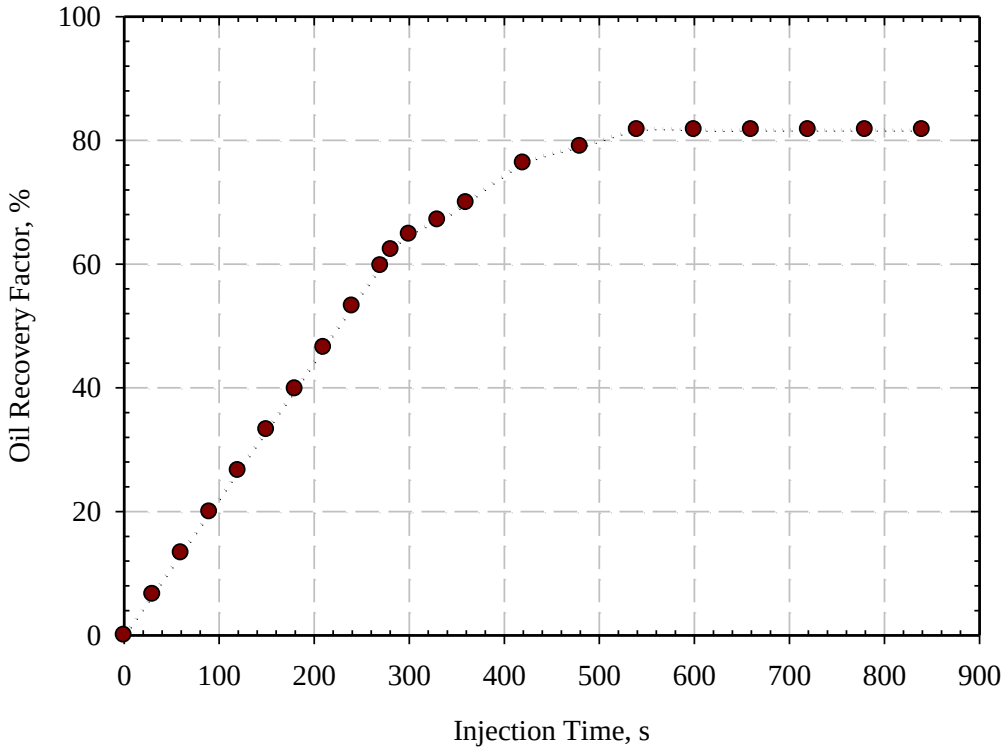

Figure 6.9: Oil recovery versus injection time for a primary water flooding scenario in a test micro-model.

A cumulative oil recovery of 81.7% was observed for water flooding, with 62.3% recovery at the water breakthrough.

Wettability analysis:

Wettability studies in micro-models are considered beneficial in thoroughly examining the wetting behaviour of the porous media using careful laboratory observations. Since the observations are limited to grain size, the entire porous medium (i.e., global wettability) may behave significantly different, compared to the local wettability behaviour. Therefore, during an overall examination of the micro scale model, it was observed that the entire model contains both water- and oil-wet areas. It was believed that detailed image processing and statistical analysis were required to achieve conclusive observations of the wettability phenomenon of the micro-model. For the micro-model used in this study, analysis of magnified snapshots showed that in most of the micro-model sections, the model was mixed-wet toward oil-wet during the oil imbibition and water flooding stages conducted in run #1.

Figure 6.10 depicts segments that were observed to be oil-wet along with the sections that can be considered as mixed- or water-wet pores. The red, blue, and yellow circles represent the oil-, water-, and mixed-wet segments, respectively.

From **Figure 6.11**, it was concluded that in most of the micro-model segments (i.e., over 50%) the oil phase is spread over the grain surface as a very thin layer indicating the oil-wetting behaviour of the micro-model in this run.

Contact angle analysis:

The topic of contact angle has received significant interest from both basic and applied points of view. It plays an essential role in various oil recovery phases and

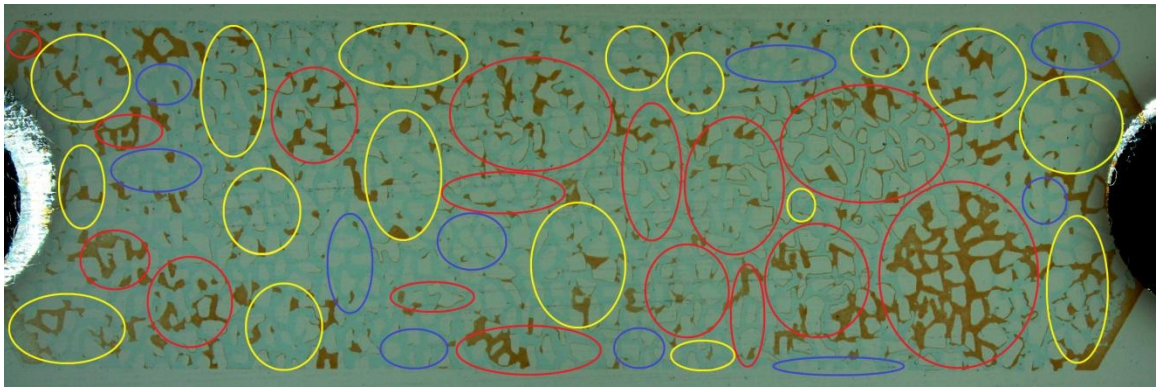

Figure 6.10: Wettability distribution after run #1: water flooding without connate water saturation. (red: oil-wet, yellow: mixed-wet, and blue: water-wet).

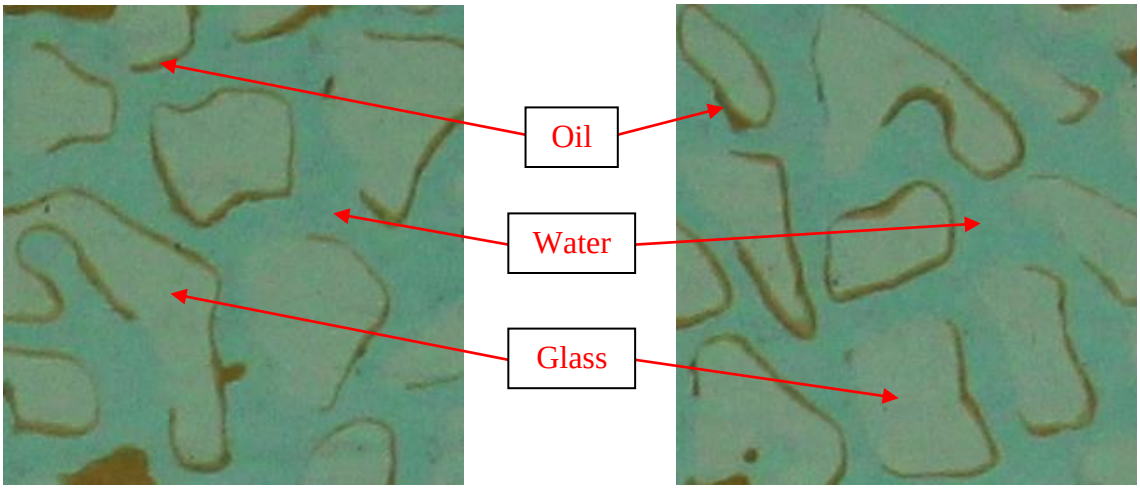

Figure 6.11: Selected magnified segments of the micro-model pointing out the oil-wet nature of the glass micro model in run #1.

processes. During this study, careful attention was taken to observe the contact angle of various fluids on the glass grain surface. These observations at different sections of the micro-model confirmed conclusion of the oil-wet nature of the glass micro-model previous section. The oil and brine ganglia spread over the glass grains were analyzed and as illustrated in **Figure 6.12**. The contact angle was measured for different segments of the micro-model. Results of the contact angle measurements revealed that the glass surface of the micro-model was mixed-wet to oil-wet as was concluded in the wettability analysis.

Trapping mechanisms:

Careful observation during this study showed that a substantial portion of the initial oil saturation remained trapped inside the micro-model due to oil-wet nature of the micro-model. As depicted in **Figure 6.13a**, the image processing results showed that about 18.3% of the original oil in-place remained in the micro-model (i.e., S_{or} = 18.3%). However some evidence of oil ganglia trapping through snap-off and pore-doublet mechanisms were also noticed during this run. Selected sections of the micro-model that are illustrated in **Figure 6.13b** and **c** represent the trapped oil ganglia by snap-off and pore-doublet mechanisms, respectively.

6.5.5. Run #2: Initial waterflooding with connate water saturation

In this run, conventional waterflooding was carried out after establishing connate water and initial oil saturations. Initially the model was fully saturated with water at an operating pressure of P = 2.1 MPa and temperature of T = 19 °C. The injection rate was q_{inj} = 0.05 cm^3/min for both water and oil injection and the flooding was stopped after

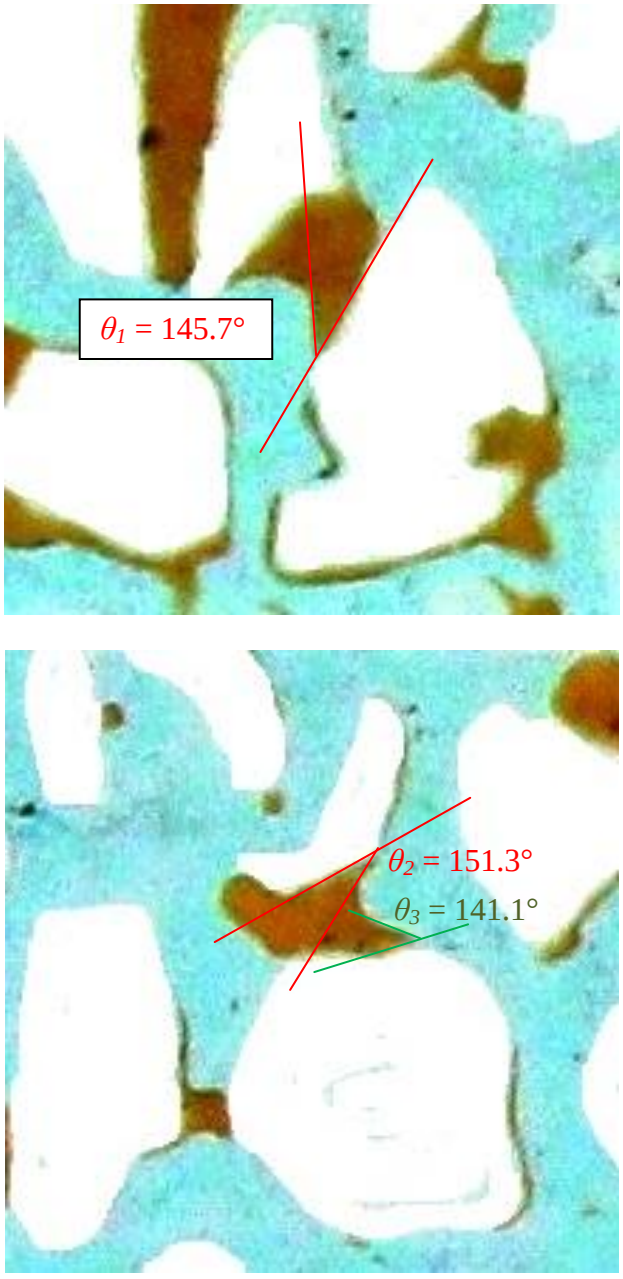

Figure 6.12: Selected magnified images for the purpose of contact angle determination during run #1.

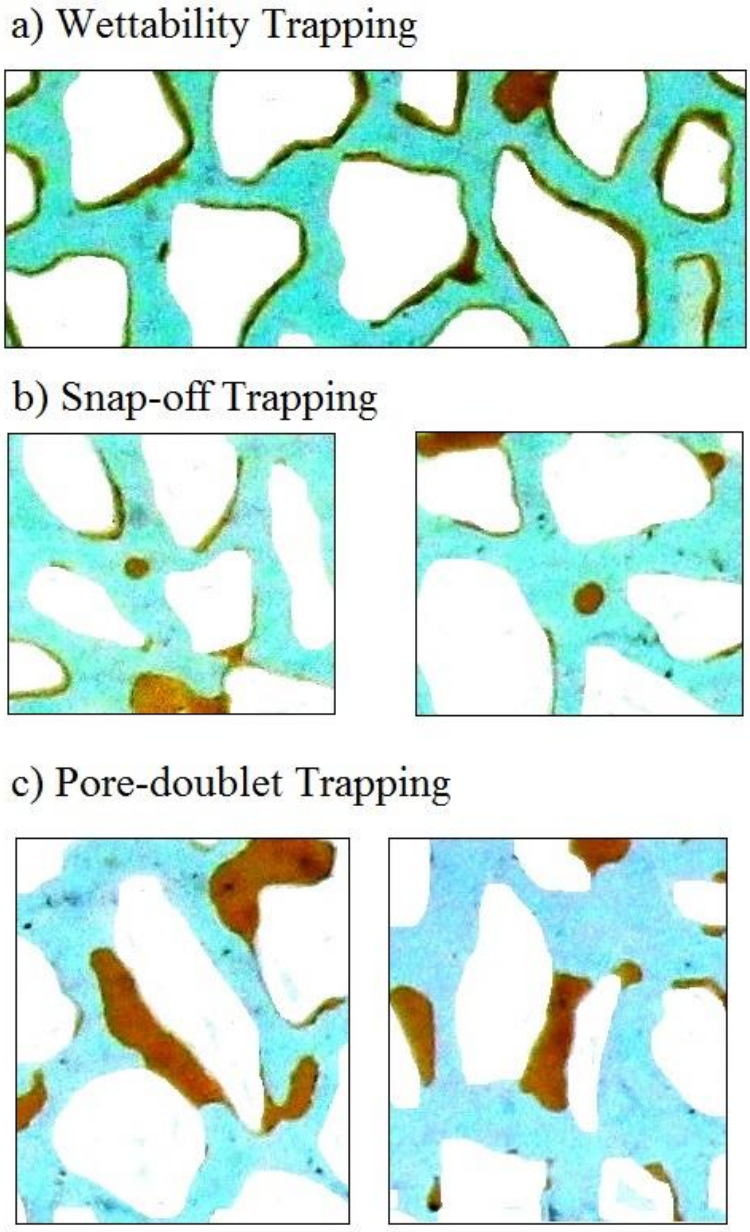

Figure 6.13: Different oil trapping mechanisms observed in the micro-model during run #1.

injection of about 5 pore volumes (i.e., 1.55 cm^3). The results of the image analysis revealed that the irreducible water and initial oil saturations were 5.2% and 94.8%, respectively. The snapshots of the water saturated micro-model along with the micro-model with established connate water are illustrated in **Figures 6.14a** and **b**, respectively. Relatively low connate water saturation demonstrated that the micro-model can be considered an oil-wet system as various parts of the image show that the oil ganglia tended to stick to the grains. However, in some sections the contact angle analysis showed that the glass surface behaved as a water-wet system, as it is illustrated in **Figure 6.15**.

6.5.6. Run #3: Secondary carbonated water injection

For this run, initial water flooding was conducted followed by oil flooding to establish connate water saturation. Afterwards, secondary carbonated water flooding was conducted at P = 2.1 MPa and T = 19 °C. **Figure 6.16a-f** depict the saturation distribution during this run. Carbonated water breakthrough was observed at t = 314 s when 0.262 cm^3 or 0.84 PV were injected. The oil recovery at breakthrough was calculated to be 70.4% of original oil in-place, which is about 8.1% higher than the water flooding recovery factor at breakthrough. Finally, a total of 91.1% of the original oil in-place was produced during this run which was about 9.4% higher than the recovery of the water flooding scenario.

The images of the saturation distribution at the end of water flooding, along with the carbonated water injection scenarios, are compared in **Figure 6.17**. It is observed that the SCWI was able of recovering more oil when compared to water flooding under identical operating conditions and a difference of 9.4% was observed in the cumulative

(a)

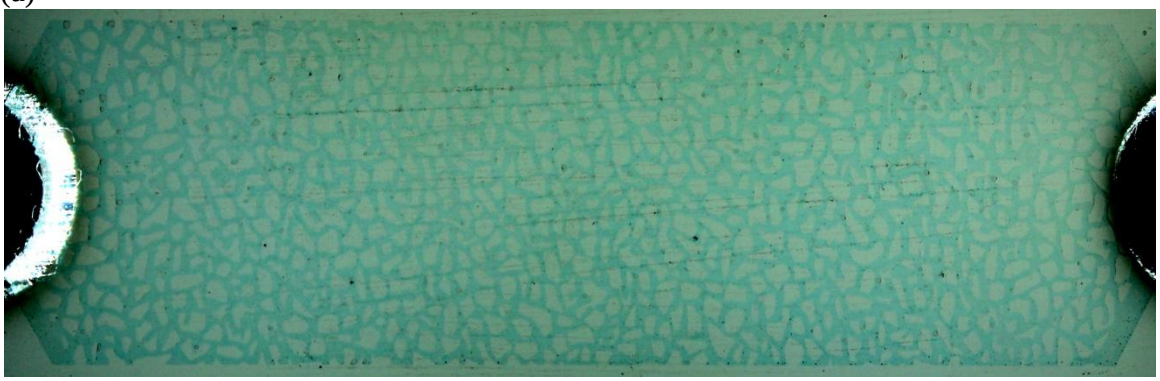

(b)

Figure 6.14: a) Fully saturated micro-model with water and b) initial oil flooding to establish connate water saturation (S_{wc}) and initial oil saturation (S_{oi}).

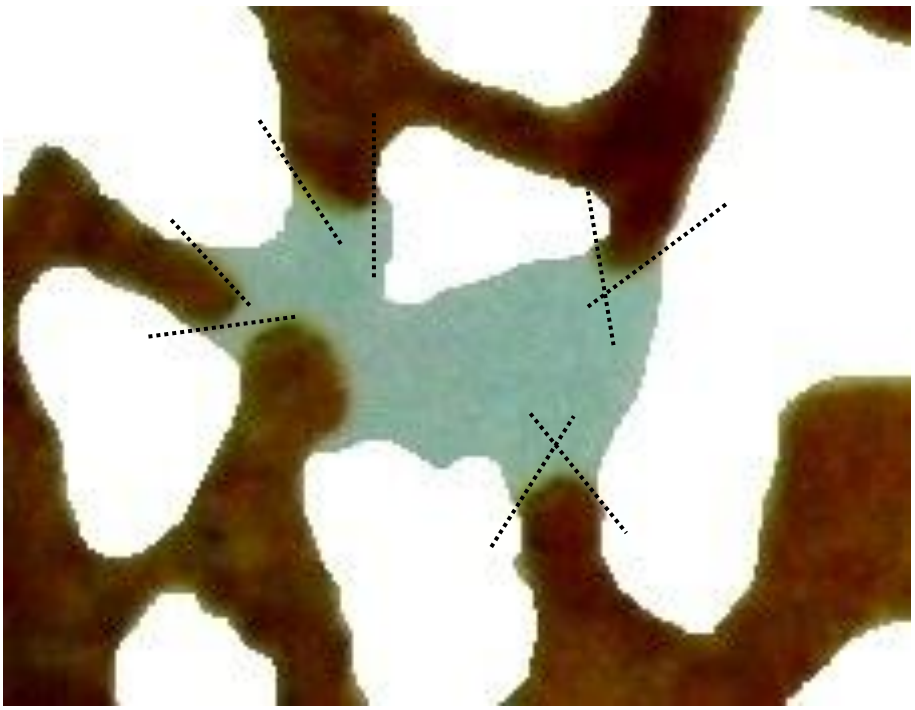

Figure 6.15: Magnified image of water-wet sections of the micro-model and corresponding contact angles in run #2.

a: (t = 0)

b: (t = 173 s)

c: (t = 355 s)

(Continued on next page …)

d: ($t = t_{BT}$ = 314 s)

e: (t = 920)

f: (t = 1800)

Figure 6.16: carbonated water front advance in the micro-model at different injection times.

oil recovery of the two methods. It was observed that the main trapping mechanism during the initial water flooding was by wettability trapping due to the oil-wet nature of the micro-model. However, less wettability trapping was observed during secondary carbonated water flooding, which shows significant potential for SCWI to improve oil recovery from oil-wet reservoirs by modifying the wettability of the porous medium from oil-wet to mixed- or water-wet. **Figure 6.18** compares the magnified snapshots of selected sections of the micro-model to demonstrate the observation of wettability alteration during carbonated water injection.

Analysing the wettability nature of the micro-model during both WF and SCWI revealed that the wettability of the porous system in many sections of the model was altered from oil-wet to water-wet. This shows the beneficial role of CWI in assisting the recovery of the in-placed oil by improving the wettability of the porous medium toward the water-wet condition.

6.5.7. Run #4: Tertiary carbonated water injection

The procedure for the tertiary CWI test was initiated by water flooding the micro-model in which original oil and connate water saturation were previously established. After completing the primary water flooding by injection of about 5 pore volumes of the micro-model (i.e., 1.55 cm^3), carbonated water was injected at the flow rate of q_{inj} = 0.05 ml/min, pressure of P = 300 2.1 MPa, and temperature of T = 19 °C. **Figure 6.19** illustrates selected micro-model images at different sequences of the primary water flooding and tertiary carbonated water injection. The results showed that the carbonated water front gradually advances from injection towards the production side and subsequently the residual oil ganglia were swept up and eventually produced. The study

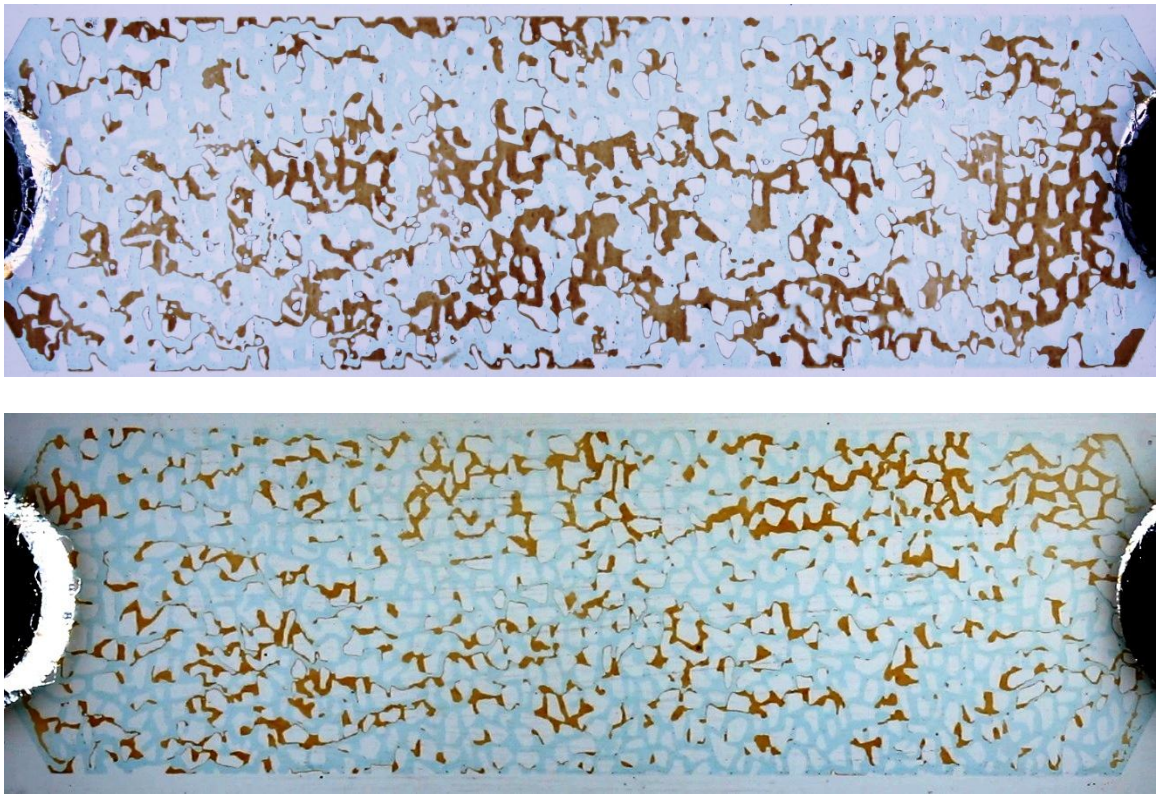

Figure 6.17: Comparative observation of the saturation distribution at the end of waterflooding (a) and secondary carbonated water injection (b).

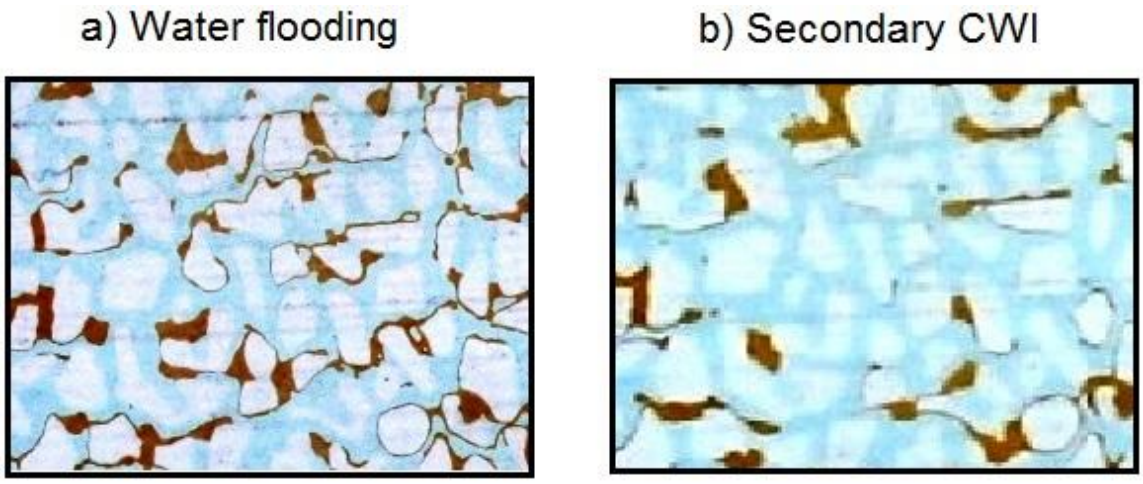

Figure 6.18: Comparative observation of the wettability condition at the end of water flooding (a) and secondary carbonated water injection (b).

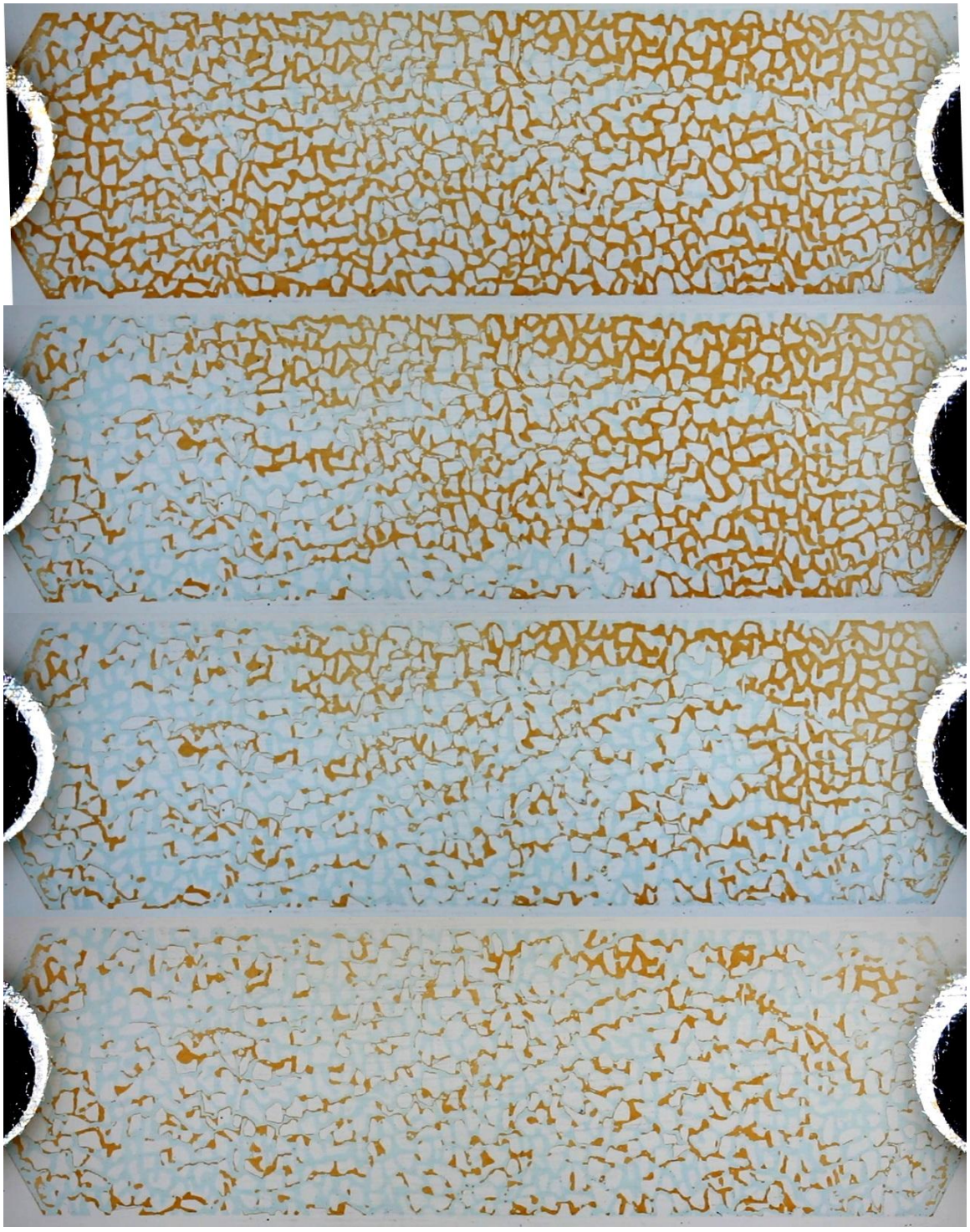

(Continued on next page …)

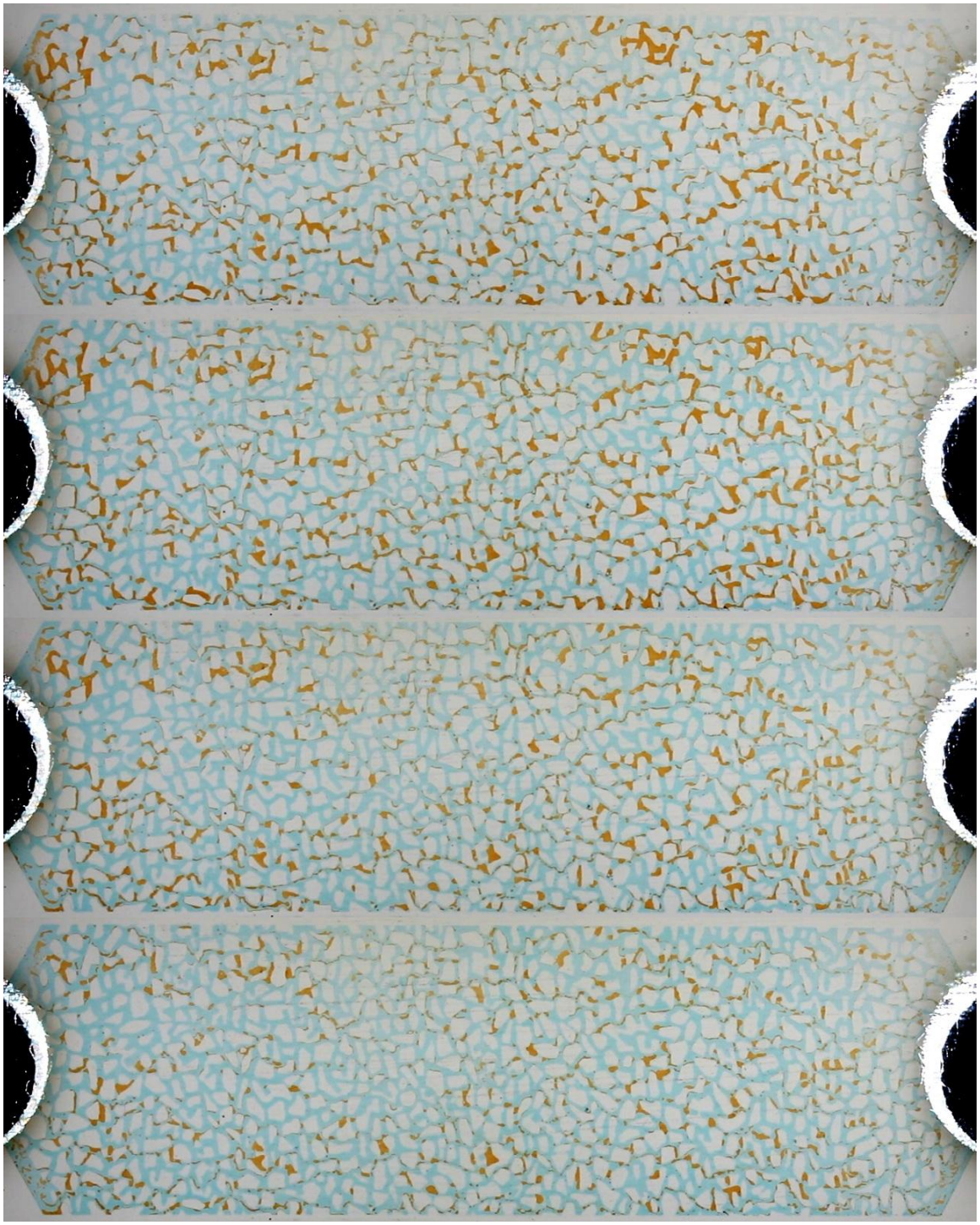

Figure 6.19: Chronological progress of the primary water flooding followed by tertiary carbonated water flooding.

prepared the carbonated water using the same physical characteristics as the injection brine. However, a slight colour contrast was added in order to visually differentiate the two brine phases in the micro-model and distinguish the location of the front between the carbonated water and that of water. This was achieved by adding 0.1 ml more of the blue dye to the carbonated brine so it could be clearly distinguished in the high resolution images. After conducting the tertiary CWI test, it was observed that the CWI was capable of recovering more oil and reducing the residual oil saturation after the primary water flooding. Compared to the primary water flooding scenario, a reduction of about 7.7% in residual oil saturation was observed when CWI was implemented in the tertiary mode, which shows a large potential of tertiary CWI in improving light oil production.

Figure 6.20 illustrates a magnified section of the micro-model indicating the capability of tertiary carbonated water flooding for recovering trapped oil ganglia after primary water flooding. It was observed in the figure that the residual oil was trapped by sticking to the oil-wet grains and the trapped oil in the dead end pores and cavities in the model were produced when tertiary CWI was implemented. The reason for this was the introduction of carbonated water into the micro-model and later the CO_2 mass transfer from brine to the oil phase resulted in changes from the wettability from an oil-wet to water-wet condition, which greatly improved the release of residual oil. The process behind this was the CO_2 dissolution into the oil phase leading to oil swelling and viscosity reduction, which enhanced the sweep efficiency and ultimately improved the oil recovery.

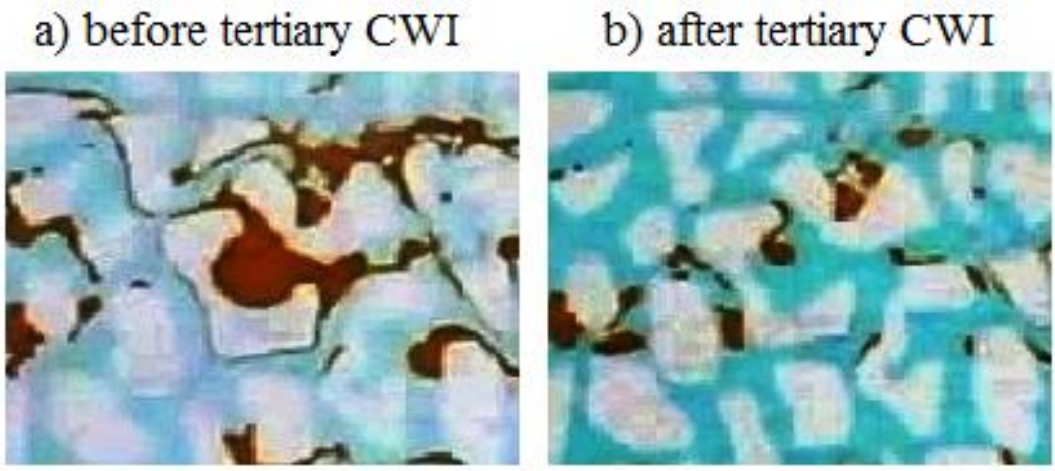

Figure 6.20: Production of the trapped oil during carbonated water injection.

6.5.8. Run #5: Extended tertiary carbonated water injection

The tertiary carbonated water injection run was extended to about 20 PV of the injected carbonated water. As depicted in **Figure 6.21**, continuation of carbonated water injection was found to be beneficial in terms of oil recovery and about 3.1% of extra oil was produced when the carbonated water injection was continued to higher injected PV. This clearly showed that the CO_2 mass transfer from the brine phase to the oil phase takes place continuously over a period of time. Even after a relatively longer period of carbonated water injection time, CO_2 diffusion into the oil phase promotes the recovery of the residual oil ganglia because the oil phase is not fully saturated with CO_2 at experimental pressure and temperature and is still capable to dissolving more CO_2 as the injection time increases.

Analysis of the selected magnified images of the micro-model in run #4 and #5 demonstrated that the effectiveness of carbonated water injection lasts for a long period of time (even after 20 PV of injected carbonated water) as depicted in Figure 6.21.

6.6. Chapter summary

In this study, a visual glass micro porous medium, called a micro-model, was successfully designed, manufactured, and tested in order to observe the details of various mechanisms during carbonated water injection. The results of 5 successful micro-model flooding experiments were summarized in this chapter and the results were analyzed carefully to investigate the wettability and contact angle behaviour of the entire system under different injection scenarios.

a) run #4: TCWI after 5 PV injection

b) run #5: TCWI after 20 PV injection

Figure 6.21: Comparative observation of the effect of injection time on the performance of tertiary carbonated water injection.

Wettability analysis of the micro-model at initial stages (i.e., establishment of S_{wc} and S_{oi}) clearly showed that the glass micro-model behaves as an oil-wet environment for the fluids used in this study. Therefore, during the initial oil saturation process, the oil phase occupied most of the pore spaces and relatively low connate water saturation was observed. Moreover, analysis of the wetting phase after primary water flooding revealed that the majority of the residual oil remained trapped due to the oil-wet nature of the glass micro-model. In addition, carbonated water injection was observed to be successful in modifying the wettability towards water-wet and evidence of beneficial wettability alteration was noticed for both secondary and tertiary carbonated water flooding scenarios.

Overall, the micro-model study of the carbonated water injection confirmed the successfulness of this method in enhancing the oil recovery. It was also concluded that the CWI can increase the oil recovery by 9.4% and 7.3% for secondary and tertiary scenarios, respectively, compared to the conventional water flooding.

Micro-model results demonstrated that continuation of the tertiary carbonated water flooding even 5 PV of carbonated water injection, improved the oil recovery unremittingly. It was concluded that since the residual oil is always brought in contact with fresh carbonated water, the CO_2 mass transfer to the residual oil phase could continue for a considerable time and would continue to enhance oil recovery. Therefore, it can be concluded that carbonated water injection is considered as endless injection scenario, compared to other techniques such as primary water flooding, and can definitely be a practical alternative to conventional water flooding.

CHAPTER SEVEN: Conclusions and Recommendations

7.1. Conclusions

An experimental study on carbonated water injection foe Enhanced Oil Recovery was carried out using an unconsolidated sand-pack system, light oil sample (mixture of few samples) from the Bakken formation in Saskatchewan, Canada, with viscosity of μ_o = 2.76, and synthetic brine (2 wt.% NaCl). Both secondary and tertiary CWI tests were performed to evaluate the performance of CWI in terms of oil recovery and CO_2 storage under different injection strategies and operating conditions. The results of this study led to the following conclusions:

Phase behaviour studies:

- Since a finite amount of CO_2 dissolves in water and consequently in the oil phase, maximum solubility of CO_2 in brine is a limiting factor in the CWI process and limits oil swelling, viscosity reduction, and maintains residual oil saturation.

- The CO_2 solubility in both brine and fresh water was measured at two constant temperatures of T = 25 and 40°C and various saturation pressures. The results showed that the CO_2 solubility in brine is a function of pressure, temperature, and salinity.

- The solubility of CO_2 in brine increases with increased pressure at constant temperature and salinity. In addition, the impact of pressure on CO_2 solubility

diminishes as the pressure of the system increases. Therefore, the solubility of CO_2 increases more substantially at lower pressures than at higher pressures. Moreover, the solubility of CO_2 in brine decreases when temperature increases from T = 25 to 40 °C, at constant pressure of P = 4.1 MPa and salinity of s = 0.3492 mole NaCl/kg water. The comparison of the CO_2 solubility in water and synthetic brine (2 wt.% NaCl) indicated that the addition of salt (i.e., NaCl) to the water leads to a reduction in CO_2 solubility.

- The CO_2 solubility in the oil phase is directly proportional to the pressure and inversely proportional to the operating temperature. The CO_2 solubility increases steadily with pressure at two constant temperatures of T = 25 and 40 °C. However, the increase is m noticeably higher for temperature of T = 25 °C compared to T = 40 °C.

- At a constant temperature, the swelling factor increases with pressure until the light hydrocarbon extraction pressure, P_{ext} is reached, at which time most of the light to medium hydrocarbon groups are vapourized into the gaseous CO_2 phase. For pressures higher than P_{ext}, the oil shrinks and the oil swelling factor decreases because more hydrocarbons are extracted at higher pressures and the capability of CO_2 to extract the hydrocarbon components improves.. Furthermore, the oil swelling factor is higher at lower temperatures and the light component extraction pressure increases when the temperature of the CO_2–oil system increases.
- Existence of threshold CO_2 solubility, χ_{th}, in the oil phase is a required condition for the extraction of major light to medium hydrocarbon groups. This threshold

CO_2 solubility was approximately χ_{th} = 33.21 gr CO_2/100 gr oil for the oil sample in this study. In addition, the threshold CO_2 solubility was found to be independent of temperature and was the same for all swelling/extraction tests performed at different experimental temperatures.

Carbonate water injection studies

- The ultimate oil recovery of both secondary and tertiary CWI is consistently greater than that of conventional WF at various operating pressures ranging from P = 0.7 MPa to 10.3 MPa and two constant operating temperatures of T = 25 °C and 40 °C. For instance, at the pressure of P = 10.3 MPa and temperature of T = 25 °C, injection of CW was able to improve the conventional WF oil recovery by about 19.0% and 12.5% OOIP respectively for secondary and tertiary scenarios. This demonstrates the vast potential of CWI to improve oil recovery from virgin light oil reservoirs compared to conventional WF.

- CWI in light oil reservoirs is also beneficial for CO_2 storage. A large fraction (in the range of 40% to 60%) of total volume of injected CO_2 was dissolved in the injected CW and stored at the end of the CWI flooding.

- Operating pressure plays a significant role in the oil recovery process by CWI. Experimental results revealed that oil recovery by CWI can be increased by 14.21% and 8.03% for secondary and tertiary schemes, respectively, when pressure increased from P = 1.4 to 10.3 MPa. In addition, it was found that the cumulative oil recovery of both secondary and tertiary CWI improved

considerably for pressures up to P = 5.6 MPa when the experimental temperature was set to T = 25 °C. While for the ranges of P > 5.6 MPa the oil recovery using CWI increases only slightly. This was because at the constant temperature of T = 25 °C, the CO_2 solubility in brine increased considerably to a certain pressure and then was maintained neart the same level.

- The performance of CWI was different for different injection schemes (i.e., secondary and tertiary CWI). The results of flooding experiments at constant operating conditions showed that CWI in the secondary scheme improved the oil recovery more noticeably than in the tertiary CWI scheme. For instance, the cumulative oil recovery for secondary water flooding was 8.03% higher than when CW was injected in the tertiary scheme with all experimental conditions held consistent (i.e., P = 6.9 MPa, T = 25 °C, q_{inj} = 1.0 cm^3/min, and CL = 100%).
- The amount of oil recovery and CO_2 storage during CWI is dependent on other operating parameters such as temperature and CW characteristics (e.g., carbonation level). At a constant pressure, the cumulative oil recovery using CWI increase with reduced temperature and increased carbonation level. However, CW injection rate was found to have negligible influence on ultimate oil recovery using CWI when the other operating parameters were constant.

- The phase behaviour simulation study used the WINPROP module of CMG software. The experimental results of CO_2 solubility, swelling/extraction, IFT, and MMP determination tests, as well as the basic properties data were used to tune the PR-EOS. The final fluid model was examined by comparing the

simulated results with the experimental data. It was observed that the fluid model could accurately reproduce the various experimental data.

- The compositional simulator module of CMG, GEM, was used to simulate the laboratory sand-pack flooding tests of this study. The tuned PR-EOD fluid model developed formerly was imported to a flooding simulation model to represent the experimental fluids. The history data comparison successfully simulated the results for oil, brine, and CO_2 production as well as the differential pressure across the sand-pack in fair agreement with those obtained from the flooding experiments.
- It was concluded that the CMG simulation package is fairly capable in modeling the phase behaviour of the fluids used in this study. Additionally, the results from the compositional simulator, GEM, were able to accurately reproduce the results of the flooding tests.

Micro-model studies

- The performance of CWI was examined through sequences of carefully designed micro-model tests in order to visualize the CWI process and investigate the detailed recovery mechanisms. Wettability behaviour, contact angle analysis, and residual oil trapping mechanisms were studied using image processing tools.
- It was observed that the main mechanism trapping oil in the micro-model is the wettability trapping due to oil-wet nature of the micro-model. Evidence of other

trapping mechanisms such as snap-off and pore-doublet mechanisms were also observed during the flooding tests.

- It was found that CWI injection was capable of changing the wettability of the glass micro-model from oil-wet to a water-wet condition. Micro-model observations revealed that the wettability of the system was gradually modified as the carbonated water injection proceeds. It was concluded that carbonated water injection can be considered as a beneficial IOR technique that is capable in effectively changing the wettability of mixed- to oil-wet reservoirs to a more favourable water-wet condition.
- Continuation of carbonated water injection for more than 5 pore volumes of the micro-model was found to be advantageous in recovering an additional 3.1% of original in-place oil. It was found that the main mechanism that contributes this additional recovery is continued dissolution of CO_2 into the oil phase and subsequent oil swelling and viscosity reduction, which ultimately led to improved mobility of the residual oil ganglia in the micro-model.

7.2. Recommendations

- Although laboratory studies using recovered oil samples resulted in a beneficial understanding around the performance of CWI, further laboratory investigations using live oil samples are recommended for both phase behaviour and flooding tests. In addition, conducting the CWI flooding experiments using real reservoir cores provides more realistic and field-like conclusions.
- It has been reported that the injection brine salinity might have significant influences on the performance of water flooding. Therefore, it is highly recommended to perform CWI flooding test at various type of salts (e.g. $CaCl_2$ and $MgCl_2$) as well as various concentrations (e.g. 5%, 10%, and 15%) in order to investigate the effects of brine composition on the performance of CWI. In this regard, a preliminary study on the effect of various salts and their concentrations on the CO_2 solubility is necessary.
- Corrosion problem has been considered as one of the drawbacks of CWI which mostly happens in surface facilities and the pipes inside the wellbore. Detailed investigation of the effects of CWI process on various pipings and equipments is highly recommendes particularly when CWI is considered to be implemented in field scale.
- It is also recommended to upscale the laboratory simulations into field-scale simulations. Both hypothetical and real field models could be used to examine the performance of CWI in larger scale models. Comparative evaluation of the performance of CWI with that of CO_2 flooding and CO_2 WAG flooding in field-scale may lead to additional results with beneficial operating parameters.

- The micro-model test in this study consisted of analyzing the recovery and trapping mechanisms at pore level by careful visualizations. However, another important and fundamental parameter that plays a significant role in any solvent-based EOR techniques is the diffusion coefficient. Analysis and examination of the diffusion process could be accomplished by a combination of the micro-model visualization tests and appropriate mathematical modeling. The results could be useful in gaining a better understanding of the details of recovery mechanisms.
- The micro-model of this study was prepared based on a heterogeneous sand stone micro pattern. However, various trapping mechanisms could be studied individually by designing suitable micro channels representing the desired flow networks. Different snap-off and pore-doublet trapping mechanisms could be studied in relation to the effect of various network micro pattern characteristics.
- It is also recommended to calculate the Capillary Number in micromodel tests in order to investigate the degree of the importance of various forces inside the micromodel, particularly, viscous and capillary forces.
- It is also recommended to systematically compare the performance of CWI with those of CO_2 injection and CO_2 WAG injection. The results could be compared in terms of ultimate oil recovery, breakthrough time, sweep efficiency, and CO_2 storage capacity.
- During micro-model experiments, some evidence was observed that indicated carbonated water may flow in different pore channels and not follow the flow paths taken by the previously injected flood water. Therefore, recommended

study to investigate the effectiveness of post water flooding after CWI is recommended. In general, micro-model examination of CWI in relation to other IOR/EOR techniques, such as CO_2 flooding and water flooding could be beneficial in further maximizing the recovery performance of the target reservoir.

REFRENCES

Abedini, A, Torabi, F., Parametric Study of the Cyclic CO_2 Injection Process in Light Oil Systems, Industrial and Engineering Chemical Research, 2013, 52 (43), 15211–15223.

Abedini, A., Mosavat, N., Torabi, F., Determination of Minimum Miscibility Pressure of Crude Oil– CO_2 System by Oil Swelling/Extraction Test, Energy Technology, Wiley, 2014, 2 (5), 431–439.

Abedini, A., Torabi, F., and Mosavat, N., Predicting Solvent Concentration Profile in the Porous Media Using Various Numerical Solutions to Convection–Dispersion Equation, Journal of Mathematics and System Science, 2012, 2, 409–419.

Abedini, A., Torabi, F., Oil Recovery Performance of Immiscible and Miscible CO_2 Huff-and-Puff Processes, Energy Fuels, 2014, 28 (2), pp 774–784.

Al-Jabra, M., Al-Anazi, B. D., A Comparison Study of the CO_2–Oil Physical Properties Literature Correlations Accuracy Using Visual Basic Modelling Technique, Journal of NAFTA, 2009, 60 (5), 287–291.

Amyx, J.W., Bass, D.M. and Whiting, R.L., Petroleum Reservoir Engineering, Mcgraw-Hill Book Company, 1960, 133–210.

Armitage, P. and Dawe, R.A., What Is the Rheology of Foam in Porous Media? A Micromodel Study, presented at the International Symposium on Oilfield Chemistry in Houston, Texas, USA, February 8–10, 1989, Paper SPE 18495.

Asghari, K., Nasehi Araghi, M., Ahmadloo, F., Utilization of CO_2 for Improving the Performance of Waterflooding in Heavy Oil Recovery, presented at Canadian

International Petroleum Conference, Calgary, Alberta, Canada, June 16-18, 2009, Paper 2009-130.

Bahralolom, I.M., and F.M. Orr JR., Solubility and Extraction in Multiple Contact Miscible Displacements: Comparison of N_2 and CO_2 Flow Visualization Experiments, SPE Reservoir Evaluation, 1988a, 3(1), 213–219.

Bahralolom, I., R.E. Bretz and F.M. Orr JR., Experimental Investigation of the Interaction of Phase Behaviour with Microscopic Heterogeneity in a CO_2 Flood, SPE Reservoir Evaluation, 1988b, 3(2), 662–672.

Bai, B., Liu, Y., Coste, J., and Li, L., Preformed Particle Gel for Conformance Control: Transport Mechanism through Porous Media, SPE Reservoir Evaluation, 2007, 10(2), 176–184.

Bamberger, A., Sieder, G., and Maurer, G., High-Pressure (Vapor plus Liquid) Equilibrium in Binary Mixtures of (Carbon Dioxide plus Water or Acetic Acid) at Temperatures from 313 to 353 K, Journal of Supercritical Fluids, 2000, 17, 97–110.

Bon, J., and Sarma, H.K., A Technical Evaluation of a CO_2 Flood for EOR Benefits in the Cooper Basin, presented at the SPE Asia Pacific Oil and Gas Conference and Exhibition, Perth, Australia, October 18-20, 2004, Paper SPE 88451.

Bora, R., Chakma, A., and Maini, B.B., Experimental Investigation of Foamy Oil Flow Using a High Pressure Etched Glass Micromodel, Proceedings SPE Annual Technical Conference and Exhibition, Denver, Colorado, USA, October 5–8, 2003, 91–100.

Buckley, S.E., and Leverett, M.C., Mechanism of Fluid Displacements in Sands, Transactions of the AIME, 1942, 146, 107–116.

Bui, L.H., Tsau, J.S., and Willhite, G.P., Laboratory Investigations of CO_2 near Miscible Application in Arbuckle Reservoir, presented at SPE Improved Oil Recovery Symposium, Tulsa, Oklahoma, USA, April 24–28, 2010, Paper SPE 129710-MS.

Campbell, B.T. and Orr, F.M., Flow Visualization for CO_2/Crude Oil Displacements, SPE Journal, 1985, 25(5), 665–678.

Cardoza, J.M.P., Sharif, Q.J., and Poston, S.W., Carbonated Water Imbibition Flooding: An Enhanced Oil Recovery Process for Fractured Reservoirs, presented at SPE/DOE 8th Symposium on Enhanced Oil Recovery, Tulsa, Oklahoma, April 22–24, 1992: Paper SPE/DOE 24164,

Chang, S.-H., Martin, F.D., Grigg, R.B., Effect of Pressure on CO_2 Foam Displacements: a Micromodel Visualization Study, Proceedings SPE Symposium on Improved Oil Recovery, Tulsa, Oklahoma, USA, April 17–20, 1994, 2, 11–22.

Chang, Y.B., Coats, B.K., and Nolen, J.S., A Compositional Model for CO_2 Floods Including CO_2 Solubility in Water, presented at the 1996 Permian Basin Oil and Gas Recovery Conference, Midland, Texas, USA, March 27–29, 1996, Paper SPE 35164.

Chapoy, A., Mohammadi, A.H., Chareton, A., Tohidi, B., and Richon, D., Measurement and Modeling of Gas Solubility and Literature Review of the Properties for the Carbon Dioxide–Water System, Industrial Engineering and Chemical Research, 2004, 43 (7), 1794–1802.

Chatzis. I., and Dullien F. A. L., Dynamic Immiscible Displacement Mechanisms in Pore Doublets: Theory versus Experiment, Journal of Colloid and Interface Science, 1983, 91, 199–222.

Christensen, R. J., Carbonated Waterflood Results–Texas and Oklahoma, presented at the 7th Annual Meeting of Rocky Mountain Petroleum Sections of AIME, 1961, Paper SPE 66.

Cinar, Y., K., R. Jessen, Berenblyum, R., Juanes, F., and Orr, M., An Experimental and Numerical Investigation of Crossflow Effects in Two-Phase Displacements, SPE Journal, 2006, 11(2), 216–226.

Costa, G.M.N., Rocha, P.S.M.V., Riberio, A.L.C., Menezes, P.R.F., Lima, R.C.A., and Costa, P.U.O., Rodrigues, E.A., An Improved Method for Calculating CO_2 Minimum Miscibility Pressure Based on Solubility Parameter. Journal of Petroleum Science and Engineering. 2012, 98–99, 144–155.

Cramer, S.D. The Solubility of Methane, Carbon Dioxide, and Oxygen in Brines from 0 °C to 300 °C, U.S. Department of Interior, Bureau of Mines, Washington D.C., 1982.

Crawford, H.R., Neill, G.H., Bucy, B.J., and Crawford, P.B., Carbon Dioxide A Multipurpose Additive for Effective Well Stimulation, Journal of Petroleum Technology, 1963, 237.

Danesh, A., Krinis, D., Henderson, G.D., and Peden, J.M., Asphaltene Deposition in Miscible Gas Flooding of Oil Reservoirs, Chemical Engineering Research and Design, 1988, 66, 339–344.

de Nevers, N.H., A Calculation Method for Carbonated Water Injection, SPE Journal, 1964, 9–20.

de Nevers, N.H., Carbonated Waterflooding: Is It a Lab Success and a Field Failure, World Oil, September, 1966, 93–96.

DeRuiter, R.A., Nash, L.J., Singletary, M.S., Solubility and Displacement Behavior of a Viscous Crude with CO_2 and Hydrocarbon Gases, SPE Journal of Reservoir Engineering, 1994, 9 (2), 101–106.

Diamond, L.W., Akinfiev, N.N., Solubility of CO_2 in water from -1.5 to 100 C and from 0.1 to 100 MPa: Evaluation of Literature Data and Thermodynamic Modelling, Fluid Phase Equilibria, 2003, 208(1–2), 265–290.

Dong, Y., Ishizawa, C., Lewis, E., Dindoruk, B., Carbonated Water Flood: What We Observed In Sand Pack Experiments, Presented at International Symposium of the Society of Core Analysts, Austin, Texas, USA, September 18–21, 2011, Paper SCA2011-34.

Duan, Z., and Sun, R., An Improved Model Calculating CO_2 Solubility in Pure Water and Aqueous NaCl Solutions from 273 to 533 K and from 0 to 2000 bar, Chemical Geology, 2003, 193, 257–271.

Duan, Z., Sun, R., Zhu, C., and Chou, M., An Improved Model for the Calculation of CO_2 Solubility in Aqueous Solutions Containing Na^+, K^+, Ca^{2+}, Mg^{2+}, Cl^-, and $SO4^{2-}$, Marine Chemistry, 2006, 98 (2), 131–139.

Dullien, F.A.L., Porous Media: Fluid Transport and Pore Structure; Academic Press Inc.: San Diego, California, 1992.

Dumore, J.M., Hagoort, J., and Risseeuw, A.S., A One-Dimensional Analytical Model for Carbonated Waterflooding, Shell Internal Research Report, August, 1982, RKGR.82.065.

Emera, M.K., and Sarma, H.K., A Genetic Algorithm-Based Model to Predict CO_2–oil Physical Properties for Dead and Live Oil. Presented at Canadian International Petroleum Conference, Calgary, Alberta, Canada, June 13–15, 2006, Paper SPE 2006-197.

Emera, M.K. and Sarma, H.K., Use of Genetic Algorithm to Obtain CO_2–Oil Minimum Miscibility Pressure (MMP) in Designing a CO_2 Miscible Flood, Journal of Petroleum Science & Engineering, 2005, 46, 37–52.

Enick, R.M., and Klara, S.M., CO_2 Solubility in Water and Brine under Reservoir Conditions. Chemical Engineering Communications, 1989, 90(1), 23–33.

Ennis-King, J. and Paterson, L., Role of Convective Mixing in the Long-Term Storage of Carbon Dioxide in Deep Saline Formations. SPE Journal, 2005, 10 (3), 349–356.

Exxonmobil Home Page, The outlook for energy: a view to 2040, 2013. http://www. http://corporate.exxonmobil.com/en/energy/energy-outlook (accessed June 2013).

Falls, A.H., Analysis of an Idealized Carbonated Waterflood in the South Wasson/Clearfork Formation, Shell Internal Research Report, April, 1986, BRC 8–86.

Falls, A.H., Cherubini, A.A., and Seunsom, S., The Response of South Wasson/Clearfork Crude to Carbonated Water in an Etched-Glass Model, Shell Internal Research Report, April, 1986, BRC-1350.

Flumerfelt R,W., and Li X., A Cyclic Surfactant-Based Imbibition/Solution Gas Drive Process for Low-Permeability, Fractured Reservoirs, presented at SPE 68th Annual Technical Conference and Exhibition, Houston, Texas, USA, October 3–6, 1993, Paper SPE 26373.

George, D.S., Hayat, O., and Kovscek, A.R., A Microvisual Study of Solution-Gas-Drive Mechanisms in Viscous Oils, Journal of Petroleum Science and Engineering, 2005, 46(1–2), 101–119.

Global Energy Assessment: Toward a Sustainable Future, International Institute for Applied Systems Analysis, IIASA magazine, Cambridge, Summer 2012.

Gorell, S. B., and A. H. Falls, Status of Carbonated Waterflooding Research, Shell Internal Research Report, October, 1986.

Grattoni, C. A. and Dawe, R. A., Gas and Oil Production from Waterflood Residual Oil: Effects of Wettability and Oil Spreading Characteristics, Journal of Petroleum Science and Engineering, 2003, 39(3–4), 297–308.

Green, D.W., and Willhite, G.P., Enhanced Oil Recovery, SPE Textbook Series, Richardson, TX, 1998.

Gu, F., Solubility of Carbon Dioxide in Aqueous Sodium Chloride Solution under High Pressure, Journal of Chemical Engineering of Chinese Universities, 1998, 12(2), 118–1231.

Han, J.M., Shin, H.Y., Min, B.-M., Han, K.-H., and Cho, A., Measurement and Correlation of High Pressure Phase Behaviour of Carbon Dioxide+Water System, Journal of Industrial and Engineering Chemistry, 2009,15(2), 212–216.

Hickok, C. W., and Ramsay, H. J., Case Histories of Carbonated Waterfloods in Dewey-Bartlesville Field, presented at SPE Secondary Recovery Symposium, Wichita Falls, Texas, USA, May 7–8, 1962, Paper SPE 333-MS.

Hickok, C. W., Christensen, R. J., and Ramsay, Jr. H. J., Progress Review of the K&S Carbonated Waterflood Project, Journal of Petroleum Technology, 1960, 20–24.

Hiorth, A., Cathles, L.M., Kolnes, J., Vikane, O., Lohne, A., Korsnes, R.I., and Madland, M.V., A Chemical Model for the Seawater-CO_2- Carbonate System–Aqueous and Surface Chemistry, presented at International Symposium of the Society of Core Analysts, Abu Dhabi, UAE, October 29–November 2, 2008, Paper SCA2008-18.

Hoffman, A.E., Crump, J.S., and Hocott, C.R., Equilibrium Constants for a Gas-Condensate System, Trans AIME, 1953, 198, 1–10.

Holm, L. W. Carbon Dioxide Solvent Flooding for Increased Oil Recovery. Petroleum Transactions AIME. 1959, 216, 225–231.

Holm, L. W. CO_2 Requirements in CO_2 Slug and Carbonated Water Recovery Processes. Producer Monthly. September, 1963.

Hornof, V. and Morrow, N.R. Flow Visualization of the Effects of Interfacial Tension on displacement, SPE Reservoir Evaluation, 1988, 3(1), 251–256.

IEA Greenhouse Gas R&D Programme: http://www.IEAGHG.org. Accessed May 15, 2013.

Intergovernmental Panel on Climate Change (IPCC). Climate Change 2007: The Physical Science Basis, Cambridge University Press. 2007, Cambridge, United Kingdom and New York, NY, USA, 996 pp.

Jamaluddin, A.K.M., Kalogerakis, N.E., Chakma, A., Predictions of CO_2 Solubility and CO_2 Saturated Liquid Density of Heavy Oils and Bitumens Using a Cubic Equation of State, Fluid Phase Equilibria. 1991, 64, 33–48.

Jarrell, P.M., Fox, C.E., Stein, M.H., and Webb, S.L., Practical Aspects of CO_2 Flooding, SPE Monograph, 2002, 22, 220p.

Jodecke, M., Kamps A. P.-S., and Maurer G., Experimental Investigation of the Solubility of CO_2 in (Acetone + Water) Michael, Journal of Chemical and Engineering Data, 2007, 52 (3), 1003–1009.

Jodecke, M., Xia, J., Kamps, A.P.S., and Maurer, G., Solubility of Carbon Dioxide in Aqueous, Salt-Containing Solution of Methanol or Acetone, Chem. Eng. Technol., 2004, 27 (1), 31–34.

Johnson, W.E., Lab Experiments with Carbonated Water and Liquid Carbon Dioxide as Oil Recovery Agents, Producer Monthly. November, 1952, 15.

Johnson, W.E., Macfarlane, R.M., Breston, J.N. and Neil, D.C., Laboratory Experiments with Carbonated Water and Liquid Carbon Dioxide as Oil Recovery Agents, Producers Monthly, November, 1952, 17 (1).

Kamps, A.P.S., Sing, R., Rumpf, B., and Maurer, G., Influence of NH_4Cl, NH_4NO_3, and $NaNO_3$ on the Simultaneous Solubility of Ammonia and Carbon Dioxide in Water, Journal of Chemical and Engineering Data, 2000, 45 (5), 796–809.

Kansas Geological Survey Home Page, Open-file Report 2003-33. http://www.kgs.ku.edu/PRS/publication/2003/ofr2003-33/P1-05.html (accessed January 2013).

Kavousi, A.; Torabi, F.; Chan, C. Experimental Measurement of CO_2 Solubility in heavy Oil and Its Diffusion Coefficient calculation at both Static and Dynamic Conditions, Presented at SPE Heavy Oil Conference Canada, Calgary, Alberta, Canada, June 11–13, 2013, Paper SPE 165559.

Kechut, N.I., Riazi, M., Sohrabi, M., Jamiolahmady, M, Tertiary Oil Recovery and CO_2 Sequestration by Carbonated Water Injection (CWI). presented at SPE International Conference on CO_2 Capture, Storage, and Utilization, New Orleans, Louisiana, USA, November 10–12, 2010, Paper SPE 139667.

Kechut, N.I., Sohrabi, M., Jamiolahmady, M, Experimental and Numerical Evaluation of Carbonated Water Injection (CWI) for Improved Oil Recovery and CO_2 Storage, presented at SPE EUROPEC/EAGE Annual Conference and Exhibition, Vienna, Austria, May 23–26, 2011, Paper SPE 143005.

Khatib, A.K., Earlougher, R.C, CO_2 Injection as an Immiscible Application for Enhanced Recovery in Heavy Oil Reservoirs, presented at the 1981 California Regional Meeting, Bakersfield, California, USA, March 25–26, 1981, Paper SPE 9928.

Kiepe, J., Horstmann, S., Fischer, K., Gmehling, G., Experimental determination and prediction of gas solubility data for CO_2+H_2O mixtures containing NaCl or KCl at temperatures between 313 and 393 K and pressures up to 10 Mpa, Industrial and Engineering Chemistry Research, 2002, 41, 4393–4398.

King, M.B., Mubarak, A., Kim, J.D., Bott, T.R., The Mutual Solubilities of Water with Supercritical and Liquid Carbon Dioxide. Journal of Supercritical Fluids. 1992, 5, 296–302.

Kislyakov, Y.P., Kovalenko, K.I., Babalyna, G.A., Treatment of well-Bore Area of Injection Wells with Carbonated Water, Neft Khoz, 1967, 45 (4), 41–44.

Korsnes, R.I., Madland, M.V., Vorland, K.A.N., Hildebrand H., Kristiansen, T.G., and Hiorth, A., Enhanced Chemical Weakening of Chalk Due to Injection of CO_2Enriched Water, presented at International Symposium of the Society of Core Analysts, Abu Dhabi, UAE, October 29 to November 2, 2008, Paper SCA2008-24.

Koschel, D., Coxam, J.-Y., Rodier, L., Majer, V., Enthalpy and Solubility Data of CO_2 in Water and NaCl(aq) at Conditions of Interest for Geological Sequestration, Fluid Phase Equilibria, 2006, 247 (1–2), 107–120.

Kraus, A.D., Mendoza, C.M., and Cortes, M.C., Injection of Acidulated Water of Carbonated Water, ING Petrol, 1970, 10 (1), 17–21.

Lago, M., Huerta, M. and Gomes, R., Visualization Study During Depletion Experiments of Venezuelan Heavy Oils Using Glass Micromodels, Journal of Canadian Petroleum Technology, 2002, 41(1), 41–47.

Laidlaw W.G., and Wardlaw N.C., A Theoretical and Experimental Investigation of Trapping in Pore Doublets, Canadian Journal of Chemical Engineering, 1983, 61 (5), 719–727.

Lake, L.W., Pope, G.A., Carey, G.F., and Sepehernoori, K. Isothermal, Multiphase, Multicomponent Fluid-Flow in Permeable Media. In Situ. 1984, 8(1), 1–40.

Laroche, C., Vizika, O., and Kalaydjian, F., Wettability Heterogeneities in Gas Injection: Experiments and Modelling, Petroleum Geoscience, 1999, 5(1), 65–69.

Latil, M. Enhanced Oil Recovery; Editions Technip: Paris, 1980.

Li, T.M.W., Ioannidis, M., and Chatzis, I., Recovery of Non-aqueous Phase Liquids from Ground Sources, U.S. Patent 7,300,227 B2, 2007.

Lindeberg, E., Wessel-Berg, D., Vertical Convection in an Aquifer Column Under a Gas Cap of CO_2, journal of Energy Conversion and Management, 1997, 38, S229–S234.

Liu, Y., Hou, M., Yang, G., Han, B., Solubility of CO_2 in Aqueous Solutions of NaCl, KCl, $CaCl_2$ and their Mixed Salts at Different Temperatures and Pressures, The Journal of Supercritical Fluids. 2011, 56 (2), 125–129.

Mackay, E.J., Henderson, G.D., Tehrani, D.H., and Danesh, A., The Importance of Interfacial Tension on Fluid Distribution During Depressurization, SPE Reservoir Evaluation, 1998, 1(5), 408–415.

Madland, M.V., Finsnes, A, Alkafadgi, A., Risnes, R., Austad, T., The Influence of CO_2 Gas and Carbonate Water on the Mechanical Stability of Chalk, Journal of Petroleum Science and Engineering, 2006, 51 (3–4), 149–168.

Mahers, E.G. and Dawe, R.A., Quantification of Diffusion inside Porous Media for EOR Processes by Micromodel and Holography, paper SPE 12679, presented at the SPE/DOE 4^{th} Symposium on EOR, Tulsa, Oklahoma, USA, April 16–18, 1984.

Mahers, E.G. and Dawe, R.A., The Role of Diffusion and Mass Transfer Phenomena in the Mobilisation of Oil during Miscible Displacement, presented at the 2^{nd} European Symposium on Enhanced Oil Recovery, Paris, France, November 8–10, 1982.

Mahers, E.G. and Dawe, R.A., Visualization of Microscopic Displacement Processes Within Porous Media in EOR Capillary Pressure Effects, presented at the 3rd European Meeting on Improved Oil Recovery, Rome, April 16–18, 1985.

Mao, S., Hu, J.W., Zhang, D., and Li, Y., Thermodynamic modeling of ternary CH_4-H_2O-NaCl fluid inclusions, Chemical Geology, 2013, 335, 128–135.

Martin, J.W., Additional Oil Production through Flooding with Carbonated Water, Producer Monthly, July, 1951a, 18–22.

Martin, J.W., The Use of Carbon Dioxide in Increasing the Recovery of Oil. Producer Monthly, May, 1951b, 13–15.

Mayers, E.H., Earlougher, R.C., Spivak, and A., Costa, A. Analysis of Heavy-Oil Immiscible CO_2 Tertiary Coreflood Data, SPE Reservoir Engineering, February, 1988, 69–75.

Melzer, L.S., Carbon Dioxide Enhanced Oil Recovery (CO_2 EOR): Factors Involved in Adding Carbon Capture, Utilization and Storage (CCUS) to Enhanced Oil Recovery, National Enhanced Oil Recovery Initiative, Center for Climate and Energy Solutions, 2012.

Miller, J., and Jones, R. A., A Laboratory Study to Determine Physical Characteristics of Heavy Oil after CO_2 Saturation, presented at the 1981 SPE/DOE Second Joint Symposium on Enhanced Oil Recovery, Tulsa, Oklahoma, USA, 1981, Paper SPE/DOE 9789.

Miller, J.S. and Jones, R.A., A Laboratory Study to Detennine Physical Characteristics of Heavy Oil after CO_2 Saturation, final report U.S. DOE, 1984.

Mohamed, I., He, J, Nase-El-Din, H.A., Effect of Brine Composition on CO_2/Limestone Rock Interactions during CO_2 Sequestration, Journal of Petroleum Science Research, 2013, 2 (1), 14–26.

Morrow, N.R., Lim H.T. and Ward, J.S., Effect of Crude Oil Induced Wettability Changes on Oil Recovery, SPE Formation Evaluation, 1986, 1(1), 89–103, 1986.

Mosavat, N. and Torabi, F., Performance of Secondary Carbonated Water Injection (CWI) in Light Oil Systems, Industrial & Engineering Chemistry Research, 2014, 53 (3), 1262–1273.

Mosavat, N. Rasaei, M. R. Torabi, F., Experimental Determination of Absolute and Relative Permeability in Composite Cores: Effect of Ordering, Special Topics & Reviews in Porous Media - An International Journal, 2013, 4, 33–43.

Nelson, L., Barker, J., Li, T., Thomson, N., Ioannidis, M., and Chatzis, J., A field trial to assess the performance of CO_2-supersaturated water injection for residual volatile LNAPL recovery, Journal of Contaminant Hydrology, 2009, 109, 82–90.

Nghiem, L., Shrivastava, V., Kohse, B., Hassam, M., Yang, C., Simulation of Trapping processes for CO_2 Storage in Saline Aquifers, presented at Canadian International Petroleum Conference, Calgary, Alberta, June 16–18, 2009, Paper 2009-156.

Nighswander, J.A., Kaiogerakis, N., and Mehrotra, A.K., Solubilities of Carbon Dioxide in Water and 1 wt% NaCl Solution at Pressures up to 10 Mpa and Temperatures from 80 to 200 °C. Journal of Chemical Engineering Data, 1989, 34(3), 355–360.

Orr, F. M., Heller, J. P., Taber, J. J., Carbon Dioxide Flooding for Enhanced Oil Recovery: Promise and Problems, Journal of the American Oil Chemists Society, 1982, 59 (10), 810A–817A.

Orr, F.M., Jr. and Jessen, K., An Analysis of the Vanishing Interfacial Tension Technique for Determining Minimum Miscibility Pressure, Fluid Phase Equilibria, 2007, 255, 99–109.

Owete, O.S. and Brigham, W.E., Flow Behaviour of Foam: A Porous Micromodel Study, SPE Reservoir Evaluation, 1987, 2 (3), 315–323.

Panteleev, V. G., and Tumasyan, A. B., Capillary Imbibition of Carbonated Water into an Oil-Saturated Porous Medium, Neft Khoz, 1972, 5, 64–66.

Paterson, L., Hornof, V. and Neale, G., Visualization of a Surfactant Flood of an Oil Saturated Porous Medium, SPE Journal, 1984, 24 (3), 325–327.

Perez, J.M., Poston, S.W., and Sharif Q. J., Carbonated Water Imbibition Flooding: An Enhanced Oil Recovery Process for Fractured Reservoirs, presented at SPE/DOE 8^{th} symposium on Enhanced Oil Recovery, Tulsa, Oklahoma, USA, April 22–24, 1992, Paper SPE 24164.

Pruess, K., ECO2N: A TOUGH2 Fluid Property Module for Mixtures of Water, NaCl, and CO_2, Earth Sciences Division, Lawrence Berkeley National Laboratory University of California, Berkeley, CA 94720, 2005.

Prutton, C.F., and Savage, R.L., The Solubility of Carbon Dioxide in Calcium Chloride-Water Solutions at 75, 100, 120 °C and High Pressures, Journal of the American Chemical Society, 1945, 67 (9), 1550–1554.

Ramesh A.B., and Dixon T.N., Numerical simulation of Carbonated Waterflooding in a Heterogeneous Reservoir, presented at Third Numerical Simulation of Reservoir Performance Symposium of the SPE of AIME. Houston, Texas, USA, January l0–12, 1973, Paper SPE 4075.

Ramsay, H.J.J., and Small, F.R., 1964, Use of Carbon Dioxide for Water Injectivity Improvement, Journal of Petroleum Technology, 25, 1964.

Rapoport, L.A. and Leas, W.J., Properties of Linear Waterfloods, Trans AIME, 1953, 198, 139–148.

Ren, W., Bentsen, R.G., and Cunha, L.B., A Study of the Gravity Assisted Tertiary Gas Injection Processes, Journal of Canadian Petroleum Technology, 2005, 44 (2), 26–32.

Ren, X., Wu, P., Qu, Z. and Shi, C., Studying the Scaling Mechanism of Low-Permeability Reservoirs Using Visual Real-Sand Micromodel, Proceedings SPE Eighth International Symposium on Oilfield Scale, Aberdeen, United Kingdom, May 31–Jun 1, 2006, 95–101.

Riazi, M. Pore Scale Mechanisms of Carbonated Water Injection in Oil Reservoirs. Ph.D. Dissertation, Herriot-Watt University, Edinburgh, UK, 2011.

Riazi, M., Jamiolahmady, M., and Sohrabi, M., Theoretical investigation of pore-scale mechanisms of Carbonated Water Injection, Journal of Petroleum Science and Engineering, 2011, 75, 312–326.

Riazi, M., Sohrabi, M., Jamiolahmadi, M., Ireland, S., and Brown, C., Oil Recovery Improvement Using CO_2-Enriched Water Injection, presented at SPE Europec/Eage Annual Conference And Exhibition, Amsterdam, Netherlands, June 8–11, 2009, Paper SPE 121170.

Riazi, M., Jamiolahmady, M., Sohrabi, M., Theoretical Investigation of Pore-Scale Mechanisms of Carbonated Water Injection, Journal of Petroleum Science and Engineering, 2011, 75, 312–326.

Romero, C., Alvarez, J.M., and Muller, A.J., Micromodel Studies of Polymer-Enhanced Foam Flow Through Porous Media, Proceedings - SPE Symposium on Improved Oil Recovery, Tulsa, Oklahoma, USA, April 13–17, 2002, 532–541.

Romero-Zeron, L. and Kantzas, A., The Effect of Wettability and Pore Geometry on Foamed-Gel-Blockage Performance, SPE Reservoir Evaluation, 2007, 10 (2), 150–163.

Rumpf, B., Nicolaisen, H., Ocal, C., and Maurer, G., Solubility of Carbon Dioxide in Aqueous Solutions of Sodium Chloride: Experimental Results and Correlation, Journal of Solution Chemistry, 1994, 23, 431–448.

Sabirzyanov, A.N., Shagiakhmetov, R.A., Gabitov, F.R., Tarzimanov, A.A., Gumerov. F.M., Water Solubility of Carbon Dioxide under Supercritical and Subcritical Conditions, Theoretical Foundations of Chemical Engineering, 2003, 37(1), 51–53.

Sankur, V., Creek, J.L., Di Julio, S.S. and Emanuel, A.S., A Laboratory Study of Wilmington Tar Zone CO_2 Injection Project, SPE Reservoir Engineering, 1986, 1 (1), 95–104.

Saxon, J., Jr., Breston, J.N., and Macfarlane, R.M., Laboratory Tests with Carbon Dioxide and Carbonated Water as Flooding Mediums, Producers Monthly, November, 1951, 16 (1), 8.

Sayegh, S.G. and Fisher, D.B., Enhanced Oil Recovery by CO_2 Flooding in Homogeneous and Heterogeneous 2D Micromodels, PAPER 2008-005, presented at Canadian International Petroleum Conference/SPE Gas Technology

Symposium Joint Conference (the Petroleum Society's 59th Annual Technical Meeting), Calgary, Alberta, Canada, 17–19 June, 2008.

Sayegh, S.G., Krause, F.F., Marcel, G., Cornellus, D., Rock/Fluid Interactions of Carbonated Brines in a Sandstone Reservoir: Pembina Cardium, Alberta, Canada, SPE Formation Evaluation, 1990, Paper SPE 19392.

Scott, J.O., and Forrester C.E., Performance of Domes Unit Carbonated Waterflood - First Stage, Journal of Petroleum Technology, 1965, 1379–1384.

Shenawi, S.H., and Wu C.H., Compositional Simulation of Carbonated Waterfloods in Naturally Fractured Reservoirs, presented at SPE/DOE Ninth Symposium on Improved Oi1 Recovery, Tulsa, Oklahoma, USA, April 17–20, 1994, Paper SPE 27741.

Shenawi, S.H., Wu, C.H, and Luan Z.A., A New Iterative Mathematical Model for the Analysis of Imbibition Carbonated Waterflood in Naturally Fractured Reservoirs, presented at SPE Permian Basin Oil and Gas Recovery Conference, Midland, Texas, USA, March 16–18, 1994, Paper SPE 27717.

Shu, W., Carbonated Waterflooding for Viscous Oil Recovery Using a CO_2 Solubility Promoter and Demoter, US Patent 4,415,032, 1983.

Simon, R., Graue, D.J., Generalized Correlations for Predicting Solubility, Swelling and Viscosity Behaviour of CO_2–Crude Oil Systems, Journal of Petroleum Technology, 1965, 17, 102–106.

Smith, J.D., Chatzis, I., and Ioannidis, M.A., A New Technique to Measure the Breakthrough Capillary Pressure, Journal of Canadian Petroleum Technology, 2005, 44 (11), 25–31.

Sohrabi Sedeh, M., Kechut, N.I. Riazi, M. Jamiolahmady, M. Ireland, S., Robertson, G.J., Coreflooding Studies to Investigate the Potential of Carbonated Water Injection as an Injection Strategy for Improved Oil Recovery and CO_2 Storage, Journal of Transport in Porous Media. 2012, 91, 101–121.

Sohrabi, M., Riazi, M., Jamiolahmady, M., Ireland, S., and Brown, C., Mechanisms of Oil Recovery by Carbonated Water Injection, SCA Annual Meeting, 2009, Paper No. 26.

Sohrabi, M., Riazi, M., Jamiolahmadi, M., Ireland, S., and Brown C., Carbonated Water Injection (CWI) studies, presented at 29th Annual Workshop & Symposium, IEA Collaborative Project on Enhanced Oil Recovery, 2008.

Sohrabi, M., Riazi, M., Jamiolahmady, M., Kechut, N.I., Ireland, S., and Robertson, G. Carbonated Water Injection (CWI) – A Productive Way of Using CO_2 for Oil Recovery and CO_2 Storage, Energy Procedia, 2011, 4, 2192–2199.

Sohrabi, M., Riazi, M., Jamiolahmadi, M., Ireland, S., and Brown C, Carbonated Water Injection (CWI) studies, in proceeding of: 29th Annual Workshop & Symposium, IEA Collaborative Project on Enhanced Oil Recovery, 2008.

Solomon, S., The Bellona Foundation- Fact sheet: CO_2 Storage, Bellona Report, May, 2007.

Solomon, S., Qin, D., Manning, M., Chen, Z., Marquis, M., Averyt, K. B., Tignor, M., and Miller, H.L., Climate Change 2007, The Physical Science Basis, Cambridge University Press: Cambridge, United Kingdom and New York, New York, USA, 2007.

Soudmand-Asli, A., Ayatollahi, S. S., Mohabatkar, H., Zareie, M., and Shariatpanahi, S. F., The in Situ Microbial Enhanced Oil Recovery in Fractured Porous Media, Journal of Petroleum Science Engineering, 2007, 58 (1–2), 161–172.

Srivastava, R.K., Huang, S.S., Dyer, S.B., and Mourits, F.M., Measurement and Prediction of PVT Properties of Heavy and Medium Oils with Carbon Dioxide, presented at the 6th UNITAR International Conference on Heavy Crude and Tar Sands, Houston, Februray 12–17, 1995.

Standing, M.B., A Set of Equations for Computing Equilibrium Ratios of a Crude Oil/Natural Gas System at Pressures below 1000 Psia, Journal of Petroleum Technology, September, 1979, 1193–1195.

Steffens, A.J.E. Modeling and Laboratory Study of Carbonated Water Flooding. Master Thesis, Delft University of technology, Delft, Netherlands, 2010.

The Engineering Toolbox, http://www.engineeringtoolbox.com/gases-solubility-water-d_1148.html, accessed January 2013.

Touboul, E., Lenormand R. and Zarcone, C., Immiscible Displacements in Porous Media: Testing Network Simulators by Micromodel Experiments, paper SPE 16954, presented at the 62nd Annual Technical Conference and Exhibition of SPE, Dallas, Texas, USA, September 27–30, 1987.

Tran, T.S., Electromagnetic Assisted Carbonated Water Flooding in Heavy Oil Recovery. Master Thesis, Delft University of Technology, Delft, Netherlands, 2009.

Tsau, J.S., Bui, L.H., Willhite, G.P., Swelling/Extraction Test of a Small Sample Size for Phase Behavior Study, presented at SPE Improved Oil Recovery Symposium, Tulsa, Oklahoma, USA, April 24–28, 2010, Paper SPE 129728-MS.

Tumasyan, A.B., Babalyan G.A., Panteleev, B.G., Khalimov, E.M., Murzagildina, I, Sh. and Ionov, V.I., Results of Field Experiment on Pumping Carbonated Water in the Stratum, Neft Khoz, 1973, 12, 31–35.

U.S. Energy Information Administration Home Page. International energy outlook 2011, 2011, DOE/EIA-0484. www.eia.gov/ieo/pdf/0484(2011).pdf (accessed February 2013)

Valtz, A., Chapoy, A., Coquelet, C., Paricaud, P., Richon, D., Vapour–Liquid Equilibria in the Carbon Dioxide–Water System: Measurement and Modelling from 278.2 to 318.2 K, Fluid Phase Equilibria, 2004, 226, 333–344.

van Dijk, C. Carbonated Water Flood. Shell Internal Research Report, March, 1965, R 1189.

Wang, J., Dong, M., and Asghari, K., Effect of Oil Viscosity on Heavy-Oil/Water Relative Permeability Curves, Fifteenth SPE-DOE Improved Oil Recovery Symposium, Tulsa, Oklahoma, USA, April 22–26, 2006.

Welker, J.R. and Dunlop, D.D., Physical Properties of Carbonated Oils; Journal of Petroleum Technology, 1963, 15 (8), 873–875.

Weyburn-Midale Carbon Dioxide Project, http://en.wikipedia.org/wiki/Weyburn-Midale_Carbon_Dioxide_Project, Cenovus Energy Inc., 2010.

Whitson, C.H., and Brule, M.R., Phase Behavior, 2000, 20, Richardson, Texas: Monograph Series, SPE.

Wilson, G., A Modified Redlich-Kwong EOS Application Physical Data Calculation, presented at the annual AICHE National Meeting, Cleveland, Ohio, USA, May 4–7, 1968.

Winston, R.S., Carbonated Waterflooding for Viscous Oil Recovery using a CO_2 Solubility Promoter and Demoter, U.S Patent 4415032, November, 1983.

Winston, R. S., Carbonated Waterflooding for Viscous Oil Recovery, U.S Patent 4441555, April, 1984.

Yang, D., Tontiwachwuthikul, P., Gu, Y, Interfacial Tensions of the Crude Oil + Reservoir Brine + CO_2 Systems at Pressures up to 31 MPa and Temperatures of 27 °C and 58 °C, Journal of Chemical Engineering Data, 2005, 50, 1242–1249 .

Zendehboudi, S., Chatzis, I., Mohsenipour, A.A., and Elkamel, A., Dimensional Analysis and Scale-up of Immiscible Two-Phase Flow Displacement in Fractured Porous Media under Controlled Gravity Drainage, Energy & Fuels, 2011, 25, 1731–1750.

APPENDIX A: Laboratory simulation results

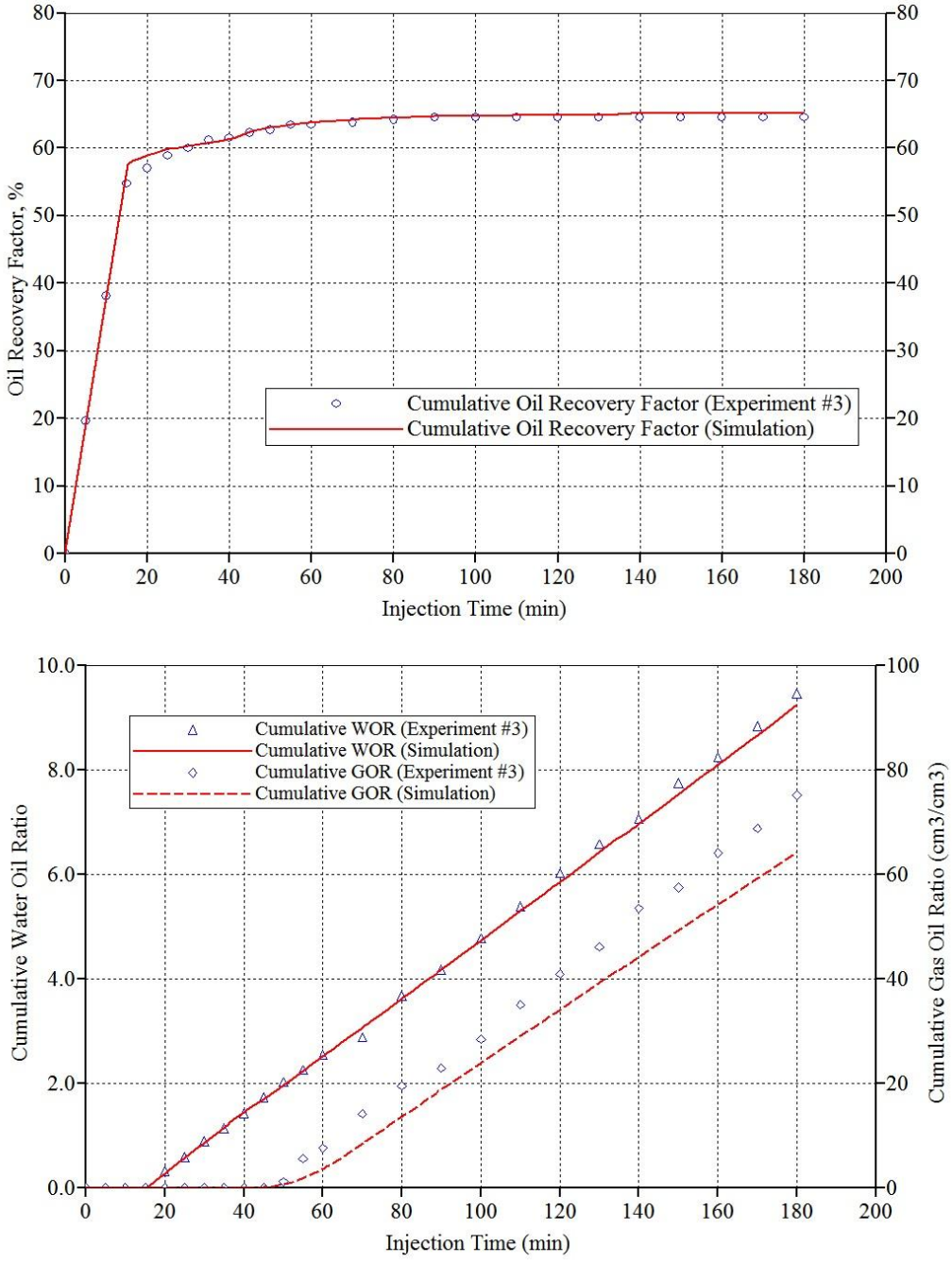

Figure A.1: Comparison of the simulated and measured cumulative oil recovery (a) and water oil ratio (b) for Test #3 (SCWI, P = 1.4 MPa, T = 25 °C, q_{inj} = 1.0 cm^3/min, CL = 100%).

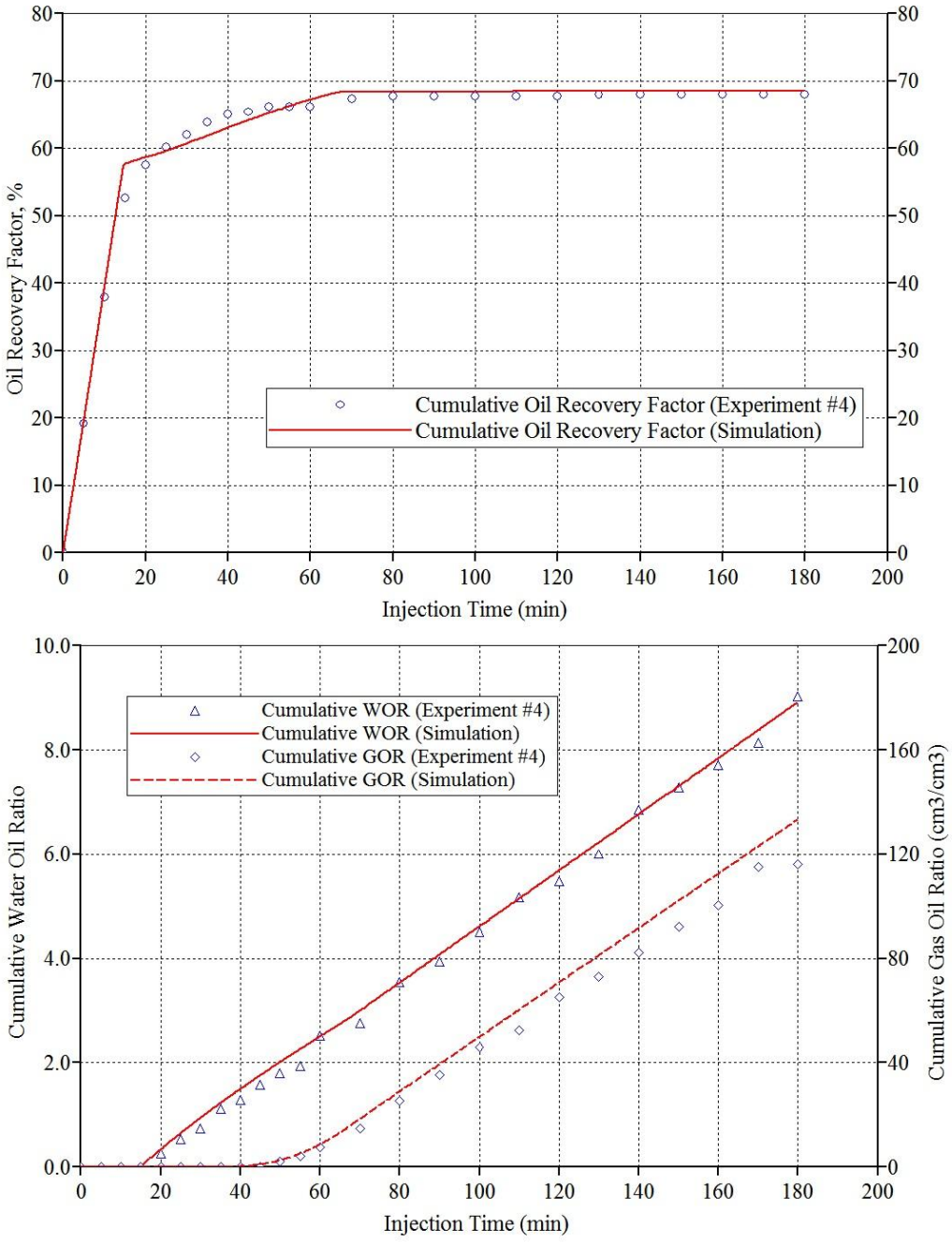

Figure A.2: Comparison of the simulated and measured cumulative oil recovery (a) and water oil ratio (b) for Test #4 (SCWI, P = 2.8 MPa, T = 25 °C, q_{inj} = 1.0 cm^3/min, CL = 100%).

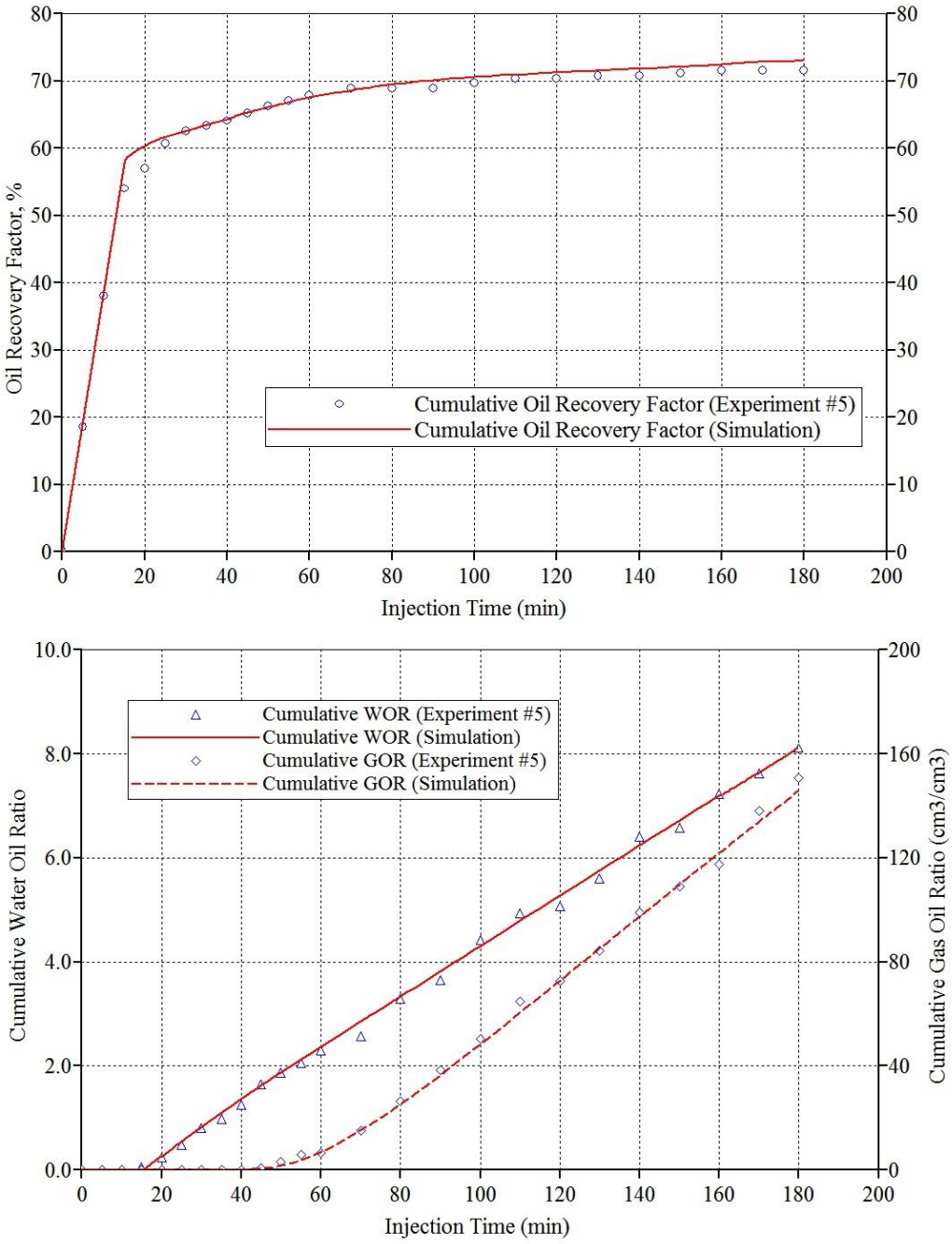

Figure A.3: Comparison of the simulated and measured cumulative oil recovery (a) and water oil ratio (b) for Test #5 (SCWI, P = 4.1 MPa, T = 25 °C, q_{inj} = 1.0 cm^3/min, CL = 100%).

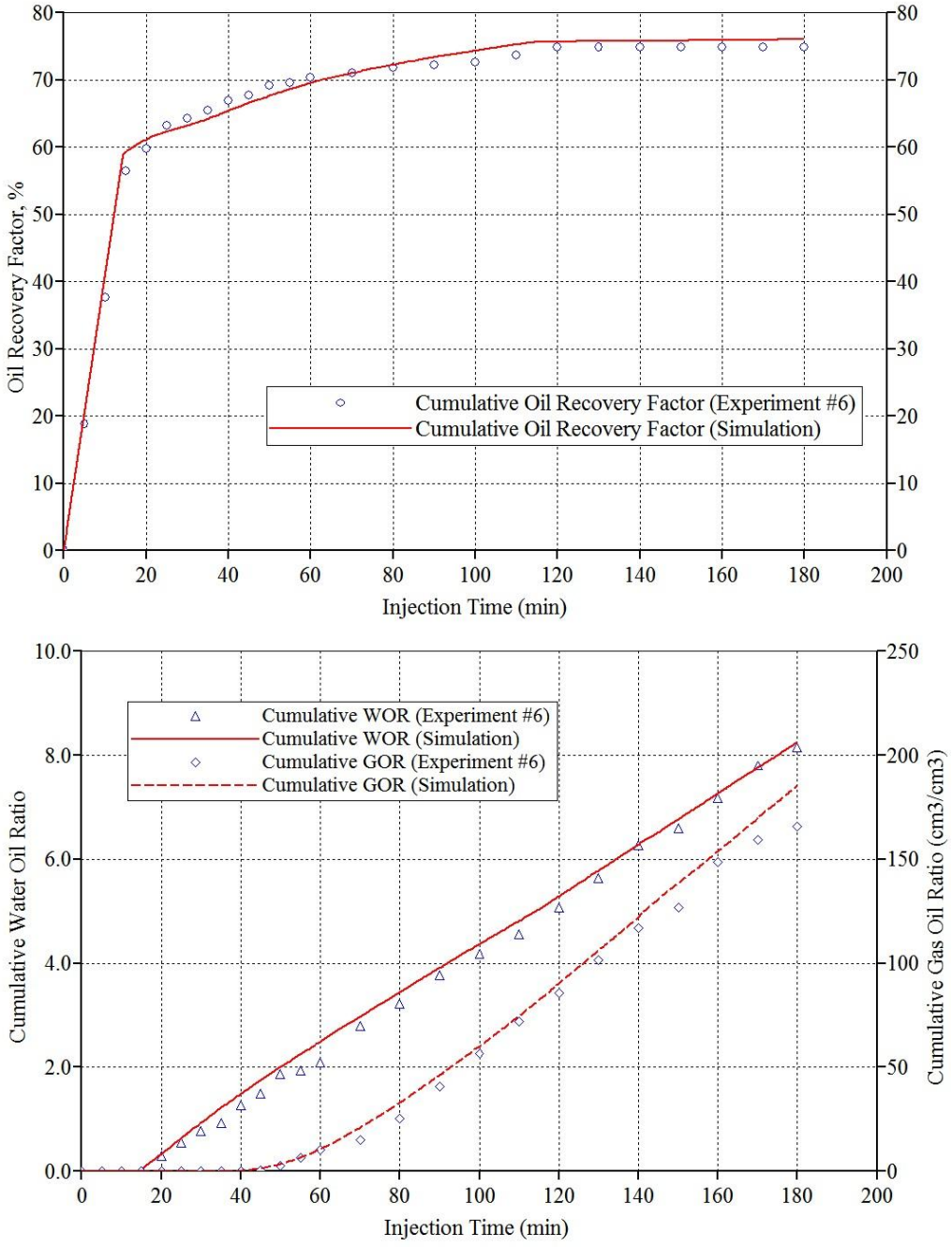

Figure A.4: Comparison of the simulated and measured cumulative oil recovery (a) and water oil ratio (b) for Test #6 (SCWI, P = 5.5 MPa, T = 25 °C, q_{inj} = 1.0 cm^3/min, CL = 100%).

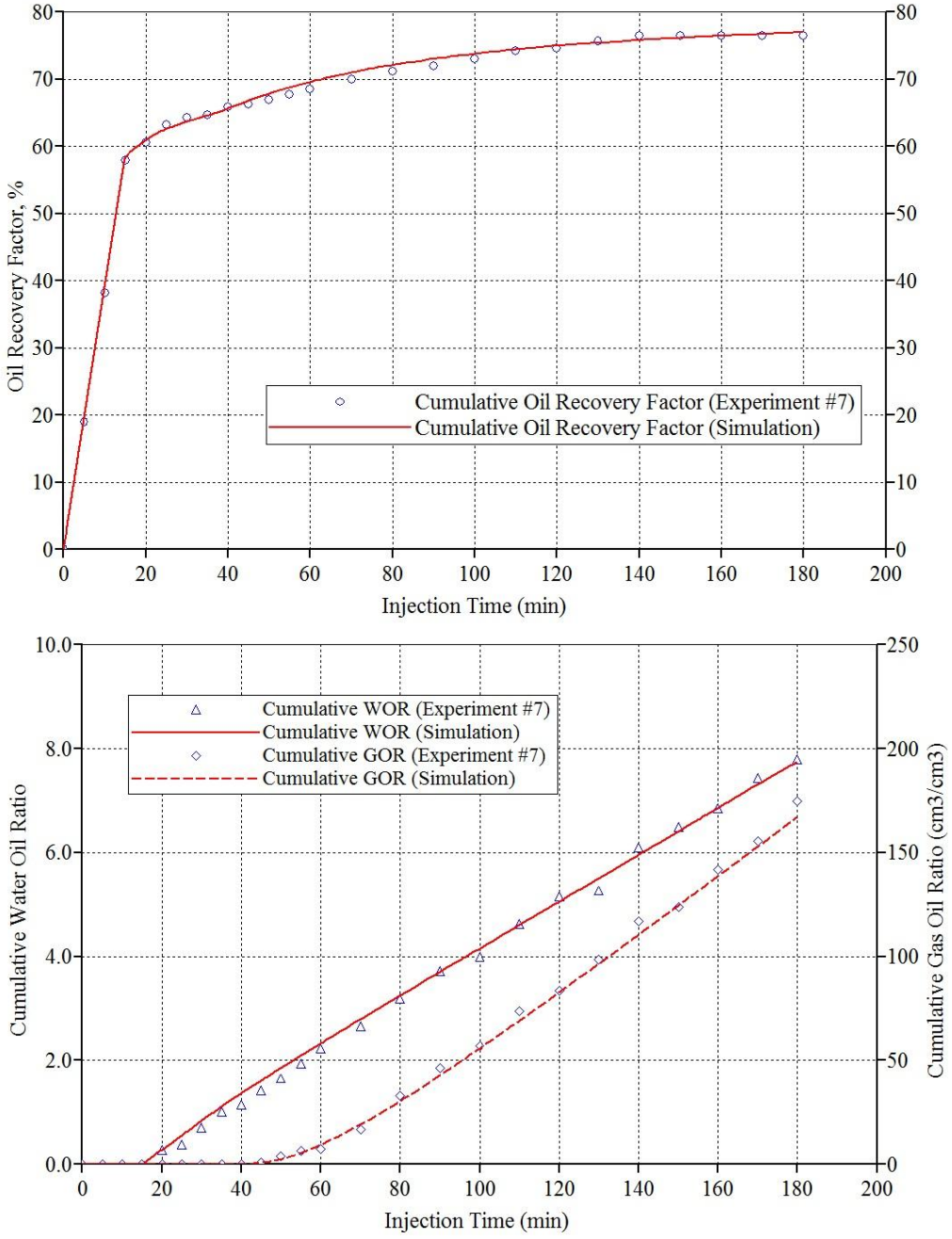

Figure A.5: Comparison of the simulated and measured cumulative oil recovery (a) and water oil ratio (b) for Test #7 (SCWI, P = 6.9 MPa, T = 25 °C, q_{inj} = 1.0 cm^3/min, CL = 100%).

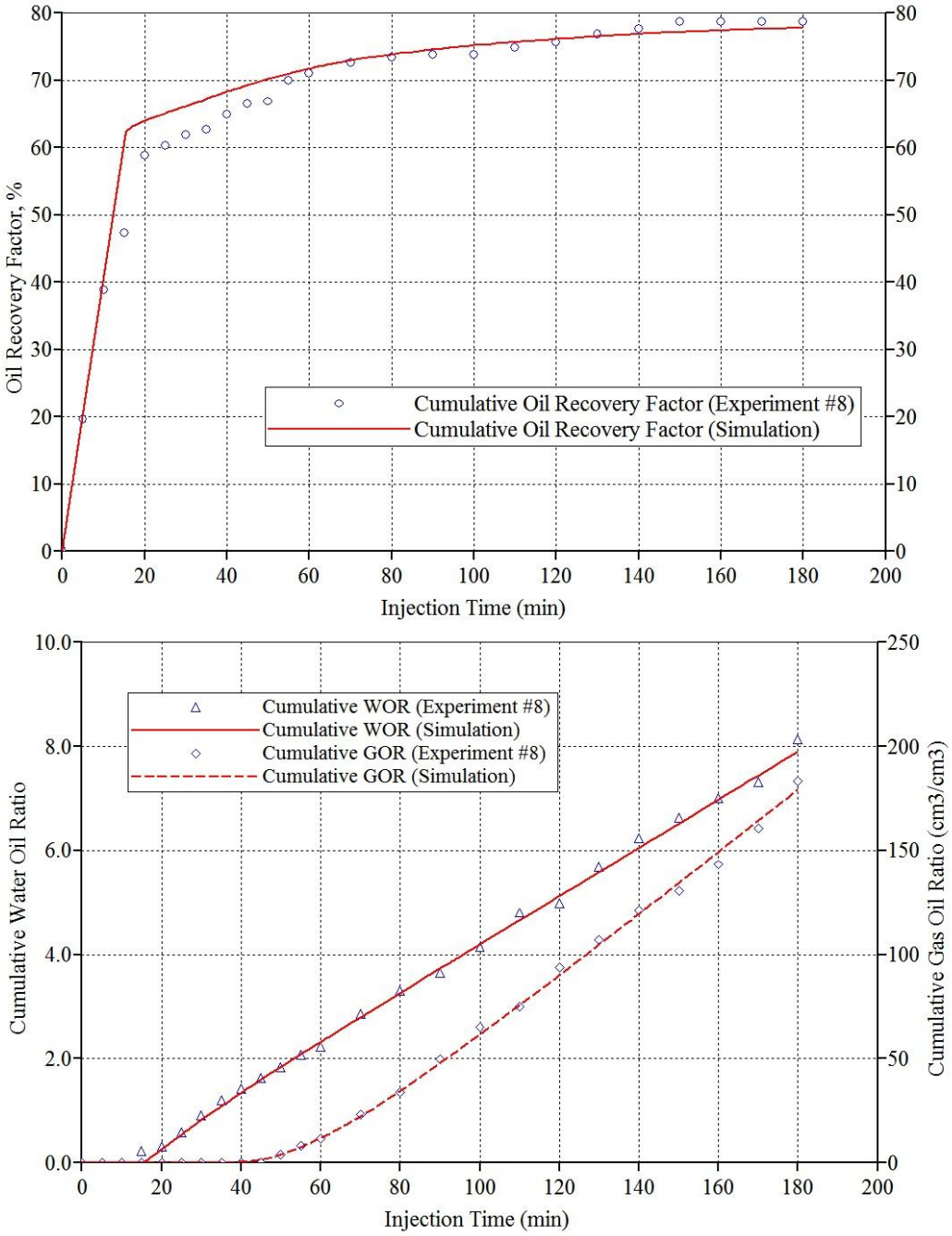

Figure A.6: Comparison of the simulated and measured cumulative oil recovery (a) and water oil ratio (b) for Test #8 (SCWI, P = 10.3 MPa, T = 25 °C, q_{inj} = 1.0 cm^3/min, CL = 100%).

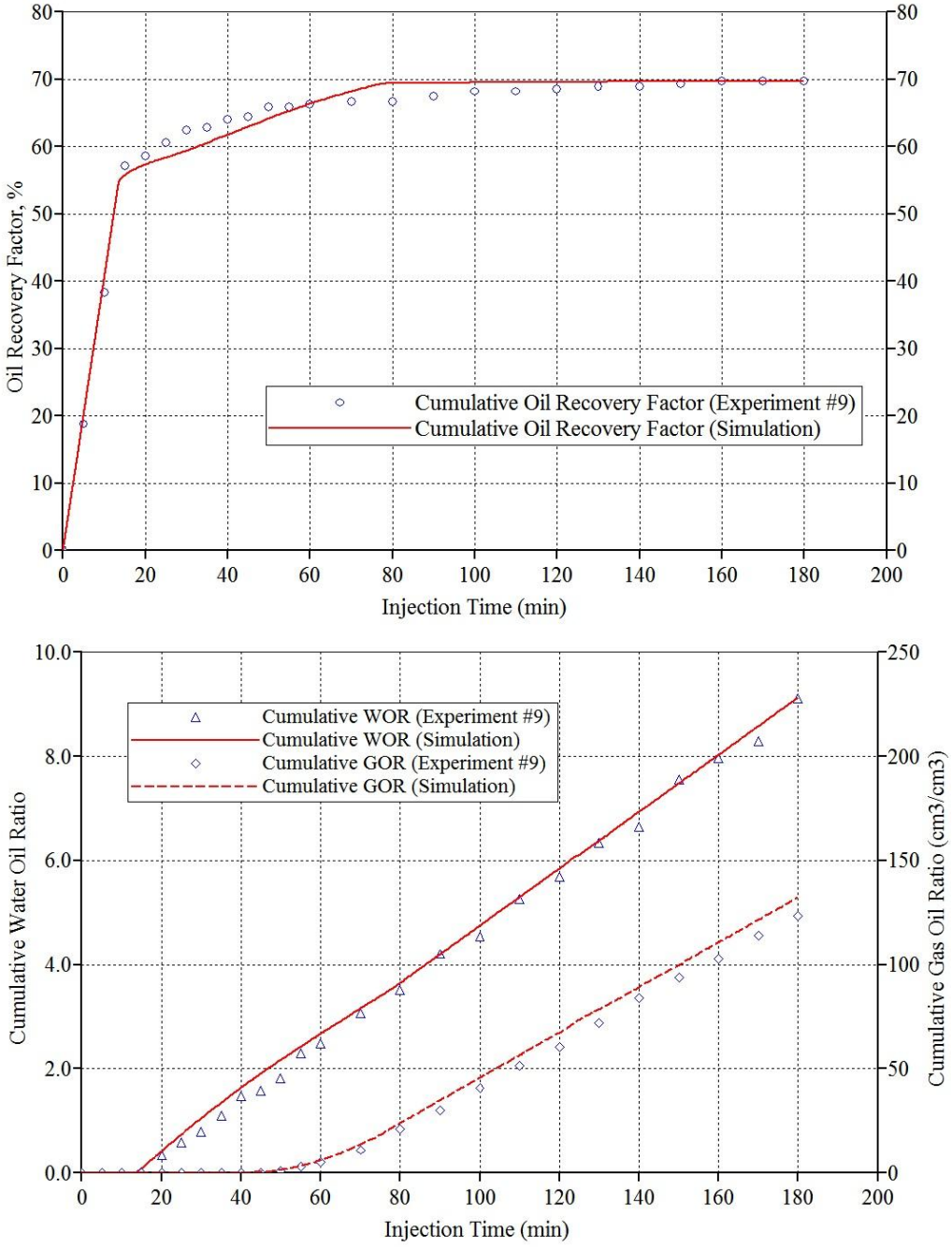

Figure A.7: Comparison of the simulated and measured cumulative oil recovery (a) and water oil ratio (b) for Test #9 (SCWI, P = 4.1 MPa, T = 40 °C, q_{inj} = 1.0 cm^3/min, CL = 100%).

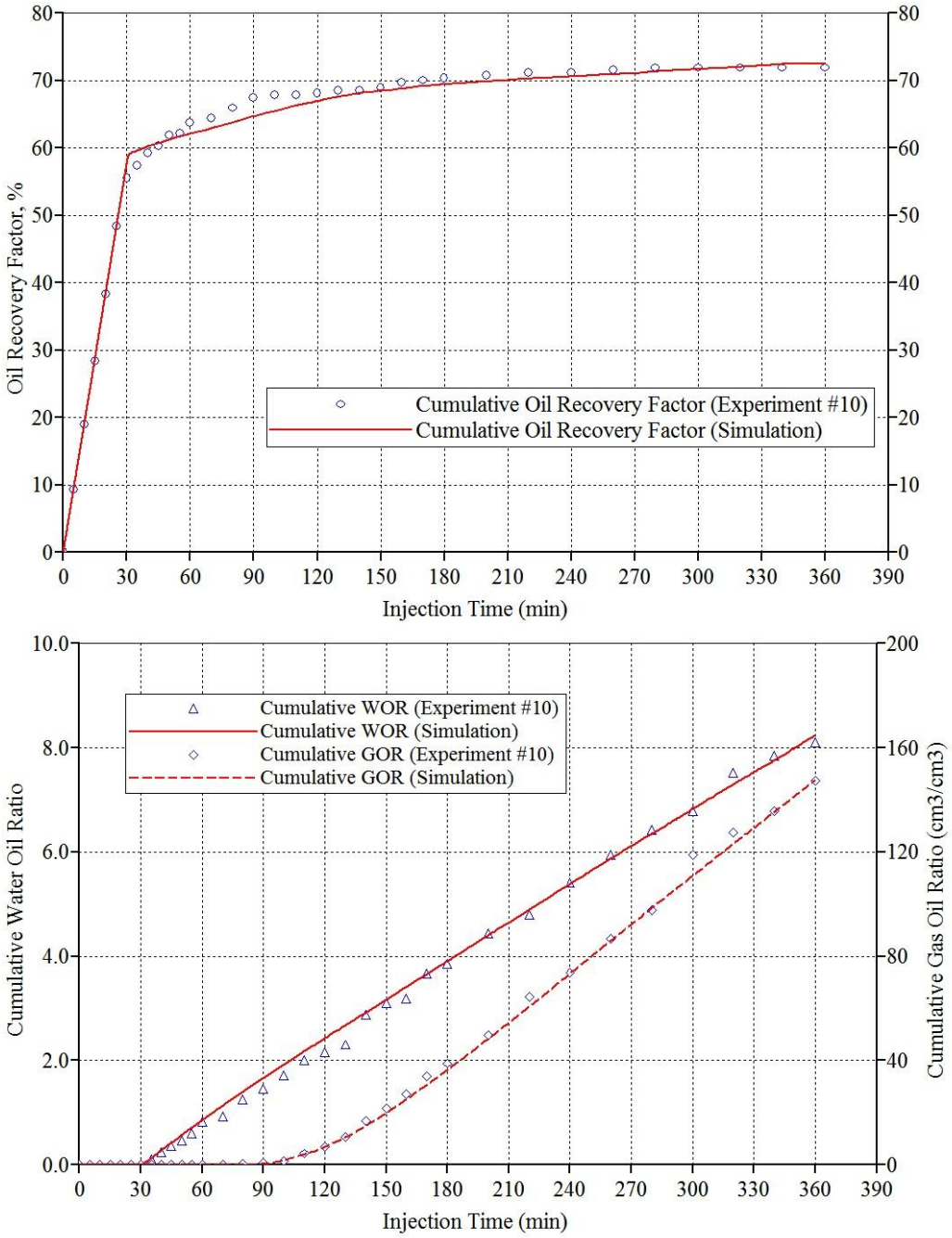

Figure A.8: Comparison of the simulated and measured cumulative oil recovery (a) and water oil ratio (b) for Test #10 (SCWI, P = 4.1 MPa, T = 25 °C, q_{inj} = 0.5 cm^3/min, CL = 100%).

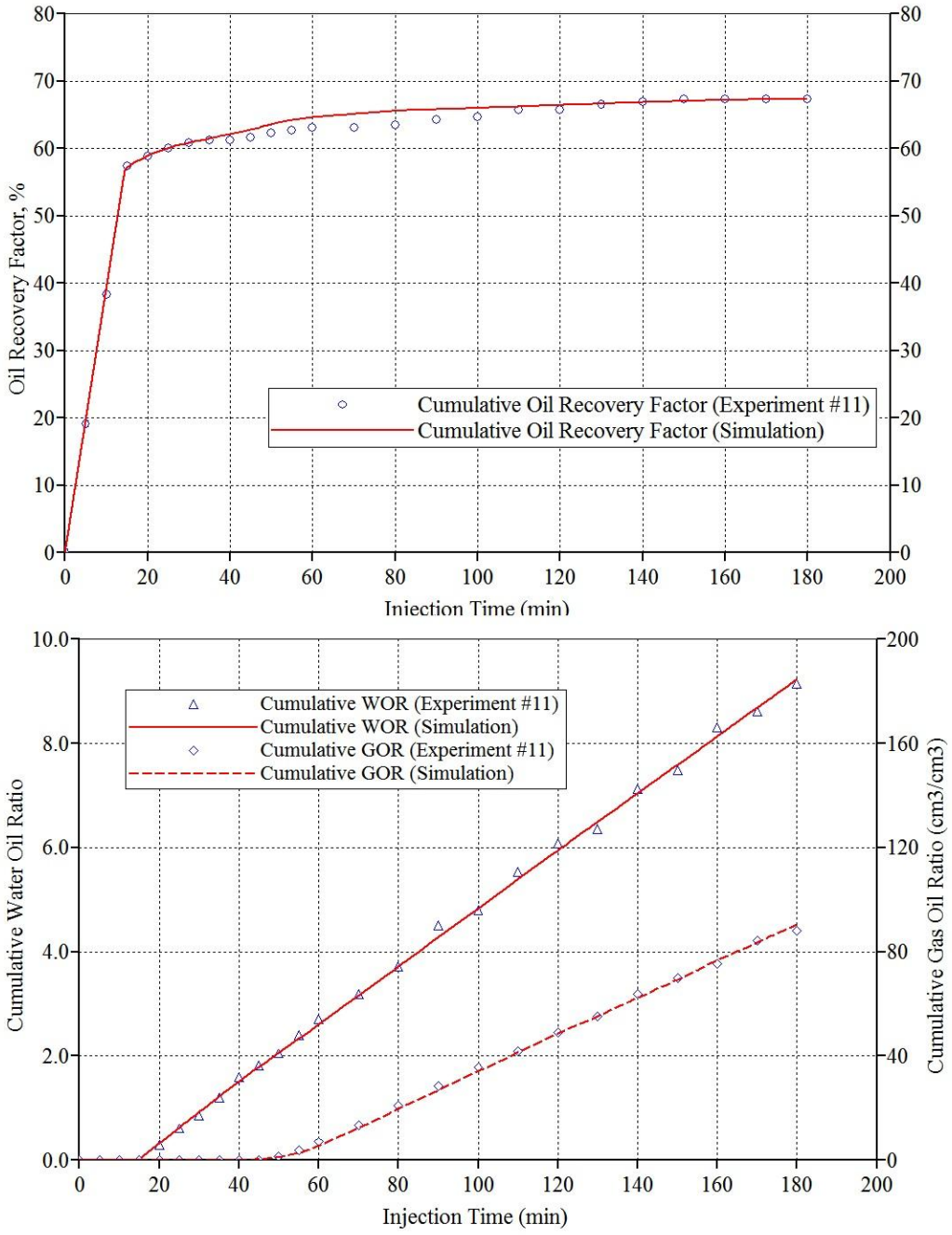

Figure A.9: Comparison of the simulated and measured cumulative oil recovery (a) and water oil ratio (b) for Test #11 (SCWI, P = 4.1 MPa, T = 25 °C, q_{inj} = 1.0 cm^3/min, CL = 50%).

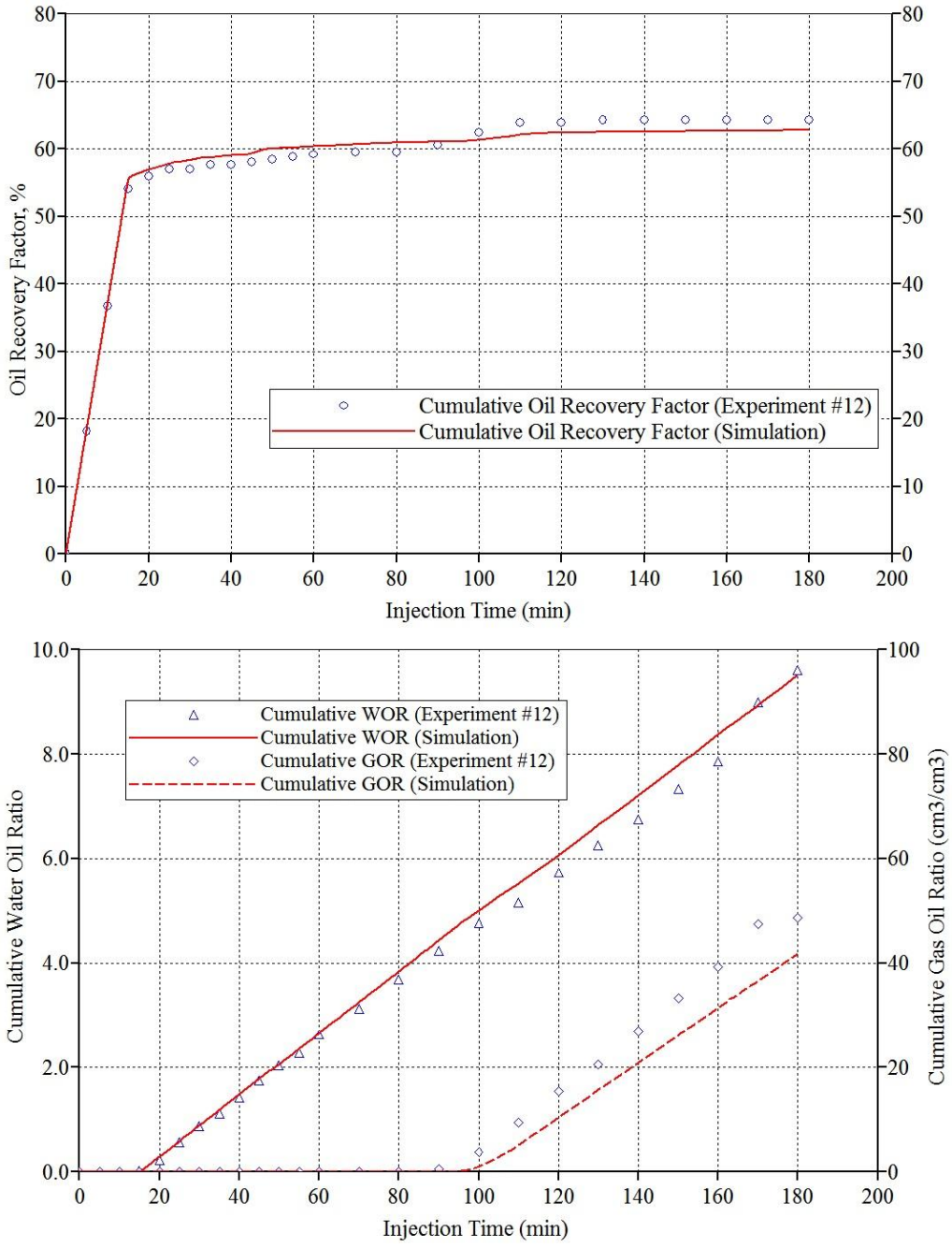

Figure A.10: Comparison of the simulated and measured cumulative oil recovery (a) and water oil ratio (b) for Test #12 (TCWI, P = 1.4 MPa, T = 25 °C, q_{inj} = 1.0 cm^3/min, CL = 100%).

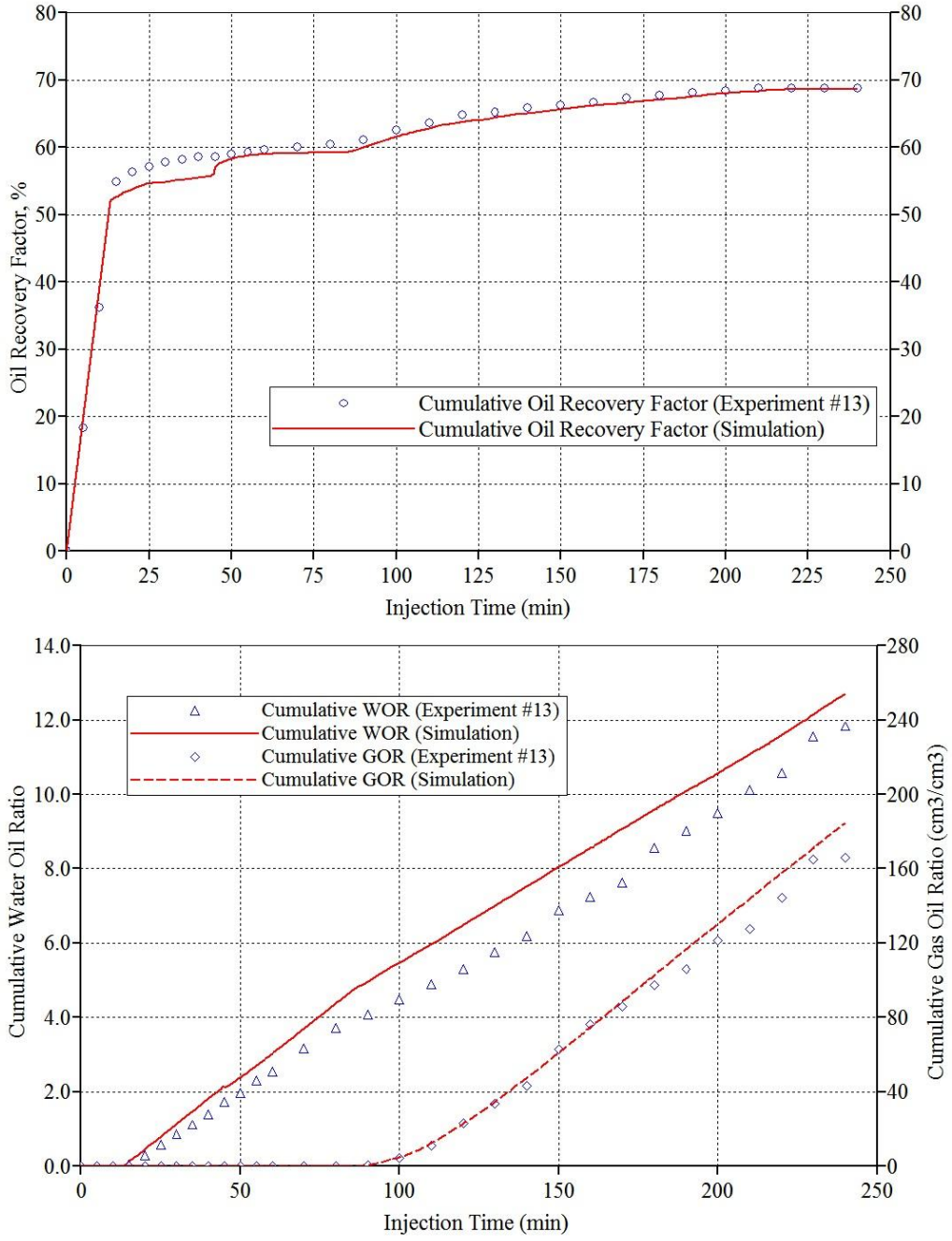

Figure A.11: Comparison of the simulated and measured cumulative oil recovery (a) and water oil ratio (b) for Test #13 (TCWI, P = 4.1 MPa, T = 25 °C, q_{inj} = 1.0 cm^3/min, CL = 100%).

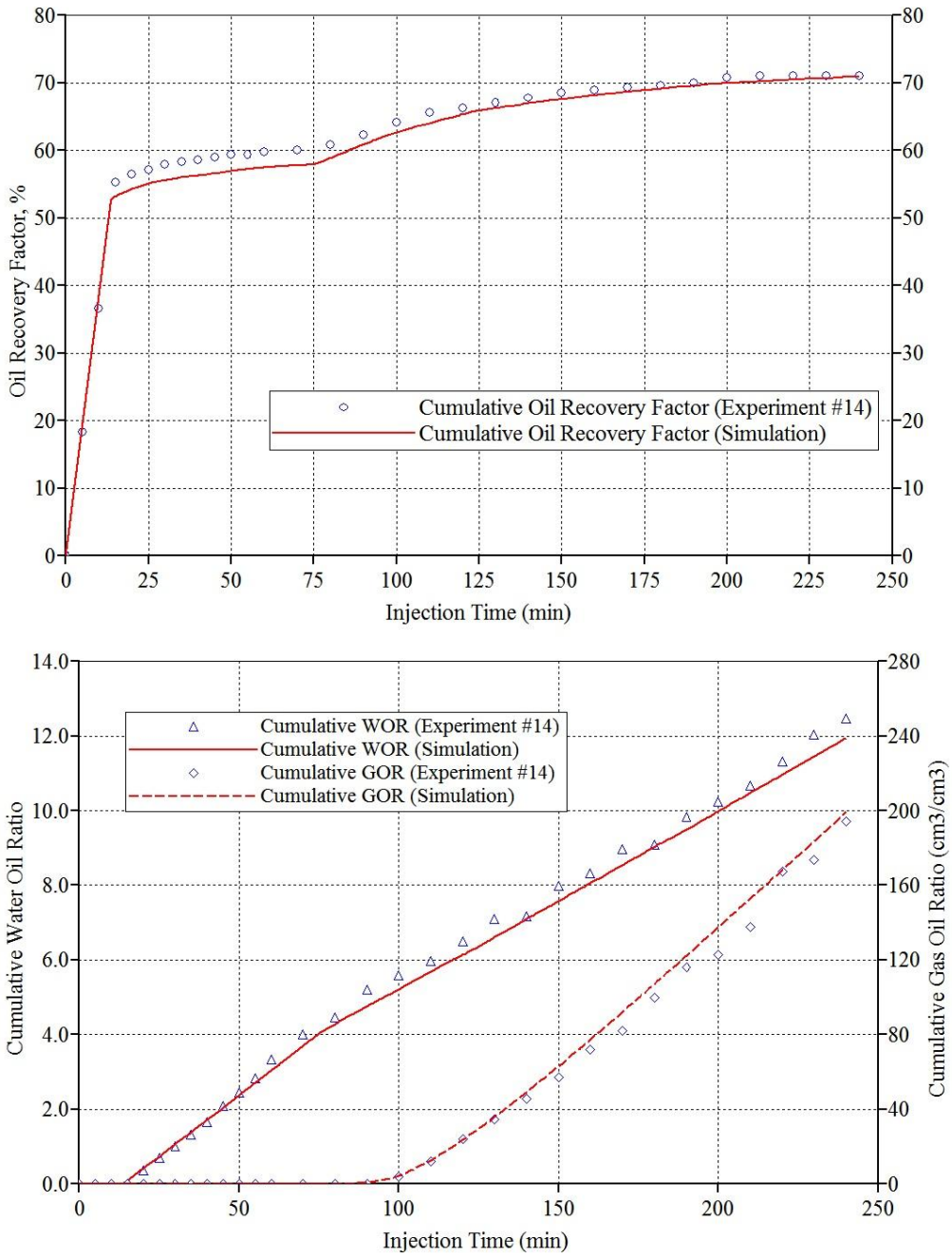

Figure A.12: Comparison of the simulated and measured cumulative oil recovery (a) and water oil ratio (b) for Test #14 (TCWI, P = 6.9 MPa, T = 25 °C, q_{inj} = 1.0 cm^3/min, CL = 100%).

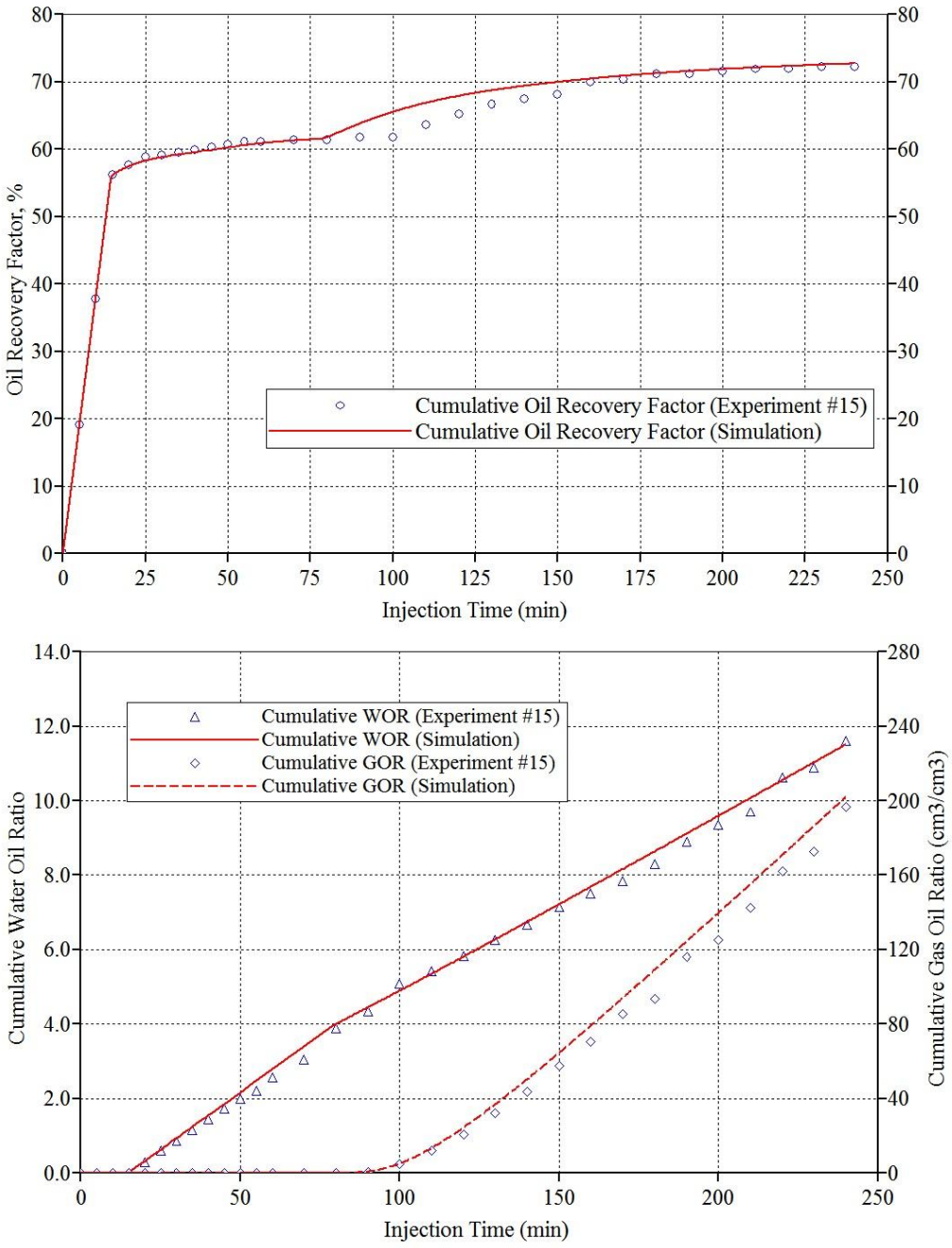

Figure A.13: Comparison of the simulated and measured cumulative oil recovery (a) and water oil ratio (b) for Test #15 (TCWI, P = 10.3 MPa, T = 25 °C, q_{inj} = 1.0 cm^3/min, CL = 100%).

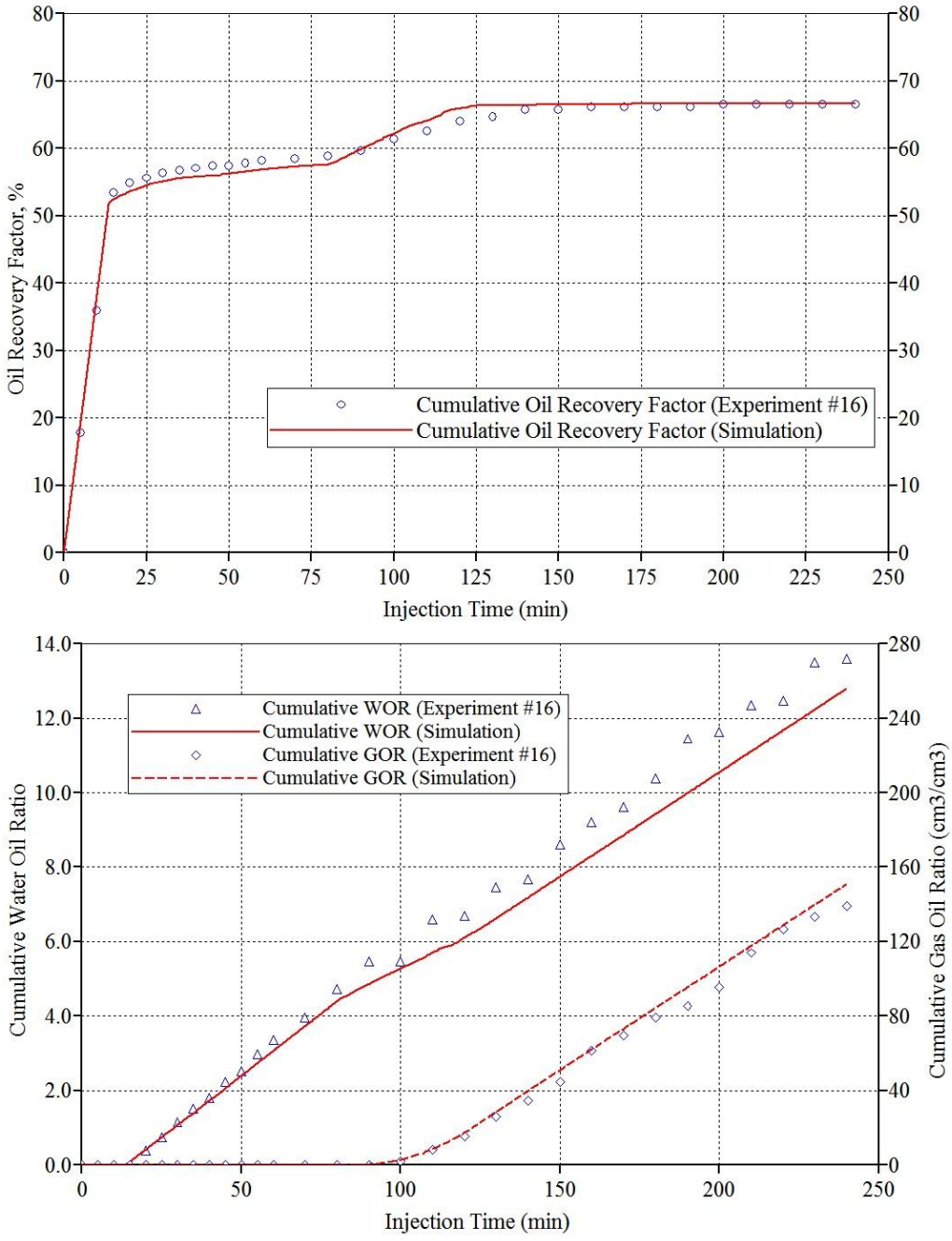

Figure A.14: Comparison of the simulated and measured cumulative oil recovery (a) and water oil ratio (b) for Test #16 (TCWI, P = 4.1 MPa, T = 40 °C, q_{inj} = 1.0 cm^3/min, CL = 100%).

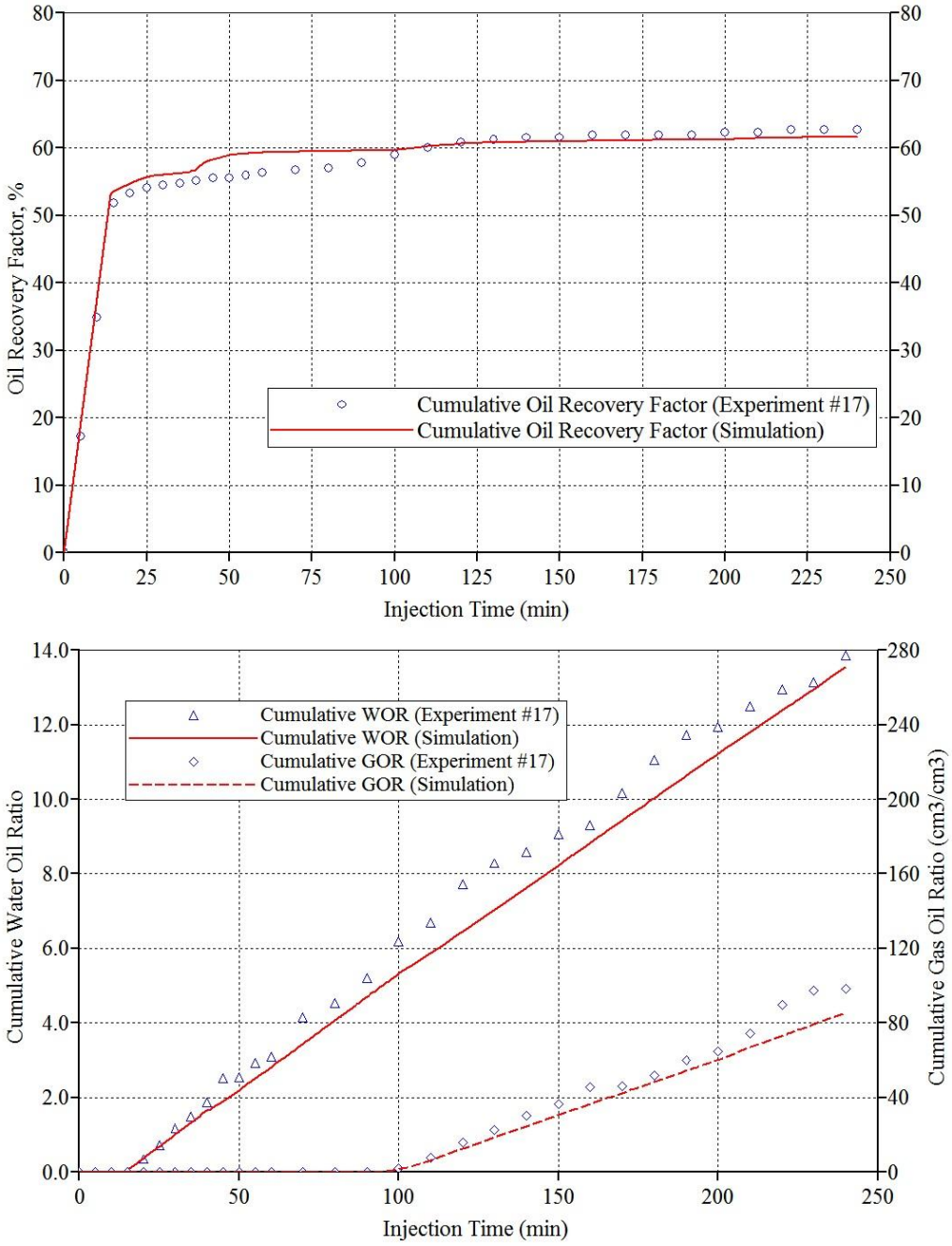

Figure A.15: Comparison of the simulated and measured cumulative oil recovery (a) and water oil ratio (b) for Test #17 (TCWI, P = 4.1 MPa, T = 25 °C, q_{inj} = 1.0 cm^3/min, CL = 50%).

APPENDIX B: MATLAB code for image processing

```
clc
workspace;  % Make sure the workspace panel is showing.
clearvars;
format longg;
format compact;
fontSize = 20;
I=imread('ia.png');
imshow(I)
background=imopen(I,strel('disk',15));
figure, imshow(background)
figure, surf(double(background(1:500:end,1:500:end))),zlim([0 255]);
set(gca,'ydir','reverse')
level=graythresh(I);
bw=im2bw(I,level);
figure, imshow(bw)
imwrite (bw,'ia_bw.png','png')
[labeled,numobjects]=bwlabel(bw,4);
numobjects
bw1=imread('ia_bw_grainwhite.png');
%imshow(bw1)
level=graythresh(bw1);
bw2=im2bw(bw1,level);
totalgrain=bwarea(bw2)
figure, imshow(bw1)
graindata=regionprops(bw2,'basic')
%imshow(bw2);
maxarea=max([graindata.Area]);
minarea=min([graindata.Area]);
num=struct2cell(graindata);
grain_areas=[graindata.Area]
nbins=45;
figure, hist(grain_areas,nbins);
title('Histogram');
 I = imread('11.jpg');
 [m, n, k]=size(I)
 for i=1:m
     for j=1:n
         r=I(i, j, 1);
         g=I(i, j, 2);
         b=I(i, j, 3);
         avg=0;
         avg=(r+g+b)/3;
         if(avg<150)
             I(i,j,1)=255;
             I(i,j,2)=0;
             I(i,j,3)=0;
             % change value to red color
         end
     end
 end
 figure,
 imshow(I),
 title('seddedImage')
bw3=imread('ia_bw_porewhite.png');
%imshow(bw1)
level=graythresh(bw3);
bw4=im2bw(bw3,level);
totalpore=bwarea(bw4)
% calculation of phase saturatuons
RGB = imread('11.jpg');
subplot(2, 1, 1);
imshow(RGB)
[x y z] = size(RGB)
RGB(1:x,1:y,1);
```

```
for i=1:13
    for j=1:y
        RGB(i,j,1)=111;
        RGB(i,j,2)=111;
        RGB(i,j,3)=111;
    end
end
for i=176:190
    for j=1:y
        RGB(i,j,1)=111;
        RGB(i,j,2)=111;
        RGB(i,j,3)=111;

    end
end
for i=1:x
    for j=517:539
        RGB(i,j,1)=111;
        RGB(i,j,2)=111;
        RGB(i,j,3)=111;

    end
end
for i=1:x
    for j=1:14
        RGB(i,j,1)=111;
        RGB(i,j,2)=111;
        RGB(i,j,3)=111;

    end
end
for i=1:x
    for j=1:y
        if RGB(i,j,3)<75
            RGB(i,j,3)=0;
            RGB(i,j,1)=0;
            RGB(i,j,2)=0;
        else
            RGB(i,j,3)=255;
            RGB(i,j,1)=255;
            RGB(i,j,2)=255;
        end
    end
end
subplot(2, 1, 2);
imshow(RGB)
```